Characterisation of the KSHV protein ORF20 and its role in innate immunity

Von der Fakultät für Lebenswissenschaften

der Technischen Universität Carolo-Wilhelmina zu Braunschweig

zur Erlangung des Grades einer

Doktorin der Naturwissenschaften

(Dr. rer. nat.)

genehmigte

D i s s e r t a t i o n

von Ulrike Diekmann geb. Lau
aus Rostock

1. Referent: Professor Dr. Lothar Jänsch
2. Referentin: Professorin Dr. Melanie Brinkmann
eingereicht am: 16.10.2018
mündliche Prüfung (Disputation) am: 21.12.2018

Druckjahr 2019

Vorveröffentlichungen der Dissertation

Teilergebnisse aus dieser Arbeit wurden mit Genehmigung der Fakultät für Lebenswissenschaften, vertreten durch den Mentor der Arbeit,
in folgenden Beiträgen vorab veröffentlicht:

Publikationen

Bussey KA, **Lau U**, Schumann S, Gallo A, Osbelt L, Stempel M, Arnold C, Wissing J, Gad HH, Hartmann R, Brune W, Jänsch L, Whitehouse A, Brinkmann MM. The interferon-stimulated gene product oligoadenylate synthetase-like protein enhances replication of Kaposi's sarcoma-associated herpesvirus (KSHV) and interacts with the KSHV ORF20 protein. PLoS Pathog 14(3): e1006937 (2018)

Tagungsbeiträge

Lau U, Bussey KA, Wissing J, Selbach M. Jänsch L, Brinkmann MM. Identification of novel type I interferon modulators encoded by Kaposi's sarcoma-associated herpesvirus (KSHV). HZI Progress Seminar, Braunschweig (2013)

Lau U, Bussey KA, Wissing J, Selbach M. Jänsch L, Brinkmann MM. Novel insights into immune modulation by the tumor virus Kaposi's sarcoma-associated herpesvirus (KSHV). HZI Progress Seminar, Braunschweig (2014)

Bussey KA, Osbelt L, **Lau U**, Stempel M, Steffens C, Wissing J, Jänsch L, Gad HH, Hartmann R, Brinkmann MM. KSHV ORF20 interacts with the oligoadenylate synthetase-like protein (OASL). (Oral and Poster Presentations) 20th International Workshop on Kaposi's Sarcoma-Associated Herpesvirus, Berlin (2017)

Posterbeiträge

Lau U, Bussey KA, Brinkmann MM. Modulation of the Type I IFN response by human Herpesvirus Kaposi's sarcoma-associated herpesvirus (KSHV). 3rd Annual PhD Retreat, Bad Bevensen (2012)

Lau U, Bussey KA, Wissing J, Konrad A, Stürzl M, Selbach M, Jänsch L, Brinkmann MM. Modulation of the Type I IFN response by KSHV ORF 20. 6th International PhD Symposium, Braunschweig (2013)

Lau U, Bussey KA, Stürzl M, Konrad A, Wissing J, Jänsch L, Selbach M, Brinkmann MM. Identification of novel type I interferon modulators encoded by Kaposi's sarcoma-associated herpesvirus. 6th International Workshop on "Interferon and Infection", Braunschweig (2013)

Lau U, Bussey KA, Stürzl M, Konrad A, Selbach M, Brinkmann MM. An unbiased KSHV ORF screen to identify novel IFNβ inhibitors. 23rd Annual Meeting of the Society of Virology, Kiel (2013)

Lau U, Bussey KA, Wissing J, Jänsch L, Brinkmann MM. Kaposi's sarcoma-associated herpesvirus-encoded ORF20 disperses the nucleolar proteins fibrillarin and eukaryotic translation initiation factor 6. 3rd ASM Conference on Viral Manipulation of Nuclear Processes, Washington, DC; USA (2014)

Lau U, Bussey KA, Wissing J, Jänsch L, Brinkmann MM. Kaposi's sarcoma-associated herpesvirus-encoded ORF20 disperses the nucleolar proteins fibrillarin and eukaryotic translation initiation factor 6. SFB 638 Symposium, Heidelberg (2014)

Lau U, Bussey KA, Wissing J, Jänsch L, Brinkmann MM. Kaposi's sarcoma-associated herpesvirus-encoded ORF20 alters localisation of nucleolar proteins. 25th Annual Meeting of the Society for Virology, Bochum (2015)

Bussey KA, **Lau U**, Schumann S, Gallo A, Osbelt L, Stempel M, Arnold J, Wissing J, Gad HH, Hartmann R, Brune W, Jänsch L, Whitehouse A, Brinkmann MM. The interferon-stimulated gene product oligoadenylate synthetase-like protein enhances replication of Kaposi’s sarcoma-associated herpesvirus (KSHV) and interacts with the KSHV ORF20 protein. 28th Annual Meeting of the Society for Virology, Würzburg (2018)

Danksagung

Ich bedanke mich bei Prof. Dr. Melanie Brinkmann für die Möglichkeit der Mitarbeit in ihrer Gruppe und zur Promotion, bei der ich an ihrer Expertise und ihrem Enthusiasmus teilhaben durfte. Ihre kritische, zielgerichtete und vorantreibende Art, sowie die nicht nachlassende Unterstützung haben mich die gesamte Zeit begleitet. Für ihre schnelle und unermüdliche Hilfe bei der Fertigstellung dieses Dokumentes bin ich ihr besonders dankbar.

Ich danke Prof. Dr. Lothar Jänsch für die Übernahme der Mentorenschaft, die von großzügiger Bereitschaft zu Gesprächen und sehr guten Ratschlägen geprägt war. Die Kooperationsarbeit in unseren Proteomicsprojekten empfand ich stets als sehr angenehm. Prof. Dr. Robert Hänsch danke ich für das große Interesse an meinem Werdegang und meiner Doktorarbeit und für die Übernahme des Prüfungsvorsitzes.

Für ihr Mitwirken an meinen Thesis Committees und die damit verbundenen Beratungen und Hilfen bedanke ich mich bei Prof. Dr. Lothar Jänsch, Prof. Dr. Andrea Kröger und Prof. Dr. Ingo Schmitz.

Ich danke ganz besonders Dr. Kendra Bussey, von der ich in unzähligen Stunden gemeinsamer Arbeit und in Gesprächen so viel gelernt habe. Ihre detailgenaue Arbeitsweise und ihr scheinbar unerschöpfliches Wissen sind mir ein Vorbild. Ihr gilt mein aufrichtiger Dank für ihre Zeit, ihr Talent und ihre Sorgfalt, aber vor allem für ihre Freundschaft.

Ein sehr großer Dank gilt Helene, Vladimir, Sripriya, Markus, Baca, Margit und allen anderen VIMM Mitgliedern für die gemeinsame Zeit, die durch die unvergleichliche Hilfsbereitschaft, die freundschaftliche Atmosphäre und natürlich auch durch die informativen, erhellenden und erbaulichen Gespräche und Pausen maßgeblich zu dieser Doktorarbeit beigetragen haben.

Worte allein reichen nicht aus, um meiner Familie, insbesondere meinem Vater, meiner Mutter und meiner Schwiegermutter meine Dankbarkeit auszudrücken, für das Vertrauen, den Glauben an mich und die nicht enden wollende Unterstützung und Hilfsbereitschaft an so vielen Fronten.

Mein ganz besonderer Dank gilt meinem unvergleichlichen Mann, Jan. Seine unübertreffliche Unterstützung, seine wissenschaftlichen und persönlichen Ratschläge, seine Zuversicht und sein Verständnis haben mich durch diese Doktorarbeit getragen.

Summary

Kaposi's sarcoma-associated herpesvirus (KSHV) is one of the seven human viruses known to date that can cause cancer. Its genome encodes more than 85 open reading frames (ORFs) and for many of them, their role in viral pathogenesis is only beginning to emerge. The host innate immune system has developed efficient strategies to fight viral infections. Initially, the cellular sensors known as pattern recognition receptors (PRRs) detect the presence of incoming viral particles. Upon binding of cytoplasmic cellular or viral RNA, the PRR RIG-I activates a signalling cascade that leads to the transcription of the type I interferons (IFN) IFNα and IFNβ. These cytokines are then secreted and bind to the type I IFN receptor (IFNAR), which induces expression of hundreds of interferon-stimulated gene products (ISGs) that generate an antiviral environment. To establish lifelong infection, KSHV has evolved sophisticated mechanisms to modulate the innate immune system of its host.

With the aim of identifying novel KSHV-encoded inhibitors of the RIG-I-mediated type I IFN response, we performed a luciferase-based reporter screen with 85 ORFs. We identified the poorly characterised KSHV ORF20 protein as a potent inhibitor of IFNα and IFNβ as well as ISG transcription. To better understand the role of ORF20 for modulation of the type I IFN response, we used the unbiased approach of quantitative affinity purification coupled to mass spectrometry (q-AP-MS) to identify cellular interaction partners of ORF20. We found that ORF20 interacted with a variety of ribosomal and nucleolar proteins. Immunofluorescence analysis revealed that ORF20 predominantly localised to the nucleolus, where it colocalised with ribosomal and nucleolar proteins. Interestingly, the distinct localisation pattern of ORF20 correlated with the dispersal of nucleolar and ribosomal proteins from the nucleolus and with an altered chromatin structure.

Furthermore, the ISG oligoadenylate synthetase-like protein (OASL) was identified as an interaction partner of ORF20 by q-AP-MS. OASL is a member of the OAS protein family and has antiviral activity against a number of RNA viruses, but its role for DNA viruses is not well understood. Others have shown that OASL amplifies RIG-I-mediated type I IFN activation by directly interacting with RIG-I. Hence, we hypothesized that ORF20 might interfere with RIG-I pathway activation by manipulating the effect of OASL on RIG-I.

We characterised the interaction of ORF20 and OASL and found that ORF20 specifically interacted with the OAS domain of OASL, but the OASL ubiquitin-like domains were not required. ORF20 did not alter colocalisation of RIG-I and OASL in the cytoplasm or the interaction between RIG-I and OASL. Surprisingly, we found that the inhibitory effect of ORF20 on RIG-I signalling was independent of OASL expression, suggesting that the interaction between ORF20 and OASL has another, yet to be identified reason. By analysing the cellular interaction partners of OASL by q-AP-MS, we found that ORF20 and OASL shared a highly similar interactome. Like ORF20, OASL interacted with numerous ribosomal and nucleolar proteins and colocalised with these proteins in the nucleolus. This finding was in accordance with the observed colocalisation of ORF20 and OASL in nucleoli. As the nucleolus is the site of ribosome biogenesis and ORF20 and OASL interact with a number of ribosomal proteins, our data suggest that the cellular protein OASL may have a role for ribosome function, which may be manipulated by the KSHV protein ORF20 to promote KSHV infection.

Table of Contents

1 Introduction

1.1 *Herpesviridae*

Herpesviruses are a highly divergent family of disease-causing viruses that are grouped together based on their morphological criteria. A herpesvirus has a large linear double stranded DNA (dsDNA) genome that ranges from 124–295 kilo base pairs (kb) in length. The DNA is enclosed by an icosahedral capsid that is surrounded by a layer of proteins, called tegument (Pellet & Roizman, 2013). The proteins of the tegument are highly ordered through specific protein-protein interactions. Upon entry, the tegument proteins are released into the cytosol of the host cell and enable immediate interactions with cellular proteins (Sathish et al. 2012). The tegument layer is enclosed by a lipid envelope spiked with viral glycoproteins that mediate attachment and entry into the host cell (Pellet & Roizman, 2013).

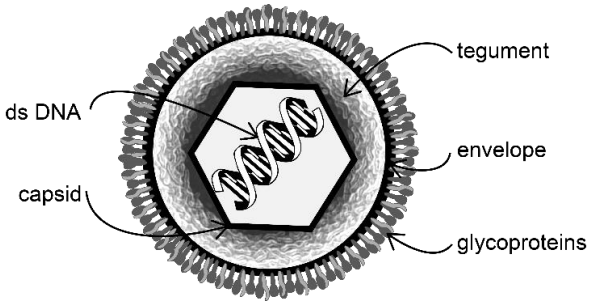

Figure 1 Herpesvirus virion structure. The linear double stranded DNA (dsDNA) is surrounded by an icosahedral capsid, embedded in a tegument layer of proteins and enclosed by lipid bilayer spiked with viral glycoproteins.

Herpesviruses can be found in every species, ranging from molluscs (*Malacoherpesviridae*), fish, and amphibians (*Alloherpesviridae*), over reptiles and birds to mammals (*Herpesviridae*) (Pellet & Roizman, 2013). Herpesviruses have coevolved with their hosts for millions of years (McGeoch & Davison, 1999). This has led to a distinct host range, as each virus has adapted perfectly to its host. Once infected, the virus persists for the entire life time of its host.

All members of the *Herpesviridae* have two alternative phases of their life cycle, a latent and a lytic phase (Miller et al. 1997). Latency allows lifelong persistence in the host. During latency, only very few viral proteins are expressed that secure stable maintenance of the viral circularised DNA as an episome in the nucleus (Renne et al., 1996), and minimize detection by the host immune system (Griffin et al. 2010). During the lytic phase, the viral DNA is replicated and packaged into the capsid and transported from the nucleus to the cytosol. The tegument is assembled in the cytoplasm together with the viral envelope that arises from cellular membranes. The infectious progeny virus is generally released by lysis of the host cell (Pellet & Roizman, 2013).

The nine human herpesviruses

To date, nine human herpesviruses have been identified. They are causing a variety of diseases, with mild to severe outcome. While every human being will be infected with at least one of the nine human herpesviruses during its lifetime, herpesviruses only cause, in most cases, mild clinical symptoms in immunocompetent individuals (Griffin et al. 2010). In immunocompromised patients however, herpesviruses can cause severe diseases and even death.

The human herpesviruses are grouped into three subfamilies based on nucleotide and protein sequence homology and genome colinearity, although the classification was originally based on biological properties (Longnecker et al., 2013). The three subfamilies are: *alphaherpesvirinae*, *betaherpesvirinae*, and *gammaherpesvirinae*.

The human alphaherpesviruses are herpes simplex virus 1 (HSV-1), herpes simplex virus 2 (HSV-2), and varicella-zoster virus (VZV). They share a variable host range, a relative short reproduction cycle, and the establishment of latent infection in sensory ganglia (Pellet & Roizman, 2013). HSV-1 and HSV-2 spread from sensory neurons to mucosal cells in their lytic life cycle. HSV-1 commonly infects orofacial surfaces and thereby causes cold sores, and less frequently keratitis and encephalitis. HSV-2 usually infects genital mucosal surfaces causing genital ulcers (Taylor et al., 2002), meningoencephalitis in neonates, and meningitis in adults (Steiner et al., 2007). VZV is causing chickenpox upon primary infection and shingles upon reactivation, which can lead to central nervous system complications such as myelitis and focal vasculopathies (Steiner et al. 2007).

The human betaherpesviruses are human cytomegalovirus (HCMV), human herpesvirus 6A (HHV-6A), human herpesvirus 6B (HHV-6B), and human herpesvirus 7 (HHV-7). They have a very restricted host range, a long reproductive cycle, and infected cells often become enlarged (cytomegalia). They can establish latency in secretory glands, lymphoreticular cells, and other tissues (Pellet & Roizman, 2013). While HHV-6B and 7 are mostly acquired during childhood and primary infections with symptoms are regarded as childhood ailments (Ward 2013), HCMV is the most common infectious cause of congenital diseases and can induce severe complications in immunocompromised patients. In the immunocompetent individual HCMV can cause febrile illness, periodontitis, and infectious mononucleosis (van Diemen & Lebbink, 2017).

The human gammaherpesviruses are Epstein-Barr virus (EBV) and Kaposi's sarcoma-associated herpesvirus (KSHV). They have a very restricted host range, as they are exclusively infecting their natural host (Pellet & Roizman, 2013). They replicate *in vitro* in lymphoblastoid cells and some types of epithelial or fibroblast cells. Latency is established in either B or T lymphocytes. EBV and KSHV are oncogenic. They are two of seven known viruses that can cause cancer in humans (Bergonzini et al. 2010). Primary infection of EBV frequently causes infectious mononucleosis (van Diemen & Lebbink, 2017). EBV is furthermore associated with several malignancies upon reactivation commonly originating from latently infected B cells or epithelial cells, like Burkitt's and Hodgkin lymphoma, or nasopharyngeal and gastric carcinoma (van Diemen & Lebbink, 2017). KSHV is described in detail in 1.2.

Currently, vaccination against herpesvirus infection can be achieved only for one of the nine herpesviruses, the alphaherpesvirus VZV. Antiviral drugs like Acyclovir, Ganciclovir, and Valganciclovir, which are recommended by the Food and Drug Administration, are used to treat life-threatening herpesvirus-caused diseases only, due to mild to tremendous side effects like nephrotoxicity, electrolyte abnormalities, and myelosuppression (Razonable, 2011). Commonly these drugs serve as competitive substrates for the viral DNA polymerase, thereby preventing viral replication (Razonable, 2011) However, there are increasing incidents of herpesvirus strains with drug resistance, emphasizing the urgency for new drugs and alternative treatments (Coen & Schaffer, 2003).

1.2 Kaposi's sarcoma-associated herpesvirus

The lymphotropic gammaherpesvirus KSHV, also called Human Herpesvirus-8 (HHV-8), was only identified in 1994 from patients with acquired immunodeficiency syndrome (AIDS)-associated Kaposi's Sarcoma (KS) (Chang et al. 1994). KSHV belongs to the genus *Rhadinovirus*, together with the closely related prototypic Herpesvirus saimiri, which infects squirrel monkeys (Pellet & Roizman, 2013). Oncogenic KSHV is the etiologic agent of three human diseases: KS, a skin tumour of endothelial origin, and the two B cell malignancies: Primary Effusion Lymphoma (PEL) and Multicentric Castleman's Disease (reviewed in Antman & Chang, 2000) (Damania & Cesarman, 2013).

1.2.1 Kaposi's Sarcoma

The disease KS is named after the Hungarian dermatologist Moritz Kaposi, who first described it in the late 19th century as "idiopathic multiple pigmented sarcoma of the skin".

KS is a cancer of cells that line lymph and blood vessels. In contrast to other cancers, KS can emerge in several areas of the body at the same time (Torre et al. 2015). Histologically, KS begins with the proliferation of endothelial cells in combination with a rapid proinflammatory infiltration and abnormal leaky blood vessel expansion (Mesri et al. 2010). The tumour or KS cells are called spindle cells. These are spindle-shaped cells that express markers of the endothelium, lymphatic endothelium, and few spindle cells express markers of dendritic cells, macrophages, or smooth muscle cells (Mesri et al. 2010). It is hypothesised that KSHV infects circulating endothelial precursor cells that are driven towards a lymphatic lineage. Explanted spindle cells *in vitro* are dependent on external cytokines and growth factors, unlike other tumour cells. They are only able to induce KS-like lesions in immunodeficient mice in the presence of inflammatory cytokines (Salahuddin et al. 1988).

KS is grouped into four classes:
(i) classic KS, which is endemic predominantly in males older than 50 years in the Mediterranean, the Middle East, or Eastern Europe (Dupin et al. 1995)
(ii) African or endemic KS, also referred as sub-Sahran African childhood KS
(iii) iatrogenic KS associated with immunosuppressive therapies in transplant patients
(iv) epidemic or AIDS-related KS, which is among the leading causes of death in AIDS patients (Ganem et al. 2010, Damania & Cesarman 2013).

Before the AIDS epidemic, KS was observed only occasionally, with the exception of certain populations prone to classic KS (Torre et al. 2015). With the beginning of the human immunodeficiency virus (HIV) pandemic in the early 1980s, KS became an AIDS-defining diagnosis in HIV-positive individuals. For many years, KSHV was the most common cancer and among the leading causes of death in AIDS patients. Notably, a dual infection of HIV and KSHV increases the risk of KS by more than 1000-fold (Torre et al. 2015). Since the 1990s antiretroviral treatment (ART) for HIV is available. Consequently, in populations were AIDS patients are treated with ART, KS has become a rare diagnosis again. In subequatorial African countries, where ART is not obtainable, KS is one of the most common forms of cancer with significant morbidity and mortality and is even diagnosed in young children (Sinfield et al. 2007, Parkin 2006). Although treatment for KS exists, none is curing the KSHV infection.

1.2.2 KSHV epidemiology

The malignancy KS strongly reflects the KSHV seroprevalence rates (Mesri et al. 2010). In northern Europe, Asia, and the United States less than 10% of the population carry KSHV, but in most of sub-Saharan Africa, overall seroprevalence is more than 50%. The Mediterranean region has intermediate seroprevalence rates of 10–30% (Mesri et al. 2010). However, it is possible that the overall seroprevalence of KSHV is underestimated, as individuals with low viral loads might have been diagnosed as false negative (Mesri et al. 2010).

The route of KSHV transmission is not completely understood. Evidences show that KSHV can be transmitted through sexual-contact, as observed in gay men (Q. Cai et al. 2010), or saliva, as mother-to-child transmission in Africa has been reported (Pauk et al. 2000) and KSHV has been detected in oral fluids (Martró et al. 2007). Furthermore, *in vitro* replication in primary oral-derived epithelial cells shows that KSHV can be transmitted within the oral epithelium in healthy immunocompetent men (Duus et al. 2004). But additional routes of transmission, like other body fluids, cannot be excluded (Pauk et al. 2000). Since KSHV seroprevalence rates are highly different within the population, KSHV may not be easily transmitted. Furthermore, factors like the viral load, influenced by the degree of exposure to infected persons, may impact transmission (Pauk et al. 2000). Additional factors that may influence establishment of KSHV infection are genetic variants of the host, environmental factors, timing and possibly route of infection (Mesri et al. 2010).
Similarly, there are factors that influence the outcome of KSHV infection, since not all KSHV infected individuals develop cancer. It has been shown that KSHV itself has oncogenic potential, because it can transform cells and manipulate cellar homeostasis (Salahuddin et al. 1988, Damania & Cesarman 2013). Concurrent pathogenic infections, like co-infection with HIV-1, HCMV, or EBV seem important for progression of KSHV-induced tumours (Thakker & Verma, 2016).

1.2.3 KSHV genome and life cycle

Like all herpesviruses, KSHV has a complex genome and a biphasic life cycle. The dsDNA genome is 165–175 kb long and encodes for at least 85 known open reading frames (ORFs), 12 micro RNAs (miRNAs) and several non-coding RNAs (Chandran 2010, Damania & Cesarman 2013). KSHV has at least 12 genes that are unique for KSHV, namely K1-K12, while most other ORFs share homologies with other herpesviruses (Pellet & Roizman, 2013).
KSHV can infect multiple cell types *in vivo* and *in vitro* (Damania & Cesarman, 2013). Consequently, multiple human cell lines have been used to study KSHV, for example primary and transformed B cells, HEK293T cells, THP-1 monocytic cells, and HeLa epithelial cells. Furthermore, non-human cell lines can be infected by KSHV, such as monkey cells (e.g. Vero cells), hamster cells (e.g. CHO cells), or mouse cells (e.g. NIH3T3 fibroblasts).

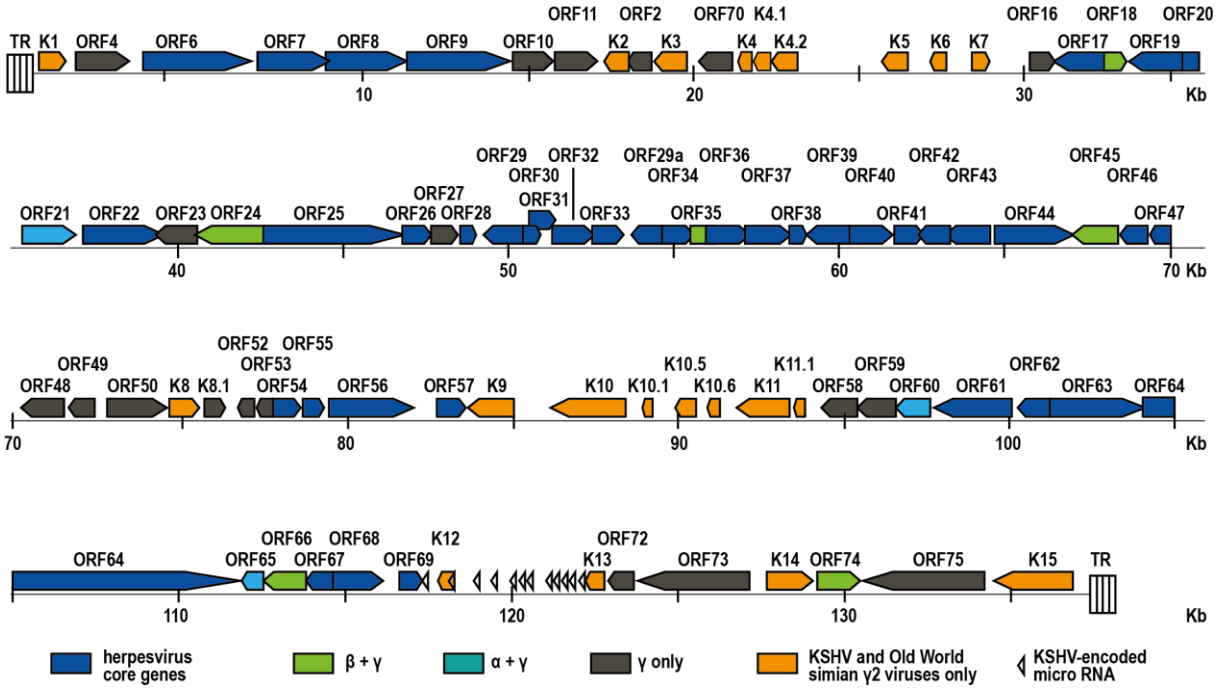

Figure 2 KSHV genome map. The viral dsDNA genome is 165–175 kb long and encodes for at least 85 known open reading frames (ORFs). Arrows indicate ORFs, and the arrowhead shows the direction of transcription. Genes that are conserved between KSHV and related alpha-(α) or beta-(β)-herpesviruses are shown in turquois or green, respectively. Unique genes of KSHV and old world simian gamma(γ) 2 herpesviruses are depicted in orange (adapted from Damania & Cesarman 2013).

As mentioned earlier, the biological cycle of a herpesvirus consists of initiation of infection, latency, and lytic replication (Miller et al. 1997, Pellet & Riozman 2013). Upon primary infection, KSHV viral particles enter the host cell and are transported along the microtubule network to the nucleus (Akula et al. 2001, Chandran 2010, Damania & Cesarman 2013). The dsDNA of KSHV is released into the nucleus where it can be replicated (lytic replication) or maintained as a circular episome (latency) (Damania & Cesarman, 2013). In the latent phase, the viral genome circularises, assembles with histones for chromatin organisation, and attaches firmly to the host chromosomal DNA. KSHV establishes viral latency in B cells by default (Renne et al. 1996, Ballestas et al. 1999), where multiple copies of the viral genome are maintained as extrachromosomal episomes and are replicated in synchrony with cell division (McGeoch & Davison 1999). During latency, only a limited number of viral genes (latent genes) are expressed that ensure maintenance of the viral episome, drive cell proliferation and prevent apoptosis, but no infectious virions are produced (Mesri et al. 2010, Zhong et al. 1996). It is described that external factors like UV exposure, co-infections, or cellular stress induce reactivation from latency and consequently lytic infection (Pellet & Roizman, 2013). For KSHV, a periodic lytic reactivation has been reported (Sun et al. 1999, Miller et al. 1997). During lytic infection, the viral DNA is linearized and viral genes are expressed in a highly regulated cascade (Damania & Cesarman 2013, Pellet & Riozman 2013). First, immediate-early (α) genes are expressed independently of de novo protein synthesis, followed by early (β) gene expression. Next, leaky-late (γ_1) genes are expressed followed by true late (γ_2) gene expression. The viral DNA itself is amplified by the rolling circle mechanism that generates long head-to-tail concatemers of viral genomes (Aneja & Yuan, 2017). The majority of the newly expressed proteins and the amplified DNA are assembled into mature virions, which are released by

lysis of the host cell and initiate infection in uninfected cells (Aneja & Yuan 2017, Pellet & Riozman 2013). This constant primary infection of new cells is crucial for viral propagation (Sathish et al. 2012). Importantly, the lytic as well as the latent viral life cycle of KSHV contribute to oncogenesis.

1.3 KSHV ORF20

KSHV-encoded ORF20 belongs to the herpesvirus core genes (Figure 2), as it is conserved in all three subfamilies (Jacobson et al. 1989). This indicates that the ancestral gene aroused 180-220 million years ago before the formation of the herpesvirus subfamilies (Nascimento et al 2009). ORF20 belongs to the UL24 gene family, which was defined by the corresponding HSV-1 gene UL24. The UL24 gene family shares five regions of high sequence similarity (Jacobson et al. 1989), and a putative endonuclease motif PD-(D/E)XK with no corresponding enzymatic or biological activity (Knizewski et al. 2006). This potential endonuclease motif is conserved in human alpha- and betaherpesviruses, but not in the human gammaherpesviruses EBV, KSHV or murine gammaherpesvirus 68 (MHV68) (Steffens, 2015).

1.3.1 Functions of the UL24 gene family members

Studies of HSV-1 UL24-deficient strains showed that UL24 is important for viral replication and reactivation from ganglia (Jacobson et al. 1989), for export of virus particles from the nucleus to the cytoplasm (Lymberopoulos et al. 2011), and for the subcellular distribution of viral glycoproteins involved in fusion (Abdeljelil et al. 2013). In cell culture, UL24 was not required for viral growth (Pearson & Coen, 2002). The UL24 protein mediates dispersal of the nucleolar proteins nucleolin and B23, whereby the function depends on the conserved N-terminal domain and the putative endonuclease motif (Lymberopoulos & Pearson 2007, Bertrand & Pearson 2008, Lymberopoulos et al. 2011). The implications of nucleolar dispersal for the herpesviral life cycle are not known.

The betaherpesvirus HCMV encodes the UL24 homologue UL76. It was shown that UL76 activates the NF-κB pathway and induces an ATM kinase-mediated DNA damage response, leading to expression of the cytokine interleukin 8 (IL-8) (Costa et al. 2013). Furthermore, UL76 interacts with the S5a protein of the ubiquitin proteasome system, which influences the formation of replication compartments and induces formation of nuclear aggresomes, which sequester polyubiquitinated proteins and thereby influence protein homeostasis (Lin et al. 2013).

The murine gammaherpesvirus MHV68 encodes the UL24 gene member ORF20, a non-essential, virion-associated protein with late replication kinetics (Bortz et al. 2003, Ebrahimi et al. 2003). MHV68 ORF20 overexpression is described to induce cell cycle arrest in the G2 phase prior to mitosis, leading to apoptosis of the cells (Nascimento & Parkhouse 2007). In this study, human HEK293T and HeLa cells as well as murine NIH3T3 cells were infected with lentiviral constructs expressing MHV68 ORF20. The viral protein was detected in the nucleus of transduced cells. The transduced cells seemed enlarged, expressed reduced levels of the mitosis marker phospho-histone H3, and showed increased levels of cyclin B and phosphorylated cyclin-dependent kinase 2 (Cdk2). This suggests that ORF20 may block the progression of the cells to mitosis by influencing the level of the Cdk2-cyclin B complex.

A similar approach was used to study HSV-1, HCMV and KSHV UL24 homologues and showed that they may inactivate the mitotic cyclinB/Cdk2 complex, leading to cell cycle arrest and apoptosis (Nascimento et al. 2009). Another study described that HCMV UL76 and HSV-1 UL24 may contribute to cell cycle arrest at the G1/S transition. In that study more than 200 herpesviral proteins were screened for their potential to induce a cell cycle arrest using a HeLa reporter cell line (Paladino et al. 2014).

1.3.2 Properties of KSHV ORF20

KSHV-encoded ORF20 is a poorly characterised protein. It is localised in the nucleus and nucleolus in transiently transfected cells (Sander et al. 2008). A recent study of our group identified two predicted nucleolar localisation signals (NoLS) in the ORF20 protein sequence: between amino acid (aa) 184 and 203 (IRKVLSKVPKKPKMDRGGKI) and between aa 218 and 250 (HHGRNKKGRPWTAQPTRA KSRTKDKGTPAFPRA). Subsequent analysis of various ORF20 deletion mutants indicated that the aa sequences 155 to 208 were important for nucleolar localisation (Osbelt, 2016). A systematic approach to identify cellular interaction partners of KSHV proteins, which used transient transfection of KSHV ORFs for affinity-purification coupled to mass spectrometry, found coiled-coil domain-containing protein 86 (CCDC86) as cellular interaction partner of ORF20 (Davis et al. 2015). CCDC86 is a poorly described protein, with nucleolar localisation and the ability to bind RNA (Castello et al. 2012).

The ORF20 gene is encoded by nucleotides 35.391 to 34.429 within the KSHV genome. This sequence encodes a 660-nucleotide mRNA, that is translated into ORF20 full length (FL), a protein of 320 aa with a predicted molecular mass of 35 kDa (GenBank: AKE33056.1) (Russo et al. 1996). Its translation starts at the first methionine. In the database, a second ORF20 protein is described, which will be designated as ORF20 B in this study. It is encoded by nucleotides 35.202 to 34.429 and its translation starts with the second ATG in frame with ORF20 FL, which is methionine 64. ORF20 B encodes a 257 aa protein with a predicted molecular mass of 28 kDa (GenBank: ABD28871.1).
During the course of this study, a third form of KSHV ORF20 was described, ORF20 A (Arias et al. 2014). Arias and colleagues used ribosome footprinting to determine alternative start codons. They found that the CTG codon located at nucleotide 35.322 is a start codon. The predicted protein consists of 297 aa and has a predicted molecular mass of 32 kDa. The mRNA of ORF20 and the potential three isoforms are shown in Figure 3.

Gene overlaps, as reported for ORF20, are common for herpesviruses. An additional transcriptional start at an internal methionine, located downstream of the first start codon, results in a shorter protein e.g. for HSV-1 UL26 and UL26.5. The resulting proteins share an identical sequence, but can have nonetheless different functions (Pellet & Roizman 2013). For ORF20, a functional relevance of the ORF20 A and ORF20 B isoforms, or a functional difference of the three ORF20 isoforms has not been described. Studies with KSHV ORF20 were predominantly performed with the full length form, from which all three isoforms, ORF20 full length, ORF20 A, and ORF20 B can be expressed.

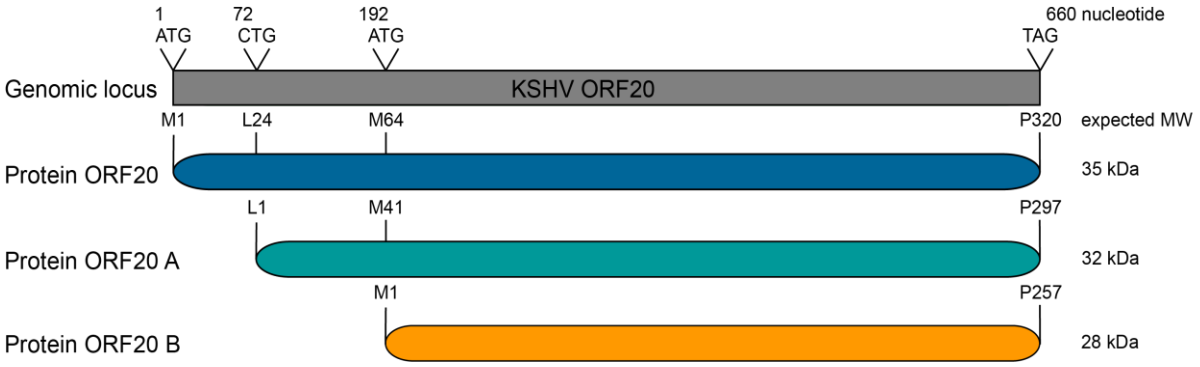

Figure 3 KSHV ORF20-encoded protein isoforms. Full length ORF20, starting at methionine 1, encodes a 320 aa protein, while ORF20 A starts at leucine 24 (aa 1-297), and ORF20 B starts at methionine 64 (aa 1-257) (adapted from Bussey et al. 2018).

1.4 Innate immune responses to KSHV infection

Pathogens like herpesviruses demonstrate nicely how important it is for the host to mount an effective innate and adaptive immune response, as immunocompromised individuals are not able to control viral infection and often consequently suffer from herpesvirus-caused diseases. Exemplary, inborn or developed deficiencies in the T cell response to KSHV can result in childhood KS (Jackson et al. 2016). In the absence of a functional immune system, the odds are in favour of the virus.

The innate immune response is the first line of defence against invading pathogens and furthermore activates and modulates the adaptive immune response. It plays a key role in the control of herpesviral infections (Dixit & Kagan 2013, Damania & Cesarman 2013). Cells of the innate immune response detect invading pathogens with a set of germ line-encoded pattern recognition receptors (PRRs) that recognize pathogen-associated molecular patterns (PAMPs). PAMPs are conserved structures, which either are essential biosynthetic products of the pathogens, or, in the case of viruses, nucleic acids, that occur as virus genomes or replication intermediates (Dixit & Kagan, 2013). Upon activation of PRRs by their respective PAMPs, signalling cascades are activated that lead to the activation of transcription factors, the interferon (IFN) regulatory factors (IRFs) and NF-kB. These transcription factors then initiate the transcription of the type I IFNs IFNα and IFNβ and proinflammatory cytokines. Secreted IFN binds to the type I IFN receptor (IFNAR) and thus triggers a signalling cascade that leads to the transcription of interferon-stimulated genes (ISGs) (Dixit & Kagan 2013). Cytokines, type I IFNs and ISGs ultimately create an antiviral environment that limits viral replication and prevents further spread of the infection.

1.4.1 Detection of KSHV infection by pattern recognition receptors

KSHV can be detected by PRRs of the innate immune system via its nucleic acids (Dixit & Kagan 2013). PRRs that detect nucleic acids are Toll-like receptors (TLRs) in the endosome, cytosolic retinoic acid inducible gene (RIG)-I-like receptors (RLRs), the cytosolic receptors cyclic GMP-AMP (cGAMP) synthase (cGAS), and nuclear receptor IFNγ-inducible protein 16 (IFI16) (Figure 4).

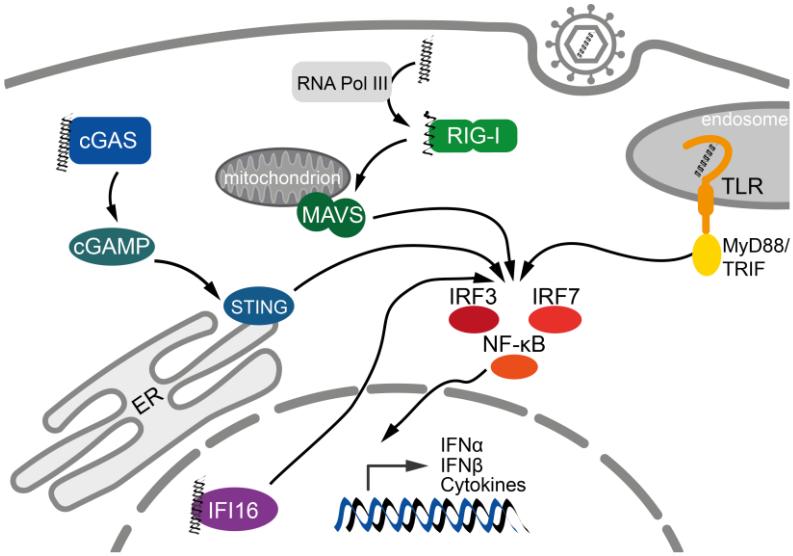

Figure 4 Detection of viral nucleic acids by pattern recognition receptors. Activation of PRRs induces a signalling cascade that leads to the activation and nuclear translocation of the transcription factors IFN regulatory factors (IRF3 and IRF7) and NF-kB and subsequent production of cytokines and type I IFNs.
TLRs sense viral DNA and RNA in the endosome of specialized immune cells and induce signalling via their respective adaptors MyD88 or TRIF. Cytosolic DNA is detected by the sensor cyclic GMP-AMP (cGAMP) synthase (cGAS). cGAS synthesises the second messenger cGAMP upon activation, which activates a signalling cascade via ER-resident stimulator of interferon genes (STING). IFNγ-inducible protein 16 (IFI16) is activated by viral DNA in the nucleus. The cytosolic RNA sensor retinoic acid inducible gene I (RIG-I) detects viral RNA. It also indirectly recognizes DNA via RNA polymerase III. RIG-I initiates signalling via its adaptor protein mitochondrial antiviral signalling protein (MAVS).

Endosomal TLRs detect endocytosed viral nucleic acids

TLRs are expressed in specialised immune cells like macrophages and dendritic cells and each cell type shows a distinct expression profile (Dixit & Kagan 2013). The endosomal TLRs TLR3, TLR7/8, and TLR9 detect nucleic acids that have reached the endosomes through endocytosis or autophagy (Kawai & Akira 2010). TLR3 is activated by dsRNA, while TLR7 recognizes single stranded RNA (ssRNA) and TLR9 CpG rich DNA (Kawai & Akira 2010).

Several studies have shown that TLRs play a role in KSHV infection (Damania & Cesarman 2013). Upon primary infection, KSHV components, presumably viral or cellular mRNA or micro RNAs incorporated in the tegument, activate TLR3 in monocytes and induce IFNβ and chemokine production. In plasmacytoid dendritic cells (pDCs), TLR9 is activated by KSHV infection (West et al. 2011). Whether TLR7 can sense KSHV infection has not been described yet, but it has been shown that stimulation of TLR7/8 in latently infected PEL cells can induce KSHV reactivation and propagation (Damania & Cesarman 2013).

cGAS detects viral DNA in the cytoplasm

The cytoplasmic innate immune receptor cGAS detects cytosolic DNA, which can be found for example in cells infected with DNA viruses or in tumour cells (Wu et al. 2013, Sun et al. 2013). Upon activation, cGAS catalyses the synthesis of 2'3'-cGAMP from ATP and GTP (Ishikawa & Barber 2008). This second messenger activates the endoplasmic reticulum (ER)-resident adapter stimulator of interferon genes (STING), inducing translocation of STING to the ER-Golgi-intermediate compartment and the Golgi apparatus (Chen et al. 2016). During this trafficking process STING recruits and activates TANK binding kinase 1 (TBK1), which enables activation of IRF3 and subsequent induction of type I IFN expression

(Ishikawa & Barber 2008, Chen et al. 2016). The cGAS pathway underlies a positive feedback mechanism, as IFNs induce cGAS gene expression via the IFNAR, which results in an enhanced cGAS-induced immune response (F. Ma et al. 2015). Activation and protein levels of cGAS and its pathway components are tightly regulated to control aberrant pathway activation, which is important to prevent autoimmune and inflammatory diseases (Chen et al. 2016, Galluzzi et al. 2018).

Studies showed that infection with KSHV is detected by cGAS and activates the cGAS/STING pathway (Z. Ma et al. 2015). At the same time, KSHV manipulates the cGAS-mediated immune response. KSHV-encoded vIRF1 was shown to inhibit interaction of TBK1 and STING, thereby preventing signal transduction and subsequent type I IFN activation (Z. Ma et al. 2015). KSHV-encoded tegument protein ORF52 directly binds to cGAS and the DNA detected by cGAS, resulting in the inhibition of cGAS enzymatic activity (Wu et al. 2015). The cytosolic receptor cGAS furthermore contributes to the regulation of reactivation from latency, and KSHV-encoded cytoplasmic variants of the major latency protein LANA directly interact with cGAS/STING to antagonise cGAS function. This promotes KSHV reactivation from latency (Zhang et al. 2016).

IFI16 detects viral DNA in the nucleus

Innate immune cells can also detect DNA in the nucleus. The DNA sensor IFI16 primarily localises to the nucleus, where it senses KSHV and other herpesvirus genomes, resulting in the activation of an inflammasome response and cytokine production (Kerur et al. 2011, Ansari et al. 2015). Interaction of IFI16 with HSV-1 DNA in the nucleus was shown to induce IFI16 translocation to the cytoplasm and subsequent activation of the STING pathway and type I IFN production (Ansari et al. 2015). Nuclear IFI16 is stabilised through interaction with cGAS, enhancing detection of viral DNA and viral genome complexes in the nucleus (Orzalli et al. 2015), demonstrating the complexity and interlinkage of innate immunity. IFI16 is a lytic replication restriction factor in KSHV infected cells, as it was shown to function as a transcriptional repressor, and IFI16 protein levels correlated with KSHV lytic reactivation (Roy et al. 2016). KSHV has evolved mechanisms to overcome IFI16-induced suppression by inducing the degradation of IFI16 via the proteasome pathway during lytic reactivation (Roy et al. 2016).

RLRs detect viral RNA from actively replicating virus

Actively replicating viruses are characterized by the presence of double stranded RNA products. These RNAs can be detected by the innate immune system through cytosolic RLRs like RIG-I and Melanoma differentiation associated gene 5 (MDA-5) (Yoneyama et al. 2004, Yoneyama et al. 2005). RLRs are expressed in most cell types (Dixit & Kagan 2013). RIG-I and MDA-5 are structurally highly related proteins. They are characterised by a central ATPase domain containing a DExD/H box helicase domain and a C-terminal domain (CTD). Both RLRs detect different RNA species but activate the same signalling cascade, leading to the activation of type I IFN, proinflammatory cytokines, and expression of ISGs (Yoneyama et al. 2005, Dixit & Kagan 2013). Upon activation, both receptors directly interact with the adaptor protein mitochondrial antiviral signalling protein (MAVS), which promotes signalling pathways that activate the transcription factors NF-kB, IRF3, and IRF7 (Meylan et al. 2005, Seth et al.

2005). MDA-5 preferentially binds high molecular weight (HMW) dsRNA, while RIG-I binds ssRNA with secondary RNA structures such as hairpin or panhandle conformations and short dsRNA, both equipped with 5'-triphosphate motifs (Lee et al. 2016). Furthermore, RIG-I emerged as an important sensor for DNA viruses like the herpesviruses EBV, HSV-1, and KSHV (Chiu et al. 2009, Cheng et al. 2007), and is described in detail in the following section.

1.4.2 RIG-I mediates type I IFN activation upon KSHV infection

The cytosolic RNA receptor RIG-I detects RNA viruses, but moreover is able to recognize infections with DNA viruses, such as herpesviruses. This is achieved by the enzyme RNA polymerase III, which transcribes AT-rich dsDNA into dsRNA with a 5'-triphosphate moiety (Ablasser et al. 2009). Additionally, RNA polymerase III transcribes herpesvirus-encoded small RNAs, which can be found in the tegument layer. These RNA polymerase III transcription products can be recognised by RIG-I, whereby they directly interact with the sensor and subsequently activate RIG-I signalling (Ablasser et al. 2009).

RIG-I consists of a central DExD/H-box helicase domain, a C-terminal domain (CTD) and two N-terminal caspase activation and recruitment domains (CARDs). Its activation is tightly controlled by several posttranslational modifications to avoid autoimmunity and other pathological conditions.
The current model of RIG-I activation is depicted in Figure 5 (Gack 2014).

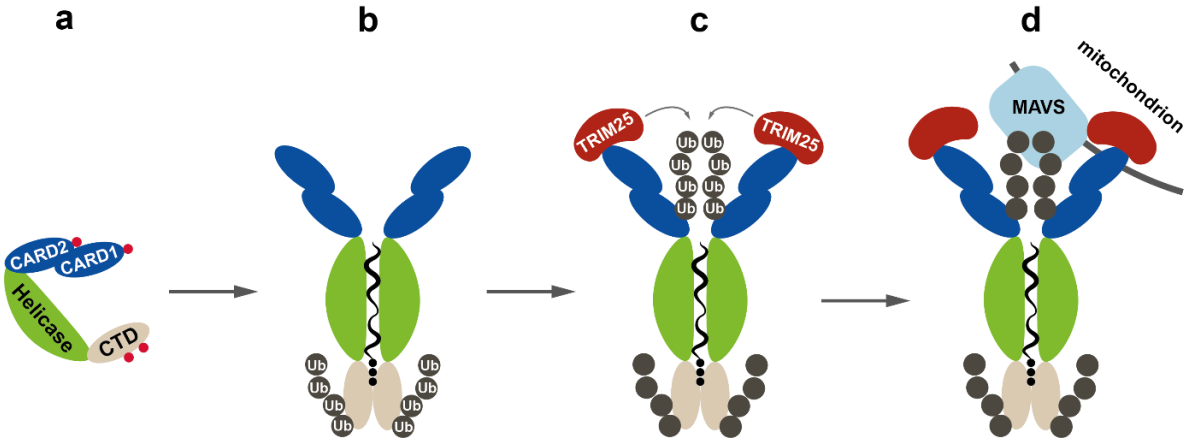

Figure 5 Activation of RIG-I. (a) The monomer is kept inactive by phosphorylation (indicated by red dots) of the CTD and the two CARDs. (b) Binding of RNA by the CTD and helicase domain, dephosphorylation of the CTD and CARDs, and attachment of Lys63-linked ubiquitin chains at the CTD induces a conformational change and subsequent dimerization of RIG-I. (c) Exposed CARD1 recruits the ubiquitin E3 ligase TRIM25, which mediates Lys63-linked ubiquitination of CARD2. (d) Activated RIG-I interacts with MAVS at the mitochondrion, resulting in MAVS-mediated type I IFN signalling (adapted from Gack 2014).

The inactive RIG-I monomer is phosphorylated at the CARDs (Ser8 and Thr170) and CTD (Thr770 and Ser845/855) and shows a closed conformation. Binding of viral RNA by the CTD and helicase domain in combination with CTD dephosphorylation and Lys63-linked ubiquitination induces a conformational change of RIG-I and enables RIG-I dimerization. The exposed CARDs are dephosphorylated, which allows interaction of CARD1 and TRIM25, a RING-dependent ubiquitin E3 ligase belonging to the tripartite motif (TRIM) protein family. TRIM25 initiates attachment of Lys63-linked ubiquitin chains at Lys172 in CARD2. As an additional control level, ubiquitination/deubiquitination regulates TRIM25 proteasomal degradation (Pauli et al. 2014). Ubiquitination of the CARDs allows RIG-I oligomerization and binding to the adaptor protein MAVS, located at the mitochondrial membrane. MAVS induces

antiviral signalling, whereby IRF3 and IRF7 are activated, which induce IFNα and IFNβ gene expression and subsequent ISG induction.

RIG-I-mediated innate immune responses play an important role during KSHV infection, as cells devoid of RIG-I show increased susceptibility to KSHV infection and increased lytic replication of KSHV (Inn et al. 2011). Upon primary infection, as well as upon reactivation, depletion of RIG-I or MAVS results in reduced IFNβ induction and enhanced KSHV transcription (West et al. 2014). It was shown that KSHV encodes a viral deubiquitinase, namely ORF64, that reduces TRIM25-dependent ubiquitination of RIG-I, leading to diminished IFNβ activity (Inn et al. 2011). Thus, RIG-I signalling seems important to control lytic reactivation of KSHV and KSHV evolved at least one mechanism to antagonise RIG-I signalling.

1.4.3 The type I interferon antiviral response

Type I IFNs play a central role in the innate immune response. Their production enables the establishment of an antiviral state, both in virus-infected cells and uninfected bystander cells. Furthermore, these secreted polypeptides contribute to the modulation of the innate immune response by promoting antigen presentation and natural killer cell functions. In addition, type I IFNs activate the adaptive immune response, as they shape the antigen-specific T and B cell responses and immunological memory.

The IFNs constitute a family which consists of 13 partially homologous IFNα subtypes in humans (14 in mice), a single IFNβ and several poorly defined single gene products (IFNε, IFNτ, IFNκ, IFNω, IFNδ and IFNζ) (Pestka et al. 2004). The ratio of the produced family members varies depending on the infected tissue, the virus and the species of the host. IFNα and IFNβ are the best studied type I IFNs. They are rapidly produced upon PRR recognition, and subsequently induce a set of gene transcriptions that interfere with multiple stages of the viral replication cycle through various mechanisms (McNab et al. 2015).

Transcriptional control of type I IFNs

Type I IFN induction is tightly regulated and is primarily controlled at the transcriptional level by the interferon regulatory factors (IRFs), where IRF3 and IRF7 have a pivotal role, although IRF1, IRF5, and IRF8 can also induce IFNα and IFNβ transcription (Honda & Taniguchi 2006). The constitutively expressed transcription factors are activated upon PRR-mediated signalling by phosphorylation at their C-terminus. This induces nuclear translocation of the IRFs and formation of IRF homo- and heterodimers. The activated dimers subsequently bind to the promoter region of IFNα and IFNβ genes and initiate their transcription (Sathish & Yuan 2011). The central theory is that IRF3 induces an initial wave of IFNα4 and IFNβ production, which triggers IRF7 transcription. The increased cytoplasmic ratio of IRF7 mediates a positive feedback loop. Both IRF3 and IRF7 induce a second wave of gene transcription, including additional IFNα-encoding genes (McNab et al. 2015, Honda & Taniguchi 2006). The transcription factor NF-κB is required as a cofactor for IRF-mediated transcriptional induction of IFNα and IFNβ (McNab et al. 2015).

IFNα/IFNβ-mediated signalling

Released IFNβ and all IFNα subtypes initiate type I IFN-mediated signalling in an autocrine and paracrine fashion by binding to the IFN receptor IFNAR, a heterodimeric trans-membrane receptor composed of one IFNAR1 and one IFNAR2 subunit (Ivashkiv & Donlin 2013). The induced ligation of the IFNAR activates two protein tyrosine kinases, the Janus kinase 1 (JAK1) and tyrosine kinase 2 (TYK2). In the canonical pathway (Figure 6), the activated tyrosine kinases phosphorylate cytosolic signal transducer and activator of transcription 1 and 2 (STAT1, STAT2). STAT1 and STAT2 dimerize and form together with IRF9 the ISG factor 3 (ISGF3) complex. This transcription complex travels into the nucleus, where it can initiate expression of several hundreds of interferon-stimulated genes (ISGs), of which a large number encodes antiviral effector proteins which apply a multitude of antiviral mechanisms (Schoggins et al. 2011). Besides the canonical pathway, IFNAR activation can induce a diversity of signalling pathways, like the phosphoinositide 3-kinase (PI3K)–mammalian target of rapamycin (mTOR) pathway or mitogen-activated protein kinase (MAPK) pathway and signalling through STAT1 homodimers or other STATs.

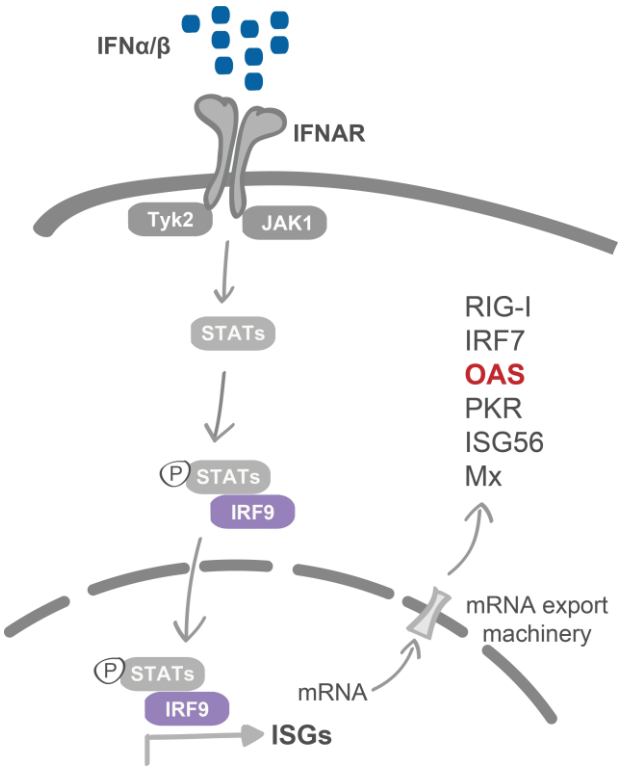

Figure 6 Canonical IFN receptor (IFNAR) signaling. Secreted IFNα and IFNβ bind to the two subunits of IFNAR. IFNAR subsequently activates Janus kinase 1 (JAK1) and tyrosine kinase 2 (TYK2), which activate signal transducer and activator of transcription 1 and 2 (STAT1, STAT2) by phosphorylation. Together with IRF9, STAT1 and STAT2 form the ISG factor 3 (ISGF3) transcription complex that traffics to the nucleus. By binding to responsive promoters, ISGF3 can induce expression of several hundreds of interferon-stimulated genes (ISGS) that shape the antiviral immune response, for example RIG-I, IRF7, OAS, PKR, ISG56 and the Mx protein family.

The complexity of type I IFN activation and IFNAR signalling allows the host to mount specific innate and adaptive immune responses against different viruses, as well as other invading pathogens. Conterminously, different virus infections induce specific sets of ISGs that aim to disrupt the viral life cycle (McNab et al. 2015).

Interferon-stimulated genes (ISGs)

ISGs interfere with the viral life cycle at distinct stages through pleiotropic effects, as one ISG can have multiple functions or its function can have varying outcomes (Sathish & Yuan 2011). Among the hundreds of ISGs that have been identified are broadly acting antiviral effectors and factors with more precise virus specificity. But each viral species is susceptible to multiple antiviral genes (Schoggins et

al. 2011). Noteworthy, some ISGs have been shown to act beneficial for the virus by enhancing viral replication and can therefore be regarded as proviral ISGs (Schoggins et al. 2011). ISGs that are described to target and disrupt the viral life cycle are dsRNA-dependent serine/threonine protein kinase R (PKR), ISG56, ISG54, ISG60, myxovirus resistance A (MxA), 2'-5'-oligoadenylate synthetase (OAS), and the interlinked RNaseL (Sathish & Yuan 2011).

The ISG MxA, which belongs to the Mx family GTPases, directly targets viral replication of ssRNA viruses by binding viral capsids and other viral components in the cytoplasm and sends them to degradation (Sadler & Williams 2008).

PKR mediates suppression of global translation by inactivating the key translation factor eukaryotic translation initiation factor 2A (eIF2A) through phosphorylation (Ivashkiv & Donlin 2013). Noticeably, the host cell simultaneously maintains translation of host defence effectors, like ISGs.

ISG54, ISG56, and ISG60 belong to the interferon-induced proteins with tetratricopeptide repeats (IFIT) protein family, and are also called IFIT1, IFIT2, and IFIT3, respectively. They interfere with the host protein translation-initiation machinery by interacting with key factors like the translation initiation factor eIF3 (Abbas et al. 2013, Terenzi et al. 2006). ISG56 furthermore senses and binds viral ssRNA and prevents viral mRNA translation, while ISG60 bridges TBK1 to MAVS at the mitochondrion, which enhances TBK1-mediated activation of IRF3 (Vladimer et al. 2014). Another study showed that ISG56 influences type I IFN production as a negative-feedback regulator by inhibiting TBK1 dependent IRF3 phosphorylation (Y. Li et al. 2009).

The high number of ISGs suggests that the IFN system uses multiple and overlapping strategies to ensure a single outcome like translational inhibition, as illustrated by the introduced PKR and IFITs.

1.4.4 Antiviral mechanisms of the OAS family

Another group of ISGs are the 2'-5'-oligoadenylate synthetase (OAS) proteins. They were first identified as inhibitors of protein synthesis that were highly induced by type I IFNs and dsRNA (Roberts et al. 1976, Kerr et al. 1977). The human OAS protein family consists of four proteins: OAS1, OAS2, OAS3, and OASL (Figure 7).

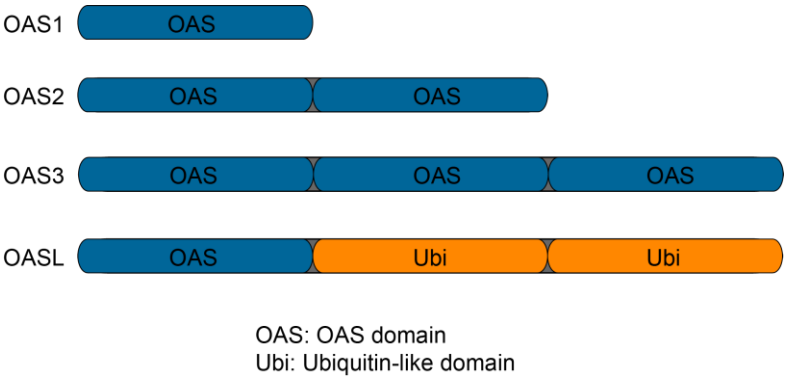

Figure 7 The human oligo-adenylate synthase (OAS) family members. The four OAS proteins OAS1, OAS2, OAS3, and OAS-like protein (OASL) are characterised by an OAS domain. Following their names OAS1-3 contain 1, 2, or 3 OAS domains, harbouring the character-istic 2'-5'-oligoadenylate synthetase activity. OASL has as an N-terminal OAS domain, which is lacking OAS enzymatic activity. Its C-terminal ubiquitin-like domain consists of two homologues ubiquitin moieties. All OAS family members possess antiviral activity.

OAS1-3 contain one, two, or three OAS domains, respectively (Hovanessian & Justesen 2007). They are activated by binding to viral dsRNA and ssRNA in the cytosol, upon which they catalyse the synthesis of 2'-5'-linked oligoadenylates from ATP as a substrate. This second messenger activates the latent endoribonuclease RNaseL, upon which it degrades cytosolic RNA of cellular and viral origin and broadly inhibits protein synthesis and limits viral propagation (Hovanessian & Justesen 2007, Hornung et al. 2014) This OAS-induced antiviral RNA decay pathway is shown in Figure 8. Interestingly, OAS and the cytosolic PRR cGAS share key structural and functional properties (Hornung et al. 2014).

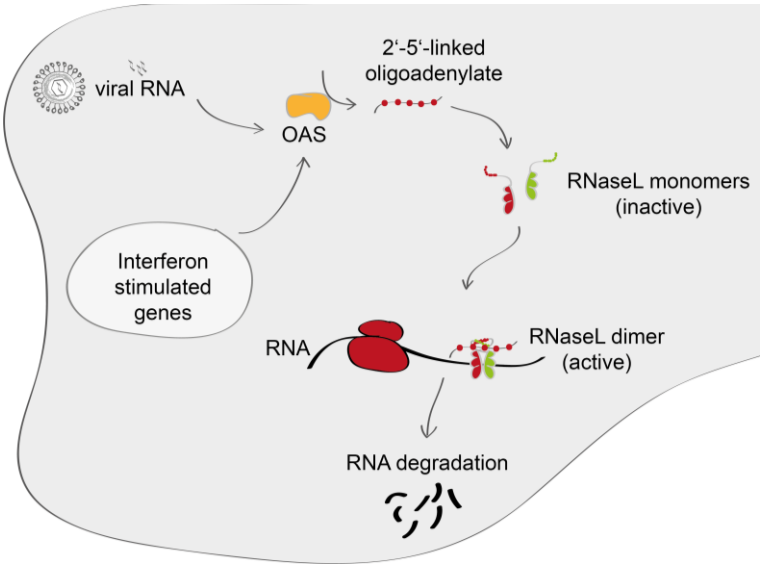

Figure 8 OAS family members induce RNA degradation. The interferon stimulated genes products OAS1, OAS2, and OAS3 bind viral RNA in the cytoplasm and produce 2'-5'-linked oligoadenylates. These second messenger molecules activate RNase L enzymes by inducing RNase L dimerization. Activated RNase L degrades host and viral RNA, thus inhibiting protein synthesis and viral propagation.

OASL possesses unique antiviral activity among OAS family members

The fourth member of the OAS protein family (Figure 7) is the oligoadenylate synthetase-like (OASL) protein, also called p59. OASL lacks the 2'-5' OAS activity of OAS1-3 (Hartmann et al. 1998). OASL was identified as a signature protein in the host response to IFN antiviral activity (Schoggins et al. 2011) that is induced by type I IFN signalling and IRF3 activation (Melchjorsen et al. 2009). OASL contains two domains (Figure 7). At its N-terminus it harbours an OAS domain with significant changes in its sequence compared to OAS1 in the P-loop, the essential aspartates in exon 2, and in the CFK tripeptide motif, involved in oligomerization of OAS1 and OAS2, which is changed to a CCY motif in OASL (Hartmann et al. 1998, Hovanessian & Justesen 2007). The C-terminal domain, called the Ubiquitin-like domain, is homologous to a tandem repeat of two ubiquitin moieties, but lacks the characteristic C-terminal diglycine motif that is essential to attach ubiquitin to cellular proteins (Hartmann et al. 1998, Jentsch & Pyrowolakis 2000). OASL has antiviral activity that requires the Ubiquitin-like domain. Overexpression of OASL was shown to possess antiviral activity against the ssRNA viruses picornavirus, encephalomyocarditis virus, hepatitis C virus, poliovirus, equine artevirus, and Newcastle disease virus and additionally showed mild effects against influenza A virus and measles virus (Marques et al. 2008, Schoggins et al. 2011, Schoggins et al. 2014). OASL did not inhibit replication of the following ssRNA viruses: human immunodeficiency virus type-1, yellow fever virus, West Nile virus, chikungunya virus, Venezuelan equine encephalitis virus, coxsackie B virus, Sindbis virus, o'nyong-nyong virus, human parainfluenza virus type 3, respiratory syncytial virus, and bunyamwera virus. OASL did not inhibit the DNA virus vaccinia (Schoggins et al. 2011). Its role for the alphaherpesvirus HSV-1 is

controversial, as one study did not observe inhibitory effects, while another did (Marques et al. 2008, Zhu et al. 2014).

In mice two OASL isoforms, mOASL1 and mOASL2, are expressed (Choi et al. 2015). The amino-acid sequence of mOASL1 shows a higher aa identity to human OASL (74% identity) than mOASL2 (49% identity) (Eskildsen et al. 2002). Unlike human OASL, mOASL2 has a functional OAS activity that requires dsRNA binding and seems to be an evolutionary intermediate of OAS1 and OASL (Eskildsen et al. 2003).

1.4.5 KSHV evades type I IFN production and type I IFN-mediated signalling

The fact that KSHV encodes a multitude of genes that evade the type I IFN response illustrates the important impact of these cytokines on viral infections (Sathish & Yuan 2011). An effective evasion of the onset of type I IFN initiation is crucial for KSHV to invade the cell and establish infection, as well as to reactivate from latency (McNab et al. 2015).

The broad repertoire of type I IFN antagonists seems necessary to manipulate the host immune response at distinct stages during the viral life cycle: upon entry, during replication, latency, or reactivation (Paludan et al. 2011). Moreover, the IFN pathway is quite complex and KSHV needs to manipulate specific checkpoints of the IFN pathway to ensure its own replication (Paludan et al. 2011). The evolution of several proteins that aim at the same objective ensures the targeted outcome, in this case the inhibition of IFN signalling (Pellet & Roizman 2013). Several studies showed that KSHV targets upstream molecules such as sensors and adaptors, as well as downstream signalling molecules (Brulois & Jung 2014). The millions of years of coevolution with its host has enabled the herpesviruses to adapt and shape the innate immune response for their own benefit (Gack 2014).

1.5 Aim of this study

The oncogenic herpesvirus KSHV is extremely successful, as it has adapted perfectly to its human host and establishes a lifelong infection. KSHV can cause several severe diseases like Kaposi's sarcoma (KS), Primary Effusion Lymphoma (PEL) and Multicentric Castleman's Disease. Notably, these diseases are frequently linked to an immunocompromised status of the host. To prevent KSHV-associated diseases and cancer, pharmaceuticals that target either primary infection, establishment of latency, or lytic reactivation are required (Aneja & Yuan 2017). In the first instance, a detailed understanding of the underlying mechanisms of viral infection and viral modulation of the host is urgently needed.

A key element of the innate immune system is the production of type I IFNs, especially IFNα and IFNβ, as these cytokines mediate the establishment of an effective antiviral state in an autocrine and paracrine fashion. KSHV infection, however, is marked by an impaired type I IFN response, and different herpesvirus-encoded factors are known to target multiple aspects of PRR-induced type I IFN induction. Nonetheless, our knowledge is far from complete. The function of many KSHV ORFs is still unknown and continuously new aspects of the innate immune system are revealed, highlighted by the recent identification of the cytosolic DNA sensor cGAS. Importantly, the study of individual KSHV ORFs sheds light on multiple aspects of viral paradigms on one side and cellular host functions on the other side.

Aim 1: Identification of novel KSHV-encoded inhibitors of the type I IFN response downstream of the PRR RIG-I. The cytosolic RNA receptor RIG-I has emerged as an important sensor for the detection of viruses. Activation of RIG-I by viral nucleic acids initiates a signalling cascade that results in the induction of the key cytokines IFNα and IFNβ. To achieve the first aim, 85 ORFs of a KSHV library were screened in a luciferase reporter assay for their ability to modulate IFNα4 or IFNβ promoter induction upon activation of RIG-I signalling. The results were validated in multiple cell lines of different species. KSHV-encoded ORF20 was identified as a novel inhibitor of the type I IFN response.

Aim 2: Characterisation of the newly identified modulator of the type I IFN response. KSHV ORF20 was analysed by basic molecular methods, determining apparent protein sizes and subcellular localisation of ORF20 and the isoform ORF20 B. We found that ORF20 and ORF20 B localised to the cytoplasm, nucleus and nucleoli and showed distinct localisation phenotypes. The cellular interactome of ORF20 was studied by affinity purification coupled to SILAC-based mass spectrometry, revealing cellular protein interactions. We found that ORF20 interacted with several nucleolar proteins, and thus raised a third aim. Furthermore, the interferon-induced protein OASL was identified as a potential interaction partner of ORF20, therefore a fourth aim was raised.

Aim 3: Analysis of the influence of KSHV ORF20 on nucleolar proteins. To achieve this aim, we first validated the interaction of ORF20 and ORF20 B with endogenous nucleolar proteins by co-immunoprecipitation. We analysed the subcellular localisation and quantified the expression of selected nucleolar proteins in the absence and presence of KSHV ORF20 and ORF20 B by immunofluorescence microscopy. We found that ORF20 and ORF20 B induced dispersal of nucleolar proteins. Subsequently, immunoblotting of endogenous nucleolar proteins was performed to analyse if ORF20 or ORF20 B influenced the total protein level of nucleolar proteins. Localisation and induction of nucleolar dispersal of the UL24 homologue MCMV M76 was analysed by immunofluorescence to study if the function was conserved in the UL24 gene family.

Aim 4: Analysis of the interaction between ORF20 and OASL and its impact on OASL function. We validated the interaction of ORF20 and OASL by co-immunoprecipitation and their localisation by immunofluorescence. During the course of this study, OASL was described to interact with the RIG-I receptor and to enhance RIG-I-mediated type I IFN induction. Consequently, we aimed to determine if ORF20 inhibited type I IFN signalling by inhibiting the effect of OASL on RIG-I. We analysed the RIG-I and OASL interaction in the presence and absence of ORF20 using immunofluorescence and co-immunoprecipitation. We further determined the influence of ORF20, OASL, as well as their interaction on RIG-I-induced ISG56 expression using co-transfections and immunoblotting and on ISG56 and IFNβ promoter induction using a luciferase-based reporter assay. Finally, the interactome of OASL was analysed by affinity-purification coupled to mass spectrometry to unravel unknown cellular interaction partners that could hint to a new function of OASL.

2 Materials and Methods

2.1 Materials and Reagents

2.1.1 Materials

Table 1 Commercially available materials

Material	Source
Amersham Hyperfilm ECL	GE Healthcare, Freiburg, Germany
Coverslips, 12 mm	Thermo Scientific, Schwerte, Germany
DynaMag – 2 Magnet, magnet stand	Thermo Scientific, Schwerte, Germany
M columns	Miltenyi Biotec, Bergisch Gladbach, Germany
MiniMACS separator	Miltenyi Biotec, Bergisch Gladbach, Germany
NuPAGE 4-12% Bis-Tris Protein Gels	Thermo Scientific, Schwerte, Germany
Protein LoBinding tubes	Eppendorf, Köln, Germany
Whatman Protran BA85 nitrocellulose membrane	GE Healthcare, Freiburg, Germany
96-well cell culture white microplate	Greiner Bio-One, Frickenhausen, Germany

2.1.2 Reagents and Enzymes

Table 2 Commercially available reagents

Reagent	Source
Agar	BD Bioscience Pharmingen, San Diego, US
Agarose	Sigma-Aldrich, Seelze, Germany
Ampicillin (100 mg/ml)	Sigma-Aldrich, Seelze, Germany
Bolt LDS Sample buffer (4x)	Thermo Scientific, Schwerte, Germany
Bolt Reducing Agent (10x)	Thermo Scientific, Schwerte, Germany
Bovine serum albumin (BSA)	Sigma-Aldrich, Seelze, Germany
Complete EDTA-free protease inhibitor cocktail tablets	Roche, Penzberg, Germany
Complete protease inhibitor cocktail tablets	Roche, Penzberg, Germany
Dialyzed fetal bovine serum (FBS)	Thermo Scientific, Schwerte, Germany
DMEM for SILAC, deficient in L-lysine and L-arginine	Thermo Scientific, Schwerte, Germany
Fermentas dNTP set, 100 mM	Thermo Scientific, Schwerte, Germany
Fetal Calf Serum (FCS)	Sigma-Aldrich, Seelze, Germany
Fugene HD	Promega, Mannheim, Germany
G418 (Geneticin)	Invivogen, San Diego, USA
Gibco DMEM, High glucose	Life Technologies, Darmstadt, Germany
Glutamine	Life Technologies, Darmstadt, Germany
GlycoBlue (15 mg/ml)	Life Technologies, Darmstadt, Germany
HEPES (1 M)	Thermo Scientific, Schwerte, Germany
Hoechst 33342	Thermo Scientific, Schwerte, Germany
IPA300 immobilized protein A affinity resin	RepliGen Corporation, Lund, Sweden
L-Arginine-HCl (Arg 0)	Thermo Scientific, Schwerte, Germany
L-Arginine-HCl, 13C6 (Arg 6)	Thermo Scientific, Schwerte, Germany
L-Glutamine, 200 mM	Life Technologies, Darmstadt, Germany
Lipofectamine 2000 transfection reagent	Life Technologies, Darmstadt, Germany
L-Lysine-2HCl (Lys 0)	Thermo Scientific, Schwerte, Germany
L-Lysine-2HCl, 13C6, 15N2 (Lys8)	Thermo Scientific, Schwerte, Germany
Lumi-Light Western Blotting Substrate	Roche, Penzberg, Germany

Reagent	Source
MEM non-essential amino acids (100x)	Life Technologies, Darmstadt, Germany
MES SDS Running buffer	Thermo Scientific, Schwerte, Germany
Nonfat dry milk	J.M. Gabler-Saliter Milchwerk GmbN & Co. KG, Obergrünzburg, Germany
NuPAGE Transfer Buffer	Thermo Scientific, Schwerte, Germany
O'GeneRuler 1kb Plus DNA ladder	Thermo Scientific, Schwerte, Germany
Opti-MEM	Life Technologies, Darmstadt, Germany
Orange DNA loading dye (6x)	Thermo Scientific, Schwerte, Germany
PageRuler plus prestained protein ladder	Thermo Scientific, Schwerte, Germany
PCR Master Mix 2x	Thermo Scientific, Schwerte, Germany
Pfu Ultra High Fidelity Reaction Buffer with $MgSO_4$	Agilent, Böblingen, Germany
Pierce Protein G Magnetic Beads	Thermo Scientific, Schwerte, Germany
Poly-D-lysine hydrobromide, average molecular weight: 30,000-70,000	Sigma-Aldrich, Seelze, Germany
Poly-D-lysine hydrobromide, average molecular weight: 75,000-150,000	MP Biomedicals GmbH, Eschwege, Germany
ProLong Gold Antifade Mountant	Thermo Scientific, Schwerte, Germany
Restore Plus Western Blot Stripping Buffer	Thermo Scientific, Schwerte, Germany
Sodium pyruvate, 100 mM	Life Technologies, Darmstadt, Germany
SuperSignal West Femto Maximum Sensitivity Substrate	Thermo Scientific, Schwerte, Germany
T4 DNA ligase buffer (5x)	Thermo Scientific, Schwerte, Germany
Trypsin-EDTA 0.25% (1x)	Life Technologies, Darmstadt, Germany

Table 3 Commercially available kits

Kit	Source
BC assay: Protein Assay Kit	Interchim, Montlucon, France
Dual-Luciferase Reporter Assay System	Promega, Mannheim, Germany
Nucleo Spin Plasmid Kit	Macherey-Nagel, Düren, Germany
NucleoSpin Gel and PCR Clean-up	Macherey-Nagel, Düren, Germany
QIAGEN Plasmid Purification Maxi Kit	Qiagen, Hilden, Germany
QIAquick Gel Extraction Kit	Qiagen, Hilden, Germany
µMACS c-myc Isolation Kit	Miltenyi Biotec GmbH, Bergisch Gladbach, Germany

Table 4 Enzymes

Enzyme	Source
Alkaline Phosphatase (1 U/µl)	Sigma-Aldrich, Seelze, Germany
Benzonase Nuclease, ultrapure	Sigma-Aldrich, Seelze, Germany
Fermentas FastDigest *Bgl*II, *EcoR*I, *Hind*III, *Nhe*I, *Pme*I, *Xho*I	Thermo Scientific, Schwerte, Germany
Fermentas T4 DNA Ligase (5 U/µl)	Thermo Scientific, Schwerte, Germany
Pfu DNA Polymerase (2.5 U/µl)	Thermo Scientific, Schwerte, Germany
Pfu Ultra High Fidelity DNA polymerase	Agilent, Böblingen, Germany
T4 DNA ligase (5 U/µl)	Thermo Scientific, Schwerte, Germany

2.1.3 Buffers and Solutions

All buffers and solutions were prepared in ultrapure water from a Milli-Q integral water purification system (EMD Millipore), except as noted.

Table 5 Buffers and solutions

Buffer / Solution	Amount of ingredient	
Agarose gel (1% / 2%)	1 / 2 g/L in TAE (1x)	Agarose
Blocking solution for IF	10% 1% in PBS (1x)	FCS BSA
Blocking solution with BSA for IB	50 g/L in TBS-T (1x)	BSA
Blocking solution with milk for IB	50 g/L in TBS-T (1x)	nonfat dry milk
Blotting buffer	25 mM 192 mM 0.05% 20%	Tris base (TRIZMA) Glycine SDS Methanol
IP Lysis Buffer (SILAC IP Lysis Buffer)	50 mM, pH 7.4 150 mM 1% 0.25%	Tris-HCl NaCl Nonidet P-40 (IGEPAL CA-630) in ddH2O Sodium deoxycholate add protease inhibitors (25x) before use
NaAcetate	2.5 M	Sodium acetate, pH 5.0
NuPAGE MES Running Buffer (20x)	50 mM 50 mM 0.1% 1 mM	MES Tris Base SDS EDTA
Orange G (5x)	100 mM 10 mM 45% (v/v) 0.001% 0.125%	Tris-HCl EDTA Glycerol Xylene Cyanol Orange G
PBS, pH 7.4	137 mM 2.7 mM 10 mM 1.8 mM	NaCl KCL Na_2HPO_4 x 2 H_2O KH_2PO_4
PFA fixation solution, pH 7.4	4% in PBS (1x)	PFA
Poly-D-lysine (50 µg/ml 100 µg/ml)	50/ 100 µg/ml	Poly-D-lysine
RIPA-100 lysis buffer	20 mM 100 mM 10 mM 1% 0.5% 0.1% 1x	Tris-HCl (pH 7.5) NaCl EDTA Triton X-100 Sodium deoxycholate SDS add protease inhibitor (25x) before use
SDS electrophoresis buffer (1x)	25 mM 192 mM 0.1%	Tris Glycine SDS
SDS loading buffer (4x)	250 mM 8% 0.04% 40% 12.5%	Tris-HCl SDS Bromphenol blue Glycerol β-mercaptoethanol (add before use)
SDS separating gel (10% acrylamide)	12.2 ml 7.5 ml 10 ml 0.3 ml 0.04 ml 0.04 ml	ddH_2O 1.5 mM Tris-HCl (pH 8.8) 30% Acrylamide 10% SDS TEMED 25% APS

Buffer / Solution	Amount of ingredient	
SDS separating gel (12% acrylamide)	10.2 ml	ddH_2O
	7.5 ml	1.5 mM Tris-HCl (pH 8.8)
	12 ml	30% Acrylamide
	0.3 ml	10% SDS
	0.04 ml	TEMED
	0.04 ml	25% APS
SDS solution (20%)	20%	SDS
SDS stacking gel (5% acrylamide)	5.75 ml	ddH_2O
	2.5 ml	0.5mM Tris-HCl (pH 6.8)
	1.7 ml	30% Acrylamide
	0.1 ml	10% SDS
	0.02 ml	TEMED
	0.03 ml	25% APS
TAE (50x), pH 7.5	50 mM	EDTA
	2.5 M	Tris-acetate
TBS (1x), pH 7.6	20 mM	Tris
	137 mM	NaCl
TBS-T (1x)	1%	TBS
	0.1%	Tween 20
Towbin Tris-glycine transfer buffer (1x)	25 mM	Tris base
	192 mM	Glycine
	0.05%	SDS
	20%	Methanol
Triton-X-100 (10%)	10%	Triton-X-100
	in PBS (1x)	

2.1.4 Bacteria and bacterial growth media

In this study, *Escherichia coli* DH10B with the following genotype was used: F- mcrA Δ(*mrr-hsd*RMS-*mcr*BC) Φ80*lac*ZΔM15 Δ*lac*X74 *rec*A1 *end*A1 *ara*D139 Δ(*ara leu*) 7697 *gal*U *gal*K *rps*L *nup*G λ-.

Table 6 Bacterial growth medium

Medium	Components	
LB medium	2%	Trypton
	0.5%	Yeast extract
	10 mM	NaCl
	10 mM	MgCl2
	10 mM	MgSO4
	20 mM	Glucose
SOC medium	2%	Tryptone
	0.5%	Yeast extract
	10 mM	NaCl
	10 mM	$MgCl_2$
	10 mM	$MgSO_4$
	20 mM	Glucose

2.1.5 Antibodies

Table 7 Primary antibodies and their working dilutions used for immunoblotting (IB), immunoprecipitation (IP), and immunofluorescence (IF)

Antibody (Anti-)	Species	Source, Order number	Working dilution IB	IF	IP
DDX21	rabbit	MBL, #RN090PW	1/1000 - 1/3000 in milk (o/n 4°C)		

Antibody (Anti-)	Species	Source, Order number	Working dilution IB	IF	IP
eIF6	rabbit, monoclonal	Cell Signaling, #3833	1/1000 in BSA (o/n 4°C, 3 h RT)	1/1000 - 1/500 (o/n 4°C)	1/50
fibrillarin	rabbit	Cell Signaling, # 2639	1/4000 in BSA (o/n 4°C, 3 h RT)	1/500 (o/n 4°C)	
FLAG	mouse, monoclonal	Sigma-Aldrich, # F1804	1/2000 in milk (1 h RT) 1/5000 in milk (o/n 4°C)	1/500 (1 h RT)	
FLAG	rabbit, polyclonal	Sigma-Aldrich, #F7425	1/2000 in BSA (o/n 4°C)	1/800 (1 h RT)	1/200
IFIT1	rabbit, polyclonal	Cell Signaling, #12082	1/500-1/1000 in BSA (3 h RT)		
IRF3	rabbit, polyclonal	Santa Cruz, # sc-9082		1/50 (o/n 4°C)	
L7a	rabbit	Cell Signaling, # 2415	1/1000 in BSA (o/n 4°C)	1/200 (o/n 4°C)	
c-Myc	mouse, monoclonal	Cell Signaling, # 2276	1/5000 in milk (1 h RT) 1/8000 in milk (o/n 4°C)	1/1000 (1 h RT; o/n 4°C)	
c-Myc	rabbit	Sigma-Aldrich, #C3956	1/1000 in milk (1-2 h RT) 1/2000 in milk (o/n 4°C)	1/500 (1 h RT)	1/200
c-Myc-HRP	rabbit, polyclonal	Sigma-Aldrich, # A5598	1/1000 in milk (o/n 4°C)		
c-Myc-Alexa Fluor-488	mouse, monoclonal	Cell Signaling, #2279		1/100 (1 h RT)	
OASL	rabbit	Abgent, #WA-PA6230	1/1000 in milk (3 h RT) 1/1000 in milk (o/n 4°C)		
RIG-I	rabbit, polyclonal	Cell Signaling, #3743	1/500-1/2000 in BSA (o/n 4°C)		
tubulin	mouse	Sigma-Aldrich, #T6199-200UL	1/2000 in milk (1 h RT)		
V5	mouse	Invitrogen, #R960-25	1/5000 in milk (o/n 4°C)	1/200 (1h RT) 1/500 (o/n 4°C)	1/200-1/250
V5-HRP	mouse	Invitrogen, #R961-25	1/3000 in milk (1 h RT) 1/4000 in milk (o/n 4°C)		
V5-Alexa Fluor-647	mouse	Life Technologies, # 451098		1/500 (1-3 h RT)	

Table 8 Secondary antibodies and their working dilutions used for immunoblotting (IB) and immunofluorescence (IF)

Antibody	Species	Source, Order number	Working dilution **IB** (45-60 min RT)	**IF** (60 min RT)
Anti-mouse IgG + IgM (H+L)-HRP (A4a)	goat, polyclonal	Dianova (115-035-068)	1/5000	
Anti-rabbit IgG (H+L)-HRP (B4c)	goat, polyclonal	Dianova (111-035-045)	1/20,000	
Anti-Mouse IgG (H+L) - Alexa Fluor-488 (A12c)	goat, polyclonal	Invitrogen (A11029)		1/400
Anti-Mouse IgG (H+L) - Alexa Fluor-594 (A13c)	goat, polyclonal	Invitrogen (A11005)		1/200
Anti-mouse IgG (H+L) – Alexa Fluor-647 (A19c)	goat, polyclonal	Invitrogen (A21235)		1/400

Antibody	Species	Source, Order number	Working dilution IB (45-60 min RT)	IF (60 min RT)
Anti-rabbit IgG (H+L) - Alexa Fluor-488 (B12c)	goat, polyclonal	Invitrogen (A11008)		1/400
Anti-rabbit IgG (H+L) - Alexa Fluor-594 (B13c)	goat, polyclonal	Invitrogen (A11037)		1/500

2.1.6 Plasmids

The following plasmids and expression constructs were used in this study. Plasmids that were cloned in this study are listed in Table 14 (2.2.1).

Table 9 KSHV expression constructs, origin University of Erlangen, Germany; (Sander et al. 2008)

ORF	Library No	Plasmid Name	Vector Backbone
K1	1	pAB39	pcDNA3.1(-)/Myc-HisA
ORF 4	2	pcHHV8-ORF4	pcDNA4/myc-His
ORF 6	3	pcHHV8-ORF6	pcDNA4/myc-His
ORF 7	4	pcHHV8-ORF7	pcDNA4/myc-His
ORF 8	5	pAB38	pcDNA3.1(-)/Myc-HisA
ORF 9	6	pcHHV8-ORF9	pcDNA4/myc-His
ORF 10	7	pcHHV8-ORF10	pcDNA4/myc-His
ORF 11	8	pcHHV8-ORF11	pcDNA4/myc-His
K2	9	pcvIL6-Myc-His	pcDNA3.1(-)/Myc-HisA
ORF 2	10	pcDNA4-ORF2	pcDNA4/myc-His
K3	11	pcorfK3	pcDNA4/myc-His
ORF 70	12	pcHHV8-ORF70	pcDNA4/myc-His
K4	13	pcDNA4-orfK4	pcDNA4/myc-His
K4.1	14	pcDNA4-orfK4.1	pcDNA4/myc-His
K4.2	15	pcDNA4-orfK4.2	pcDNA4/myc-His
K5	16	pcorfK5	pcDNA4/myc-His
K6	17	pcDNA4-orfK6	pcDNA4/myc-His
K7	18	pcDNA4-orfK7	pcDNA4/myc-His
ORF 16	19	pcDNA4-orf16	pcDNA4/myc-His
ORF 17	20	pcHHV8-ORF17	pcDNA4/myc-His
ORF 18	21	pcorf18	pcDNA4/myc-His
ORF 19	22	pcHHV8-ORF19	pcDNA4/myc-His
ORF 20	23	pcorf20	pcDNA4/myc-His
ORF 21	24	pcDNA4-orf21	pcDNA4/myc-His
ORF 22	25	pAB40	pcDNA3.1(-)/Myc-HisA
ORF 23	26	pcorf23	pcDNA4/myc-His
ORF 24	27	pcDNA4-orf024	pcDNA4/myc-His
ORF 25	28	pcHHV8-ORF25	pcDNA4/myc-His
ORF 26	29	pcHHV8-ORF26	pcDNA4/myc-His
ORF 27	30	pcorf027-MET2	pcDNA4/myc-His
ORF 28	31	pcDNA4-orf28-Myc	pcDNA4/myc-His
ORF 29	32	pcDNA4-ORF29	pcDNA4/myc-His
ORF 30	33	pcDNA4-orf30	pcDNA4/myc-His
ORF 31	34	pcDNA4-orf31	pcDNA4/myc-His
ORF 32	35	pcDNA4-orf32	pcDNA4/myc-His

ORF	Library No	Plasmid Name	Vector Backbone
ORF 33	36	pcDNA4-orf33	pcDNA4/myc-His
ORF 34	37	pcDNA4-orf34	pcDNA4/myc-His
ORF 35	38	pcDNA4-orf35	pcDNA4/myc-His
ORF 36	39	pcDNA4-orf36	pcDNA4/myc-His
ORF 37	40	pcHHV8-ORF37	pcDNA4/myc-His
ORF 38	41	pcHHV8-ORF38	pcDNA4/myc-His
ORF 39	42	pAB41	pcDNA3.1(-)/Myc-HisA
ORF 40/41	43	pcDNA4-ORF40/41_genomic	pcDNA4/myc-His
ORF 42	44	pcorf42	pcDNA4/myc-His
ORF 43	45	pcorf43	pcDNA4/myc-His
ORF 44	46	pcorf44	pcDNA4/myc-His
ORF 45	47	pcorf45	pcDNA4/myc-His
ORF 46	48	pcorf46	pcDNA4/myc-His
ORF 47	49	pcorf47	pcDNA4/myc-His
ORF 48	50	pcorf48	pcDNA4/myc-His
ORF 49	51	pcorf49	pcDNA4/myc-His
ORF 50	52	pAB45	pcDNA3.1(-)/Myc-HisA
K8	53	pcDNA4-K8_genomic	pcDNA4/myc-His
K8.1 beta	54	pcorfK8.1beta	pcDNA4/myc-His
ORF 52	55	pcorf52	pcDNA4/myc-His
ORF 53	56	pcorf53	pcDNA4/myc-His
ORF 54	57	pcorf54	pcDNA4/myc-His
ORF 55	58	pcDNA4-orf55	pcDNA4/myc-His
ORF 56	59	pcDNA4-orf56	pcDNA4/myc-His
ORF 57	60	pcDNA4-orf57_genomic	pcDNA4/myc-His
K9	61	pcHHV8-ORFK9	pcDNA4/myc-His
K10	62	pcK10_genomic	pcDNA4/myc-His
K10.5	63	pAB46	pcDNA3.1(-)/Myc-HisA
K11	64	pcDNA4-K11-cDNA	pcDNA4/myc-His
ORF 58	65	pcorf58	pcDNA4/myc-His
ORF 59	66	pcHHV8-ORF59	pcDNA4/myc-His
ORF 60	67	pcHHV8-ORF60	pcDNA4/myc-His
ORF 61	68	pcHHV8-ORF61	pcDNA4/myc-His
ORF 62	69	pcHHV8-ORF62	pcDNA4/myc-His
ORF 63	70	pcHHV8-ORF63	pcDNA4/myc-His
ORF 64	71	pcHHV8-ORF64	pcDNA4/myc-His
ORF 65	72	pcHHV8-ORF65	pcDNA4/myc-His
ORF 66	73	pcHHV8-ORF66	pcDNA4/myc-His
ORF 67	74	pcHHV8-ORF67	pcDNA4/myc-His
ORF 67.5	75	pcHHV8-ORF67.5	pcDNA4/myc-His
ORF 68	76	pcHHV8-ORF68	pcDNA4/myc-His
ORF 69	77	pcorf69	pcDNA4/myc-His
K12	78	pcHHV8-ORFK12	pcDNA4/myc-His
ORF 71/K13	79	pcDNA4-orfK13	pcDNA4/myc-His
ORF 72	80	pcHHV8-ORF72	pcDNA4/myc-His
ORF 73	81	pcDNA3-LANA (Schulz)	pcDNA3
K14	82	pAB73	pcDNA3.1(-)/Myc-HisA

ORF	Library No	Plasmid Name	Vector Backbone
ORF 74	83	pcHHV8-ORF74	pcDNA4/myc-His
ORF 75	84	pcHHV8-ORF75	pcDNA4/myc-His
K15	85	pcDNA4-ORFK15-3AG	pcDNA4/myc-His

Table 10 Vector and reporter plasmids

Construct (internal code)	Promoter and Insert	Backbone	Origin
pcDNA3.1(+) (V20)	CMV promoter, empty vector	pcDNA3.1(+)	Invitrogen
pcDNA4 myc/His A (V21)	CMV promoter, empty vector	pcDNA4	Invitrogen
pVV21 (V53)	IFNα4-Firefly luciferase (murine IFNα4 promoter)	pGL3basic	Thomas Michiels, UCL Belgium
pGL3b-IFNbeta-Luc s (V49)	IFNβ-Firefly luciferase (murine IFNβ promoter)	pGL3basic	Stefan Lienenklaus, HZI
pRL-TK (V48)	TK-Renilla luciferase (thymidine kinase promoter)	pRL	Promega

Table 11 Expression constructs

Construct (internal code)	Backbone	Insert	Origin
pcDNA4 myc/His LacZ (V25)	pcDNA4	lacZ-myc/his	Invitrogen
pcDNA3.1(-) Cal NS1 (L153)	pcDNA3.1(-)	2009 (pH1N1 influenza) NS1	Kendra Bussey, Brinkmann group
M76-V5	pcDNA3.1/V5-His	MCMV M76-V5	Ann Hill, Oregon Health and Science University
OASL-a-V5 (L202)	pcDNA3.1	hOASL-a-His/V5	Rune Hartmann, Aarhus University
OASL-aΔUbi-V5 (L203)	pcDNA3.1	hOASL-aΔUbi-His/V5	Rune Hartmann, Aarhus University
OAS1-V5 (L204)	pcDNA3.1	hOAS1-His/V5	Rune Hartmann, Aarhus University
myc-OASL-a (L205)	pRK5-myc	myc-hOASL-a	Erguang Li, Nanjing University
myc-OASL-b (L206)	pRK5-myc	myc-hOASL-b	Erguang Li, Nanjing University
myc-OASL-d 8L207)	pRK5-myc	myc-hOASL-d	Erguang Li, Nanjing University
pCAGGS FLAG-RIG-I (L257)	pCAGGS	FLAG-hRIG-I	Andreas Pichlmair, Max Plack of Biochemistry
Flag-RIG-I K172R (L346)	pCAGGS	Flag-hRIG-I, with K172R mutation	Christine Standfuß-Gabisch, Kendra Bussey, Brinkmann group
Flag-RIG-I T55I (L344)	pCAGGS	Flag-hRIG-I, with T55I mutation	Christine Standfuß-Gabisch, Kendra Bussey, Brinkmann group
pCAGGS FLAG-RIG-I-N (L258)	pCAGGS	FLAG-hRIG-I-N terminal domain	Andreas Pichlmair, Max Plack of Biochemistry

2.2 Methods

2.2.1 Cloning of Constructs

The basic polymerase chain reaction (PCR) used for cloning in this study is summarised in Table 12 and Table 13, with Table 12 showing the PCR ingredients and Table 13 showing the general thermocycler conditions. Briefly, PCR was performed with five cycles of DNA denaturation at 95°C, annealing of the primers at 5°C below the calculated primer binding temperature and DNA amplification at 72°C, followed by 25 cycles (construct L278), 30 cycles (construct L354), or 35 cycles (construct

L330) of denaturation at 95°C, annealing at the calculated primer binding temperature and extension at 72°C. All constructs generated in this study are listed in Table 14. DNA was amplified from indicated templates and with the indicated primer pairs (Table 14 and Table 15). Primers designed in this study were synthesized by Eurofins MWG Operon.

The ISG56-Luc reporter was generated by restriction and ligation into the vector pGL3 basic.

Table 12 PCR ingredients for DNA cloning in this study

Ingredient	Volume/Amount
DNA template	50-200 ng
Forward Primer (10 µM)	1 µl
Reverse Primer (10 µM)	1 µl
dNTPs (2,5 mM each)	4 µl
Pfu Ultra Polymerase	0.5 µl
Pfu Ultra Buffer (10x)	5 µl
ddH_20	Add up to 50 µl

Table 13 Thermocycler conditions for DNA cloning in this study

Step	Temperature [°C]	Time [s]	
1 - Initialisation	95	120	
2 - Denaturation	95	30	repeat step 2 - 4 5x
3 - Annealing	Primer specific temperature minus 5°C	30	
4 - Extension	72	60/kb	
5 - Denaturation	95	30	repeat step 5 - 7 25x, 30x, or 35x
6 - Annealing	Primer specific temperature	30	
7 - Extension	72	60/kb	
8 - Extension	72	600	
9 - Stop	4	pause	

Table 14 Constructs generated in this study

Construct (code)	Destination vector	Template	Primers	Restriction sites
ORF20-V5 (L278)	pcDNA3.1(+)	KSHV library (pcorf20-HHV8 C382)	667 & 668	*HindIII* / *EcoRI*
ORF20 B-myc/His (L354)	pcDNA4A	KSHV library (pcorf20-HHV8 C382)	845 & 846	*HindIII* / *PmeI*
OASL-a-myc (L330)	pcDNA3.1(+)	hOASLa pRK5-myc (L205) (Guo et al. 2012)	730 & 731	*NheI* / *HindIII*
ISG56-Luc (V90)	pGL3basic	pNiFTy 2-56k-SEAP (V57)	-	*XhoI* / *HindIII*

Table 15 PCR primers used for DNA cloning

No	Name	Sequence (5'→3')
667	HindIIIORF20for	CcggcttgttcaggtccaGGCGGGTCCGGGgtaagcctatccctaaccctctcctcggtctcgattctacgtagGAATTC
668	ORF20V5EcoRIrev	CCATGAATTCctacgtagaatcgagaccgaggagagggttagggataggcttaccCCCGGACCCGCCtggacctgaacaagccgG
845	HindIIIshort ORF20for	GCATAAGCTTGCCACCatggtacgtccaaccgagg
846	HisPmeIRev	gcgggtttaaactcaatggtg

730	NheIOASLfo	GCATGCTAGCGCCACCatggcactgatgcaggaac
731	OASLmycHindIIIrv	CCATAAGCTTctacaggtcctcctcggagatcagcttctgctcttcgaagggccctctagaactggctggaaacagagc

After PCR, 6x Orange DNA loading dye (Fermentas) was added to the PCR product and an agarose gel matrix (1% agarose in TAE) was used to separate the amplified DNA by size. The intercalating agent ethidium bromide (EtBr) was used to visualize the PCR products under ultraviolet (UV) light. PCR products were cut out of the gel, transferred to 1.5 ml tubes, and purified using the QIAquick Gel extraction Kit (Qiagen).

Restriction, Ligation and Transformation

The PCR product and the destination vector backbone were digested at 37°C for 20–30 min as described in Table 16 using the restriction sites shown in Table 14 and the corresponding enzymes. Restriction digest of the vector backbone was terminated by addition of 6x Orange DNA loading dye. An agarose gel matrix was used to separate linearized vector and the QIAquick Gel extraction Kit was used to purify the vector (as described earlier). Digested PCR product was purified using the NucleoSpin Gel and PCR Clean-up kit (Machery-Nagel) and was eluted in 50 µl H_20.

Table 16 Composition of restriction digest for PCR products and vectors

Component	Digestion of PCR Product	Digestion of Destination Vector
PCR product or vector	25 µl eluate from gel extraction	2 µg
Fast Digest Buffer (10x)	3 µl	2 µl
Fast Digest Enzyme 1	1 µl	1 µl
Fast Digest Enzyme 2	1 µl	1 µl
Alkaline Phosphatase	-	1 µl
Final volume	Add up to 30 µl with H_20	Add up to 20 µl with H_20

6.5 µl digested PCR product were ligated into 1 µl digested destination vector by combination with 2 µl T4 Ligase Buffer and 0.5 µl T4 DNA Ligase from the Rapid DNA Ligation Kit (Fermentas). Components were incubated for 20 min at RT and were added to 50 µl competent *E.coli* (DH10B) cells on ice for transformation. Cells were incubated for 1h on ice and were subsequently heat shocked at 42°C for 30 sec followed by a 2 min incubation on ice. 150 µl SOC medium was added to the cells. Cells were plated out on LB-Ampicillin plates and incubated overnight at 37°C. About 8 to 14 colonies were picked and resuspended in 10 µl H_2O for colony PCR. For overnight cultures, 4 ml of LB-Amp were inoculated with a colony.

Colony PCR and controls

Colony PCR was performed with the ingredients shown in Table 17, the primers listed in Table 18 and with the Colony PCR thermocycler conditions shown in Table 19. Clones that showed the expected fragment sizes after colony PCR were chosen for plasmid preparation of a 4 ml overnight culture using the NucleoSpin Plasmid Kit (Machery-Nagel).

Table 17 Colony PCR ingredients

Ingredient	Volume
PCR Master Mix (2x)	5 µl
Forward Primer (10 µM)	0,2 µl
Reverse Primer (10 µM)	0,2 µl
10 µl colony suspension in H_2O	2 µl
ddH_20	To a final volume of 10 µl

Table 18 Primers for colony PCR and sequencing

No	Name	Sequence (5'→3')	Generated plasmid
598	T7 for	TAATACgACTCACTATaggg	L278, L330, L354
599	BGH rev	TAGAAggCACAgTCgAgg	L278, L330, L354
269	RVprim3 For	C TAGCAAAATA GGCTGTCCC	V90
270	RVprim4 Rev	GACGATAGTCATGCCCCGCG	V90

Table 19 Thermocycler conditions for colony PCR

Step	Temperature [°C]	Time	
1 - Initialisation	95	5min	
2 - Denaturation	95	30	repeat 40x
3 - Annealing	53	30	
4 - Extension	72	60/kb	
8 - Extension	72	600	
9 - Stop	4	pause	

Protein expression from the cloned constructs was tested by transfection of 293T cells (2.2.4) and subsequent immunoblotting (2.2.6) for ORF20-V5, ORF20 B-myc, and OASL-myc. ISG56-Luc expression was tested in a luciferase reporter assay in HeLa S3 cells upon NDV infection (2.2.9.1). All inserts of the generated plasmids were completely sequenced by Eurofins Genomics using the primers listed in Table 18.

2.2.2 Cell lines and Cell Culture

Cells (Table 20) were cultured with the appropriate medium (Table 21) in 10 cm dishes at 37°C in a humid atmosphere with 7.5% carbon dioxide. Cells were passaged 2–3 times per week. For that, the medium was aspirated, cells were washed with 1x PBS and detached with trypsin-EDTA treatment for 4–5 min at RT. Trypsin was inactivated by addition of the four-fold volume medium containing FCS. The appropriate number of cells was diluted in a new dish with fresh medium.

Stable cell lines were generated by transfection of linearized vector and selection with antibiotics as described in 2.2.3.

Table 20 Cell lines

Cell line	Description	Source
Vero	African green monkey (*Cercopithecus aethiops*) epithelial kidney cell line with hypodiploid chromosome count	ATCC (CCL-81)
NIH3T3	NIH Swiss mouse embryo fibroblasts	ATCC (CRL-1658)

HeLa S3	Human epithelial adenocarcinoma cell line, clonal derivate of the parent HeLa line (see ATCC CCL-2)	ATCC (CCL-2.2)
HEK293T (VIMM)	human embryonic kidney cell line transformed with the SV40 large T antigen and adenovirus 5´ DNA fragments	ATCC (CRL-3216)
HEK293T (VH)	As above	Veit Hornung
HEK293T VIMM pcDNA	HEK293T VIMM cells stably expressing empty vector pcDNA3.1; neomycin resistant	This study
HEK293T VIMM OASL-a-V5	HEK293T VIMM cells stably expressing OASL-a-V5; neomycin resistant	This study
HEK293T VH pcDNA	HEK293T VH cells stably expressing empty vector pcDNA3.1; neomycin resistant	This study
HEK293T VH OASL-a-V5	HEK293T VH cells stably expressing OASL-a-V5; neomycin resistant	This study

Table 21 Cell culture media

Cell line	Cell culture media
HEK293T, Vero	DMEM high glucose 10% FCS 2 mM glutamine 1% pen/strep
NIH3T3, HeLa S3	DMEM high glucose 10% FCS 2 mM glutamine 1% pen/strep 1% non-essential amino acids 1 mM Na-pyruvate
SILAC heavy medium	DMEM medium for SILAC 10% dialyzed FBS 2 mM glutamine 1% pen/strep 0.1385 mM L-Arginine-HCl, 13C6 0.22 mM L-Lysine-2HCl, 13C6, 15N2
SILAC light medium	DMEM medium for SILAC 10% dialyzed FBS 2 mM glutamine 1% pen/strep 0.1385 mM L-Arginine-HCl 0.22 mM L-Lysine-2HCl
Freezing medium	45% DMEM high glucose 45% FCS 10% DMSO

2.2.3 Generation of stable cell lines

Empty vector pcDNA3.1(+) and OASL-a-V5 expression plasmid pcDNA3.1(+) OASL-a-V5 (L202) were linearized by *Bgl*II enzyme digestion, which cuts the vector backbone upstream of the CMV promoter. The linearized vectors were purified using the NucleoSpin Gel and PCR Clean-up Kit (Machery Nagel). For transfection, 600,000 HEK293T (VH) or HEK293T (VIMM) cells were seeded in a 6 well plate and grown to a confluency of about 60%. Cells were transfected with 2.5 µg DNA and 10 µl Lipofectamine 2000 (LF) transfection reagent per well. To transfect three wells with one construct, a master mix was prepared. The appropriate concentrations of LF or linearized vector were diluted in Opti-MEM and incubated for 5 min. The diluted LF was added to the diluted vector, mixed, and incubated for 10 min. 300 µl of each transfection-mix was added dropwise to the cells of one well. 24 h later cells were trypsinised and seeded into 10 cm dishes.

48 h after transfection cells were selected for stable integration of the plasmid by G418 (neomycin) treatment. Untransfected cells were treated in parallel as a negative control. The HEK293T cells were cultured in medium containing 500 ng/ml G418 for 13 days, whereby the cells were fed with fresh selective medium 3x per week. Cell lines were frozen down in freezing medium (Table 21) and stored in liquid nitrogen. Expression of the constructs was tested by immunoblotting (2.2.6) and immunofluorescence (2.2.8).

2.2.4 Transfection

For analysis of transient protein expression, HeLa S3 cells or HEK293T cells were transfected with expression constructs using either Lipofectamine 2000 (LF) or Fugene HD transfection reagents. HeLa S3 cells or HEK293T cells were seeded with the indicated cell number in a 6 well plate in 2.5 ml medium per well or in a 24 well plate with 0.5 ml medium per well (Table 22). One day after seeding, transfection was performed (Table 22). For LF transfections, DNA (c= 100 ng/µl) and LF were each diluted in Opti-MEM medium and incubated for 5 min at RT. The diluted LF was added to the diluted DNA, mixed, incubated for 5 min at RT and added dropwise to the cells. Cells were lysed 24 h or 48 h after transfection. For transfections with Fugene HD, DNA (c= 100 ng/µl) was diluted in Opti-MEM and Fugene HD was directly added, mixed, and incubated for 5 min at RT. The DNA-transfection mix was added under the surface of the medium to the cells. Cells were lysed 24 h after transfection.

Table 22 Transfection setup per well

Cells	Size	Cell number	Transfection reagent	Description
HeLa S3/ 293T	6 well plate	600,000/well	Lipofectamine 2000	10 µl LF in 150 µl volume, 5 min incubation 4 µg DNA in 150 µl volume, 5 min incubation combine mixtures, 5 min incubation add 300 µl DNA-LF mix/well
HeLaS3	24 well plate	100,000/well	Lipofectamine 2000	1 µl LF in 25 µl volume, 5 min incubation 0.5 µg DNA in 25 µl volume, 5 min incubation combine mixtures, 5 min incubation add 50 µl DNA-LF mix/well
293T	24 well plate	200,000/well	Fugene HD	5.5 µg DNA in 26 µl total volume + 1.7 µl Fugene HD, 5 min incubation add 25 µl/well

2.2.4.1 Preparation of cell lysates

HeLa S3 cells or HEK293T cells were lysed with IP Lysis Buffer or with RIPA-100 buffer (Table 5) for subsequent immunoblotting (IB) or immunoprecipitation (IP) experiments.

Medium was aspirated. HeLa S3 cells were carefully washed with cold PBS. The appropriate amount of lysis buffer per well was added to Hela S3 cells or 293T cells: 80 µl in a 24 well plate, 200 µl in a 12 well plate, or 250 µl in a 6 well plate. Cells were incubated for 20–60 min on ice on a rocking platform to allow complete lysis of the cells. Lysates were transferred to 1.5 ml tubes and centrifuged at 20,900xg at 4°C for 10–15 min. Supernatants were transferred to new 1.5 ml tubes and were either stored at -20°C or were directly used for IB or IP.

Cell lysates for analysis of nuclear proteins

To analyse expression of nuclear and nucleolar proteins by IB, cells were lysed 24 h after transfection with 1x SDS loading buffer. For that, 4x SDS loading buffer was diluted with ultrapure H_2O to give a 1x solution. Medium of the cells was aspirated completely and the appropriate amount of 1x SDS loading buffer was added per well. To one well of a 6 well plate, 300 µl were added. The plate was incubated 10 min on ice and the lysates were transferred to 1.5 ml tubes. The tubes were rattled over a metal rack to shear the DNA. DNA and debris were pelleted by centrifugation at 20,900xg at 4°C for 60 min. A pipette tip was used to extract the sticky DNA pellet out of the tube. Lysates were stored at -20°C or were used immediately for IB.

2.2.5 Nuclear and cytosolic fractionation

The Nuclear/Cytosol Fractionation Kit (N/C kit) (Biovision) was used to lyse and fractionate cells. HeLa S3 cells were seeded in a 6 well plate the day before transfection and were subsequently transfected with Lipofectamine 2000 as described (2.2.4). 24 h after transfection, cells were trypsinised and counted. 1-2x10^6 cells were pelleted by centrifugation at 5.000xg for 5 min. All further steps were strictly performed on ice or at 4°C, and precooled buffers and materials were used. The pelleted cells were washed with 1 ml PBS, transferred to a new 1.5 ml tube and pelleted by centrifugation at 5.000xg for 3 min. The supernatant was removed completely. Cells were resuspended in 200 µl CEA-B buffer (N/C kit) supplemented with DTT (N/C kit) and protease inhibitors and incubated for 15 min. 11 µl Cytosol Extraction Buffer-B (N/C kit) was added and sample was mixed by pipetting. After an incubation for 60 sec, the sample was mixed again by pipetting and fractionated by centrifugation at maximum speed for 5 min. The supernatant containing the cytosolic fraction was transferred to a fresh tube. The pellet was washed two times with 200 µl PBS and centrifuged at maximum speed for 5 min to remove cytosolic remnants. The pellet was lysed in 100 µl Nuclear extraction buffer (N/C kit) supplemented with DTT (N/C kit) and protease inhibitors by vortexing on the highest setting for 15 sec. Sample was incubated for a total of 40 min, and vortexing was repeated every 10 min. The insoluble debris was pelleted by centrifugation at maximum speed for 10 min and the supernatant containing the nuclear fraction was immediately transferred to a fresh 1.5 ml tube. In parallel, a control sample with whole cell lysate was prepared by lysing the cells in IP Lysis Buffer with protease inhibitors as described in 2.2.4.1.

Protein concentration of all samples was determined in replicates by colorimetric protein assay using the BC Assay: Protein Assay Kit (Interchim) according to the protocol. Samples were diluted with H_2O to equal protein concentrations of 0.5 µg/µl and were loaded onto a 10% SDS gel. Electrophoresis and immunoblotting were carried out as described in the following section (2.2.6).

2.2.6 Gel electrophoresis and Immunoblotting

Protein expression and protein sizes were analysed by gel electrophoresis followed by immunoblotting. Precooled solutions were used. Working steps were performed on ice.

2.2.6.1 Sodium dodecyl sulphate polyacrylamide gel electrophoresis (SDS-PAGE)

Cell lysates were supplemented with SDS loading buffer (4x) to a final concentration of 1x. Samples were boiled at 95°C for 5 min to ensure denaturation of proteins. 20–30 µl of sample were loaded onto

a self-poured SDS gel and proteins were separated at 20 mA for about 90 min. 10% and 12% polyacrylamide gels were used in this study, depending on the size of the proteins to be detected.

2.2.6.2 Bis-Tris gel electrophoresis

Bis-Tris gradient gels were used for IB with antibodies against specific endogenous proteins or for sequential antibody staining on the same membrane using more than two different primary antibodies. The neutral pH environment of Bis-Tris gels allows conservation of protein integrity in the sample and reduced protein modifications. The gradient of the gels ensured optimal protein separation. Sample buffer (SB) was prepared by mixing Bolt LDS Sample buffer (4x) and Bolt Reducing Agent (10x) (both Thermo Scientific) according to the manufacturer's protocol. Lysate samples were combined with SB in a 2:1 ratio (e.g. 20 µl sample and 10 µl SB) and were heated at 70°C for 10 min to denature the proteins. 30 µl sample-SB mix was loaded per lane to a 12 well NuPAGE 4-12% Bis-Tris Protein Gel (Thermo Scientific). The gel was run at 130 V for about 60 min with MES SDS Running buffer (Thermo Scientific) to optimise separation of small and medium sized proteins.

2.2.6.3 Immunoblotting (IB)

After separation by gel electrophoreses, proteins were transferred to a nitrocellulose membrane with a pore size of 0.45 µm using a tank blotting system filled with precooled (4°C) Blotting Buffer (Table 5). Blotting of SDS gels was performed at constant current of 350 mA for 60 or 75 min, Bis-Tris gels with NuPAGE Transfer Buffer (Thermo Scientific) at 90 V for 120 min.

Membranes were blocked with 5% milk or 5% BSA in TBS-T overnight at 4°C or 60 min at RT. Membranes were subsequently incubated in primary antibody (Table 7) diluted in 5% milk or 5% BSA in TBS-T for 60–120 min at RT or overnight at 4°C. Membranes were washed 3x with TBS-T for 5–10 min at RT, followed by 45–60 min incubation with secondary antibodies coupled to horseradish peroxidase (HRP) diluted in 5% milk in TBS-T (Table 8). Membranes were washed as described before and incubated 5–10 min in HRP-activated chemiluminescent substrate. As substrate Roche Lumi-Light Western Blotting Substrate (Lumilight) or Thermo Scientific SuperSignal West Femto Maximum Sensitivity Substrate (Femto) for more sensitive applications was used. Antibody binding was visualised using high performance X-ray films.

To detect additional proteins on the same membrane, the membrane was washed as described before and incubated in 2 ml Restore PLUS Western Blot Stripping Buffer for 15–30 min at RT. The membrane was washed and blocked in 5% milk or 5% BSA in TBS-T overnight at 4°C or for 60 min at RT. The membrane was than treated with a primary and secondary antibody, washed and developed as described before.

2.2.7 Immunoprecipitation and Co-Immunoprecipitation

For immunoprecipitation (IP) and co-immunoprecipitation (Co-IP), 600,000 HeLa S3 or 800,000 293T cells were seeded in 2.5 ml medium per well in a 6 well plate. The day after seeding, cells were transfected with Lipofectamine 2000 as described in 2.2.4 with the following modifications for Co-IP: HeLa S3 cells were transfected with two constructs per sample in a 2:1 ratio using 2.6 µg and 1.3 µg

DNA, respectively. 293T cells were transfected in a 1:1:1 ratio with three different constructs per sample using 1.33 µg of each construct for transfection.
HeLa S3 cells were lysed 24 h after transfection, while 293T cells were lysed 36 h after transfection. For lysis, medium was aspirated and cells were washed with cold PBS. All following working steps were performed on ice and with precooled solutions. 250 µl IP Lysis Buffer of RIPA-100 buffer supplemented with protease inhibitors were added per well. Cells were scraped, transferred to a 1.5 ml tube, and lysed in an end-over-end shaker for 60 min. The lysate was cleared by centrifugation at 20,900xg for 10 min. The supernatant was transferred to a new 1.5 ml tube. 45 µl of the lysate was combined with 15 µl SDS loading buffer (4x) as input control. 300 µl IP Lysis buffer or RIPA-100 buffer was added to the remaining lysate to adjust the volume to 500 µl.

IP and Co-IP with protein A agarose beads

For IP or Co-IP with protein A agarose beads, the lysate was first precleared to diminish unspecific binding of the proteins to the beads during affinity purification. 40 µl of 50% protein A agarose bead slurry was pre-equilibrated in IP lysis buffer or RIPA-100 buffer and afterwards incubated with the lysate for 60 min. Beads were removed by centrifugation at 8.600xg for 2 min and supernatant was transferred to a new 1.5 ml tube. Specific antibodies against the myc-, V5-, or FLAG-epitope tag were added to the precleared lysate, diluted as shown in Table 7, and incubated overnight in an end-over-end shaker at 4°C. 10 µl of 50% protein A agarose bead slurry was pre-equilibrated and diluted to a final volume of 50 µl in IP lysis buffer or RIPA-100, subsequently added to the lysate and incubated for 60 min with shaking at 4°C. To wash the sample, beads were pelleted by centrifugation at 8.600xg for 2 min and 1 ml fresh IP lysis buffer or RIPA-100 buffer was added and mixed by inverting the sample. The washing step was repeated 6 times. After the fifth washing step, the sample was transferred to a new 1.5 ml tube. After the final washing step, the volume was adjusted to 45 µl with IP Lysis buffer or RIPA-100 buffer and 15 µl SDS loading buffer (4x) was added. The sample was subjected to gel electrophoresis and immunoblotting as described in 2.2.6.

IP with protein G magnetic beads

The lysate was supplemented with specific antibodies against the myc-, V5-, or FLAG-epitope tag, diluted as shown in Table 7, and incubated overnight on a shaking platform. 20 µl Protein G Magnetic Beads slurry was pre-equilibrated in a 1.5 ml tube by adding 150 µl IP Lysis Buffer and mild vortexing. The tube was placed in a magnetic stand to collect the beads against the side of the tube. The supernatant was removed. 1 ml IP Lysis Buffer was added to the beads and mixed by mild vortexing. The tube was placed in the magnetic stand, supernatant was discarded and the lysate-antibody mixture was added and incubated for 60 min at RT on a shacking platform. The sample was placed in the magnetic stand, the supernatant containing the unbound proteins was removed and the beads were washed with 500 µl IP Lysis Buffer and gentle mixing. The washing step was repeated three times. The beads were transferred to a fresh tube after the second washing step. The proteins were eluted from the beads by adding 65 µl SDS loading buffer (1x) and heating the sample at 95°C for 10 min. The beads were magnetically separated from the sample and the supernatant was transferred to a fresh tube and analysed by immunoblotting (2.2.6).

2.2.8 Immunofluorescence (IF)

Glass coverslips were acidified and washed before use to allow attachment of the cells. Coverslips were washed shaking in 60% ethanol (100% p.a.) and 40% HCl (100% p.a.) for 20 min, then washed three times with deionised H_2O, dried on filter paper, heat sterilised, and stored under sterile conditions.

HeLa S3 cells were seeded in a 24 well plate equipped with glass coverslips at a density of 70,000 cells in 0.5 ml medium per well. Cells were transfected the next day with LF as described in 2.2.4. Briefly, 0.5 µg DNA and 1 µl LF were each diluted in Opti-MEM to a total volume of 25 µl and incubated for 5 min at RT. The mixtures were combined, mixed, and incubated for 5 min at RT. 50 µl of the complexes were added dropwise to the cells. To transfect multiple constructs per sample, equal DNA amounts of each construct were used: 0.25 µg DNA for each of two constructs and 0.166 µg DNA for each of three constructs. Cells were fixed 24 h after transfection as described in 2.2.8.1.

50,000 NIH3T3, 80,000 Vero, or 200,000 HEK293T cells were seeded in 0.5 ml medium per well in a 24 well plate. The next day, cells were transfected with LF as described above. 24 h after transfection, cells were trypsinised and splitted in a 1:3 or 1:4 ratio and seeded in a 24 well plate equipped with glass coverslips. For 293T cells, coverslips were coated with 100 µg/ml poly-D-lysine for 20 min at RT before plating. The next day, 48 h after transfection, cells were fixed as described in 2.2.8.1.

2.2.8.1 Fixation of cells

Cells were fixed either with PFA or with methanol and PFA, depending on the antibodies used for IF. To fix the cells with PFA, the medium was aspirated and 300 µl 4% PFA in PBS (37°C) were carefully added per well and cells were incubated for 20 min at RT. PFA was aspirated and the cells were washed three times with PBS (4°C). After the last washing step, 1 ml PBS was added per well to prevent the sample from drying out.

To fix the cells with methanol and PFA, medium was aspirated and 500 µl methanol (-20°C) were carefully added to the cells and incubated for 5 min at -20°C. The cells were subsequently treated with 4% PFA and washed with PBS as described above. The fixed samples were either stored at 4°C or were directly subjected to IF labelling. As methanol permeabilises the membranes, methanol and PFA fixed sample preparation was continued with without permeabilization.

2.2.8.2 Antibody labelling and Hoechst staining

PFA fixed samples were permeabilised in 500 µl 0.1% TritonX-100 in PBS for 5 min at RT and were washed three times with PBS. Methanol and PFA fixed samples were directly subjected to blocking, as methanol permeabilises the cells.

Blocking solution, primary antibody solution, and secondary antibody solution were prepared with 1% BSA in PBS. Coverslips were blocked cell-side down in 50 µl blocking solution (10% FCS in PBS) per coverslip on parafilm for 60 min. Coverslips were directly transferred to 50 µl primary antibody solution. Primary antibodies were diluted and incubated as shown in Table 7. To stain with two primary antibodies, one antibody raised in mouse and one antibody raised in rabbit were used in together. After incubation, coverslips were washed three times in PBS and were incubated for 60 min in the dark on parafilm in 50 µl secondary antibody solution containing the fluorochrome-linked mouse or rabbit specific antibodies. For dilutions see Table 8. Coverslips were washed as described before. Hoechst staining

(1/500 of a 1 mg/ml stock solution) of the DNA was either performed in combination with the last antibody incubation step, by adding Hoechst to the antibody solution, or by incubation of the coverslip in 30 µl Hoechst in PBS for 60 min in the dark, after secondary antibody staining. Samples were washed three times, mounted on glass microscope slides with Prolong Gold and were dried overnight at 4°C in the dark.

To detect three proteins in parallel by IF, a third primary antibody conjugated to a fluorochrome was used, ultimately combining Alexa-488, Alexa-594, and Alexa-647 fluorochromes for IF. For that, coverslips were labelled with two different primary and secondary antibodies as described earlier. Subsequently coverslips were again blocked in 10% FCS for 60 min at RT, followed by incubation in 50 µl solution of primary antibody conjugated to a fluorochrome (e.g. V5-Alexa Fluor-647, Table 7) and Hoechst reagent (1/500). Coverslips were washed three times with PBS and mounted on glass microscope slides as described before.

2.2.8.3 Imaging and quantification

Images were acquired with a 60x objective using a Nikon ECLIPSE Ti-E inverted microscope equipped with a PerkinElmer Ultraview spinning disk confocal device and Volocity software (Improvision). Images were processed with Volocity and Photoshop software.

For quantification, each coverslip was viewed along a fictional grid and unbiased images were captured of all ascertained stained cells. Images were analysed and evaluated manually, differentiating localisation and brightness of the fluorescence signals of the labelled proteins, and taking the health of the cell into account.

2.2.8.4 IRF3 localisation

HeLa S3 cells were seeded on coverslips and were left untransfected or transfected the next day with LF as described earlier (2.2.8). 24 h after transfection, samples were infected with Newcastle disease virus (NDV) to induce IRF3 nuclear localisation, or left uninfected. For that, medium was aspirated and cells were carefully washed with PBS. 250 µl Opti-MEM was added to unstimulated samples and 250 µl Opti-MEM with NDV diluted 1/100 was added to stimulated samples. Cells were incubated for 1 h at 37°C. 1 ml fresh medium was added to each sample and cells were incubated for additional 11 h. Unstimulated and NDV infected samples were fixed 36 h after transfection with methanol and PFA as described in 2.2.8.1. Coverslips were blocked with 10% FCS in 1% BSA in PBS for 60 min at RT and were labelled with primary antibodies against the myc epitope tag and endogenous IRF3 diluted in 50 µl 1% BSA in PBS as shown in Table 7. Coverslips were incubated for 60 min in fluorochrome-linked secondary antibody diluted in 1% BSA in PBS as shown in Table 8 and were labelled with 50 µl Hoechst in PBS (1:500 of 1 mg/ml stock solution in PBS) for 5 min. Coverslips were washed three times with 1x PBS after all incubation steps. Coverslips were mounted in Prolong Gold on glass microscope slides and were dried overnight at 4°C. Imaging and quantification was performed as described in 2.2.8.3.

2.2.9 Luciferase-based reporter assays

2.2.9.1 KSHV library screen

100,000 HeLa S3 cells were seeded in a volume of 0.5 ml medium per well in a 24 well plate. The day after seeding, transient transfection was performed using Fugene HD. 2 µg DNA, comprising of 500 ng IFNα4- or IFNβ-Firefly luciferase reporter (Table 10), 50 ng TK-Renilla luciferase reporter (Table 10) and 1450 ng KSHV library plasmid (Table 9) or control plasmid (Table 11 or Table 14), were diluted in Opti-MEM to a total volume of 100 µl. 6 µl Fugene HD were added to the diluted DNA, mixed, and incubated for 5 min at RT. 25 µl transfection mix was added per well. 24 h after transfection, medium was aspirated and cells were washed with 1 ml PBS. For unstimulated conditions, 250 µl Opti-MEM were added per well. NDV was diluted in Opti-MEM to a ratio of 1/100 for IFNα4 reporter assays and 1/500 for IFNβ reporter assays and 250 µl were added per well (=stimulated samples). Cells were incubated for 60 min at 37°C and 500 µl of fresh medium were added to stop the infection. 24 h after infection, cells were lysed in 80 µl 1x Passive Lysis Buffer (Promega) supplemented with protease inhibitors for 20 min at RT on a plate shaker. Samples were further treated and analysed as described in 2.2.9.3.

2.2.9.2 RIG-I mediated IFNβ and ISG56 induction

200,000 HEK293T cells (VIMM and VH) were seeded in a volume of 0,5 ml medium per well in a 24 well plate. The day after seeding, transient transfection was performed using 2 µg DNA and 6 µl Fugene HD per well. For ISG reporter assays, 100 ng ISG56-Firefly luciferase reporter (Table 14), 50 ng TK-Renilla luciferase reporter (Table 10), and 906 ng of two different genes of interest (GOI) plasmids (Table 11 or Table 14) were diluted in Opti-MEM to a total volume of 100 µl. For IFNβ reporter assays, 500 ng IFNβ-Firefly luciferase reporter (Table 10), 50 ng TK-Renilla luciferase reporter (Table 10) and 725 ng of two different GOI plasmids (Table 11 or Table 14) were diluted in Opti-MEM to a total volume of 100 µl. 6 µl Fugene HD were added to the diluted DNA, mixed, and incubated 5 min at RT. 25 µl of transfection mix were added per well. 48 h after transfection, 80 µl of 1x Passive Lysis Buffer (Promega) supplemented with protease inhibitors were added per well. The cells were lysed for 20 min at RT on a plate shaker. Samples were further treated and analysed as described in 2.2.9.3.

2.2.9.3 Dual luciferase reporter measurement and analysis

Samples from 2.2.9.2 were transferred to 1.5 ml tubes and stored on ice. A tube was flicked to mix the sample and 10 µl sample were transferred to a white bottom plate. Firefly and Renilla luciferase activity were measured separately using the Promega 20/20 Glomax luminometer with the ‘Promega Protocols’ ‘DLR’ with Dual Injector protocol. First, Firefly luciferase activity was measured by application of 50 µl Luciferase Reagent II (LARII) to the sample. Subsequently, 50 µl Stop&Glo reagent (S&G) was added to the sample to stop the Firefly luciferase light reaction and measure the Renilla luciferase activity. Light reactions were measured for 2 sec each.

Firefly luciferase expression was controlled by the IFNα4, IFNβ, or ISG56 promoters that were cloned upstream of the Firefly luciferase gene. Renilla luciferase expression, however, was under control of the constitutive thymidine kinase promoter and served as a control for the transfection efficiency and health status of the cells. For analysis of the data, the Firefly luciferase values were divided by the Renilla

values. To determine IFNα4, IFNβ, or ISG56 promoter fold induction upon stimulation, stimulated values were divided by unstimulated values.

2.2.10 Interactome studies and SILAC

Low passage HeLa S3 cells were used for stable isotope labelling with amino acids in cell culture (SILAC). HeLa S3 cells either incorporated 'heavy' 13C6 L-arginine and 13C6 15N2 L-lysine or 'light' L-arginine and L-lysine during 10 days of cell culture into their proteins. At the beginning of incorporation, three wells of a 24 well plate were prepared with 25,000 HeLa S3 in 0.5 ml heavy or light SILAC medium (Table 5) per well. Cells were washed, trypsinised, resuspended and expanded in fresh SILAC medium every second day. 10 days later, heavy or light labelled HeLa S3 cells were seeded into two 15 cm dishes each, plating 7.6–6.9x10^6 cells in 23 ml heavy or light SILAC medium per dish. The next day, light and heavy HeLa S3 cells were transfected with 48.5 µg DNA and 100 µl LF per dish. Transfection mixtures were prepared in polystyrene tubes. 100 µl LF and 48.5 µg DNA were each diluted in a total volume of 2.4 ml in SILAC medium and incubated for 5 min at RT. The diluted DNA was added to the diluted LF, carefully mixed, and incubated for 15 min at RT. The complete transfection mixture was added dropwise to the cells per 15 cm dish. A forward and a crossover experiment were performed in parallel. For the forward experiment, heavy labelled HeLa S3 cells were transfected with myc-tagged ORF20, ORF75, or OASL, while light labelled HeLa S3 cells were transfected with LacZ-myc as a control. In the crossover experiment the constructs were transfected vice versa.

To analyse the interactome of OASL upon stimulation, 12 h after transfection heavy and light labelled HeLa S3 cells of the forward and crossover experiment were infected with NDV. For this, the medium was taken off and the cells were carefully washed once with PBS. NDV was diluted 1/500 in 5 ml SILAC medium, added to the cells, and incubated for 1 h at 37°C. To stop infection, 20 ml heavy or light SILAC medium was added to the plate and incubated for 14 h at 37°C.

Cells were lysed 24 h or 36 h after transfection. Cells were carefully washed three times with cold PBS. The plate was placed on ice and 1 ml IP lysis buffer (Table 5) supplemented with EDTA-free protease inhibitors was added. The cells were detached with a cell scraper and the lysate was transferred to a 2 ml low protein binding (LoBind) tube (Eppendorf). 2 µl Benzonase of a 1:10 working dilution were added to digest DNA and RNA. The lysate was incubated for 60 min at 4°C on a rotating platform and cell debris was pelleted by centrifugation at 20,817xg for 10 min at 4°C. The supernatant was transferred to a new 2 ml LoBind tube. For IP, 75 µl of anti-myc MicroBeads (Miltenyi kit) were added to the lysate and incubated for 60 min at 4°C on a rotating platform. Corresponding heavy and light sample of the forward or crossover experiment were combined and mixed in a new LoBind tube immediately before affinity purification (AP). Combined samples were applied to M Columns (Miltenyi) placed in a µMACS Separator (Miltenyi), whereby the columns were equilibrated with 200 µl IP lysis buffer before AP. On-column beads were washed 4x with 200 µl cold IP lysis buffer and 2x with Miltenyi Wash Buffer 2 (Miltenyi) to remove detergent that would interfere with mass spectrometry (MS). The bound proteins were eluted from the beads stepwise in 10 min intervals by application of 3x 100 µl 100 mM glycine (pH 2.5). The eluate was collected in a 2 ml LoBind tube. Protein precipitation was performed by sequential addition of 70 µl 2.5 M Na-Acetate (pH 5.0), 40 µl Tris-HCl (20 mM, pH 8.2), 1 µl GlycoBlue coprecipitant, and 1600 µl 100% Ethanol (p.a). The samples were mixed by inverting the tubes after each step.

Samples were incubated overnight at 4°C on a rocking platform. The next day, proteins were pelleted by centrifugation at 17.949xg for 60 min at 4°C. The supernatant was carefully removed completely and the protein pellet was airdried at RT. Further sample preparation and MS were conducted by Josef Wissing of the Cellular Proteome Research Group at the HZI.

First, an in-solution digest was performed, converting the proteins to peptides with the endopeptidases Lys-C and trypsin. The protein pellet was resuspended in 20 µl 8 M urea in 0.5 M triethylammonium bicarbonate buffer (TEAB buffer). 20 µl 20 mM Tris-(2-carboxyethyl)-phosphine-hydrochloride (TCEP) and 20 µl TEAB buffer were added to reduce the protein disulphide bonds between the cysteines. The cysteines were blocked and alkylated by addition of 2 µl 200 mM methyl methane thiosulfonate (MMTS). Lys-C was added to a final ratio of 50:1 (protein: protease), incubating the sample more than 2 h at 25°C. H_2O was added until the urea concentration was below 2 M. The proteins were further digested by addition of trypsin with a final ratio of 50:1 and overnight incubation at 37°C. Subsequently, all fluid was evaporated in a SpeedVac (Eppendorf). Peptides were desalted with a RP18 clean up with STAGE-TIP purification using LiChrosorb® RP-18 material (Sigma Aldrich, Merck). RP-18 material was equilibrated by successive washing with elution buffer (60% acetonitrile (ACN) in water supplemented with 0.2% trifluoroacetic acid (TFA)) and washing buffer (3% ACN in water containing 0.2% TFA). First, the peptides were resolubilized in 20 µl washing buffer and adsorbed to the RP18 material. Peptides were washed 4–5 times with washing buffer, and were eluted with 2–3x 20 µl elution buffer. Peptides were dried in a SpeedVac to remove the organic phase and were resolubilized in 12 µl washing buffer.

Liquid chromatography coupled to tandem mass spectrometry (LC-MS/MS) analyses were performed on a Dionex UltiMate 3000 n-RSLC low flow liquid LC system (Thermo Scientific) connected to an LTQ Orbitrap VelosPro mass spectrometer (Thermo Scientific). First, the sample was washed with washing buffer containing 0.1% formic acid (FA) on a C18 pre-column (3 µm, Acclaim, 75 µm x 20 mm, Dionex) at a flow rate of 6 µl/min. The sample was fractionated by liquid chromatography on a C18 analytical column (3 µm, Acclaim PepMap RSLC, 75 µm x 25 cm, Dionex) at 35 µl/min with a linear 180 min gradient of 0-80% ACN in 0.1% FA. The LC system was run with Chromeleon Software (version 6.8, Dionex), embedded in the Xcalibur software (version 2.1, Thermo Scientific). The eluate from the column was electro-sprayed (Pico Tip Emitter Needles, New Objectives) into the mass spectrometer controlled by Xcalibur software run in the data-dependent mode. Peptide fragmentation was performed with the CID mode in the ion trap. Peptide identification of the generated MS/MS raw data was performed with Proteome Discoverer 1.3.0.339 software using a human protein database extracted from SwissProt on a Mascot server (V. 2.4, Matrix Science) using the following search parameters: enzyme, trypsin; maximum missed cleavages, 1; fixed modification, methyl methane thiosulfonate (C); variable modification, oxidation (M), peptide tolerance, 5 ppm; MS/MS tolerance, 0.5 Da, and Arg6 and Lys8 as variable modifications for quantification.

Data analysis was part of this study, using the Proteome Discoverer Software with the following filter parameters: maximum peptide rank to 1, peptide confidence to medium and Masco Score to at least 25. Heavy/light values of each identified protein were transformed into heavy/light $\log_2$ fold change values, to facilitate analysis.

3 Results

3.1 Identification of KSHV ORF20 as a novel type I interferon modulator

3.1.1 KSHV ORF20 negatively modulates the type I IFN response downstream of RIG-I

To establish infection, the human gammaherpesvirus KSHV must circumvent antiviral innate immunity. As the virus has co-evolved with its human host for millions of years, it has evolved sophisticated mechanisms to manipulate its host, but our knowledge of these mechanisms is far from complete. A crucial antiviral response is mediated by the type I IFNs IFNα and IFNβ. Their production is initiated by PRRs upon detection of invading pathogens, which initiate a signalling cascade with multiple proteins and post-transcriptional modifications, and this ultimately results in the transcriptional induction of type I IFNs.

The identification and characterisation of novel KSHV-encoded antagonists of the type I IFN system can lead to the identification of promising targets for antiviral therapeutics. The identification of the mechanism of manipulation, moreover, can reveal novel insights into the mode of action of the innate immune system and its components.

We aimed to identify novel proteins encoded by KSHV with the ability to interfere with type I IFN signalling downstream of RIG-I, a PRR which belongs to the family of RIG-I-like receptors (RLRs). The RNA helicase RIG-I is activated by viral RNA and DNA. Upon ligand binding RIG-I induces a signalling cascade involving the mitochondrial antiviral signalling protein (MAVS), a central node in intracellular RLR transduction pathways, which ultimately leads to the production of type I IFNs.

Newcastle disease virus (NDV) is known to induce a strong IFNβ and IFNα4 response via RIG-I. To identify KSHV-encoded proteins that negatively modulate the type I IFN response, we used cell lines that were transiently transfected with single ORFs of the KSHV library, consisting of 85 ORFs (Sander et al. 2008), or an empty vector control. We infected these cells with NDV and measured the transcriptional induction of IFNβ and IFNα4 in a luciferase-based reporter assay. Beforehand, we analysed the responsiveness of IFNβ- or IFNα4-luciferase reporters in different cell lines to NDV infection. We identified Vero cells and HeLa S3 cells as ideally suited for IFNβ assays, and NIH3T3 cells and HeLa S3 cells for IFNα4 assays (experiments performed by Kendra Bussey, data not shown).

The experimental setup for the KSHV library screen was as follows: We cotransfected Vero, NIH3T3, or HeLa S3 cells with a single KSHV ORF or empty vector control and a reporter plasmid encoding the Firefly luciferase gene under control of either the IFNβ or IFNα4 promoter together with a Renilla luciferase reporter plasmid for normalisation. At 24 h post transfection (p.t.) cells were left unstimulated or were infected with NDV. 21 h later cells were lysed and Firefly and Renilla luciferase production was measured. The Firefly luciferase values were normalised to the corresponding Renilla luciferase values. Subsequently, stimulated values were divided by unstimulated values to illustrate IFNβ or IFNα4 fold induction. Cotransfection of a plasmid coding for the NS1 protein of influenza A virus was used as a positive control for inhibition of IFNβ or IFNα4 induction, as NS1 was described to prevent type I IFN activation by targeting ubiquitin ligase TRIM25-mediated activation of RIG-I (Gack et al. 2009) and activation of the crucial downstream transcription factor interferon regulatory factor 3 (IRF3) (Talon et

al. 2000, Gack et al. 2009). Figure 44 in the Appendix shows the normalised data scaled to the empty vector control. While most KSHV ORFs did not strongly influence the cellular response to NDV, we found several KSHV ORFs that inhibited the IFNα4 and IFNβ promoter induction more than 50% after NDV stimulation compared to the empty vector control.

Based on these results, we chose selected KSHV ORFs (ORF10, ORF11, ORF20, ORF23, ORF36, ORF54, ORF55, K10, ORF64, and ORF75) for further small scale experiments in HeLa S3 cells (Figure 9).

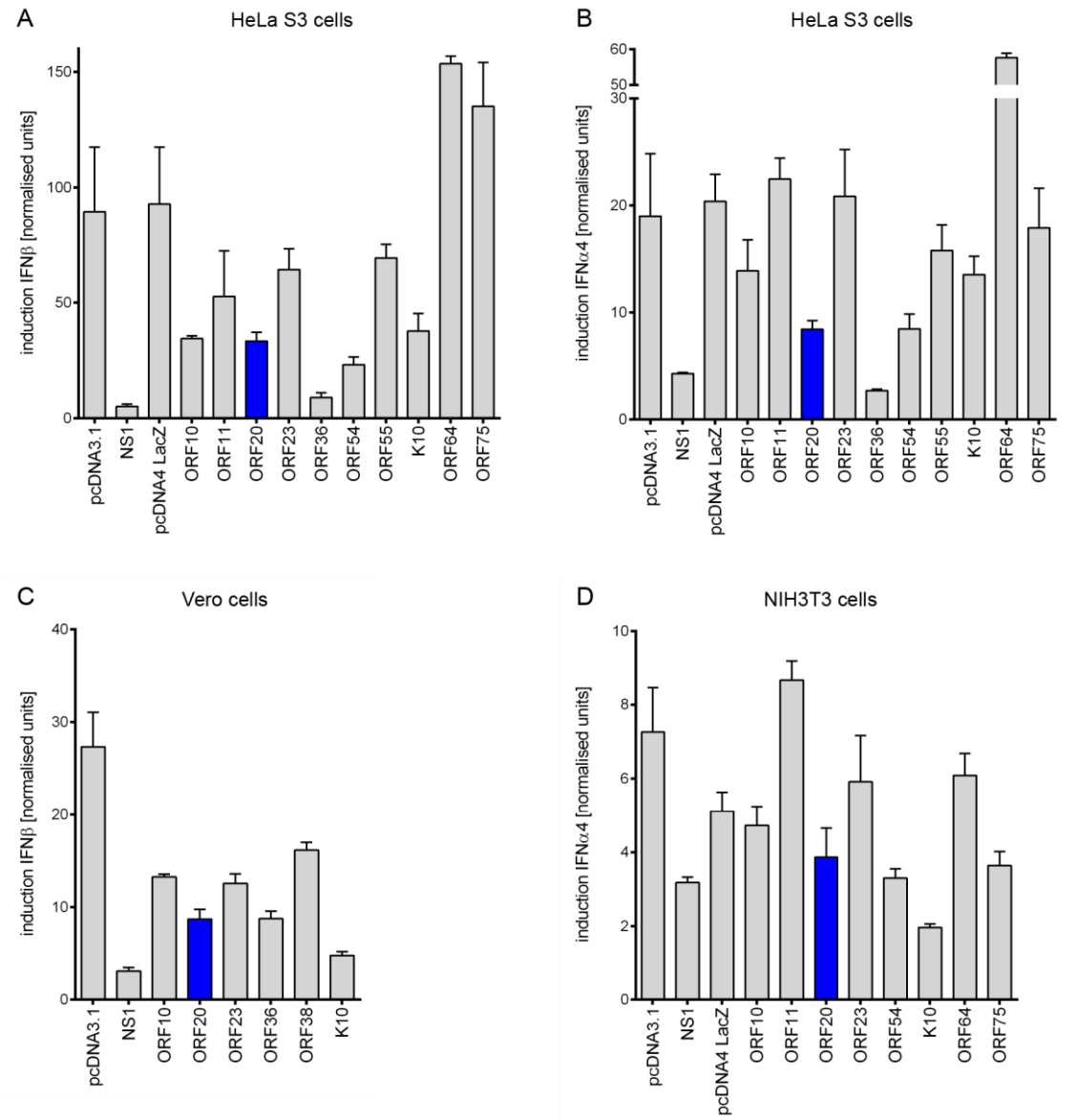

Figure 9 Identification of KSHV ORFs that negatively modulate the RIG-I-induced type I IFN response upon NDV infection. HeLa S3 cells (A and B), Vero cells (C), or NIH3T3 cells (D) were transfected with three constructs: IFNβ-Firefly luciferase (A and C) or IFNα4-Firefly luciferase (B and D), Renilla luciferase, and the indicated vector construct. 24 h p.t. cells were left unstimulated or stimulated with Newcastle disease virus (NDV). 21h later cells were lysed and luciferase activity was measured. Firefly luciferase values were normalised to the corresponding Renilla values. The NS1 protein of influenza A virus was used as a positive control for inhibition of RIG-I signalling. The data shows averages with standard deviation from three independent experiments with the exception of pcDNA4 LacZ, ORF20 and ORF23 (n=2) in D.

In every experiment we included the NS1 protein as a positive control, as described earlier. The β-galactosidase enzyme (LacZ) was used as a negative control, as well as an empty vector control, to which the values of the KSHV ORFs were compared (Figure 9 A and B).

The IFNβ response to NDV in HeLa S3 cells was impaired in the presence of 6 out of 10 analysed KSHV ORFs: ORF10, ORF11, ORF20, ORF36, ORF54, and K10. Of these, KSHV ORF20, ORF36, and ORF54 also downmodulated IFNα4 induction in HeLa S3 cells, while ORF10, ORF11, and K10 had no strong inhibitory effect on the IFNα4 promoter. KSHV ORF23, ORF55, and ORF75 showed comparable values to the vector controls and did not influence the IFNβ or IFNα4 response in HeLa S3 cells, while ORF64 seemed to enhance the response.
We repeated the assay in Vero and NIH3T3 cells for some of the KSHV candidates (Figure 9 C and D). In accordance with the HeLa S3 data, KSHV ORF10, ORF20, ORF36, and K10 reduced IFNβ induction in Vero cells, and KSHV ORF20 and ORF54 inhibited IFNα4 induction in NIH3T3 cells. We did not analyse KSHV ORF11 and ORF54 in Vero cells, and ORF36 in NIH3T3 cells.

We found that KSHV ORF20, ORF36, and ORF54 were able to block the IFNβ and IFNα response to NDV infection in different cell lines. While previous studies have described ORF36 (Hwang et al. 2009) and ORF54 (Madrid & Ganem, 2012) as antagonists of the type I IFN response, ORF20 has not been described as a modulator of the IFNβ and IFNα4 response downstream of RIG-I.

3.1.2 Expression analysis of KSHV ORF20 by IB and IF

As we identified KSHV ORF20 as a novel inhibitor of the type I IFN response, we sought to determine its detailed function. We began our exploration of ORF20 by basic molecular analysis of the protein, as ORF20 is a barely described protein with a scarcely ascribed function. In the NCBI protein database two forms of KSHV ORF20 are listed, a full length 320 amino acid (aa) version (GenBank: AKE33056.1) and a shorter version, which starts with the second methionine in frame of the ORF20 sequence, resulting in a 257 aa protein (GenBank: ABD28871.1). We will refer to the 320 aa version as “ORF20” and to the 257 aa version as “ORF20 B” (1.3.2 Introduction).
We received ORF20 as pcDNA4 ORF20-myc construct as part of the KSHV library (Sander et al. 2008). We cloned pcDNA4 ORF20 B-myc, using pcDNA4 ORF20-myc as a template.

Protein sizes of KSHV ORF20

ORF20 has a calculated protein size of 35,1 kilodaltons (kDa) and ORF20 B has a predicted protein size of 28,4 kDa. To examine the apparent protein sizes of ORF20-myc and ORF20 B-myc, constructs were transiently expressed in HEK293T or HeLa S3 cells, lysed 24 h p.t., and analysed by anti-myc immunoblotting (Figure 10).

We found that ORF20 B-myc expressed a single protein band of about 29 kDa in both cell lines. Interestingly, ORF20-myc showed protein sizes of about 35 kDa and 29 kDa, which seemed to correlate

with the detected protein size of ORF20 B-myc, in HEK293T and HeLa S3 cells. This suggests that the ORF20 construct was expressing both, the full length and the shorter version of KSHV ORF20.

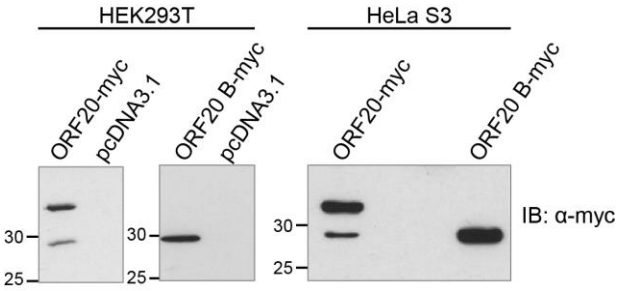

Figure 10 Protein sizes of KSHV ORF20-myc and ORF20 B-myc in HEK293T and HeLa S3 cells. Transient expression of pcDNA4 ORF20-myc and pcDNA4 ORF20 B-myc was analysed by anti-myc immunoblotting. Cells expressing empty vector pcDNA3.1 were used as negative control. Left margin shows molecular mass in kilodaltons (kDa).

Subcellular localisation of KSHV ORF20

Next we analysed the subcellular localisation of KSHV ORF20 by immunofluorescence (IF), as localisation of a protein is closely associated with its function. We transiently transfected human HeLa S3 cells on glass coverslips with ORF20-myc, fixed the cells 24 h p.t. with methanol and 4% paraformaldehyde (PFA), and labelled with antibody against the myc-tag to detect ORF20. Specificity of the antibody was tested in untransfected cells (data not shown). The DNA was stained with Hoechst. Images were obtained by confocal microscopy (Figure 11 A). To rule out that the observed localisation was cell type or species specific, we additionally analysed human HEK293T cells, murine NIH3T3 cells, and African green monkey Vero cells transfected with ORF20-myc. In contrast to the HeLa S3 cells, HEK293T, NIH3T3, and Vero cells were trypsinised and seeded onto coverslips 24 h p.t. and fixed 48 h p.t. (Figure 11 B, C, and D).

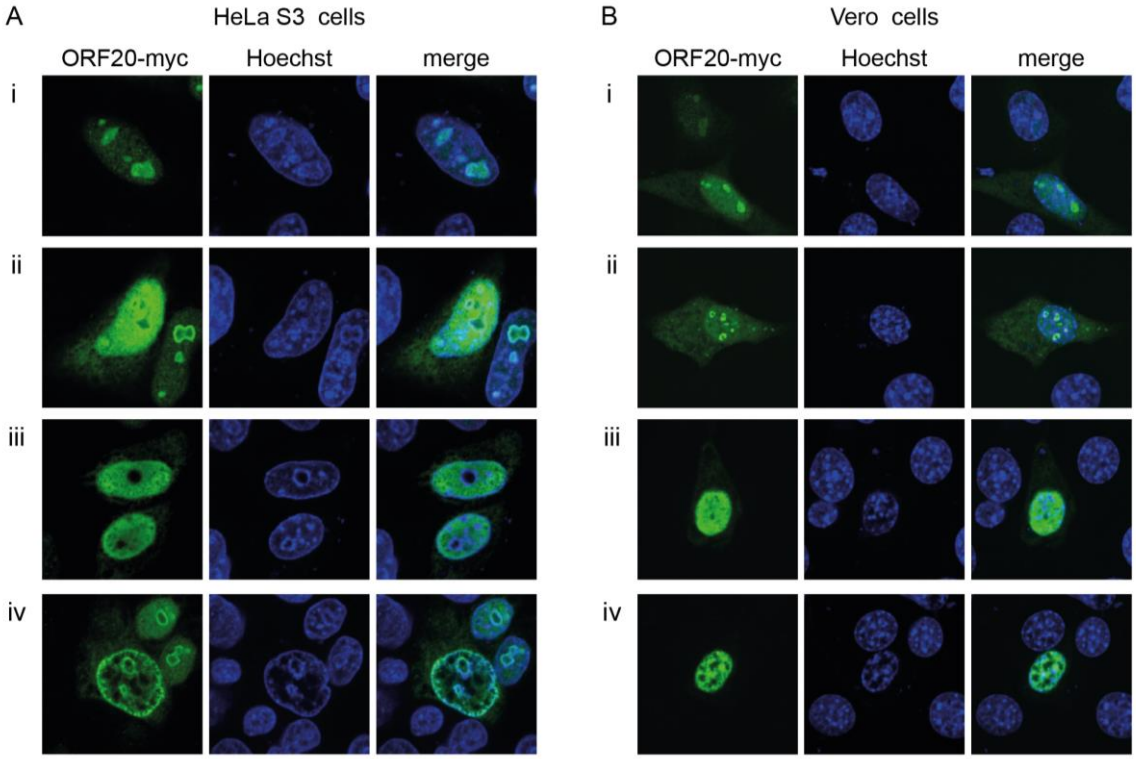

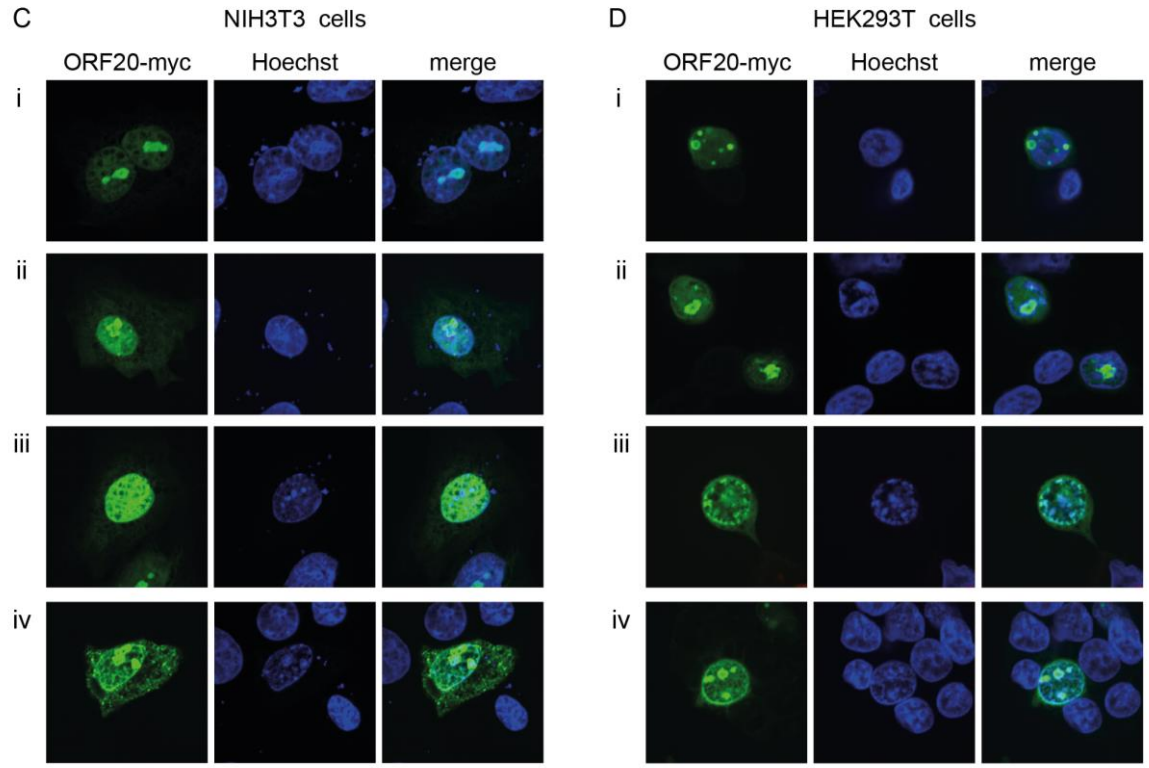

Figure 11 KSHV ORF20-myc is localised in the nucleolus, nucleus, and cytoplasm in different phenotypes. Cells were transfected with ORF20-myc. HeLa S3 cells (A) were fixed 24 h p.t., while HEK293T (B), NIH3T3 (C), and Vero (D) cells were fixed 48 h p.t. with methanol and PFA. Samples were subjected to anti-myc IF. DNA was stained with Hoechst. Images were obtained by confocal microscopy with 60x magnification and are representative of at least 3 independent experiments.
ORF20-myc is localised in the nucleoplasm and the nucleolus (i). ORF20-myc is distinctly expressed at the nucleolar border and in the cytoplasm and nucleoplasm (ii). ORF20-myc is expressed in the nucleoplasm but is omitted from the nucleolus (iii). ORF20-myc is strongly enriched at the nucleolar border and at nuclear border (iv).

We found that the intracellular localisation of KSHV ORF20-myc was similar in all analysed cell lines, irrespective of human, murine, or monkey origin. Namely, ORF20-myc was primarily localised in the nucleolus, but was also present in the nucleus and to some extent in the cytoplasm. This observation was in accordance with published data about the intracellular localisation of full length ORF20-myc in HeLa cells (Sander et al. 2008). Sander and colleagues analysed 85 KSHV ORFs and differentiated crudely between nuclear, cytoplasmic, or both nuclear and cytoplasmic localisation and categorised ORF20 as primarily nuclear. Precisely, the study depicts six ORF20-myc expressing Hela cells, which show the ORF20 protein in the nucleoplasm and distinctly in the nucleolus, while a cytoplasmic localisation was not clearly visible.

We found on closer inspection of our data that localisation of ORF20-myc was more diverse and could be differentiated into four particular localisation phenotypes, further named ORF20-i, ORF20-ii, ORF20-iii, and ORF20-iv (Figure 12). Phenotype ORF20-i showed localisation of ORF20 in the nucleoplasm plus a distinct signal in the whole nucleolus. This localisation phenotype was exclusively detected in cells with a weak or moderate fluorescent signal of ORF20 (Figure 11 i). The most phenotype ORF20-ii, showed distinct ORF20 expression at the nucleolar border. These cells were with or without additional weak expression of ORF20-myc in the nucleoplasm and cytoplasm (Figure 11 ii).

Cells of the third localisation phenotype, ORF20-iii, strongly expressed ORF20 in the nucleoplasm, but showed no nucleolar localisation of ORF20 (Figure 11 iii). In contrast to the other phenotypes, cells showing the ORF20-iv localisation phenotype expressed ORF20 distinctly at the nuclear border but little in the nucleoplasm. These cells additionally showed strong expression of ORF20-myc at the nucleolar border and some showed additional expression of ORF20-myc in the cytoplasm (Figure 11 iv).
The four localisation phenotypes of ORF20 are illustrated in Figure 12.

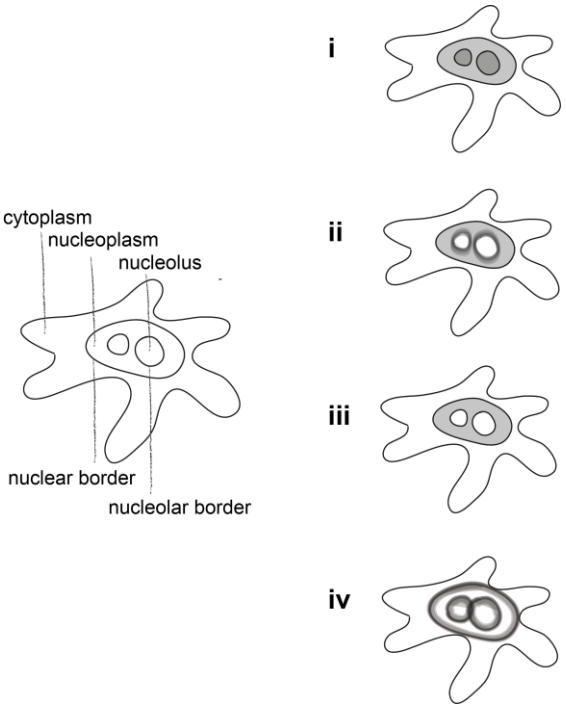

Figure 12 Illustration of the localisation phenotypes of KSHV ORF20. ORF20 is localised in the nucleoplasm and in the whole nucleolus (**ORF20-i**). ORF20 is localised in the nucleoplasm and at the nucleolar border (**ORF20-ii**). ORF20 is localised in the nucleoplasm but omitted from the nucleolus (**ORF20-iii**). ORF20 is localised at the nuclear periphery and the nucleolar border (**ORF20-iv**).

Besides the localisation signal of ORF20, we found particular alterations in the DNA staining in many ORF20-myc expressing cells. Strikingly, cells with localisation phenotype ORF20-ii, ORF20-iii, and ORF20-iv showed a different DNA staining compared to untransfected cells or cells with phenotype ORF20-i (Figure 11 ii to iv). The stained DNA was no longer equally distributed within the nucleoplasm but was exclusively located at the border of the nucleolus and nucleus, while omitted from the nucleoplasm, resembling cells with marginalized or condensed DNA. This effect could most clearly be seen in HeLa S3 cells (Figure 11 A), when compared to the other cell types, possibly due the size of the nuclei.

Subsequently, we analysed the localisation of ORF20 B-myc, the shorter form of ORF20, in HeLa S3 cells (Figure 13). The samples were processed as described earlier.

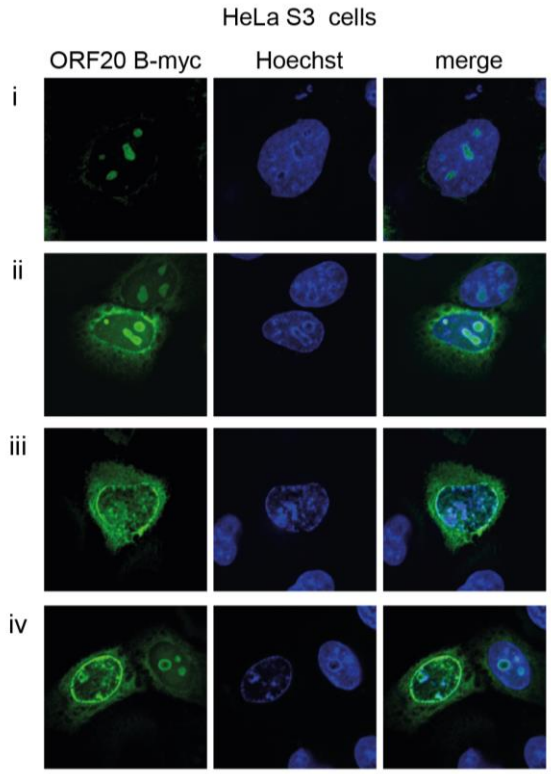

Figure 13 KSHV ORF20 B-myc is localised in the nucleolus, the nucleus, and the cytoplasm in HeLa S3 cells. Cells were transfected with ORF20 B-myc and fixed 24 h p.t with methanol and PFA. Samples were subjected to anti-myc IF and Hoechst staining of the DNA. Images were obtained by confocal microscopy with 60x magnification and are representative of at least 3 independent experiments. ORF20 B-myc is weakly expressed in the nucleus, but enriched in the complete nucleolus (**i**). ORF20 B-myc is localised in the cytoplasm, the nucleus and strongly enriched in ring-shaped nucleoli (**ii**). ORF20 B-myc is expressed in the cytoplasm and nucleus, but is omitted from the nucleolus (**iii**). ORF20 B-myc is strongly enriched in ring-shaped nucleoli and at the nuclear lamina (**iv**).

ORF20 B-myc showed the same localisation patterns as ORF20-myc, as it was expressed in the nucleolus, the nucleus and the cytoplasm. Moreover, ORF20 B-myc showed the same distinct four phenotypes (illustrated in Figure 12). We found cells that showed ORF20 B expression in the whole nucleolus next to moderate expression in the nucleoplasm (Figure 13 i), reflecting the ORF20-i localisation phenotype. A subset of cells showed localisation of ORF20 B in the nucleoplasm and strong enrichment at the nucleolar border (Figure 13 ii), characterising the ORF20-ii phenotype, while another subset of cells, the ORF20-iii phenotype, showed strong nucleoplasmic but no nucleolar expression of ORF20 B (Figure 13 iii). Furthermore, the ORF20-iv phenotype was detected, showing cells with intense expression ORF20 B at the nuclear border and the nucleolar border (Figure 13 iv).

As observed for ORF20-myc (Figure 11 ii to iv), we also detected altered DNA staining in HeLa S3 cells with ORF20 B localisation phenotype ORF20-ii, ORF20-iii, and ORF20-iv, where we observed a strong signal for Hoechst stained DNA at the nuclear border and surrounding the nucleolus, but a diminished signal in the nucleoplasm (Figure 13 ii to iv). ORF20-myc and ORF20 B-myc could not be distinguished by intracellular localisation studies, as they did look alike.

To verify the intracellular localisation of ORF20, we analysed the expression of V5-tagged KSHV ORF20 in nuclear and cellular fractions of HeLa S3 cell lysates by immunoblotting.

Cells were transfected with KSHV ORF20-V5 or empty vector pcDNA3.1 as control and lysates were processed with a nuclear/cytosol fractionation kit. Expression of ORF20-V5 was detected by anti-V5 immunoblotting. Detection of the exclusively cytoplasmic protein tubulin and the exclusively nuclear protein Lamin A/C by immunoblotting served as control for purity of the fractions (Figure 14).

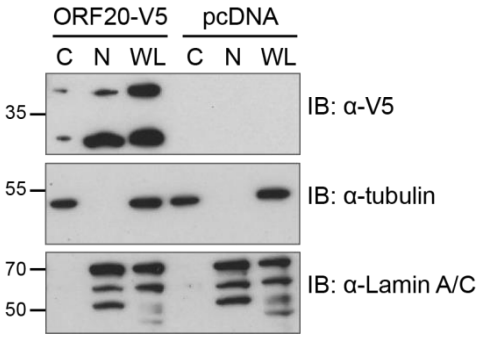

Figure 14 Expression of KSHV ORF20-V5 in the nucleus and cytoplasm of HeLa S3 cells. Immunoblot analysis of nuclear (**N**) and cytoplasmic (**C**) fractions compared to whole cell lysates (**WL**) of cells transiently transfected with ORF20-V5 or empty vector control pcDNA3.1. Tubulin served as a control for cytoplasmic proteins, while Lamin A/C served as a control for nuclear proteins. The experiment was repeated twice. Left margin shows molecular mass in kilodaltons (kDa).

We found that ORF20-V5 was expressed in both, the nuclear and the cytoplasmic fraction, confirming our IF microscopy results, where we found ORF20-myc located in the nucleus, including the nucleolus, and the cytoplasm. While the 29 kDa form compared to the 35 kDa form of ORF20-V5 seemed to be enriched in the nuclear fraction (Figure 14), a replicate of the experiment did not show this (data not shown).

3.1.3 Identification of KSHV ORF20 cellular interaction partners by q-AP-MS

We next addressed the question with which proteins of the human host cell KSHV ORF20-myc interacted. Since most cellular functions are dependent on direct and indirect protein-protein interactions (PPI), information about these interactions might give valuable insight into protein function of KSHV ORF20.

We used affinity purification (AP) combined with quantitative mass spectrometry (q-AP-MS), as this approach allows the unbiased detection of PPIs in their native cellular environment and maintains all relevant post-translational modifications. Furthermore, the composition of entire protein complexes, indicating the function of large molecular machines, can be detected (Paul et al. 2011). To distinguish true interaction partners from co-purifying contaminants, the quantitative proteomic method of stable isotope labelling by amino acids in cell culture (SILAC) was used, as it is an easy and very accurate approach for cell culture experiments (Paul et al. 2011). For that, two experiments were performed in parallel: the first one with the sample and the second one with a suitable control. A suitable control is expected to have no interaction partners, but should resemble the actual bait protein as close as possible. In our case bait protein and control shared the same vector backbone and the same epitope tag. The abundance of proteins in APs, of the actual sample and the control, was compared. Non-specific contaminants have a 1:1 ratio, while true interaction partners are more abundant in the actual sample (Paul et al. 2011). Proteins of both samples can be distinguished by MS through labelling of the proteins with different isotopes of an amino acid during cell culture, introducing a measurable mass shift

for each peptide of a protein between both samples. The workflow of co-IP coupled to SILAC mass spectrometry is shown in Figure 15 A.

We labelled HeLa S3 cells with either light or heavy isotopes of arginine and lysine for 10 days in cell culture. Heavy labelled cells were transfected with pcDNA4 ORF20-myc, while light labelled cells were transfected with pcDNA4 LacZ-myc as a control. A crossover experiment with swapped isotope labels was performed in parallel, which served as biological replicate, while the label switch should result in reciprocal SILAC ratios for true interaction partners (Paul et al. 2011). In the crossover experiment heavy labelled cells were transfected with pcDNA4 LacZ-myc and light labelled cells with pcDNA4 ORF20-myc. The cells were lysed 24 h p.t. in 1% NP-40 and 0.25% sodiumdeoxycholate containing buffer and immunoprecipitation was performed with myc magnetic beads. For the forward experiment lysates of the heavy labelled cells expressing ORF20-myc and light labelled cells expressing LacZ-myc were combined for affinity purification, while for the crossover experiment heavy labelled cells expressing LacZ-myc and light labelled cells expressing ORF20-myc were combined. Eluates were processed for mass spectrometry and analysed by liquid-chromatography coupled to tandem mass spectrometry (LC-MS/MS), performed by Josef Wissing of the Cellular Proteome Research group at the HZI. The results were bioinformatically analysed and Proteome Discoverer software by Thermo Scientific was used to evaluate the results, apply peptide filters (2.2.10 Materials and Methods), and calculate heavy/light values, based on the relative intensity, representing the relative abundance of a heavy labelled protein to its light labelled protein partner. The values were transformed into $\log_2$ fold changes for each protein of the forward and crossover experiment (Figure 15 B/C, Table 24 Appendix) to facilitate the analysis.

We found that KSHV ORF20-myc interacted with 28 of 47 known human large ribosomal subunit proteins (e.g. 60S ribosomal proteins L7a (L7a), L36 (L36), and acidic ribosomal protein P0 (LA0)) and 14 of 33 known human small ribosomal subunit proteins (e.g. 40S ribosomal protein S12 (S12)) (Khatter et al. 2015). Additionally, a variety of nucleolar proteins like rRNA 2'-O-methyltransferase fibrillarin, eukaryotic translation initiation factor 6 (eIF6), and nucleolar RNA helicase 2 (DDX21) were identified, but scarcely cytoplasmic proteins were detected as binding partners. Interestingly, most of the identified binding partners were described to be able to bind RNA or DNA. Notably, we found an interferon stimulated gene product (ISG) (Schoggins et al. 2011) with antiviral properties (Marques et al. 2008) as a potential interaction partner of ORF20-myc, namely 2'-5'-oligoadenylate synthase-like protein (OASL) (Figure 15 B and C).

We wondered whether binding of KSHV ORF20 to a large portion of ribosomal proteins was artificial, and therefore analysed the interactome of another KSHV protein, to compare the results. We chose KSHV ORF75, a mainly nuclear protein, that is expressed to some extent in the cytoplasm but not in the nucleolus. We performed the experiment with ORF75-myc as described for ORF20-myc above. We detected no ribosomal proteins as potential interaction partners of ORF75-myc (Table 25 Appendix), showing that interaction with ribosomal proteins was specific for ORF20-myc.

A

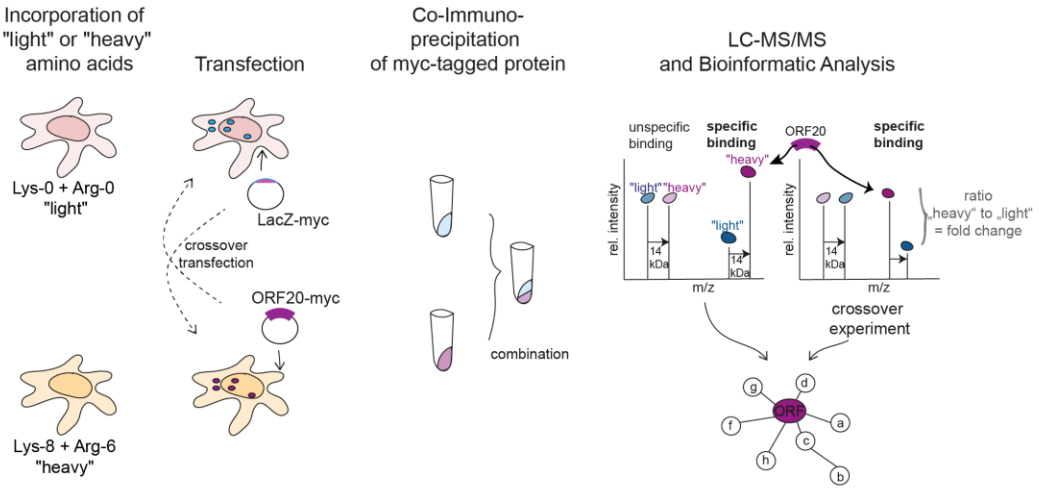

B

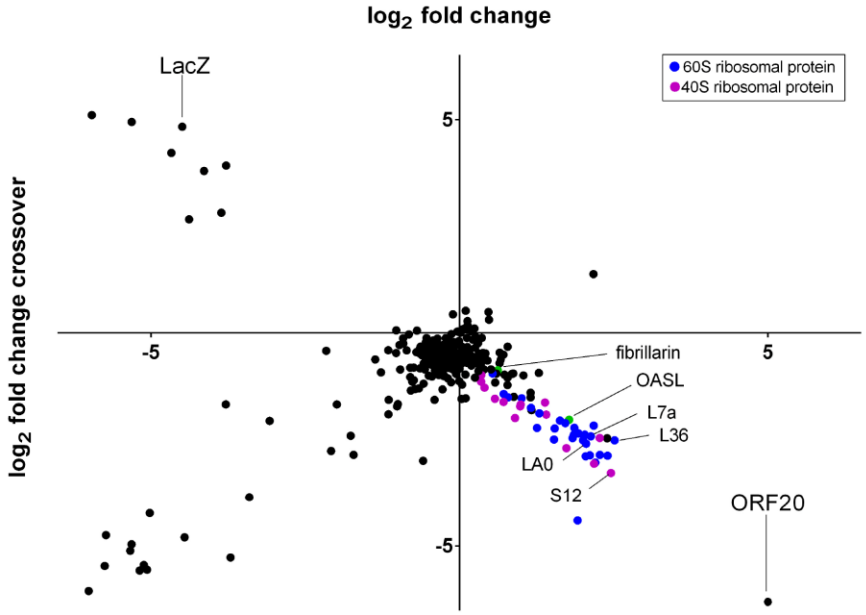

C

protein name	log_2 fold change	log_2 fold change crossover
ORF20	4,99	-6,31
eIF6	n.d.	-4,47
L36	2,51	-2,51
S12	2,45	-3,28
L7a	2,13	-2,42
LA0	2,05	-2,60
OASL	1,77	-2,04
DDX21	1,34	n.d.
fibrillarin	0,62	-0,88

Figure 15 Interactome of KSHV ORF20-myc in Hela S3 cells analysed by q-AP-MS. HeLa S3 cells incorporated heavy or light amino acids in 10 days of cell culture. Heavy labelled cells were transfected with ORF20-myc and light labelled cells with LacZ-myc as a control. 24 h p.t. cells were lysed and subjected to anti-myc IP. After IP, heavy and light samples were combined. Eluates were precipitated, prepared for MS, and analysed by LC-MS/MS. The relative intensity of a heavy labelled protein to its light labelled protein partner was used to calculate a "heavy/light-fold change" for each protein pair. In parallel a label switch experiment (crossover) was performed, were light labelled cells expressed ORF20-myc and heavy labelled cells LacZ-myc (**A**). Potential cellular protein interaction partners of ORF20 and non-specific contaminants are shown. Values of the "heavy/light-fold change" for each protein pair were transformed into log_2 fold changes and graphed together with the log_2 fold changes of the crossover experiment. Peptide filters were applied during bioinformatical analysis. Proteins that were identified only in the forward or crossover experiment are not shown (**B**). Many ribosomal proteins like L36 and S12, ribosome-associated proteins like LA0, nucleolar proteins like fibrillarin and DDX21, and the antiviral interferon stimulated gene product OASL were identified as potential binding partners of ORF20 (**C**).

3.2 Characterisation of the KSHV ORF20 interaction with nucleolar proteins

3.2.1 KSHV ORF20 interacts with nucleolar proteins

Given the nucleolar localisation of ORF20 and the potential protein interactions with nucleolar proteins like fibrillarin, DDX21, eIF6, and ribosomal L7a identified by q-AP-MS, we sought to further determine the role of ORF20 in the nucleus and especially in the nucleolus.

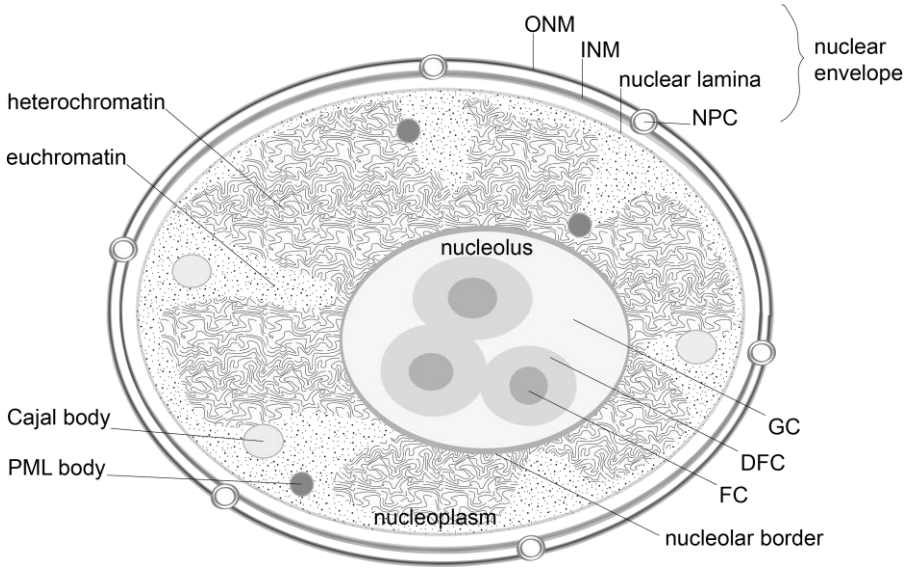

Figure 16 Nuclear organisation and compartments. Outer nuclear membrane (ONM), inner nuclear membrane (INM), and nuclear lamina (in animal cells) form the nuclear envelope. The envelope is perforated by nuclear pore complexes (NPC). The portion of the nuclear lumen close to the envelope is called the nuclear periphery. Condensed DNA, the Heterochromatin, lies in a characteristic “cartwheel” structure, while the lightly packed Euchromatin fills the nucleoplasm. The nucleus encompasses serval non-enveloped compartments, like PML bodies, Cajal bodies, and one or more nucleoli. A nucleolus harbours three subregions, the outer granular component (GC), the inner fibrillar component (FC), and between these the dense fibrillar component (DFC). Adapted from (Mekhail & Moazed 2010, Wei 2003, Morimoto & Boerkoel 2013)

The nucleus of an animal cell is encompassed by a nuclear envelope, built by an outer nuclear membrane (ONM) and an inner nuclear membrane (INM), which are perforated by nuclear pore complexes (NPC). Lamins form the nuclear lamina, which connects the INM with the DNA at the nuclear periphery (Mekhail & Moazed 2010). The nuclear DNA is classically divided into condensed packed Heterochromatin, associated with transcriptionally repressive DNA, which forms a “cartwheel” structure in the nucleus, and the lightly packed Euchromatin, being transcriptionally active, which fills the nucleoplasm (Luo et al. 2009). Next to the DNA, serval highly dynamic compartments, like promyelocytic leukaemia (PML) bodies, Cajal bodies, and one or more nucleoli are located in the nucleus (Figure 16). The nucleolus is described to have multiple functions. Primarily, the nucleolus is the site of ribosome-biogenesis, which forms around clusters of ribosomal DNA (rDNA) genes during interphase, concentrating machineries for transcription and processing of ribosomal subunits (Boisvert et al. 2007). The human ribosome itself comprises of a large subunit (60S) containing the 28S, 5S and 5.8S rRNA chains and 47 proteins, including L7a, and a small subunit (40S) possessing a single 18S rRNA-chain and 33 proteins (Khatter et al. 2015). The nucleolus further consists of three subregions termed fibrillar

centre (FC), dense fibrillar component (DFC), and granular component (GC). While transcription mainly occurs at the border between the centralized FC and surrounding DFC, ribosome subunit assembly takes place in the outer GC, where most proteins concentrate (Figure 16). Proteomic studies have shown that the nucleolus is associated with more than 700 human proteins, and is subjected to highly dynamic changes in its protein composition under different metabolic conditions. While approximately 30% of the nucleolar proteins are associated with ribosome biogenesis, others have been described to have functions in cell-cycle regulation, proliferation, stress sensing, innate immune responses, and viral infection (reviewed in Boisvert et al. 2007 and Ni et al. 2012). In the following some nucleolar proteins that are of interest for this study will be introduced.

The major nucleolar protein nucleolin is a multifunctional protein essentially involved in all aspects of ribosome biogenesis, like transcription of rDNA, modification and processing of pre-ribosomal RNA (rRNA), and assembly and transport of ribosome subunits and proteins. Upon cellular stress nucleolin relocalises from the nucleolus to the nucleoplasm by complex formation with cellular tumour antigen p53. Downregulation of nucleolin increases expression of p53, inhibits RNA polymerase I transcription, and causes blockage of the cell in G_2 phase (reviewed in Tajrishi et al. 2011).

The methyltransferase fibrillarin is highly conserved and indispensable for development in mice (Newton et al. 2003). It is involved in processing pre-rRNA (Tollervey et al. 1993) and translational control (Marcel et al. 2013). While normally located in the DFC and GC regions, fibrillarin leaves the nucleolus after transcriptional shut down in prophase, correlating with the disintegration of the nuclear envelope (Boisvert et al. 2007).

The RNA helicase DDX21 has a multifaceted role in multiple steps of ribosome biogenesis and regulation of transcriptional and post-transcriptional steps, which is associated with its ability to sense the transcriptional status of RNA polymerase I and II (Calo et al. 2014). While normally located in the nucleolus, in breast cancer cell lines DDX21 is frequently located in the nucleus but not the nucleolus, furthermore DDX21 protein expression levels correlate with cell proliferation (Zhang et al. 2014). Interestingly, DDX21 has been associated with viral infection, as it has been shown to restrict Influenza A virus replication early in infection, but to be counteracted by the viral NS1 protein later in infection (Chen et al. 2014).

Eukaryotic initiation factor 6 (eIF6) controls biogenesis and maturation of the 60S subunit in the nucleolus (Miluzio et al. 2009). In the cytoplasm binding of eIF6 to the 60S subunit controls joining of the 80S ribosome complex, a process that is rate-limiting for translation (Ceci et al. 2003). Furthermore, eIF6 mediates translation downstream of growth factors, and depletion of eIF6 in human cells specifically supresses miRNA-mediated regulation of target protein and mRNA levels (Chendrimada et al. 2007).

First we aimed to verify the protein interactions of ORF20-myc with nucleolar proteins by co-IP and immunoblotting. The nucleolar proteins L7a and DDX21 were selected for this experiment based on the availability and quality of antibodies for endogenous proteins that were identified in the ORF20 interactome. Additionally, we tested whether ORF20 B-myc would bind these proteins as well. As

controls we used the bacterial protein LacZ and the cellular protein OASL, which was also identified as potential ORF20 interaction partner (Figure 15 B and C).

HeLa S3 cells were transfected with ORF20-myc, ORF20 B-myc, LacZ-myc, or OASL-a-myc. The cells were harvested in lysis buffer containing 1% NP-40 and 0.25% sodiumdeoxycholate 24 h p.t. and were subsequently used for anti-myc co-IP using protein A agarose beads, pulling down the myc-tagged protein and its binding partners. The eluates were analysed by immunoblotting using antibodies against L7a and DDX21, and successful IP of the bait proteins was verified with an anti-myc antibody (Figure 17).

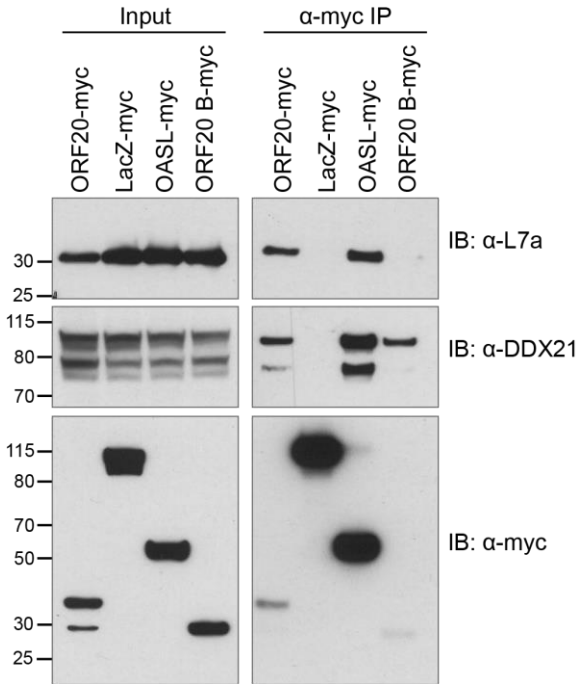

Figure 17 KSHV ORF20, ORF20 B and OASL co-precipitate with the endogenous nucleolar proteins L7a and DDX21. HeLa S3 cells were transfected with ORF20-myc, ORF20 B-myc, LacZ-myc, or OASL-myc and were lysed 24 h p.t. with 1% NP-40 and 0.25% sodium deoxycholate. Samples were subjected to anti-myc immunoprecipitation and were analysed by immunoblotting with antibodies against L7a, DDX21 or the myc epitope respectively. LacZ-myc served as negative control. Left margin shows molecular mass in kilodaltons (kDa). Experiment was performed once

First, we verified the expression of endogenous L7a and DDX21 and myc-tagged proteins in whole cell lysates. Ribosomal protein L7a has a predicated size of 30 kDa and an apparent size of 32 kDa according to the manufacturer of the anti-L7a antibody. DDX21 was referred to have two isoforms in the UniProt database, a full length version of 783 aa and an isoform lacking 68 aa at the N-terminus, resulting in two proteins with the predicted sizes of 88 kDa and 80 kDa, respectively. The anti-DDX21 antibody used in this study is described to detect a strong band at 95 kDa, a very faint band at 90 kDa, and an intermediate band at 80 kDa in HeLa cells. All analysed proteins were detected at the anticipated sizes in the whole cell lysates, including L7a at about 32 kDa and DDX21 at about 95 kDa and 78 kDa with additional faint bands at 90 kDa and 75 kDa, probably reflecting the two isoforms and additional unspecific bands, as the faint bands were not detected after immunoprecipitation.

We found that ORF20-myc co-immunoprecipitated the ribosomal protein L7a and the two isoforms of nucleolar helicase DDX21, even though after IP we could only weakly detect the 35 kDa band of

ORF20-myc, and were unable to detect the 29 kDa band. ORF20 B-myc was detected very faintly after myc-IP, indicating that the IP of ORF20 B worked poorly. But strong co-precipitation of the upper band of DDX21 and faint bands for the lower form of DDX21 and the L7a protein with ORF20 B were observed, showing that ORF20 B, like full length ORF20, was able to interact with L7a and DDX21. Our negative control LacZ-myc did not co-immunoprecipitate with DDX21 or L7a, which showed that the proteins did not unspecifically bind to the beads or the myc tag. Interestingly, OASL-myc interacted clearly with both proteins.

These findings revealed that the nucleolar proteins DDX21 and L7a co-immunoprecipitated with ORF20 and ORF20 B, clearly showing interaction of these proteins and confirming our q-AP-MS data. Notably, the antiviral protein OASL, which is described to be located mainly in the cytoplasm and partially in the nucleolus (Rebouillat et al. 1998) and which was found by us to interact with KSHV ORF20 by q-AP-MS, also bound to endogenous DDX21 and L7a.

3.2.2 KSHV ORF20 alters the subcellular localisation of nucleolar proteins

To extend the findings gained by interaction studies with q-AP-MS and co-IP followed by immunoblotting, we analysed whether ORF20 and ORF20 B would colocalise with the nucleolar proteins fibrillarin, L7a, DDX21, eIF6, and nucleolin (introduced in 3.2.1.) by IF microscopy. Colocalisation of two proteins by IF does not necessarily indicate a direct protein-protein interaction, but is actually a prerequisite for protein-protein interaction. Localisation of proteins in the same subcellular area can furthermore indicate a similar or connected protein function, as specific cellular activities and mechanisms are often concentrated in distinct cellular areas.

As control for a specific colocalisation with nucleolar proteins, we included in this experiment two proteins of other distinct nuclear bodies: coilin, the scaffold protein of Cajal bodies, which are involved in pre-mRNA splicing and in ribosomal RNA processing (Machyna et al. 2014) and PML, essential for the formation of PML-nuclear bodies (PML bodies). PML bodies are structurally and functionally heterogeneous and are associated with apoptosis, proliferation, genome stability, and antiviral responses (Bernardi & Pandolfi 2007).

HeLa S3 cells were transfected with ORF20-myc, ORF20 B-myc, or the control plasmid LacZ-myc and fixed 24 h later. Samples were labelled with murine anti-myc and rabbit antibodies against endogenous nucleolin, DDX21, eIF6, L7a, fibrillarin, PML, or coilin, followed by treatment with secondary Alexa-488 and Alexa-594 fluorochrome-linked antibodies against murine and rabbit primary antibodies, respectively. Hoechst staining was used to visualize the DNA. Images were obtained by confocal microscopy (Figure 18).

As expected, our control protein LacZ-myc was localised in the cytoplasm and weakly in the nucleoplasm of HeLa S3 cells if the cells expressed high levels of LacZ, and exclusively in the cytoplasm if the cells expressed low levels of LacZ. LacZ-myc did not colocalise with endogenous nucleolin, as nucleolin was strongly expressed in the nucleolus and moderately in the cytoplasmic area that surrounded the nucleus. Nucleolar localisation of nucleolin was clearly detected in every cell, independent of LacZ expression (Figure 18 A top panel). KSHV ORF20 colocalised with nucleolin in the nucleolus in a large fraction of transfected cells (Figure 18 A middle panel). Interestingly, we found that

some ORF20-myc expressing cells were lacking nucleolar expression signals of nucleolin (Figure 18 B middle panel, white arrow heads). Consequently, no colocalisation of ORF20 and nucleolin was detected in these cells. Likewise, ORF20 B-myc expressing cells colocalised with nucleolin in the nucleolus (Figure 18 A bottom panel), or nucleolin expression was absent in the nucleolus (Figure 18 B bottom panel, white arrow heads). Colocalisation of nucleolin with ORF20 or ORF20 B was steadily observed in cells with localisation phenotype ORF20-i (Figure 11 i and Figure 13 i), where the KSHV proteins were weakly to moderately expressed in the whole nucleolus and optionally in the nucleoplasm. A missing nucleolar expression signal of nucleolin was exclusively, but not necessarily, detected in cells showing localisation phenotype ORF20-ii, ORF20-iii, or ORF20-iv of ORF20 and ORF20 B (Figure 12). As described earlier, phenotype ORF20-ii showed strong expression of the KSHV proteins at the nucleolar border and in the nucleoplasm (Figure 11 ii and Figure 13 ii), while phenotype ORF20-iii was characterised by strong expression in the nucleoplasm omitted from the nucleolus (Figure 11 iii and Figure 13 iii), and phenotype ORF20-iv by localisation of ORF20 or ORF20 B at the nuclear and nucleolar border (Figure 11 iv and Figure 13 iv). This finding could suggest that distinct localisation patterns of ORF20 and ORF20 B induced absence of nucleolar nucleolin expression.

Endogenous DDX21 was detected exclusively in the nucleolus, in both, cells showing LacZ expression and cells not showing LacZ expression (Figure 18 B top panel), as were eIF6 (Figure 18 C top panel), L7a (Figure 18 D top panel), and fibrillarin (Figure 18 E top panel). Equally to nucleolin, we found that DDX21, eIF6, L7a, and fibrillarin colocalised with ORF20 in cells showing localisation phenotype ORF20-i (Figure 18 B - E middle panel), and were often dispersed in cells with localisation phenotype ii, iii or iv of ORF20 (Figure 18 B - E bottom panel, white arrow heads). We found the same effect of ORF20 B expression on DDX21 and eIF6 localisation, as expression of localisation phenotype ORF20 B-i was clearly associated with colocalisation of the proteins in the nucleolus (Figure 18 B and C bottom panel), while missing expression signals of DDX21 and eIF6 were found in many cells with localisation phenotype ii, iii, and iv of ORF20 B (Figure 18 B and C bottom panel, white arrow heads).

In untransfected and LacZ-myc transfected cells, the nuclear protein PML was detected in dot-like structures distributed in the nucleoplasm that represented localisation of PML bodies, as PML is part of PML bodies (Figure 18 F top panel). KSHV ORF20-myc did not colocalise with endogenous PML or influence PML localisation, as ORF20 was not expressed in dot-like structures in the nucleoplasm or affected the quantity of PML dot-like structures, respectively (Figure 18 F bottom panel).

Endogenous coilin, a marker for Cajal bodies, was detected in dot-like structures in the nucleoplasm of untransfected and LacZ-myc expressing cells, with commonly one to four Cajal bodies per cell (Figure 18 G top panel). We found that ORF20-myc expression altered expression and localisation of coilin, as cells with localisation phenotype ii, iii, and iv of ORF20 frequently lacked coilin expression, or showed translocation of coilin to the nucleolus, where it was detected in ring-like structures (Figure 18 G bottom panel, white arrow heads).

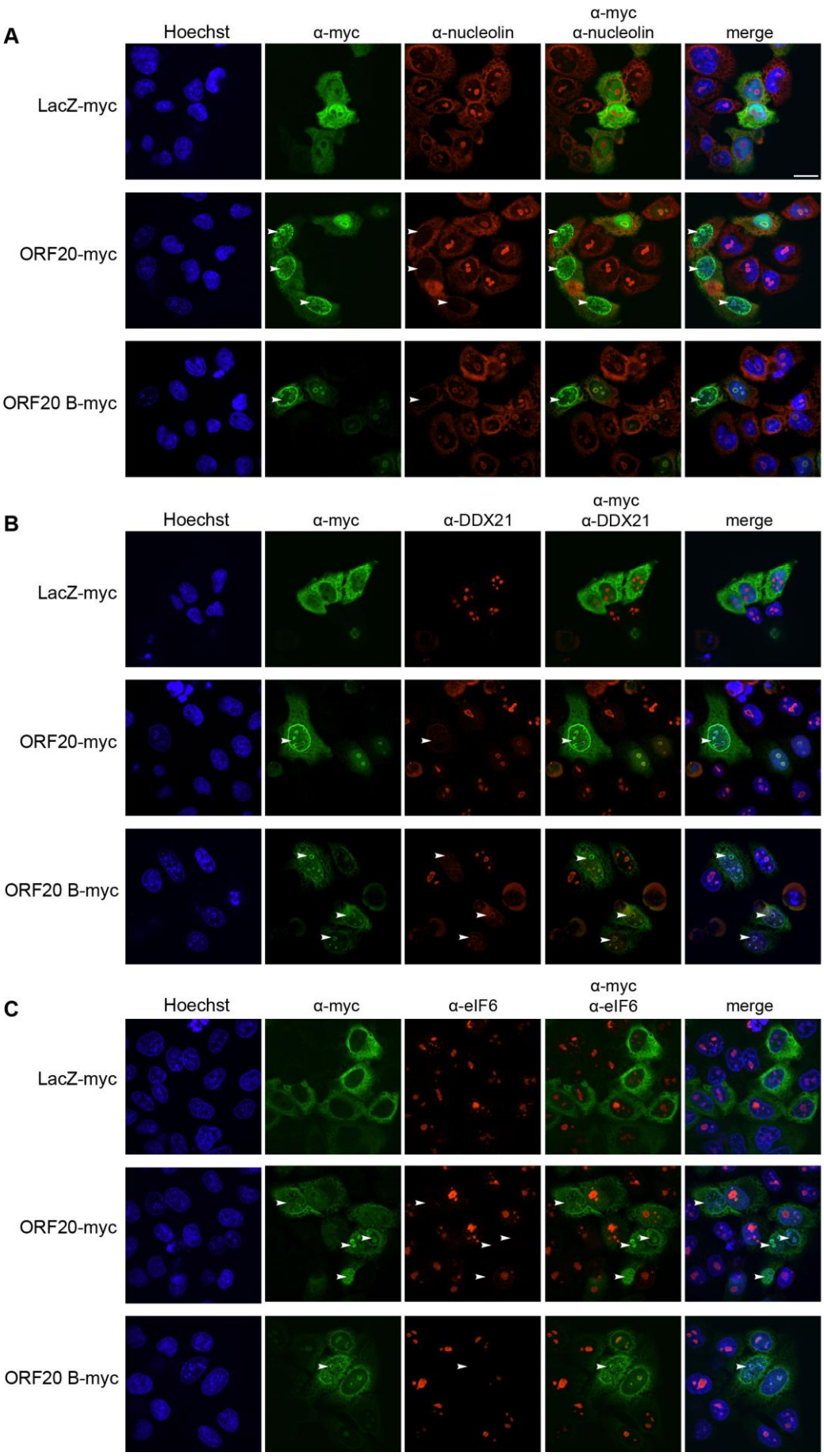
A
Hoechst
α-myc
α-nucleolin
α-myc
α-nucleolin
merge
LacZ-myc
ORF20-myc
ORF20 B-myc
B
Hoechst
α-myc
α-DDX21
α-myc
α-DDX21
merge
LacZ-myc
ORF20-myc
ORF20 B-myc
C
Hoechst
α-myc
α-eIF6
α-myc
α-eIF6
merge
LacZ-myc
ORF20-myc
ORF20 B-myc

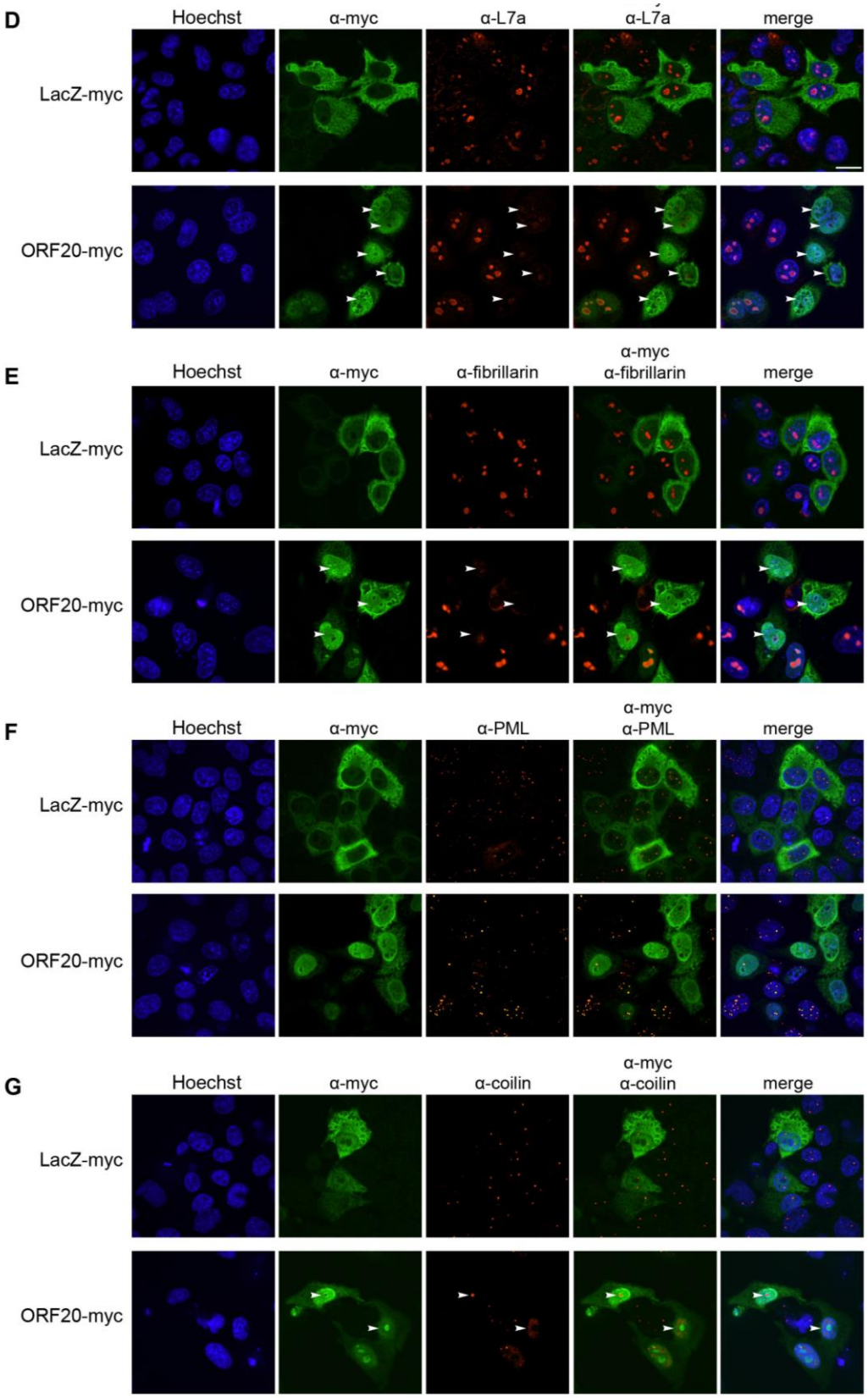

Figure 18 Nucleolar proteins colocalise with and are dispersed by KSHV ORF20 and ORF20 B. HeLa S3 cells were transfected with ORF20-myc, ORF20 B-myc, or LacZ-myc as control and fixed 24 h later. Samples were subjected to IF using antibodies against nucleolin, DDX21, eIF6, L7a, fibrillarin, PML, or coilin and myc (A-G). Nuclei were stained with Hoechst. Images were obtained by confocal microscopy with 60x magnification and are representative of 3 independent experiments. Scale bar 18 µm. White arrow heads indicate lacking nucleolar expression signals of the nucleolar proteins (A–E) and missing or altered localisation of coilin (G).

In summary we observed that ORF20 and ORF20 B colocalised with all analysed endogenous nucleolar proteins in the nucleolus, namely, nucleolin, DDX21, eIF6, L7a, and fibrillarin for ORF20 and nucleolin, DDX21, and eIF6 for ORF20 B. Interestingly, specific localisation patterns of ORF20 and ORF20 B, as seen in the localisation phenotypes ORF20-ii, ORF20-iii, and ORF20-iv, seem to results in dispersal of nucleolar proteins from the nucleolus, as detected by a missing expression signal of the proteins in the nucleolus. This effect seemed to be specific for the nucleolar localisation of the analysed proteins, as for example the cytoplasmic localisation of nucleolin was unaffected by ORF20-myc or ORF20 B-myc expression. ORF20 expression did not affect nuclear PML expression, but dispersed and altered nuclear localisation of coilin.

Quantification of nucleolar protein localisation in the presence of KSHV ORF20

We next quantified our observations to determine the percentage of cells with altered nucleolar localisation of nucleolin, DDX21, eIF6, L7a, and fibrillarin, as well as localisation of PML and coilin in their respective nuclear compartments. More than 50 cells with localisation phenotype ii, iii, or iv of ORF20-myc and ORF20 B-myc (Figure 12), and more than 50 cells expressing high levels of LacZ-myc were counted, and expression and localisation of the nuclear proteins was analysed in three independent experiments. We chose cells showing localisation phenotype ii, iii, or iv of ORF20 and ORF20 B, as the dispersal of nucleolar proteins by ORF20 or ORF20 B was exclusively detected in these cells. Cells having a strong LacZ expression signal were used as a control. Figure 19 shows the percentage of counted transfected cells per sample harbouring altered nuclear protein localisation, altered PML or coilin localisation.

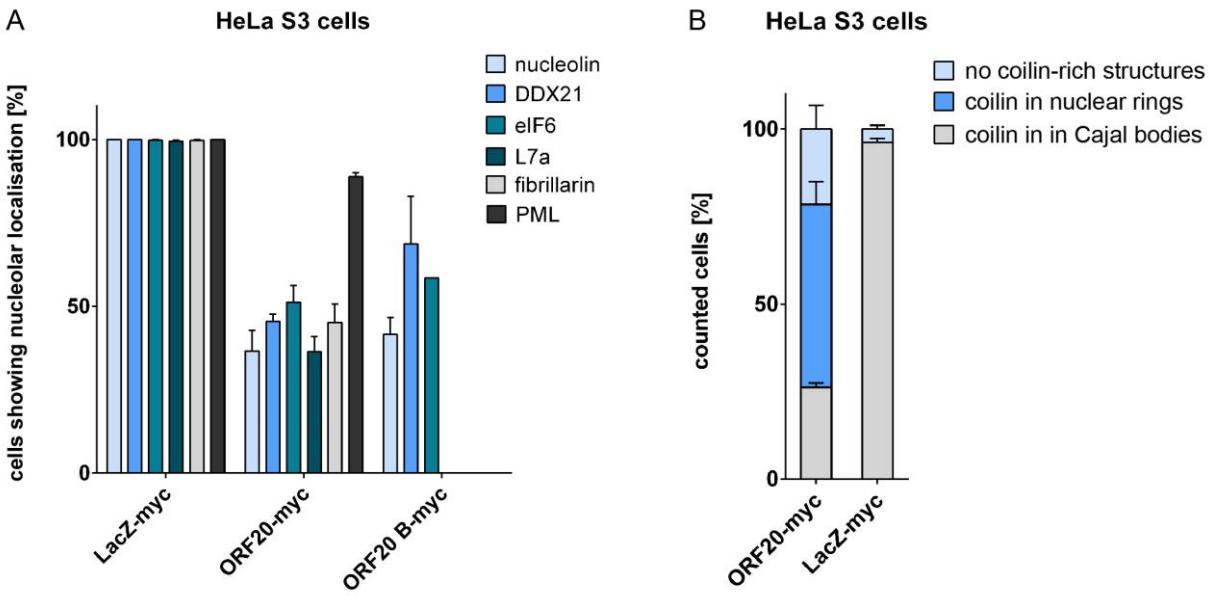

Figure 19 KSHV ORF20 and ORF20 B disperse nucleolar proteins and coilin in HeLa S3 cells. Cells were transfected with ORF20-myc, ORF20 B-myc, or LacZ-myc as a control and fixed 24 h p.t. Samples were subjected to IF using antibodies against nucleolin, DDX21, eIF6, L7a, fibrillarin, PML (A), or coilin (B) and the myc epitope. DNA was stained with Hoechst. Images were obtained by confocal microscopy. For quantification, at least 50 cells showing localisation phenotype ii, iii, or iv of ORF20-myc and ORF20 B-myc (Figure 12) or expressing LacZ-myc were analysed for subnuclear expression and localisation of the indicated endogenous proteins. The number of counted cells per sample was set to 100% to show the percentage of cells per sample with altered indicated protein localisation. Data shows averages with standard deviation from three independent experiments.

We found that in cells with localisation phenotype ii, iii, and iv of ORF20-myc nucleolar localisation of nucleolin, DDX21, eIF6, L7a, and fibrillarin was detected in approximately 36% - 50% of the cells, while in LacZ-myc expressing cells nucleolar protein localisation was detected in approximately 99,5% of the cells (Figure 19 A). In the total population of ORF20-myc transfected cells, including localisation phenotype ORF20-i, 28% - 33% of the cells showed dispersed localisation of nucleolin, DDX21, eIF6, L7a, and fibrillarin (data not shown). ORF20 B-myc significantly reduced nucleolar localisation of nucleolin (~41,6%), DDX21 (~68,8%), and eIF6 (~58,6%), but less efficiently in comparison to ORF20-myc. Localisation of PML was not significantly affected by ORF20-myc expression, as approximately 89% of the cells showed PML expression in PML bodies. In comparison, 100% of the cells expressing LacZ-myc had PML bodies.

We found that localisation of coilin was strongly altered by expression of ORF20-myc compared to LacZ-myc expressing cells, where approximately 96% of cells showed expression of coilin in Cajal bodies (Figure 19 B). ORF20-myc expression strongly correlated with translocation of coilin to the nucleolus (~52% of the cells) or the absence of coilin expression (~21,5% of the cells). Only a minority of ORF20-myc expressing cells showed coilin-rich structures reflecting Cajal bodies (~26% of the cells), indicating that ORF20-myc-dependent manipulation of subnuclear localisations was not limited to nucleoli.

Nucleolar protein localisation in the presence of KSHV ORF20 in different cell types

Next, we wanted to investigate whether the dispersal of nucleolar proteins induced by KSHV ORF20 expression was cell type specific or limited to HeLa S3 cells. We analysed expression and localisation of selected nucleolar proteins in murine NIH3T3, human HEK293T, and African green monkey Vero cells expressing ORF20-myc or LacZ-myc as a control. Cells were transfected, 24 h p.t trypsinised, and seeded onto coverslips. Samples were fixed 48 h p.t. and were subjected to IF as described earlier. Images were acquired by confocal microscopy (Figure 20). For quantification, more than 40 cells strongly expressing LacZ-myc or ORF20-myc with localisation phenotype ii, iii, and iv (Figure 12) were counted in NIH3T3 cells and HEK293T cells, while in Vero cells, due to low transfection efficiency, 14 to 43 cells were counted (Figure 21).

ORF20-myc colocalised with fibrillarin and eIF6 in the nucleolus in more than half of the analysed NIH3T3 cells (Figure 20 A and B). Similarly, we found that ORF20-myc commonly colocalised with DDX21 and eIF6 in HEK293T cells (Figure 20 C and D) and with fibrillarin, eIF6, and DDX21 in Vero cells (Figure 20, E, F, and G). In all analysed cell types, expression of ORF20-myc with localisation phenotype ii, iii, or iv frequently correlated with a missing nucleolar expression signal of fibrillarin, eIF6, and DDX21, while nucleolar expression signals were steadily detected in LacZ-myc expressing cells (100% of NIH3T3, HEK293T, and Vero cells, Figure 21). Fibrillarin was dispersed in approximately 57% of NIH3T3 cells and in about 42% of Vero cells, while eIF6 expression was absent in approximately 52% of NIH3T3, 67% of HEK293T, and 54% of Vero cells (Figure 21). About 48% of HEK293T and 43% of Vero cells lacked DDX21 expression signals in the presence of ORF20 with localisation phenotype ii, iii, or iv (Figure 21).

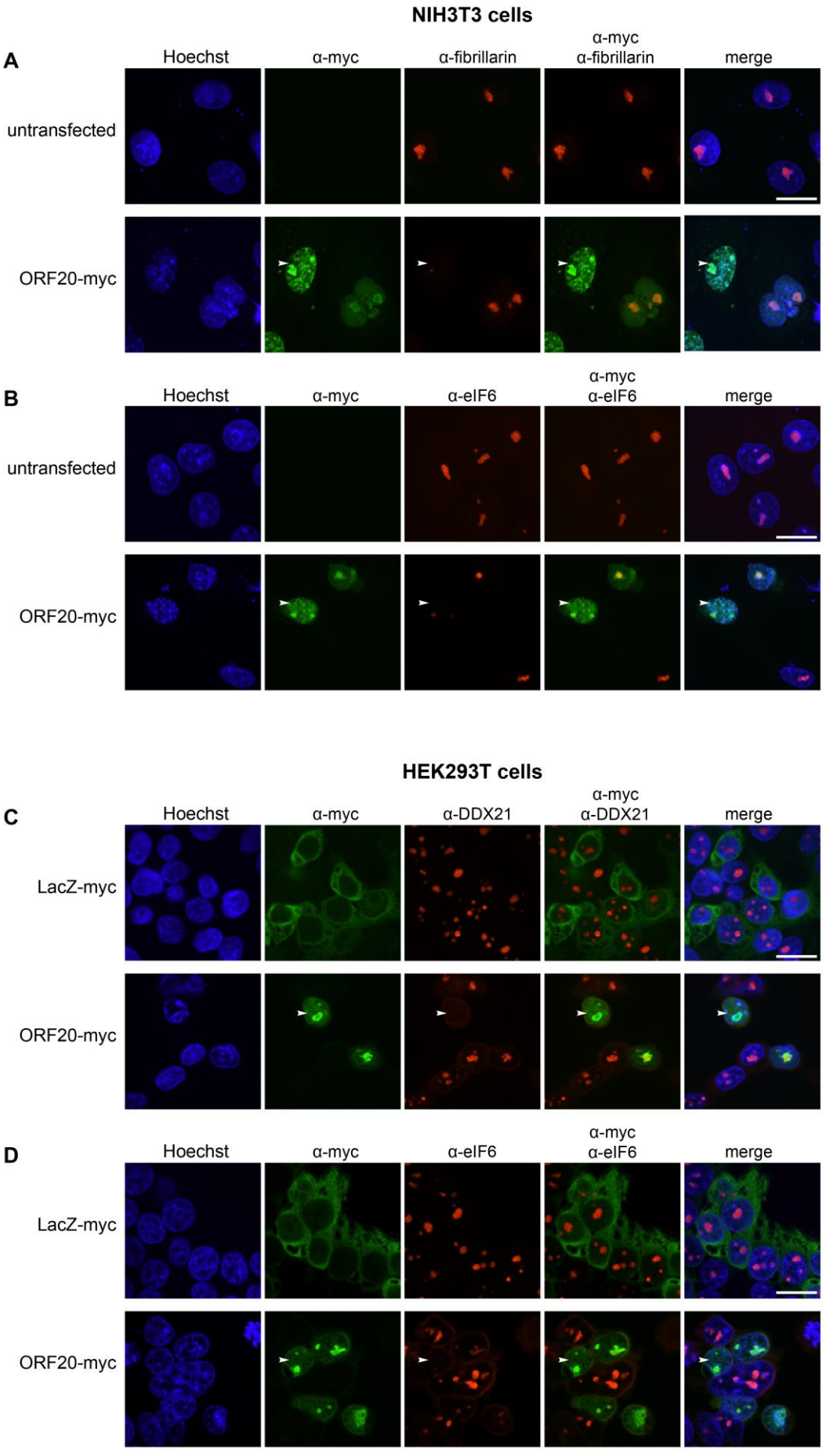
NIH3T3 cells
A
Hoechst
α-myc
α-fibrillarin
α-myc
α-fibrillarin
merge
untransfected
ORF20-myc
B
Hoechst
α-myc
α-eIF6
α-myc
α-eIF6
merge
untransfected
ORF20-myc
HEK293T cells
C
Hoechst
α-myc
α-DDX21
α-myc
α-DDX21
merge
LacZ-myc
ORF20-myc
D
Hoechst
α-myc
α-eIF6
α-myc
α-eIF6
merge
LacZ-myc
ORF20-myc

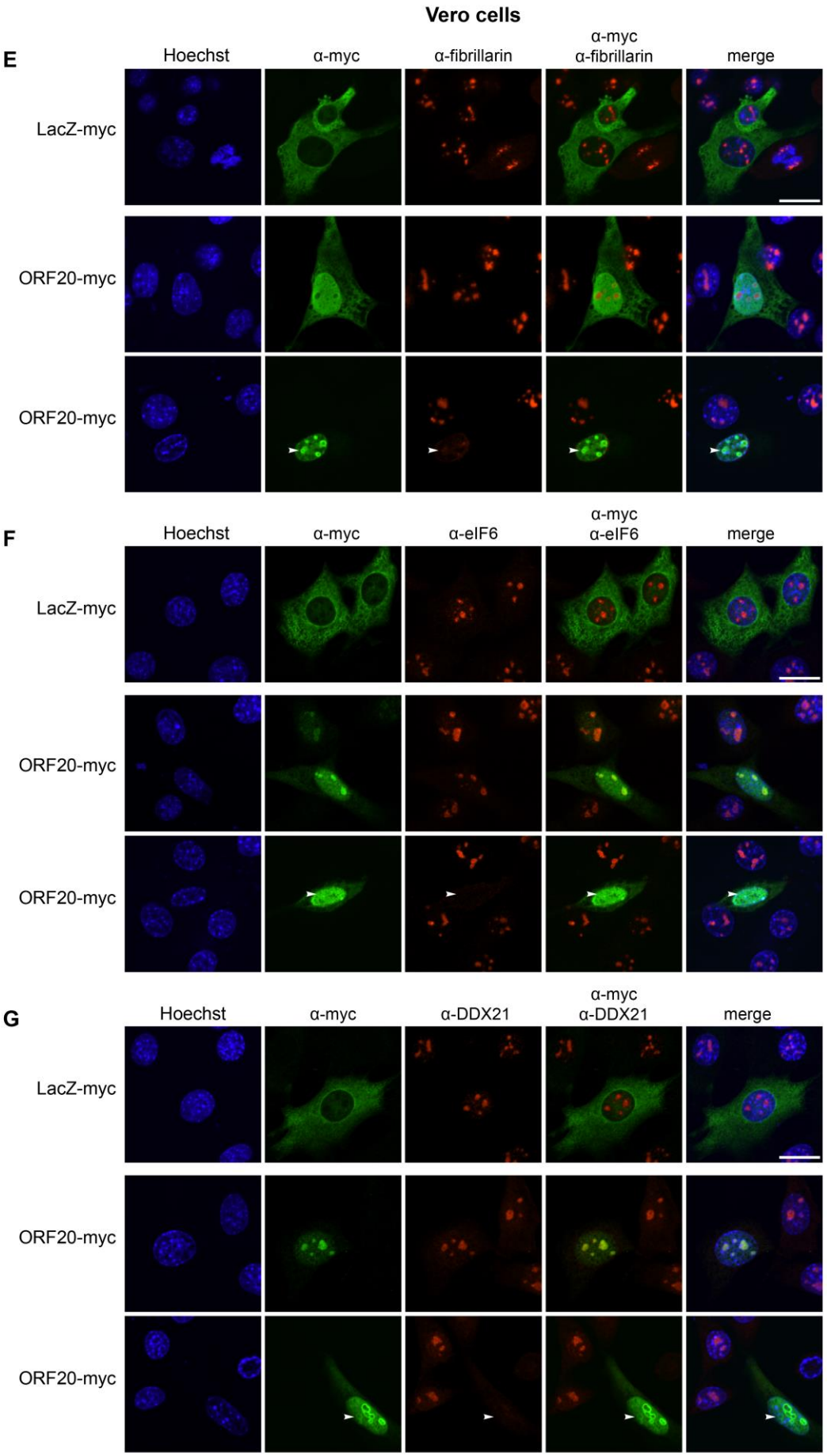
Vero cells
E
Hoechst
α-myc
α-fibrillarin
α-myc
α-fibrillarin
merge
LacZ-myc
ORF20-myc
ORF20-myc
F
Hoechst
α-myc
α-eIF6
α-myc
α-eIF6
merge
LacZ-myc
ORF20-myc
ORF20-myc
G
Hoechst
α-myc
α-DDX21
α-myc
α-DDX21
merge
LacZ-myc
ORF20-myc
ORF20-myc

Figure 20 KSHV ORF20 colocalises with and disperses nucleolar proteins in NIH3T3, HEK293T, and Vero cells. NIH3T3 (A and B), HEK293T (C and D), or Vero cells (E, F, and G) were transfected with KSHV ORF20-myc or control protein LacZ-myc. 24 h p.t. cells were seeded onto coverslips and were fixed at 48 h p.t. with methanol and 4% PFA. Samples were labelled with primary antibodies against the myc epitope and fibrillarin (A and E), eIF6 (B, D, and F), or DDX21 (C and G) followed by labelling with secondary fluorochrome-linked antibodies and Hoechst staining of the DNA. Images were obtained by confocal microscopy with 60x magnification. Experiment was performed once. Scale bar 18 µm. White arrow heads indicate lacking nucleolar expression signals of the indicated nucleolar proteins.

In summary, more than half of the analysed cells with ORF20-myc localisation phenotype ii, iii, or iv had no detectable fibrillarin, eIF6, or DDX21 signals. These values were similar among murine NIH3T3, human HEK293T, and African green monkey Vero cells (Figure 21), and were comparable to the values obtained with human HeLa S3 cells (Figure 19), showing that dispersal of nucleolar proteins induced by KSHV ORF20 was conserved throughout different cell types and cell species.

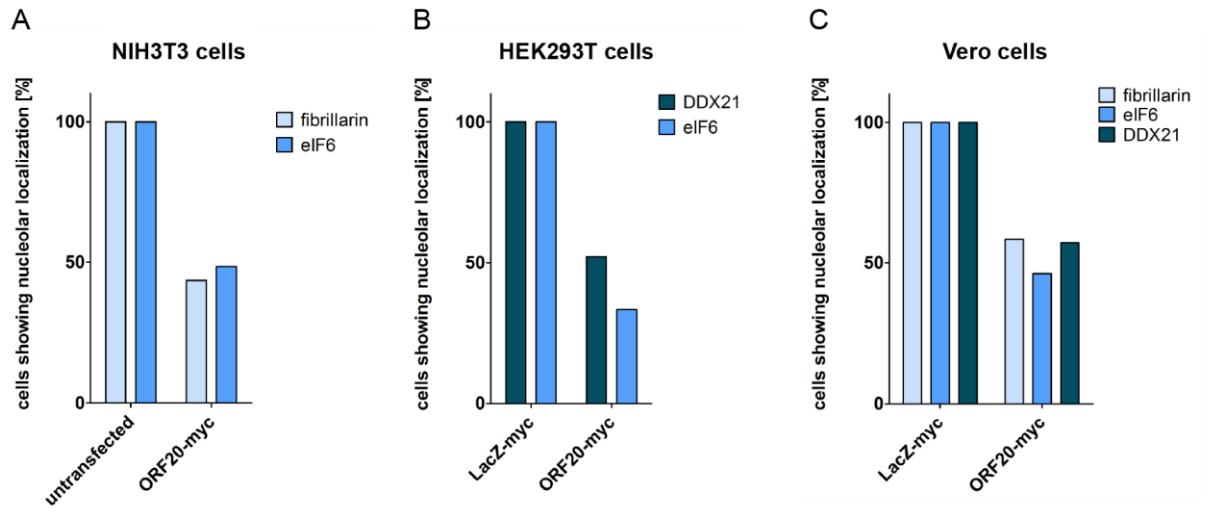

Figure 21 Nucleolar proteins are dispersed in KSHV ORF20 expressing NIH3T3, HEK293T and Vero cells. NIH3T3 (A), HEK293T (B), or Vero cells (C) were transfected with KSHV ORF20-myc, or control protein LacZ-myc. Samples were treated as described in Figure 20. For quantification, more than 40 NIH3T3 (A) or HEK293T (B) and more than 14 Vero cells (C) strongly expressing LacZ-myc or ORF20-myc were analysed for nucleolar expression and localisation of the indicated protein.

Altogether, our data showed that ORF20 and ORF20 B colocalised with nucleolar proteins and affected localisation of all analysed nucleolar proteins, namely nucleolin, DDX21, eIF6, L7a, and fibrillarin, preventing their normal enrichment and localisation in the nucleolus. Additionally, absence of nucleolar protein expression induced by ORF20 has been observed in different cell types and species, indicating that the effect was not limited to one expression system. Although ORF20 B showed the same phenotype as ORF20, the induced dispersal of nucleolar proteins was less pronounced, suggesting that ORF20 and ORF20 B might differ in their function. While PML expression in PML bodies was unaffected by ORF20, expression and localisation of coilin, the marker of Cajal bodies, was strongly altered by ORF20. Differently to PML bodies, Cajal bodies have been described to be associated with the nucleolus. This may suggest that ORF20 specifically manipulates a subset of nuclear proteins enriched in connected subnuclear compartments.

3.2.3 KSHV ORF20 does not influence total expression of nucleolar proteins

Next, we examined if KSHV ORF20 was affecting the total protein expression levels of the above-mentioned nucleolar proteins. The missing expression signal of the nucleolar proteins, detected by IF microscopy, might be caused by manipulation of transcription or protein stability, affecting the total protein levels of these proteins, or by relocation of the proteins from the nucleolus to other subcellular compartments. We analysed the protein expression of the nucleolar proteins L7a, fibrillarin, and eIF6 by immunoblotting of total cell lysates of HEK293T cells transfected with ORF20-myc and compared these to untransfected cells, or cells expressing empty vector pcDNA4 or LacZ-myc (Figure 22).

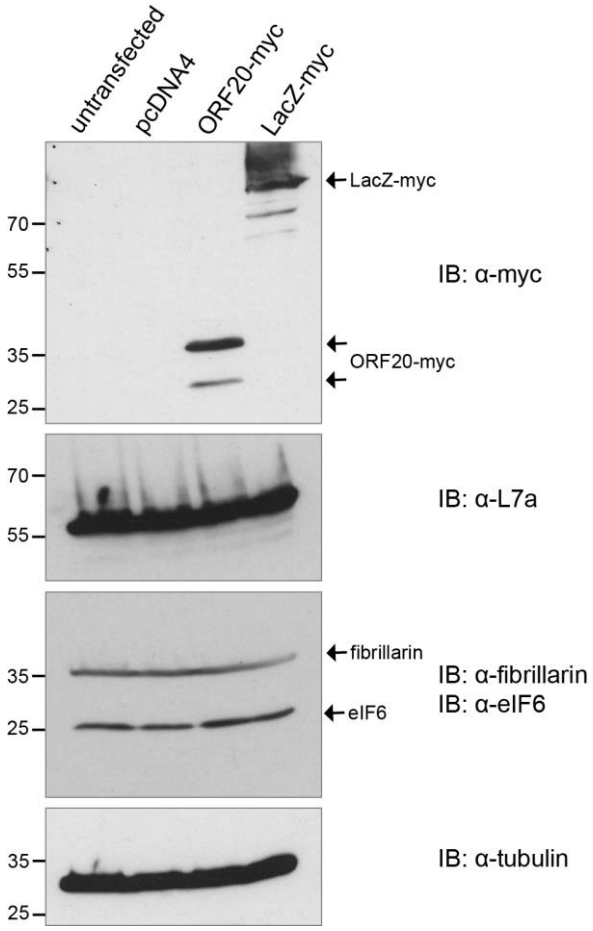

Figure 22 Protein expression levels of nucleolar proteins are not altered by KSHV ORF20-myc. HEK293T cells were transfected with ORF20-myc, LacZ-myc, or empty vector pcDNA4 or were left untransfected. Cells were lysed 24 h p.t. with 1x SDS-sample buffer. Immunoblotting of the samples was performed using antibodies against L7a, fibrillarin, eIF6, and the myc epitope. Anti-tubulin immunoblotting served as a protein loading control. Experiment was performed twice.

We found that the nucleolar proteins L7a, fibrillarin, and eIF6 were equally expressed in untransfected HEK293T cells or HEK293T cells expressing empty vector pcDNA4, LacZ-myc, or ORF20-myc. This suggests that ORF20-myc did probably not affect the protein levels of nucleolar proteins, but may cause dispersal of nucleolar proteins or inhibition of accumulation in the nucleolus.

3.2.4 The MCMV protein M76 does not affect the localisation of nucleolar proteins

KSHV ORF20 belongs to the UL24 gene family that is conserved in all herpesviruses. One family member is UL24, encoded by the alphaherpesvirus human herpes simplex virus-1 (HSV-1). Using transient transfection of UL24 and viral infection with UL24 mutants, Bertrand and colleagues showed that UL24 expressing cells lacked nucleolar localisation of nucleolin and B23. They claimed that UL24 is sufficient to induce dispersal of nucleolin and B23, and that the UL24 homology domain was indispensable for nucleolar targeting (Bertrand & Pearson 2008, Bertrand et al. 2010, Lymberopoulos et al. 2011).

As KSHV ORF20 and HSV-1 UL24 are able to disperse nucleolar proteins, we wondered whether this protein function was conserved throughout the UL24 protein family. We analysed the murine UL24 gene family member M76 encoded by the betaherpesvirus murine cytomegalovirus (MCMV), as we had C-terminally tagged M76 (M76-V5) in pcDNA3, cloned by Vladimir Magalhaes, in our lab. We transiently expressed M76-V5 in murine NIH3T3 cells and African green monkey Vero cells to analyse the subcellular localisation of M76 and to determine the influence of M76 on localisation and expression of nucleolar proteins by IF microscopy.

NIH3T3 cells were transfected with pcDNA3 M76-V5. Untransfected cells were used as a control. Cells were fixed 48 h later. Samples were labelled with primary antibodies against the myc or V5 epitope in combination with antibody against fibrillarin, eIF6, or DDX21, followed by labelling with secondary fluorochrome-labelled antibodies and DNA staining with Hoechst. Cells were visualized by confocal microscopy (Figure 23). Vero cells were transfected with pcDNA3 M76-V5 or pcDNA4 LacZ-myc as a control. Samples were treated as described earlier and analysed by confocal microscopy (Figure 24).

For quantification of the nucleolar expression signals of fibrillarin, eIF6, and DDX21 more than 40 NIH3T3 cells per sample (Figure 25 A) and 24 to 48 Vero cells per sample were analysed (Figure 25 B), whereby only cells strongly expressing M76 or LacZ were selected.

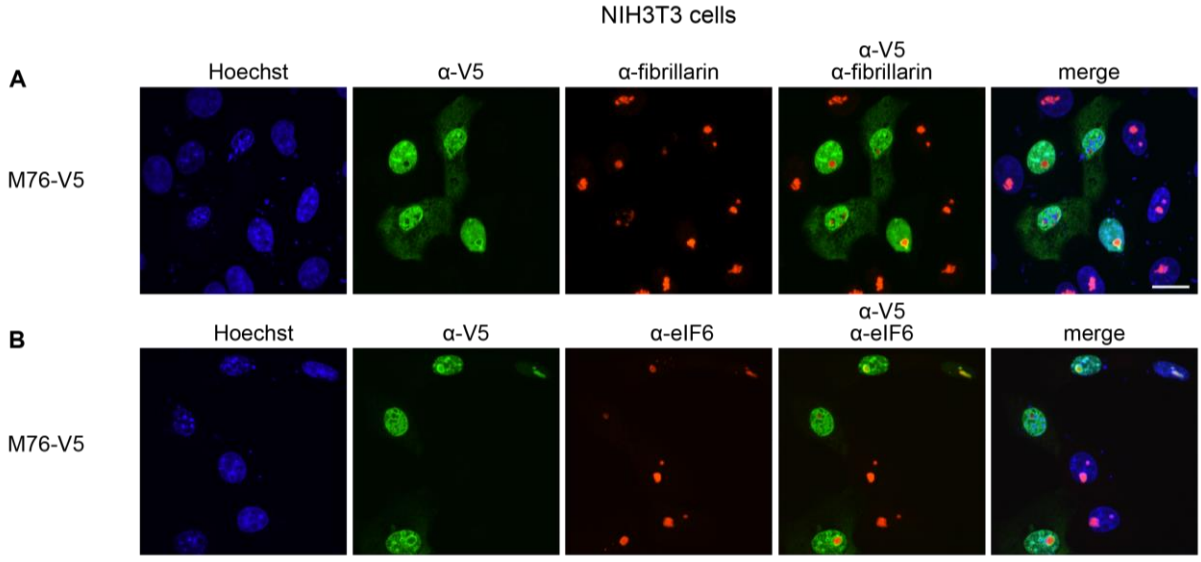

Figure 23 MCMV M76 colocalises with fibrillarin and eIF6 in the nucleolus but does not induce their dispersal in NIH3T3 cells. Cells were transfected with M76-V5. Untransfected cells were used as a control (data not shown). 24 h later cells were trypsinised, plated onto coverslips, and were fixed 24 h later with methanol and 4% PFA. Samples were subjected to anti-V5 and anti-fibrillarin (A) or anti-eIF6 (B) IF and Hoechst staining. Images were obtained by confocal microscopy with 60x magnification. Experiment was performed once. Scale bar 18 µm.

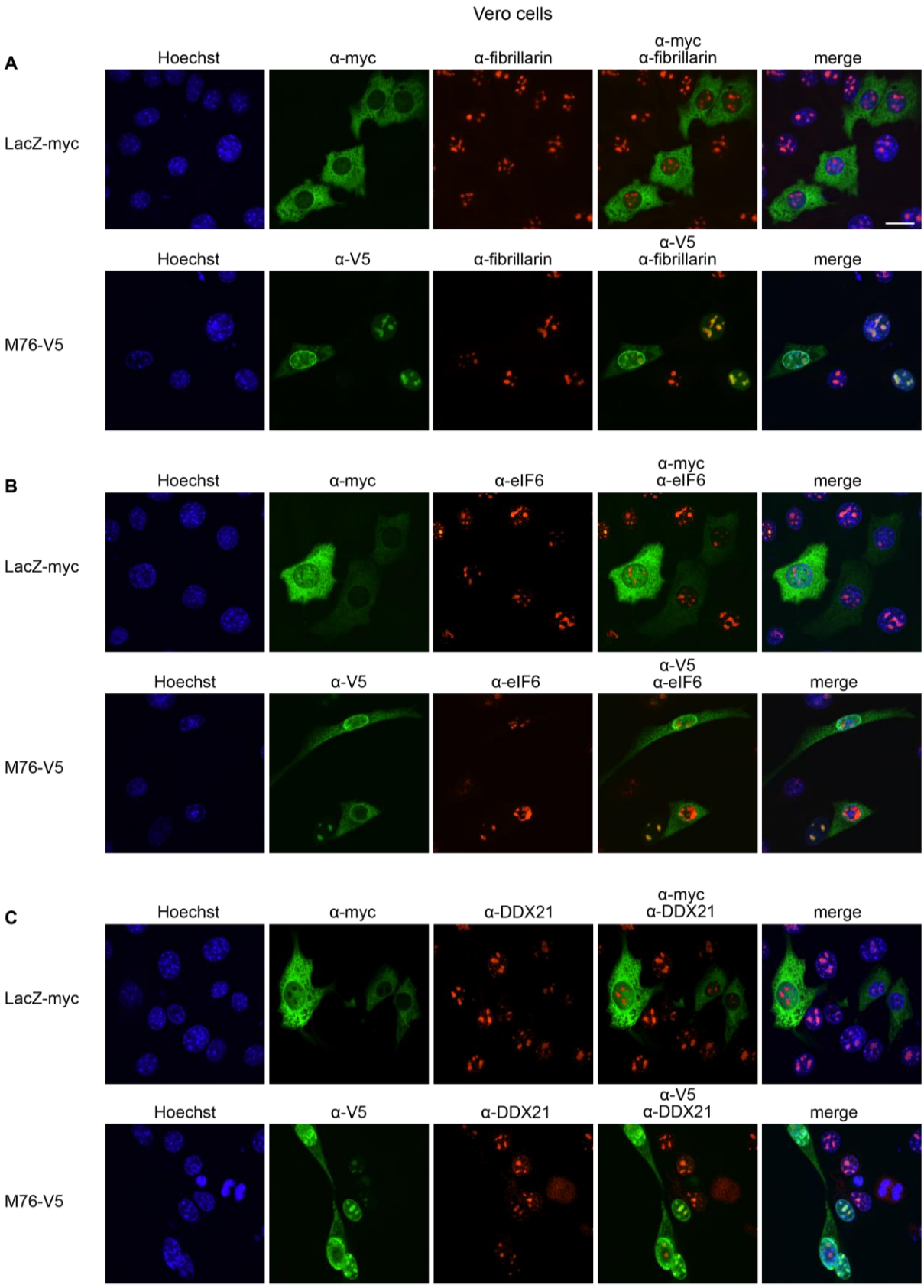

Figure 24 MCMV M76 colocalises with fibrillarin, eIF6, and DDX21 in the nucleolus but does not induce their dispersal in Vero cells. Cells were transfected with M76-V5, or LacZ-myc as control. 24 h later cells were trypsinised, plated onto coverslips, and were fixed 24 h later. Samples were subjected to IF using anti-myc or anti-V5 in combination with anti-fibrillarin (A), anti-eIF6 (B), or anti-DDX21 (C) and Hoechst staining. Images were obtained by confocal microscopy with 60x magnification. Experiment was performed once. Scale bar 18 µm.

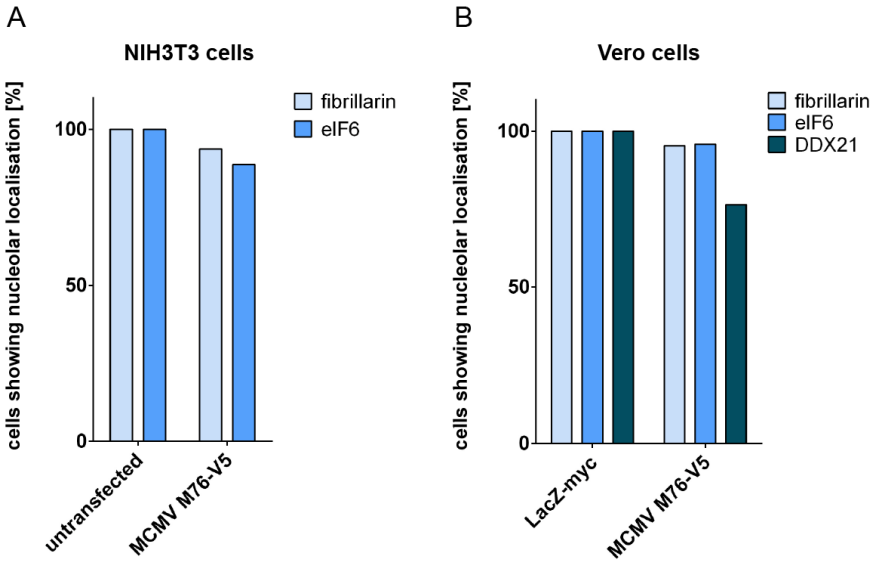

Figure 25 MCMV M76 does not disperse nucleolar proteins in NIH3T3 or Vero cells. NIH3T3 cells were transfected with M76-V5 or were left untransfected as a control (A). Vero cells were transfected with M76-V5 or LacZ-myc as a control (B). Samples were processed as described in Figure 23 and Figure 24. For quantification more than 40 NIH3T3 cells (A) and more than 28 Vero cells (B) were analysed for nucleolar expression of the indicated nucleolar proteins. Only cells strongly expressing M76-V5 or LacZ-myc were selected. Experiment was performed once.

We found that murine UL24 gene family member M76-V5 encoded by MCMV was primarily expressed in the nucleolus, and either filled the complete nucleolus or was localised at the nucleolar border (e.g. Figure 23 B and Figure 24 A lower panel). In a fraction of cells, M76-V5 was additionally detected in the nucleoplasm, at the nuclear border, and in the cytoplasm (e.g. Figure 24 A and B lower panel), or in the nucleoplasm, but omitted from the nucleolus (e.g. Figure 24 B lower panel). M76-V5 was expressed in the same subcellular structures in NIH3T3 cells (Figure 23) and Vero cells (Figure 24), irrespective of cell line and species, indicating that localisation was conserved in different cell lines from different species. The divergent localisation patterns of M76-V5 strongly resembled the localisation phenotypes we found for KSHV ORF20 (Figure 12), suggesting that localisation might be similar throughout the UL24 family. Moreover, this spectrum of localisation patterns, as described as different localisation phenotypes, might be part of the conserved function of the UL24 family proteins.

We detected in every untransfected NIH3T3 cell endogenous fibrillarin and eIF6 expression in the nucleolus (quantified in Figure 25 A). Equally, every LacZ transfected Vero cell showed endogenous fibrillarin, eIF6, and DDX21 expression in the nucleolus (Figure 24 A, B, and C, upper panels). The nucleolar proteins fibrillarin and eIF6 in NIH3T3 cells and fibrillarin, eIF6, and DDX21 in Vero cells colocalised with M76 in the nucleolus. We frequently observed M76 expressing cells that showed diminished nucleolar expression of fibrillarin, eIF6, or DDX21 (e.g. Figure 23 A and Figure 24 A), but we scarcely detected cells that completely lacked nucleolar localisation of these proteins. Quantification of our IF data emphasised that in NIH3T3 cells strong expression of M76 did not induce substantial dispersal of nucleolar proteins compared to untransfected cells, as more than 80% of the M76 expressing cells showed nucleolar expression of fibrillarin or eIF6 (Figure 25 A). Similarly, more than 80% of the counted Vero cells expressing M76 showed nucleolar localisation of fibrillarin, eIF6, and

DDX21, while this was the case for 100% of Vero cells transfected with the LacZ control (Figure 25 B), showing that MCMV encoded M76 only mildly induced dispersal of nucleolar proteins.

While the two UL24 protein family members KSHV ORF20 and HSV-1 UL24 disperse nucleolar proteins, we did not find that the family member M76 encoded by MCMV had this ability. Together our data suggest that targeting of nucleolar proteins might not be conserved throughout the UL24 protein family, or this function might be limited to members of the alpha- and gammaherpesviridae or to human herpesviruses. Although nucleolar localisation in the host cell was found for all described UL24 protein family members.

3.3 Confirmation of the antiviral protein OASL as a novel binding partner of KSHV ORF20

3.3.1 KSHV ORF20 interacts with the antiviral protein OASL

We identified the 2'-5'-oligoadenylate synthase-like (OASL) protein as a potential cellular interaction partner of KSHV ORF20 using the unbiased approach of affinity purification coupled to mass spectrometry (q-AP-MS), as shown earlier in Figure 15. We further analysed the interaction of ORF20 and OASL, since human OASL was shown to possess antiviral activity against a number of RNA viruses by inhibiting viral replication in OASL overexpressing cells (Marques et al. 2008, Ishibashi et al. 2010, Schoggins et al. 2011). While basal protein levels of OASL are low in most cells (Hartmann et al. 1998), OASL can be highly induced as it is a signature protein of the host response to interferon induced antiviral activity, being an interferon stimulated gene product (ISG) (De Veer et al. 2001, Rebouillat et al. 1998)

In contrast to other ISGs, OASL can not only be induced by type I IFNs, but is rapidly and strongly upregulated by interferon regulatory factor 3 (IRF3). IRF3 activation occurs downstream of RIG-I signalling and induces type I IFN transcription. As a consequence, OASL induction does not require functional IFN receptor (IFNAR) signalling, as it is already induced by PRR activation through IRF3 (Melchjorsen et al. 2009), implying an important role in innate antiviral immunity.

During the course of our studies, Zhu and colleagues published a mechanism by which OASL contributes to antiviral responses. They described that, after induction, OASL specifically binds to RIG-I and mediates further activation of RIG-I through its C-terminal ubiquitin-like (Ubi) domains by mimicking polyubiquitination (pUb), which is necessary for RIG-I activation and normally mediated by the ubiquitin ligase TRIM25. Activation of RIG-I by OASL or TRIM25 results in a RIG-I mediated type I IFN response. In detail, the authors showed that loss of OASL by RNA interference (RNAi) and transcription activator-like effector nucleases (TALEN)-mediated knockout, increased replication of the negative-sense single-stranded RNA viruses vesicular stomatitis virus (VSV), respiratory syncytial virus (RSV), and Sendai virus (SeV). In contrast, overexpression of OASL diminished replication of VSV, SeV, RSV, and the positive-sense single-stranded RNA virus dengue virus type 2 (DENV), and slightly reduced HSV-1 replication. OASL overexpression inhibited RNA virus replication only if RIG-I was expressed. Overexpression of full length OASL, but not OASL lacking its Ubi domains, enhanced RIG-I signalling

after stimulation, as measured by induction of IFNβ and different ISGs. Ablation of OASL reduced RIG-I signalling. The authors further showed interaction of OASL with RIG-I by co-IP and colocalisation of OASL and RIG-I in the cytoplasm and in puncta formed after SeV infection. More importantly, OASL overexpression rescued the induction of ISG60 expression if cotransfected with RIG-I signalling mutants having mutated ubiquitination sites, or in TRIM25 deficient cells, indicating that binding of OASL to RIG-I affected pUb of RIG-I (Zhu et al. 2014).

For human OASL, three isoforms have been described: OASL-a, OASL-b, and OASL-d (Figure 26 A). The dominant isoform OASL-a is a 59 kDa protein, encoded by a 1,5 kb mRNA. OASL-a is localised in the cytoplasm and the nucleolus of HeLa cells, and has a potential nucleolar localisation signal at its C-terminus (376-RKVKEKIRRTR-386; Figure 26 A at the top; Rebouillat et al. 1998). OASL-b, a 30 kDa protein, has a C-terminal truncation starting after aa 220, continuing with 35 aa sequence that differ from the OASL-a sequence, and thus lacks the C-terminal part of the OAS domain (aa 221–349) and the complete Ubi domains (aa 350–514; Figure 26 A in the middle; Rebouillat et al. 1998). Recently, OASL-d was discovered by RT-PCR amplification. Exon 4 and 5, encoding the second part of the OAS domain (aa 221–349), are deleted in OASL-d, resulting in a 44 kDa protein (Figure 26 A at the bottom; Guo et al. 2012). All isoforms are IFN-induced, but different IFNs induce distinct isoforms in different cell lines, e.g. OASL-d was exclusively induced by IFNγ and OASL-a by IFNβ in THP-1 cells (Guo et al. 2012). This could indicate that the OASL isoforms have discrete functions. OASL-b and OASL-d are sparsely described, while OASL-a has been analysed in most studies, e.g. in the study of Zhu and colleagues described earlier. If not indicated otherwise, the OASL-a isoform will be named OASL in the following.

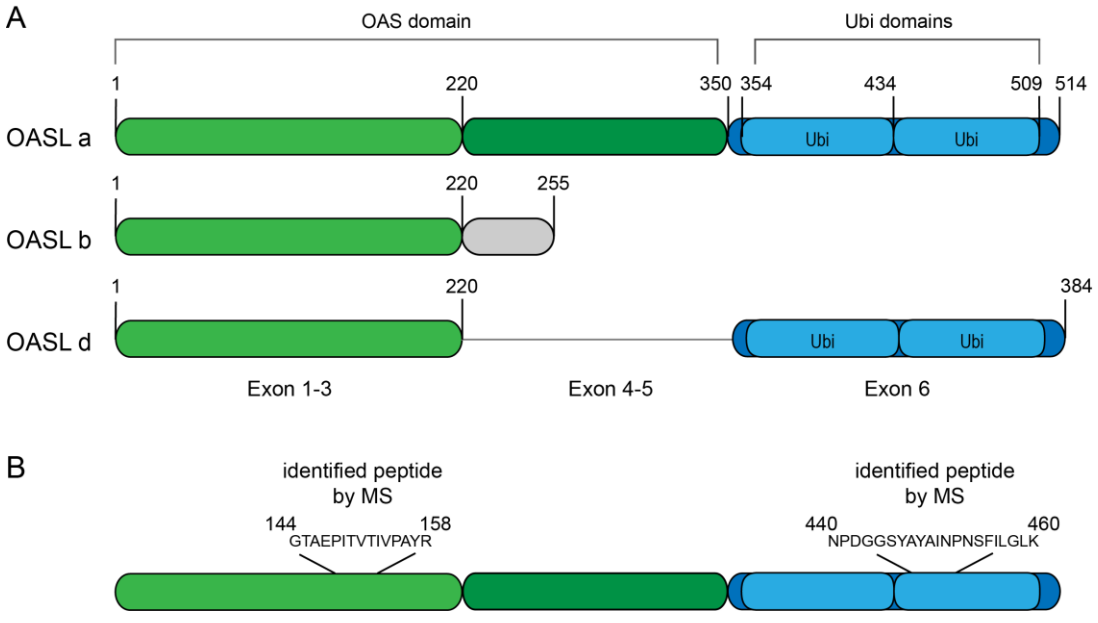

Figure 26 Human 2'-5'-oligoadenylate synthase-like (OASL) protein isoforms and OASL peptides identified by q-AP-MS of ORF20. (**A**) OASL-a is a 514 aa protein, having an N-terminal oligoadenylate synthase (OAS) domain (aa 1–349), encoded by exons 1 to 5, and two ubiquitin-like (Ubi) domains at the C-terminus (aa 354–433 and aa 434–509). OASL-b is C-terminally truncated, resulting in a 255 aa protein differing from OASL-a in the OAS domain after aa 220 and lacking the Ubi domains. OASL-d is comprised of 384 aa and lacks exons 4-5 that express the second part of the OAS domain (aa 221–349). (**B**) Two highly confident unique peptides of OASL have been identified by q-AP-MS of ORF20. The first peptide corresponds to aa 144-158 in the OAS domain, while the second peptide corresponds aa 440-460 in the Ubi domains.

KSHV ORF20 interacts with OASL by Co-IP coupled to SILAC proteomics

OASL was identified as a specific ORF20 binding partner by q-AP-MS (3.1.3. Results; Figure 15). Two highly confident peptides of OASL were identified by mass spectrometry (Figure 26 B). They were used for the calculation of heavy/light values using the program Proteome Discoverer, necessary for quantification of the interaction between bait and prey protein. The indicated OASL peptides were also manually analysed and quantified by Manfred Nimtz of the Cellular Proteome Research group (HZI).
We were wondering if the identified OASL peptides would shed light on which specific OASL isoform interacts with ORF20. The first peptide, GTAEPITVTIVPAYR, origins from the N-terminal OAS region shared by all OASL isoforms. The second peptide, NPDGGSYAYAINPNSFILGLK, located at the C-terminus in the second Ubi domain, is present in OASL-a and OASL-d, but not OASL-b. However, OASL-b cannot be excluded to interact with ORF20, since none of the peptides was exclusive for one isoform, and the first peptide could belong to all of them. To conclude, ORF20 could potentially interact with all OASL isoforms.

Confirmation of the KSHV ORF20-OASL interaction by Co-IP and Immunoblotting

Next, we aimed to verify the protein interaction of ORF20 and ORF20 B with OASL. We chose isoform OASL-a as it was described to be the most abundant isoform. Again OASL-a will further be referred to as OASL, if not indicated otherwise. We included several controls. An OASL mutant lacking the Ubi domains (OASLΔUbi) was used to analyse the impact of the Ubi domains on the binding to ORF20 and ORF20 B. OAS1 (Figure 7 Introduction), an OAS family member containing one OAS domain and a CFK motif instead of CCY in the OAS domain, allowing OAS1 to synthesise 2'-5' oligoadenylates and activate RNase L, was used as a control for specificity of the protein interaction. We received C-terminally V5-tagged OASL, OASLΔUbi, and OAS1 constructs in a pcDNA3.1 vector backbone from Rune Hartmann , Aarhus University (Marques et al. 2008). Furthermore, LacZ-myc was included as a negative control for myc-tagged ORF20 and ORF20 B.
We transfected HeLa S3 cells with myc tagged versions of ORF20, ORF20 B, or LacZ in combination with V5 tagged OASL, OASLΔUbi, or OAS1. 24 h p.t. the cells were lysed, subjected to IP using an anti-V5 antibody and protein A agarose beads, and eluates were analysed by immunoblotting with V5 and myc specific antibodies (Figure 27 A). In addition, the same experiment was performed vice versa, applying the lysates for anti-myc IP (Figure 27 B), to confirm observed protein interactions.

We verified expression of all transfected constructs by detection of the corresponding proteins at the anticipated sizes in whole cell lysates (Input) (Figure 27 A and B). We found that full length OASL-V5 co-immunoprecipitated ORF20-myc and ORF20 B-myc by anti-V5 IP, but not the control protein LacZ-myc (Figure 27 A). Similarly, ORF20-myc and ORF20 B-myc, but not LacZ-myc, co-precipitate OASL-V5 by anti-myc IP (Figure 27 B). Moreover, ORF20-myc and ORF20 B-myc interacted with OASL lacking the ubiquitin-like domain by anti-myc IP (Figure 27 B) and by anti-V5 IP (Figure 27 A). These findings confirmed our ORF20 q-AP-MS results, where we identified OASL as a potential binding partner of ORF20, and furthermore showed that the interactions of ORF20 and ORF20 B with OASL were not dependent on the Ubi domains of OASL.

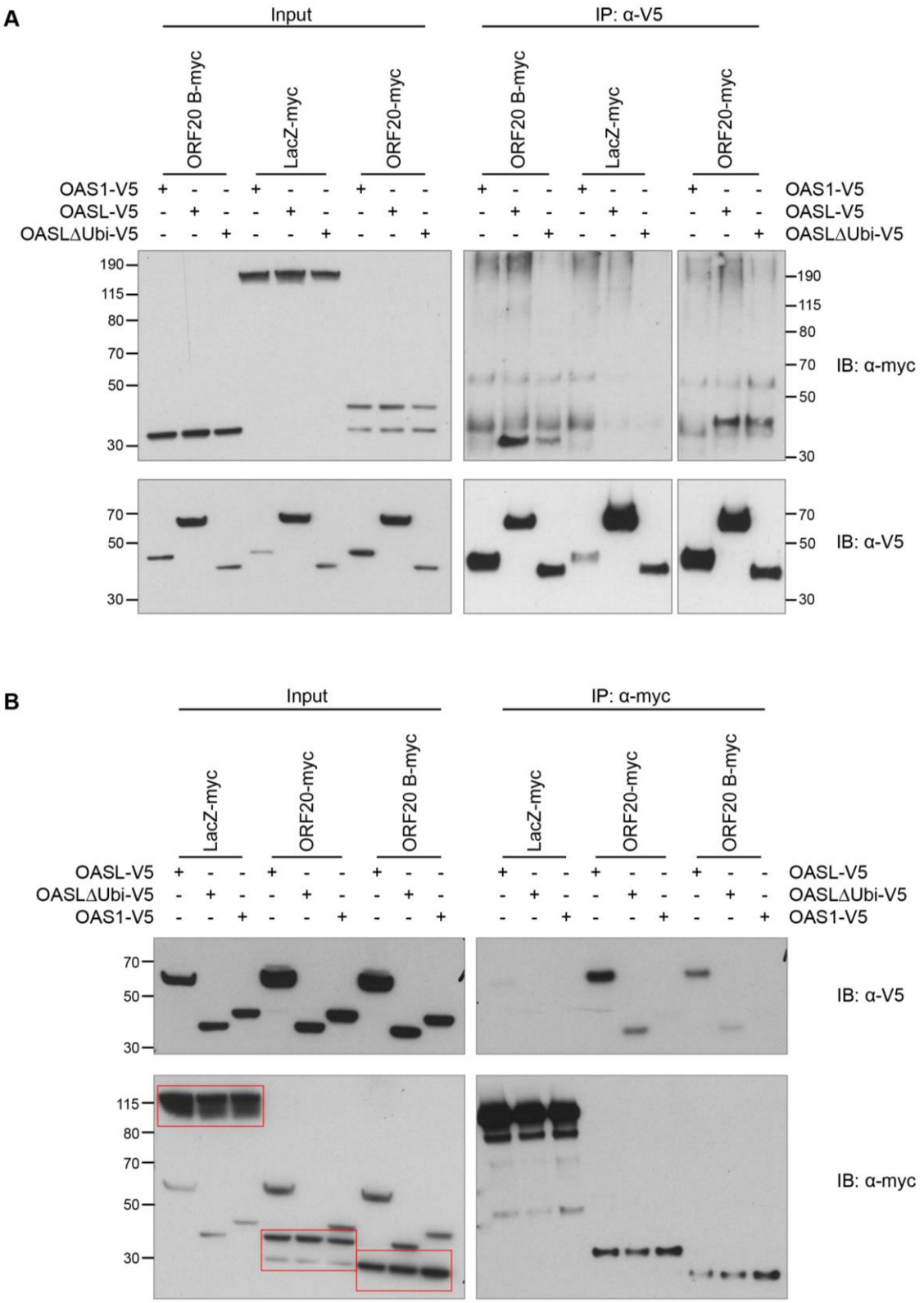

Figure 27 KSHV ORF20 and ORF20 B co-precipitate with OASL and OASLΔUbi. HeLa S3 cells were transfected with ORF20-myc, ORF20 B-myc, or LacZ-myc as a control in combination with OASL-V5, OASLΔUbi-V5, or OAS1-V5 as a control. 24 h p.t. cells were lysed in buffer containing 1% NP40 and 0.25% sodiumdeoxycholate. Lysates were subjected to anti-V5 IP (A) or anti-myc IP (B) using protein A beads. Samples were analysed by anti-myc and anti-V5 IB. Anti-Myc IP was performed twice for ORF20 B and more than three times for ORF20. Anti-V5 IP was performed once for ORF20 B and more than three times for ORF20. Red boxes in (B) highlight LacZ, ORF20, and ORF20 B expression signals in the whole cell lysates (Input). Left margin gives protein sizes in kDa.

We observed that the interaction between ORF20 and ORF20 B with OASLΔUbi-V5 was less pronounced after anti-V5 IP (Figure 27 A) and anti-myc IP (Figure 27 B), compared to the corresponding OASL-V5 samples.
This suggests that the interaction of OASLΔUbi with ORF20 or ORF20 B may be weaker than the interaction of full length OASL with ORF20 or ORF20 B. But this observation could be due to the stronger protein expression of OASL-V5 compared to OASLΔUbi-V5, as seen in the whole cell lysates. ORF20-myc and ORF20 B-myc did not co-precipitate with the OAS family member OAS1-V5 (Figure 27 A and B). This finding emphasised the specificity of the interaction of ORF20 with OASL and showed that ORF20 was specifically interacting with the OAS domain of OASL, which differs between OAS1 and OASL in small aspects like in the above mentioned CFK motif. Interestingly, only the 35 kDa but not the 29 kDa band of ORF20-myc was detected after myc-IP and after V5-IP, which might imply that the ORF20 isoforms have different binding abilities, when expressed at the same time. OASL-V5 and OASLΔ Ubi-V5 showed stronger expression signals after anti-myc IP with ORF20-myc than with ORF20 B (Figure 27 B), which might indicate that ORF20 B interacted less efficiently with full length OASL and OASL lacking the Ubi domains than ORF20.

KSHV ORF20 co-precipitates with all three OASL isoforms

To extend those findings, we studied the interaction of ORF20 with the OASL isoforms. We received N-terminally myc-tagged versions of OASL-a, OASL-b, and OASL-d in a pRK5 vector backbone from Erguang Li (Guo et al. 2012). We used myc-OASL-a as a template to clone C-terminally myc-tagged OASL-a in pcDNA3.1, to allow better comparison with OASL-V5. We transfected HeLa S3 cells with KSHV ORF20-V5 together with myc-tagged versions of OASL-a, OASL-b, OASL-d, or empty vector pcDNA3.1 as a control for background binding. We lysed the cells 24 h p.t. with IP lysis buffer containing 1% NP-40 and 0.25% sodiumdeoxycholate, as used before, and subjected the lysates to anti-myc IP. Eluates were analysed by anti-myc and anti-V5 immunoblotting (Figure 28 A).

Protein expression of the transfected constructs was verified in whole cell lysates (Figure 28 A Input). We found that the myc-tagged isoforms OASL-a and OASL-d precipitated the 35 kDa band of ORF20-V5. The 29 kDa form of ORF20-V5 was detected only very faintly after myc-IP with myc-OASL-a, which was better detectable after a longer exposure time, but is not shown here due to a simultaneous increase in background signals on the immunoblot. The weak detection of the 29 kDa band of the ORF20-derived protein suggested that the smaller form of ORF20 was able to interact with OASL-a, but less efficiently than the 35 kDa form. This observation did not seem to be due to expression differences in the 35 kDa and 29 kDa form of ORF20, as they were expressed equally in the input samples. Myc-OASL-b was detected weakly after myc-IP, which was consistent in all replicates of the experiment. This might be the reason that no detectable co-precipitation of ORF20-V5 with OASL-b-myc was observed.

Next, we wanted to perform the co-IP of ORF20-V5 with the OASL isoforms under more stringent conditions, using RIPA-100 lysis buffer for lysis of the cells and during IP, to analyse the strength of

interaction between the OASL isoforms and KSHV ORF20. We conducted the experiment as described earlier, but performed lysis and myc-IP with IP lysis buffer and RIPA-100 buffer in parallel (Figure 28 B).

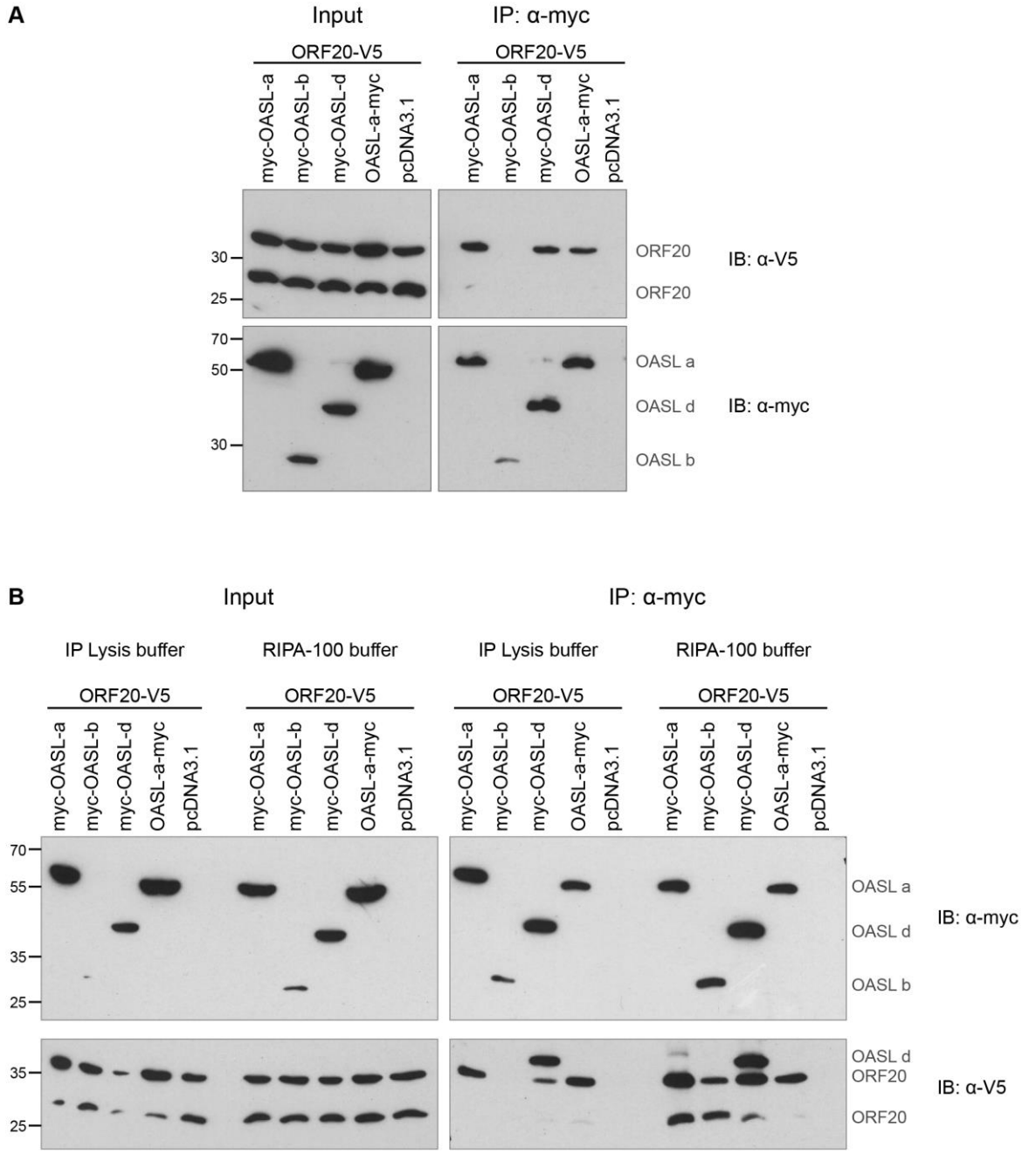

Figure 28 KSHV ORF20 co-precipitates with OASL-a and OASL-d, and weakly with OASL-b. HeLa S3 cells were transfected with ORF20-V5 and myc-tagged OASL-a, OASL-b, OASL-d, or empty vector control pcDNA3.1. 24 h p.t. cells were lysed with IP Lysis buffer containing 1% NP-40 and 0.25% sodium deoxycholate. Lysates were subjected to anti-myc IP, followed by anti-myc and anti-V5 IB of the eluates (**A**). HeLa S3 cells were transfected with ORF20-V5 and myc-tagged OASL-a, OASL-b, OASL-d, or empty vector control pcDNA3.1, lysed 24 h p.t. either with IP lysis Buffer or RIPA-100 buffer, and samples were subjected to anti-myc IP (**B**). Eluates were analysed by anti-myc and anti-V5 IB. Myc IP with IP lysis buffer was performed twice and myc-IP with RIPA-100 buffer was repeated three times. Left margin gives protein sizes in kilodaltons (kDa).

We found all transfected proteins at the anticipated sizes in whole cell lysates (Figure 28 B Input). As observed before (Figure 28 A), ORF20-V5 interacted with OASL-a and OASL-d, with the 35 kDa form of ORF20 precipitating more efficiently with the OASL isoforms than the 29 kDa form. Interestingly, we found that ORF20-V5 interacted stronger with the OASL isoforms in the presence of RIPA-100 buffer than in the presence of IP lysis buffer. With the more stringent lysis condition of RIPA-100 buffer, the ORF20-V5 signal was more pronounced and both forms of ORF20-V5 were detectable after myc-IP. Furthermore, ORF20-V5 seemed to precipitate with OASL-b, which was not observed with IP lysis buffer. This interaction seemed to be specific, as ORF20-V5 did not precipitate with the empty vector control. Considering the expression levels of the OASL isoforms in the input samples and the signal intensity of ORF20-V5 after myc-IP, ORF20-V5 seemed to interact strongly with OASL-a, moderately with OASL-d and weakly with OASL-b (Figure 28 B).

In summary, we found that ORF20 and ORF20 B interacted with the OAS domain of OASL-a, but the interaction with full length OASL-a was more pronounced in comparison to the truncated mutant of OASL lacking the Ubi domains. This suggested that the Ubi domains, are important for stable interaction of OASL and ORF20. ORF20 bound to all three OASL isoforms, yet binding to OASL-a seemed strongest and binding to OASL-b was quite weak.

3.3.2 KSHV ORF20 colocalises with OASL

We next explored whether ORF20 and OASL would colocalise within the cell, and if ORF20 could affect the cellular localisation of OASL. OASL was described to be localised in the cytoplasm and in the nucleolus of OASL-V5 transfected human epithelial HeLa and HT1008 cells (Rebouillat et al. 1998, Zhu et al. 2014). This corresponds to the subcellular localisation of ORF20, that we detected primarily in the nucleolus with additional expression in the nucleoplasm and in some cells in the cytoplasm (Figure 11). We cotransfected ORF20-myc and OASL-V5 in HeLa S3 cells and compared their localisation to cells cotransfected with LacZ-myc and OASL-V5. We also analysed localisation of OASLΔUbi-V5 expressed together with ORF20-myc or LacZ-myc, to determine the influence of the Ubi domains on the subcellular localisation of OASL and on colocalisation with ORF20. OAS1-V5 co-expressed with ORF20-myc or LacZ-myc was used as a control for the ability of ORF20 to influence localisation of cellular proteins and to determine if ORF20 unspecifically colocalised with OASL.
We transfected HeLa S3 cells with ORF20-myc or LacZ-myc in combination with OASL-V5, OASLΔUbi-V5, or OAS1-V5 and fixed the cells 24 h later. The samples were subjected to anti-myc and anti-V5 IF, and nuclei were stained with Hoechst (Figure 29).

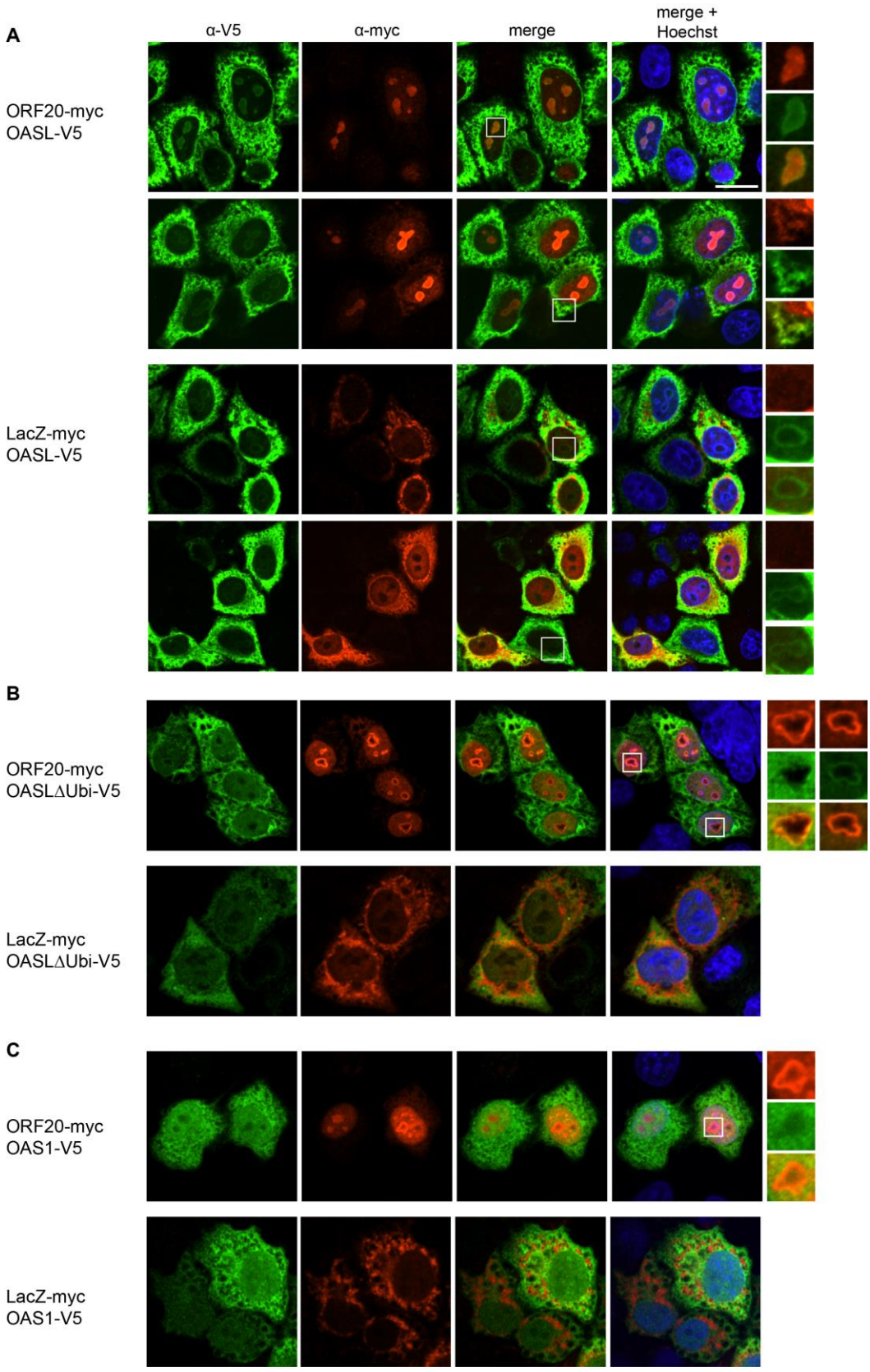

Figure 29 KSHV ORF20 colocalises with OASL in the nucleolus and in the cytoplasm. HeLa S3 cells were transfected with ORF20-myc or LacZ-myc in combination with OASL-a-V5 (**A**), OASL-aΔUbi-V5 (**B**), or OAS1-V5 (**C**). Cells were fixed 24 h p.t., subjected to anti-myc and anti-V5 IF, and staining of the DNA with Hoechst. Images were obtained by confocal microscopy with 60x magnification. Representative images of three independent experiments are shown. Two examples are shown for ORF20 and LacZ expressing cells (**A**). Scale bar 18 µm. White boxes delineate the enlarged area shown on the right side.

In accordance with previous studies, we found that OASL-V5 was expressed in the cytoplasm but not in the nucleoplasm, and in the majority of the cells OASL-V5 showed additional expression in the nucleolus or in ring-like structures at the border of the nucleolus that probably represented the GC region (Figure 29 A). We found that ORF20-myc and OASL-V5 colocalised in nucleolar structures (Figure 29 A first panel) and to some extent in the cytoplasm, if ORF20-myc was present in the cytoplasm (Figure 29 A second panel). OASL-V5 was expressed in the same subcellular regions in the presence of ORF20-myc or LacZ-myc, showing that ORF20 did not alter localisation of OASL (Figure 29 A).
OASLΔUbi-V5 was expressed in the cytoplasm, but in contrast to full length OASL, it was localised in the nucleoplasm but not in the nucleolus (Figure 29 B). A small number of cells showed nucleolar instead of nucleoplasmic expression of OASLΔUbi-V5 (Figure 29 B first panel, left enlarged area). The altered localisation of OASLΔUbi-V5 could indicate that the Ubi domains of OASL are involved in the nucleolar localisation of OASL, as in their absence we detected a broad nuclear distribution for OASLΔUbi-V5. This is consistent with the predicted nucleolar localisation signal of OASL, located in the Ubi domains (Rebouillat et al. 1998). But as a minority of OASLΔUbi-V5 expressing cells did show nucleolar localisation, nucleolar localisation of OASL could also be regulated indirectly, maybe through interaction with other, unknown proteins (Figure 29 B second panel, right enlarged area).
Cytoplasmic expressed ORF20-myc colocalised with cytoplasmic OASLΔUbi-V5 and nucleolar expressed OASLΔUbi-V5 colocalised with ORF20-myc in the nucleolus (Figure 29 B, first panel). Colocalisation of ORF20-myc and OASLΔUbi-V5 was less frequently observed, than for ORF20-myc and full length OASL (Figure 29 A second panel).
OAS1 was detected equally distributed in the cytoplasm and in the nucleoplasm, being slightly reduced in the nucleolus. OAS1 did not colocalise with ORF20 and OAS1 localisation was not altered in cells expressing ORF20-myc (Figure 29 C).

These results strengthened our findings that ORF20 interacted with both, OASL and OASLΔUbi, although interaction with OASL lacking the Ubi domains seemed to be reduced compared to full length OASL. ORF20 did not colocalise and interact with OAS family member OAS1, underlining the specificity of the interaction between ORF20 and OASL.

3.3.3 Subcellular localisation of OASL isoforms

Next we wanted to analyse the subcellular localisation of the three described OASL isoforms OASL-a, OASL-b, and OASL-d. We wanted to determine differences and similarities in their cellular expression, as this has not been studied before. These findings could help to draw back conclusions about distinct functions of the isoforms and the influence of their domains on their localisation. Furthermore, we will compare localisation of the OASL isoforms to the localisation of KSHV ORF20, to affirm our protein interaction studies between ORF20 and the OASL isoforms. As mentioned earlier, OASL-a has been described to be localised in the cytoplasm and in the nucleolus (Rebouillat et al. 1998; Zhu et al. 2014), and one study described that OASL-b is expressed in the cytoplasm (Rebouillat et al. 1998). Localisation of OASL-d has not been published. As a control for nucleolar localisation, we used anti-fibrillarin staining of the cells to visualize the nucleolus.

We transfected HeLa S3 cells with N-terminally myc-tagged OASL-a, OASL-b, OASL-d, or C-terminally myc-tagged ORF20, fixed the cells 24 h p.t., and performed anti-myc and anti-fibrillarin IF and Hoechst staining of the DNA. IF images of the subcellular localisation of OASL-isoforms are shown in Figure 30.

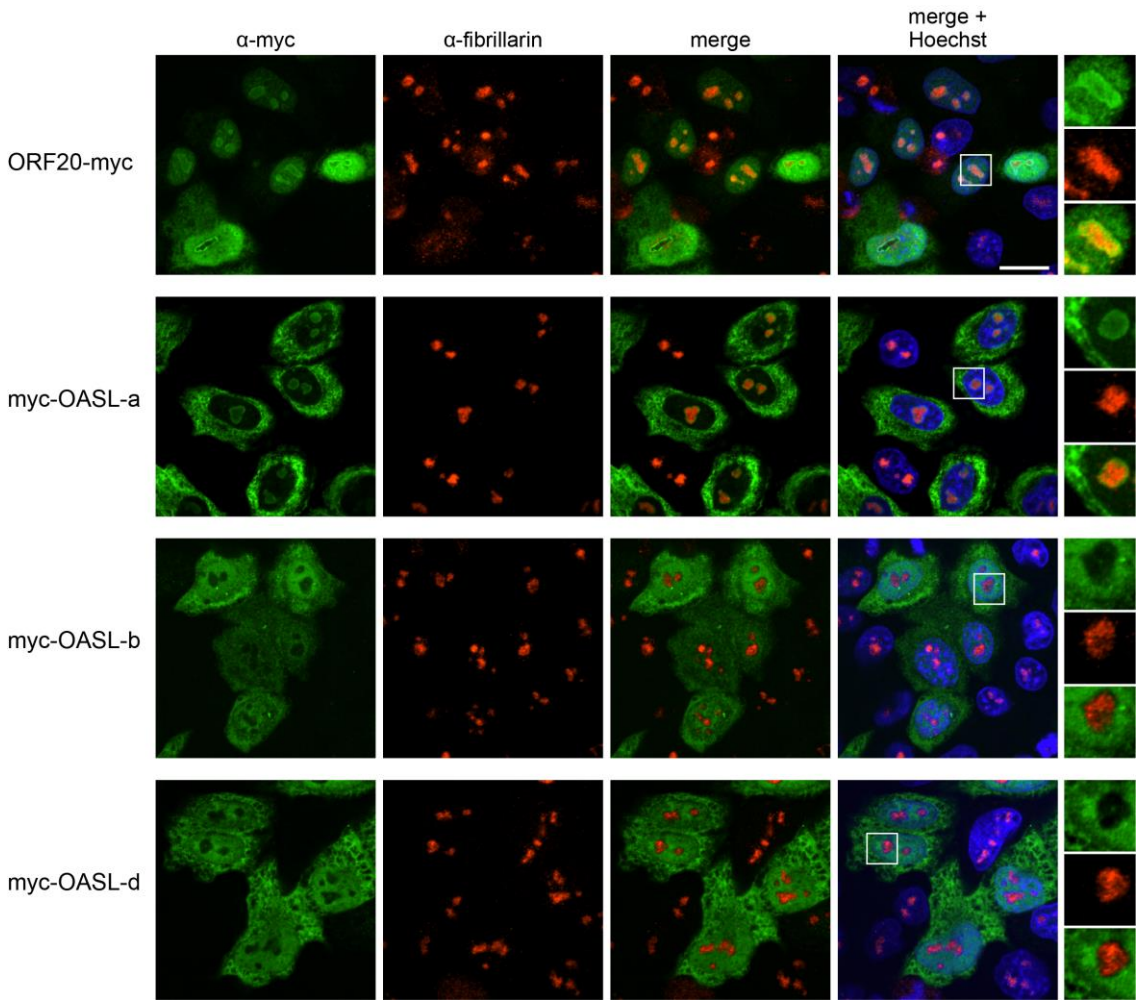

Figure 30 Human OASL-a is localised in the cytoplasm and in the nucleolus, while OASL-b and OASL-d are localised in the cytoplasm and in the nucleoplasm. HeLa S3 cells were transfected on glass coverslips with myc-OASL-a, myc-OASL-b, myc-OASL-d, or ORF20-myc. Cells were fixed at 24 h p.t. with methanol and 4% PFA and were subjected to IF with anti-myc and anti-fibrillarin antibodies. DNA was stained with Hoechst. Images were obtained by confocal microscopy with 60x magnification. Representative images of two independent experiments are shown. White boxes delineate the enlarged area shown on the right side. Scale bar 18 µm.

As observed for OASL-a-V5 (Figure 29), we detected myc-OASL-a in the cytoplasm and in the nucleolus, where it colocalised with the nucleolar protein fibrillarin. OASL-a was omitted from the nucleoplasm in all transfected cells. OASL-b and OASL-d showed similar localisation, as they were expressed in the cytoplasm and in the nucleoplasm. Both isoforms were excluded from the nucleolus and did consequently not colocalise with fibrillarin. OASL-d shares the Ubi domains with OASL-a, which possess the potential nucleolar localisation signal (NoLS) (Rebouillat et al. 1998). However, OASL-d was not expressed in the nucleolus, indicating that the predicted localisation signal may not be a true NoLS. This was in accordance with our observation that the lack of the Ubi domains did not completely diminish nucleolar localisation of OASL-a, as shown with the mutant OASLΔUbi-V5 (Figure 29 B). This suggested that the Ubi domains are not essential for nucleolar localisation of OASL. Nucleolar localisation seemed to be specific for OASL-a and not dependent on the Ubi domains or the region

encoded by exons 1-3 that is present in both OASL-a and OASL-d. However, the region encoded by exons 4-5 is only present in OASL-a (Figure 26 A) and might comprise a signal that enables OASL-a to localise to the nucleolus. Nonetheless, nucleolar localisation of OASL-a could be regulated by a different mechanism such as protein-protein interaction or posttranscriptional modification.

Due to its nucleolar localisation (Figure 30), OASL-a was the only isoform able to colocalise with ORF20 in the nucleolus, and we have shown earlier that ORF20-myc and the C-terminally V5-tagged OASL-a colocalised in the nucleolus (Figure 29 A). OASL-a, OASL-b, and OASL-d are all expressed in the cytoplasm, where they potentially could interact with ORF20 (Figure 30), which we have observed by co-precipitation of the proteins (Figure 28), although a post-lysis interaction during precipitation cannot be excluded.

3.3.4 KSHV ORF20 does not inhibit colocalisation and interaction of OASL and RIG-I

Human OASL was shown to interact with RIG-I, thereby activating RIG-I through its ubiquitin-like (Ubi) domains, which substitutes for polyubiquitination (pUb) of RIG-I that is usually mediated by interaction with TRIM25. OASL amplified the RIG-I signalling cascade leading to a more potent activation of type I IFNs and induction of ISG expression (Zhu et al. 2014).

We have found that KSHV ORF20 expression significantly inhibited RIG-I-mediated activation of IFNβ and IFNα4 reporters (Figure 9). Furthermore, we observed that ORF20 interacted with OASL (Figure 15 and Figure 27), prompting us to ask whether ORF20 negatively regulated RIG-I signalling by influencing the ability of OASL to activate RIG-I. We first analysed whether ORF20 was able to prevent the interaction between RIG-I and OASL and thereby inhibited activation of RIG-I signalling mediated by OASL.

KSHV ORF20 does not influence localisation of OASL and RIG-I

Zhu and colleagues showed colocalisation of endogenous RIG-I with stably expressed OASL-V5 in the cytoplasm of human epithelial HT1080 cells. Colocalisation is a prerequisite for interaction of proteins. We investigated whether expression of ORF20 influenced the subcellular localisation of OASL and RIG-I, or prevented their colocalisation. To do this, we analysed the localisation of transiently expressed OASL and RIG-I in HeLa S3 cells in the presence and absence of KSHV ORF20 by IF microscopy (Figure 31).

We transfected HeLa S3 cells with ORF20-myc, OASL-V5, and N-terminally Flag-tagged RIG-I in a 1:1:1 ratio. As controls, localisation of each protein alone (Flag-RIG-I, OASL-V5, or ORF20-myc), or localisation of Flag-RIG-I co-expressed either with OASL-V5 or ORF20-myc was analysed. To maintain a 1:1:1 DNA ratio in the control samples, the samples were supplemented with appropriate amounts of empty vector pcDNA3.1 for transfection. The cells were fixed 24 h later, substituted for IF using anti-myc, anti-V5, and anti-Flag antibodies and Hoechst staining and were analysed by confocal microscopy.

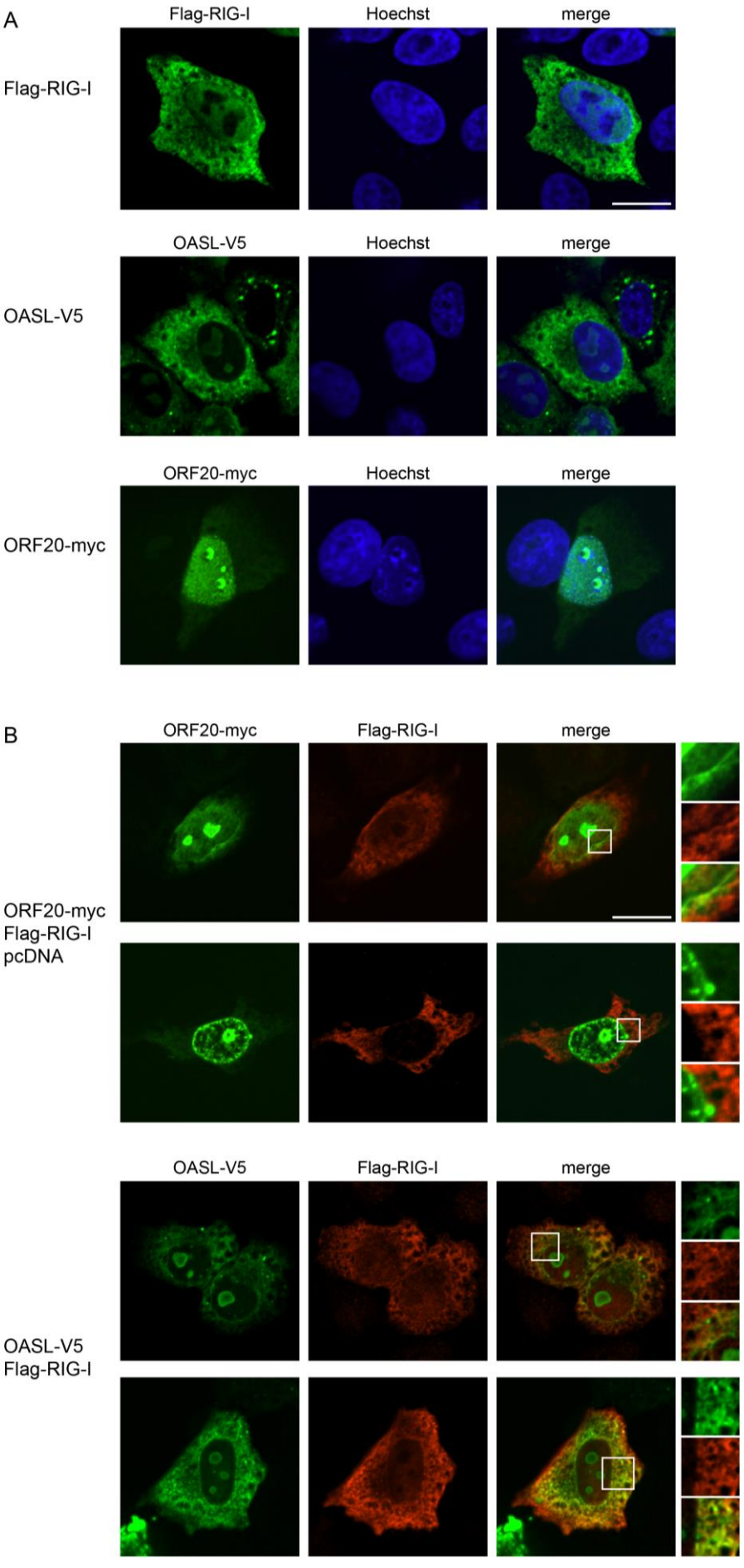
A
Flag-RIG-I
Hoechst
merge
Flag-RIG-I
OASL-V5
Hoechst
merge
OASL-V5
ORF20-myc
Hoechst
merge
ORF20-myc
B
ORF20-myc
Flag-RIG-I
merge
ORF20-myc
Flag-RIG-I
pcDNA
OASL-V5
Flag-RIG-I
merge
OASL-V5
Flag-RIG-I

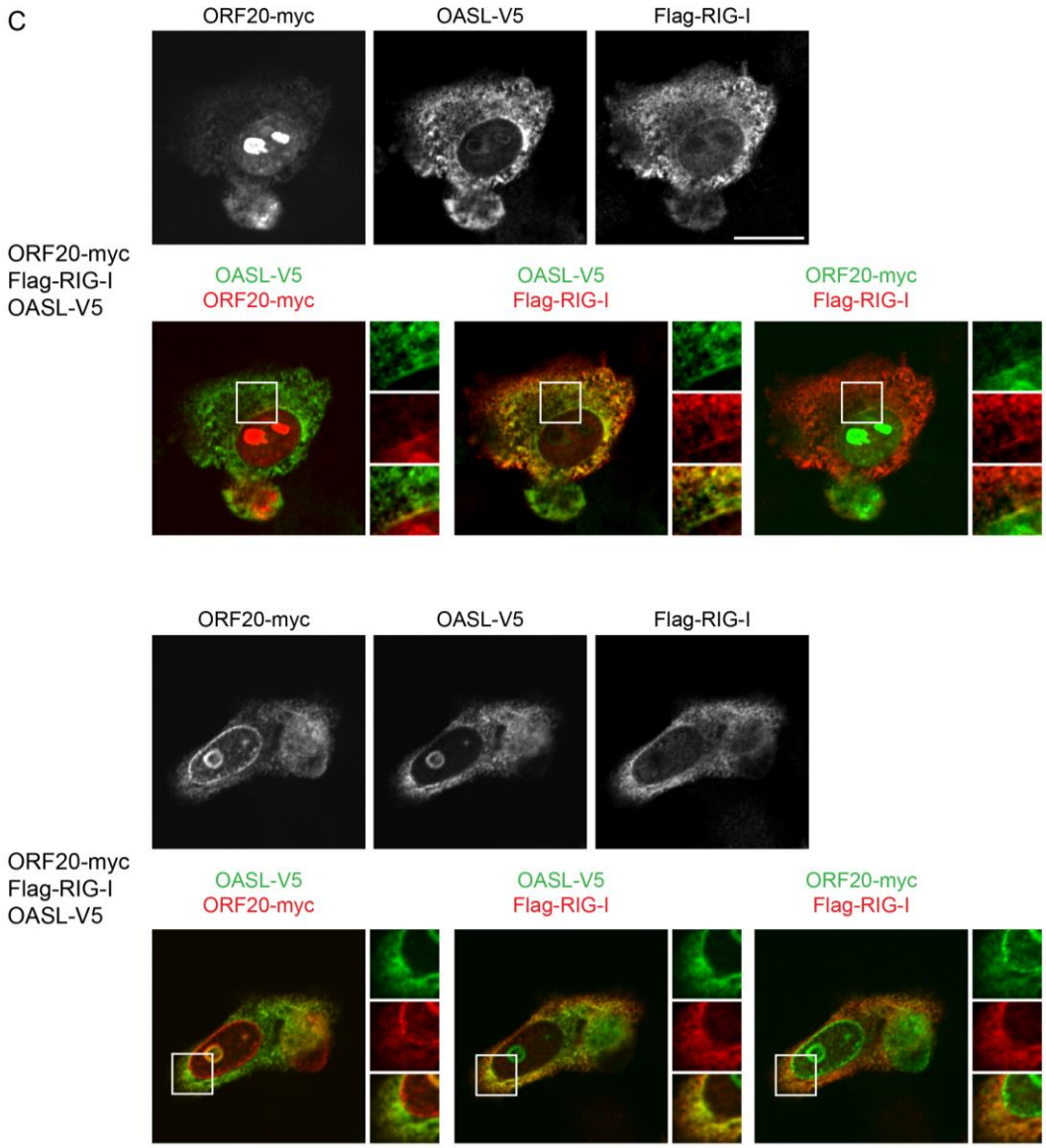

Figure 31 KSHV ORF20 does not influence colocalisation of OASL and RIG-I in the cytoplasm of HeLa S3 cells. Cells were transfected either with Flag-RIG-I, OASL-V5, or ORF20-myc in combination with empty vector pcDNA3.1 in a 1:2 ratio (**A**). Cells were transfected with Flag-RIG-I and empty vector pcDNA3.1 in combination with OASL-V5, or ORF20-myc in a 1:1:1 ratio (**B**). Cells were cotransfected with Flag-RIG-I, OASL-V5, and ORF20-myc in a 1:1:1 ratio (**C**). Cells were fixed on glass coverslips 24 h p.t. with methanol and 4% PFA. Samples were subjected to anti-myc, anti-V5, and anti-Flag IF and Hoechst staining of the DNA. Images were obtained by confocal microscopy with 60x magnification. Representative images of two independent experiments are shown. White boxes delineate the enlarged area shown on the right side. Scale bar 18 µm.

The control samples with the singly transfected constructs showed, as expected, that RIG-I was mainly localised in the cytoplasm, weakly in the nucleus, and absent from the nucleolus. OASL was localised in the cytoplasm and in the nucleolus, being enriched at the nucleolar border. ORF20 was mainly expressed in the nucleolus, but also detectable in the nucleoplasm and occasionally in the cytoplasm (Figure 31 A). We found colocalisation of OASL and RIG-I in the cytoplasm, as both proteins were expressed with a similar distribution in the cytoplasm, although OASL showed a more distinct perinuclear expression than RIG-I (Figure 31 B). No clear colocalisation was observed for cytoplasmic expressed KSHV ORF20 and RIG-I in the cytoplasm (Figure 31 B).

Analysing RIG-I, OASL, and ORF20 cotransfected cells, we found that expression of ORF20 did not alter the cellular distribution of OASL and RIG-I (Figure 31 C), since their subcellular distribution and cytoplasmic localisation was identical in the control samples that expressed only RIG-I, or OASL (Figure 31 A), or co-expressed RIG-I and OASL (Figure 31 B). Instead, cytoplasmic expressed ORF20, RIG-I, and OASL showed partial colocalisation in the cytoplasm, while simultaneously ORF20 and OASL clearly colocalised at the nucleolar border. RIG-I was not expressed in the nucleolus in the presence of ORF20 and OASL (Figure 31 C).
Our findings confirmed the published colocalisation of OASL and RIG-I in the cytoplasm and showed that KSHV ORF20 did not manipulate the localisation of either OASL or RIG-I, and consequently did not modulate the colocalisation of OASL and RIG-I.

KSHV ORF20 does not inhibit co-immunoprecipitation of OASL and RIG-I

We next wanted to investigate whether ORF20 inhibited interaction of OASL and RIG-I. OASL-V5 was shown to co-precipitate with Flag-tagged RIG-I by anti-Flag IP in HEK293T cells (Zhu et al. 2014). We aimed to reproduce the experiment published by Zhu and colleagues and to subsequently analyse whether OASL and RIG-I were interacting with each other in the presence of ORF20-myc expression.
We transfected HEK293T cells with Flag-RIG-I, OASL-V5, and KSHV ORF20-myc in a 1:1:1 ratio. Cells cotransfected with Flag-RIG-I and OASL-V5 served as positive control, since both proteins are known to co-precipitate. To maintain the DNA ratio, the constructs were cotransfected with empty vector pcDNA3.1 in a 1:1:1 ratio. In addition, RIG-I was cotransfected with ORF20-myc and empty vector pcDNA3.1, to determine if ORF20 was able to interact directly with RIG-I in the absence of OASL-V5. Flag-RIG-I, OASL-V5, and ORF20-myc were each transfected in a 1:2 ratio with pcDNA3.1 to control for unspecific binding of the proteins. The cells were lysed 36 h p.t. and were subjected to anti-Flag IP using anti-Flag antibody and protein G linked magnetic beads. The samples were analysed by immunoblotting using anti-Flag, anti-V5, and anti-myc antibodies (Figure 32).

Analysis of whole cell lysates (Input) showed that all transfected constructs were expressed. Flag-tagged RIG-I was detected at a size of about 110 kDa, representing RIG-I isoform 1, with a predicted size of about 107 kDa. The RIG-I construct seemed to additionally express a 90 kDa protein. The 90 kDa protein was not detected after anti-Flag IP. This appearance of Flag-RIG-I protein before and after IP was in accordance with the results shown by Zhu and colleagues. As described before, OASL-V5 was detected at about 60 kDa and KSHV ORF20-myc was expressed as a double band with an apparent weight of 29 kDa and 35 kDa.
We found that Flag-RIG-I co-precipitated OASL-V5, confirming the published data by Zhu and colleagues. Moreover, Flag-RIG-I co-precipitated OASL-V5 in the presence of KSHV ORF20-myc, and additionally bound ORF20-myc. Flag-RIG-I did not precipitate KSHV ORF20-myc in the absence of OASL-V5, showing that ORF20 did not directly interact with RIG-I. However, KSHV ORF20 co-precipitated with Flag-RIG-I when OASL was present. ORF20 did not affect the interaction between RIG-I and OASL, yet was detected in a protein complex with OASL and RIG-I.

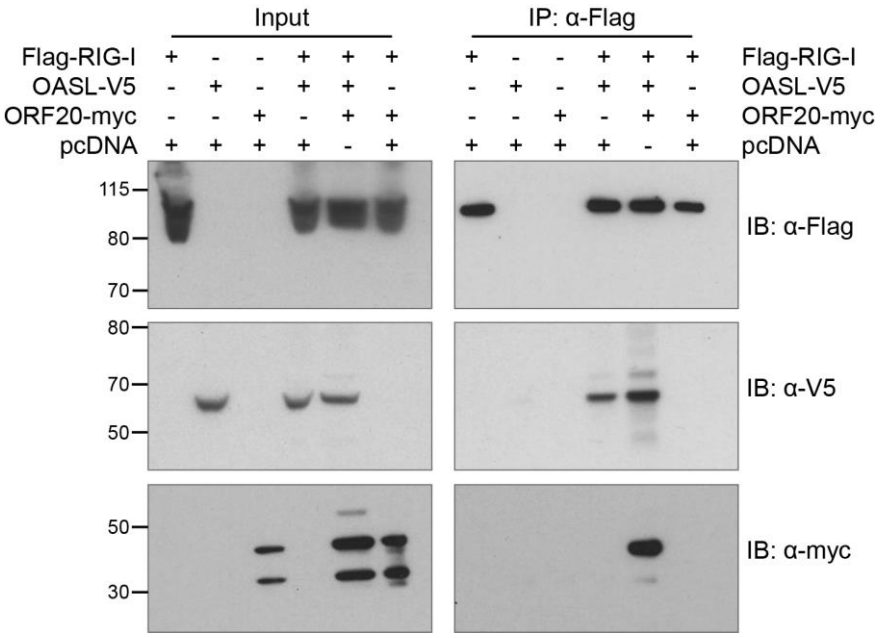

Figure 32 KSHV ORF20 co-precipitates with RIG-I and OASL and does not inhibit binding of OASL and RIG-I. HEK293T cells were either transfected in a 2:1 with pcDNA3.1 and Flag-RIG-I, OASL-V5, or ORF20-myc, or in a 1:1:1 ratio with Flag-RIG-I combined with OASL-V5 and pcDNA3.1, OASL-V5 and ORF20-myc, or ORF20-myc and pcDNA3.1. Cells were lysed 36 h p.t. in buffer containing 1% NP40 and 0.25% sodiumdeoxycholate. Lysates were subjected to anti-Flag IP using anti-Flag antibody and protein G magnetic beads. Samples were analysed by anti-Flag, anti-V5, and anti-myc immunoblotting on the same membrane. Two independent experiments were performed. Left margin gives protein sizes in kilo Daltons (kDa).

To extend those findings we repeated the co-IP experiment of RIG-I, OASL, and KSHV ORF20, but instead of using an anti-Flag IP to co-precipitate binding partners of RIG-I, we performed an anti-V5 IP to detect binding to OASL-V5. The anti-V5 IP was repeated in two independent experiments (data not shown). As observed before (Figure 27), ORF20 co-precipitated with OASL. Importantly, we found that OASL-V5 interacted with Flag-RIG-I in the absence and presence of ORF20-myc, whereby co-expressed ORF20-myc co-precipitated with OASL and RIG-I, confirming our results obtained by anti-Flag IP (Figure 32).

In summary we found that transiently expressed RIG-I and OASL colocalised in the cytoplasm and interacted with each other by co-IP, being in accordance with published data (Zhu et al. 2014). KSHV ORF20 did not interfere with this interaction, but partially colocalised with RIG-I and OASL in the cytoplasm and moreover co-precipitated with the RIG-I/OASL complex. ORF20 did not interact with RIG-I in the absence of OASL, suggesting that ORF20 indirectly bound to RIG-I by interacting with OASL.

3.3.5 OASL induces IRF3 nuclear translocation

The receptor RIG-I detects RNA derived from RNA and DNA viruses. Binding of these RNAs activates RIG-I and triggers interaction with its adaptor protein MAVS at the mitochondria. MAVS consequently forms aggregates and promotes a signalling cascade that leads to the activation of interferon regulatory factors (IRFs) by phosphorylation. IRFs subsequently dimerise and translocate to the nucleus where they act as transcription factors. IRF3 is an essential transcription factor for IFNβ transcription (reviewed

by Dixit & Kagan 2013). Detection of IRF3 nuclear translocation upon RIG-I activation is a suitable method to measure functional RIG-I signalling far downstream in the signalling cascade.
Human OASL was described to enhance RIG-I signalling. Zhu and colleagues used HEK293T cells stably expressing OASL and infected these cells with the single stranded (ss) RNA virus SeV for 12 h and analysed IRF3 dimerization by native-PAGE followed by anti-IRF3 immunoblotting and measured nuclear IRF3 in nuclear cell extracts by anti-IRF3 immunoblotting. The OASL HEK293T cell line showed slightly enhanced IRF3 dimerization and IRF3 nuclear translocation compared to control HEK293T cells, though expression of OASL was not shown in these experiments (Zhu et al. 2014).

We aimed to confirm that OASL was able to induce RIG-I signalling and subsequent nuclear translocation of IRF3. For that, we quantified nuclear IRF3 after infection with the ssRNA virus NDV in HeLa S3 cells using anti-IRF3 IF microscopy.
Firstly, we analysed localisation of IRF3 in HeLa S3 at various time points after NDV infection. The cells were either mock infected by adding medium or were infected with NDV for 1 h. The samples were fixed and subjected to IF with an anti-IRF3 antibody. We found nuclear localisation to peak at 12 h post infection (p.i.) (data not shown). The 12 h time point was consequently chosen for further stimulation experiments with NDV.
We transiently transfected HeLa S3 cells with OASL-V5, protein LacZ-myc as a control, or left the cells untransfected to control for transfection-based effects on IRF3 localisation. We additionally analysed cells transfected the OASLΔUbi mutant, as these domains were described to be indispensable for OASL function and enhancement of the RIG-I signalling pathway. The samples were mock infected or infected with NDV, fixed 12 h p.i., and were subjected to IF with an anti-IRF3 antibody in combination with an anti-myc or an anti-V5 antibody and analysed by confocal microscopy (Figure 33). To quantify nuclear localisation of IRF3, more than 64 transfected cells per sample or more than 200 untransfected cells in the untransfected control sample were counted and analysed for nuclear IRF3 expression. The number of transfected cells that showed nuclear IRF3 localisation was compared to the total number of transfected cells that were counted, likewise was the number of untransfected cells that showed nuclear IRF3 expression compared to the total number of untransfected cells that were counted (Figure 34).

We found cytoplasmic localisation of IRF3 in the vast majority of unstimulated untransfected HeLa S3 cells and no nuclear localisation of IRF3. Nuclear expression of IRF3 with only weak expression in the cytoplasm was detected in 8 of 217 unstimulated and untransfected cells (3,7%). At 12 h p.i. with NDV, nuclear localisation of IRF3 was detected in 58 of 319 cells (18,2%) (Figure 33 A and Figure 34). Similarly, nuclear localisation of IRF3 was rarely detected in unstimulated cells expressing LacZ-myc (1,2%), but was frequently detected at 12 h p.i. (46,9%) (Figure 33 B and Figure 34). These controls showed that, independent of transfection, IRF3 was mainly localised in the cytoplasm in unstimulated cells, but translocated to the nucleus in a clearly measurable manner 12 h after stimulation of the RIG-I signalling pathway with NDV.

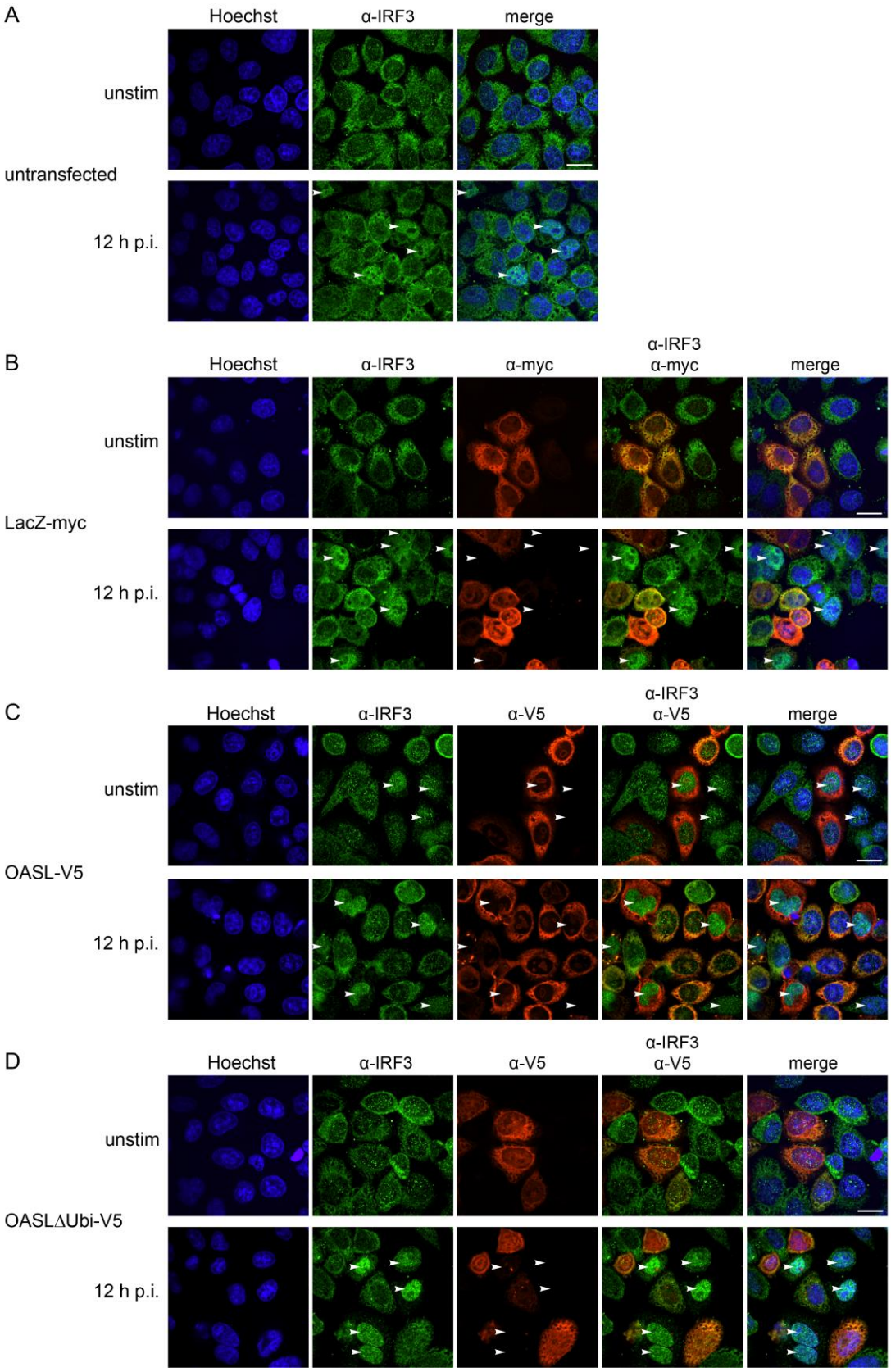

Figure 33 OASL expression enhances nuclear IRF3 localisation in unstimulated and NDV infected HeLa S3 cells. Untransfected cells or cells transfected with OASL-V5, OASLΔUbi-V5, or LacZ-myc as a control, were mock infected or were infected with NDV. Cells were fixed with methanol and 4% PFA 12 h p.i. and samples subjected to IF with anti-IRF3 and anti-myc, or anti-IRF3 and anti-V5 antibodies. DNA was stained with Hoechst. Experiment was performed once. Images were obtained by confocal microscopy with 60x magnification. White arrows heads indicate cells that show nuclear IRF3 expression. Scale bar 18 µm.

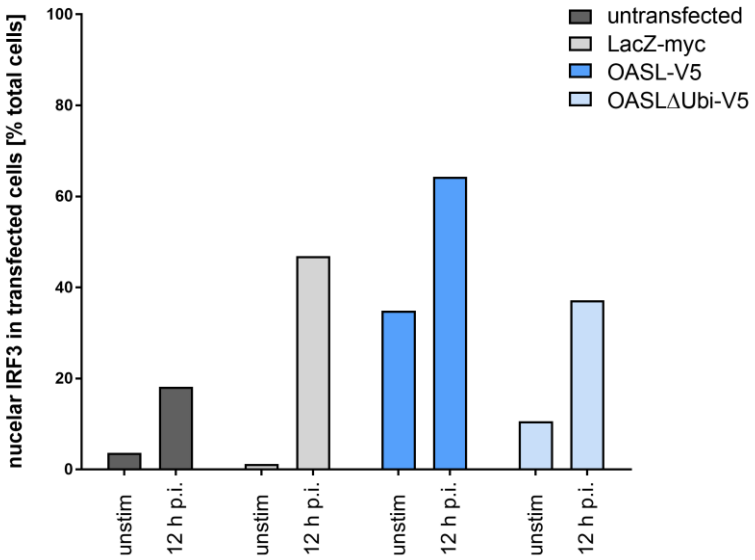

Figure 34 Nuclear localisation of IRF3 is enhanced in OASL but not OASLΔUbi expressing cells. HeLa S3 cells were left untransfected or were transfected with OASL-V5, OASLΔUbi-V5, or LacZ-myc as a control. Cells were mock infected or were infected with NDV. Samples are prepared as described in Figure 33. Per sample, more than 64 transfected or more than 200 untransfected cells were analysed for nuclear IRF3 expression. The percentage of cells that showed nuclear IRF3 localisation in the indicated sample is shown. Experiment was performed once.

In contrast, we found an increased number of cells with IRF3 nuclear localisation that expressed OASL under unstimulated as well as stimulated conditions (Figure 33 C). We detected nuclear IRF3 in 30 of 86 cells expressing OASL-V5 under unstimulated conditions (34,9%), while in LacZ-myc expressing cells 1 of 84 cells presented nuclear IRF3 (1,2%) (Figure 34). In NDV stimulated cells 92 of 143 cells expressing OASL-V5 (64,3%) and 30 of 64 cells expressing LacZ-myc (46,9%) showed nuclear IRF3 localisation, indicating that OASL expression further enhanced NDV stimulated IRF3 nuclear localisation. OASLΔUbi expressing cells, however, showed an IRF3 localisation comparable to the controls, as nuclear IRF3 localisation was detected in 10 of 94 unstimulated OASLΔUbi-V5 expressing cells (10,6%) and in 26 of 70 stimulated OASLΔUbi-V5 expressing cells (37,1%) (Figure 33 D and Figure 34).

Our data show that OASL overexpression enhanced nuclear IRF3 localisation after activation of RIG-I by the RNA virus NDV, being in accordance with the published data of Zhu and colleagues. Moreover, we found that OASL expression alone lead to an increased nuclear localisation of IRF3, in the absence of the RIG-I inducing signal by NDV. The OASLΔUbi mutant did not show these abilities, indicating that the Ubi domains were substantial for OASL to induce and enhance nuclear IRF3 localisation.

3.3.6 KSHV ORF20 alters IRF3 nuclear translocation

We have previously shown that expression of ORF20 diminished induction of IFNβ and IFNα4 transcription upon NDV-induced RIG-I signalling (Figure 9). Since we found ORF20 to interact with OASL, which enhances RIG-I signalling, we hypothesised that ORF20 might interfere with RIG-I signalling through interaction with OASL. As this protein interaction would be upstream of IRF3 activation, a reduced nuclear translocation of IRF3 should be detectable in ORF20 expressing cells compared to LacZ expressing cells or untransfected cells. In contrast, if ORF20 would interfere with type

I IFN transduction downstream of IRF3, we would expect to see no difference in IRF3 translocation upon RIG-I signalling.

Similar to the experiment described in 3.3.5, we analysed whether expression of KSHV ORF20 influenced nuclear localisation of IRF3 in unstimulated and NDV infected HeLa S3 cells. Briefly, HeLa S3 cells were transfected with ORF20-myc, while untransfected cells und LacZ-myc transfected cells served as controls. 24 h p.t. the cells were mock treated, or infected with NDV for 1 h. 12 h later, the samples were fixed and subjected to anti-IRF3 and anti-myc IF and analysed by confocal microscopy (Figure 35).

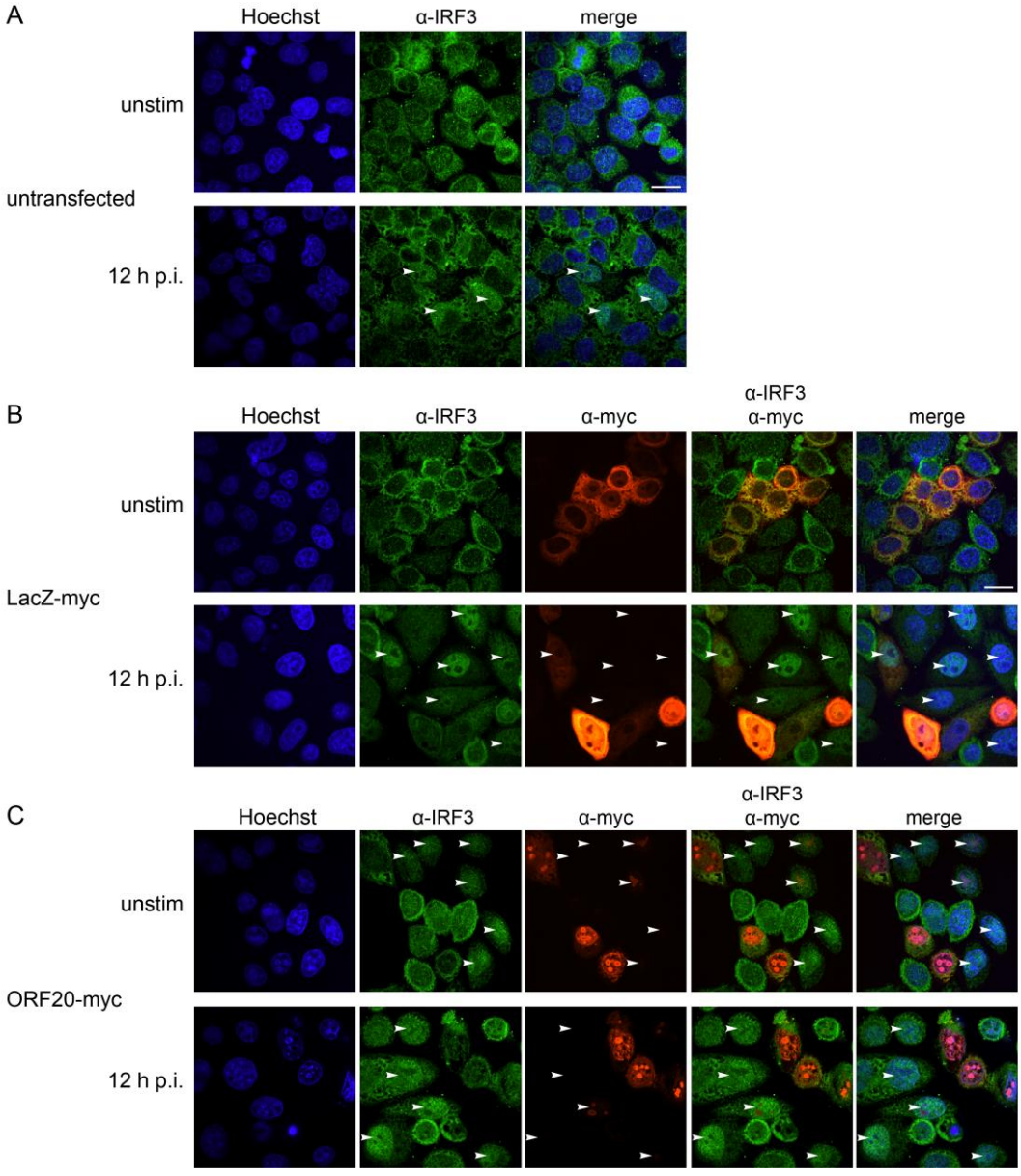

Figure 35 Localisation of IRF3 is altered in ORF20 expressing cells. HeLa S3 cells were transfected with ORF20-myc, while LacZ-myc transfected cells and untransfected cells served as control. 24 h later, cells were mock infected in medium without NDV, or were infected with NDV. Cells were fixed with methanol and 4% PFA 12 h later. Samples were subjected to anti-IRF3 and anti-myc IF and Hoechst staining. Images were obtained by confocal microscopy with 60x magnification. White arrow heads indicate nuclear localisation of IRF3. Images are representative of two independent experiments. Scale bar is 18 µm.

We found that LacZ-myc expressing cells very rarely showed nuclear localisation of IRF3 under unstimulated conditions. In these cells, IRF3 was clearly localised in the cytoplasm and not in the nucleus (Figure 35 A and B, upper panels). Nuclear IRF3 localisation, indicated by distinct expression of IRF3 in the nucleoplasm but omitted from the nucleolus, and fainter expression in the cytoplasm, was observed 12 h after infection with NDV in untransfected and LacZ-myc expressing cells (Figure 35 A and B, lower panels, white arrow heads). In accordance with our previous results (Figure 33), LacZ-myc transfected and untransfected cells showed comparable nuclear IRF3 localisation under unstimulated and stimulated conditions, indicating that the transfection itself did not significantly induce IRF3 translocation.
Localisation of IRF3 looked different in cells transfected with ORF20-myc compared to cells expressing LacZ-myc and untransfected cells. Here, in many unstimulated cells IRF3 was not equally distributed throughout the cytoplasm and seemed to be localised at the nuclear periphery and diffusely in the nucleus, including the nucleolus. This phenotype was not limited to ORF20-myc expressing cells, but was also observed in the surrounding untransfected cells (Figure 35 C upper panel, white arrow heads). Upon NDV infection (Figure 35 C lower panel) some untransfected cells and ORF20-myc expressing cells showed a faint nuclear IRF3 signal, that might have been due to nuclear translocation of IRF3 (Figure 35 C, white arrow heads). But since we could not reliably differentiate between cells showing distinct nuclear or cytoplasmic localisation of IRF3, quantification of nuclear IRF3 localisation in these images was not possible.

Our results showed that ORF20 expression caused an altered localisation of IRF3 in untransfected and RIG-I stimulated cells, as observed by absence of a proper nuclear IRF3 localisation. Our results may suggest that ORF20 manipulates IRF3 localisation or interferes with a proper IRF3 nuclear translocation, and thereby inhibits type I IFN transcription, as observed in our receptor assays (3.1.1 and 3.3.10).

3.3.7 OASL enhances RIG-I-induced ISG expression

Expression of ISGs are strongly induced through type I IFNs. The proteins ISG56 and ISG60 belong to the IFN-induced proteins with tetratricopeptide repeats (IFITs), which influence anti-viral signal transduction through various mechanisms (reviewed in Vladimer et al. 2014). Protein expression of ISG56 and ISG60, measured by immunoblotting of the endogenous proteins, can be used as readout for activity of the RIG-I signalling pathway.
Human OASL overexpression was shown to enhance ISG56 and ISG60 expression after induction of the RIG-I pathway upon SeV infection, low-molecular-weight poly(I:C) transfection, and RIG-I transfection (Zhu et al. 2014). To show that OASL enhanced RIG-I signalling by substituting for polyubiquitination (pUb) of RIG-I, the authors analysed ISG60 expression, induced by transfection of RIG-I ubiquitin-binding mutants or RIG-I wild type (WT) in the absence and presence of OASL expression. Two different RIG-I mutants were used (Zhu et al. 2014). The RIG-I T55I mutant has a mutation located in the first CARD domain of RIG-I that abolishes TRIM25 interaction, whereas the RIG-I K172R mutant has a mutation in the second CARD domain that prevents polyubiquitin attachment. Both residues are crucial for interaction with downstream signalling partners (Gack et al. 2008) (1.4.2 Introduction). Zhu and colleagues transfected HEK293T cells stably expressing OASL-V5 or empty

vector control with N-terminally Flag-tagged versions of WT RIG-I and both RIG-I mutants, or empty vector pcDNA as a control, and analysed the lysates 24 h p.t. by anti-ISG60, anti-Flag, anti-V5, and anti-actin immunoblotting. In HEK293T control cells, expression of WT RIG-I induced ISG60 expression, while RIG-I K172R and RIG-I T55I expression resulted in a diminished ISG60 expression. Stable expression of OASL-V5 in HEK293T cells slightly increased ISG60 expression in the presence of WT RIG-I and enhanced RIG-I K172R induced ISG60 expression to a level comparable with ISG60 induction by WT RIG-I in HEK293T control cells. RIG-I T55I induced less ISG60 expression than RIG-I K172R in the presence of OASL-V5 expression. The authors concluded that OASL-V5 expression partially rescued the function of the RIG-I mutants, probably by mimicking the necessary polyubiquitination of RIG-I, and moreover enhanced RIG-I signalling induced by WT RIG-I overexpression.

We aimed to reproduce this set of data published by Zhu et al. to subsequently analyse if coexpression of ORF20 was able to interfere with the OASL effect on RIG-I.
The RIG-I mutants K172R and T55I were generated in our Lab. Veit Hornung, University of Bonn, co-author in the publication of Zhu et al. provided us with the HEK293T cell line (HEK293T VH), that was used in the experiments performed by Zhu and colleagues. We included in our experiment the RIG-I mutant RIG-I-N, that encodes both CARD domains but lacks the helicase and the C-terminal domain (CTD) of RIG-I, thus being constitutively active and able to efficiently induce RIG-I signalling without stimulation by RNA ligands. RIG-I-N served as a positive control for ISG induction. Zhu et al. used ISG60 and ISG56 expression as readout of RIG-I signalling interchangeably throughout their publication. We decided for protein expression of ISG56 as readout in this experiment, due to the good quality of the commercially available antibodies.
We transfected HEK293T VH cells with N-terminally tagged WT RIG-I, RIG-I K172R, RIG-I T55I, or RIG-I-N in combination with OASL-V5, or empty vector control pcDNA, in a 1:1 ratio. To detect whether OASL-V5 expression itself was sufficient to induce ISG56 expression, OASL-V5 was cotransfected with empty vector pcDNA. 48 h p.t. cells were lysed and analysed by anti-ISG56, anti-Flag, and anti-V5 immunoblotting (Figure 36).

All transfected constructs were detected at the anticipated sizes in anti-Flag and anti-V5 immunoblots. As expected we found that WT RIG-I overexpression strongly induced ISG56 expression, and expression of the constitutive active mutant RIG-I-N induced an even stronger ISG56 expression. Expression of both RIG-I mutants induced only weak ISG56 expression compared to WT RIG-I, with the T55I mutant inducing an even lower level than the K172R mutant (Figure 36, compare upper panels lane 1 to lane 3 and 5). However, in our hands, both mutants induced a measurable ISG56 expression, showing that the single point mutations not completely abolished RIG-I signalling, as observed by Zhu and colleagues. Notably, the anti-Flag immunoblot showed that RIG-I-N was expressed much weaker than WT RIG-I, RIG-I K172R, or RIG-I T55I, but nonetheless induced the strongest ISG56 expression.

We found that coexpression of OASL-V5 with WT RIG-I enhanced ISG56 induction (Figure 36, compare upper panels lane 1 to lane 2). This was not due to OASL expression alone, since coexpression of OASL-V5 with empty vector pcDNA did not induce ISG56 expression (Figure 36, compare upper panels lane 1 to lane 9). Coexpression of OASL-V5 with RIG-I-N did not measurably increase ISG56 expression, probably because ISG56 expression was already saturated by RIG-I-N expression alone. OASL increased ISG56 expression induced by RIG-I mutants K172R and T55I, compared to the control samples where the RIG-I mutants were cotransfected with empty vector pcDNA (Figure 36, compare upper panels lane 3 to lane 4 and lane 5 to lane 6). This shows that OASL expression can partially rescue signalling activated by the RIG-I mutants that can no longer be polyubiquitinated.

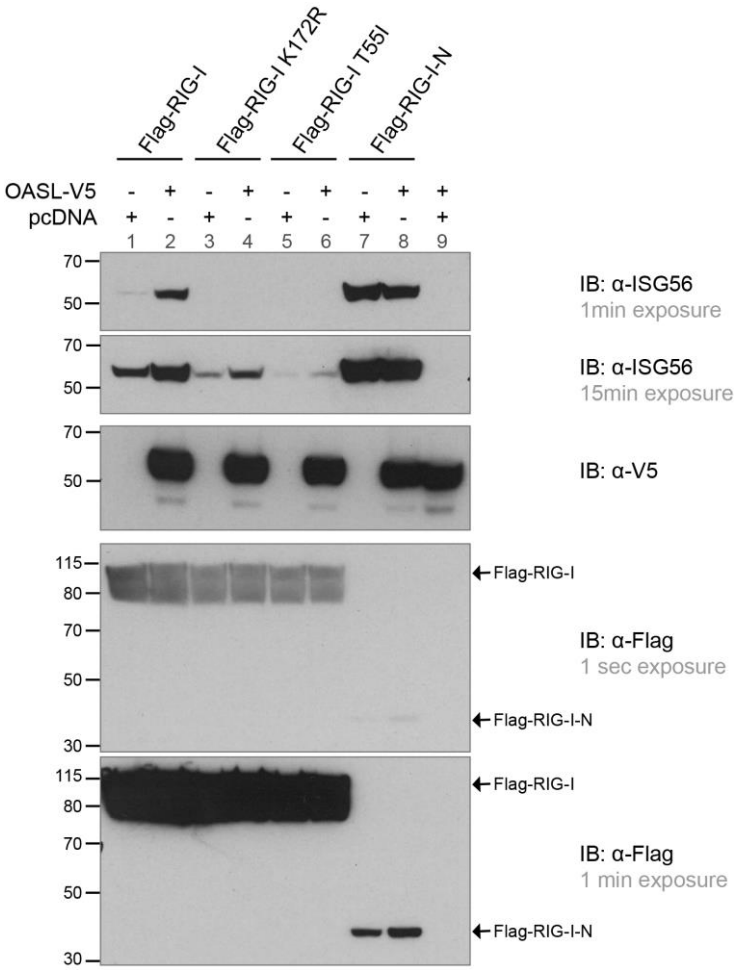

Figure 36 OASL overexpression enhances RIG-I mediated ISG56 induction and partially rescues function of RIG-I ubiquitination mutants. HEK293T VH cells were cotransfected in a 1:1 ratio with the indicated constructs. 48 h p.t. cells were lysed with RIPA-100 buffer. Lysates were subjected to NuPAGE gelelectrophoresis followed by anti-ISG56, anti-V5, and anti-Flag immunoblotting on the same membrane. One representative experiment of three independent experiments is shown. Left margin gives molecular sizes in kilodaltons (kDa).

Our results were in accordance with the data published by Zhu et al. and confirmed their finding that OASL enhanced RIG-I-induced signalling and subsequent ISG56 expression. OASL was furthermore able to substitute for ubiquitination of RIG-I, as it partially rescued ISG56 induction of the RIG-I ubiquitination mutants.

3.3.8 KSHV ORF20 does not inhibit OASL-mediated enhancement of RIG-I signalling

We confirmed that OASL expression amplified RIG-I signalling and partially rescued signalling by the RIG-I ubiquitination mutants as published by Zhu and colleagues (2014). Given the interaction and colocalisation of KSHV ORF20 with human OASL and the ability of KSHV ORF20 to inhibit the type I IFN response downstream of RIG-I, we determined whether ORF20 affected RIG-I signalling by interfering with OASL-mediated enhancement of RIG-I signalling.

Similar to the preceding experiment (3.3.7), we examined activation of the RIG-I signalling pathway by analysing ISG56 protein expression upon overexpression of WT RIG-I and RIG-I K172R in the absence and presence of OASL and KSHV ORF20. We decided to use the mutant RIG-I K172R in this experiment and to neglect the RIG-I T55I mutant, as RIG-I K172R showed a better detectable phenotype upon overexpression and upon cotransfection with OASL (Figure 36). Constitutive active RIG-I-N served as a positive control for ISG56 induction. Coexpression of RIG-I-N with ORF20 was used to analyse the influence of OR20 expression on ISG56 expression induced by RIG-I-N signalling.

We transfected HEK293T VH cells with three constructs in a 1:1:1 ratio, where Flag-RIG-I (WT) or Flag-RIG-I K172R were cotransfected with OASL-V5 plus empty vector pcDNA, OASL-V5 plus ORF20-myc, or ORF20-myc plus pcDNA. To measure the basal level of ISG56 expression induced by WT RIG-I and RIG-I K172R, the constructs were transfected with empty vector pcDNA in a 1:2 ratio in order to maintain the DNA:transfection reagent ratio. In addition, OASL-V5 was either cotransfected with pcDNA in a 1:2 ratio, or with ORF20-myc plus pcDNA in a 1:1:1 ratio. The cells were lysed 48 h after transfection and lysates were analysed by anti-ISG56, anti-Flag, anti-V5, anti-myc, anti-OASL, and anti-tubulin IB on the same membrane. By using an antibody against endogenous OASL, we aimed to detect induction of endogenous levels of OASL upon activation of RIG-I signalling. Tubulin served as a protein loading control (Figure 37).

Different to the experiment shown in Figure 36, where all constructs were transfected in a 1:1 ratio, in this experimental setup the used DNA amount was reduced from half to one third in the transfection mix. This may explain why we observed less pronounced induction of ISG56 expression in this experimental setup (Figure 37). We found that all transfected constructs were expressed, only Flag-RIG-I-N was expressed very weakly, as observed previously. In accordance with our previous results (Figure 36), expression of OASL enhanced ISG56 expression induced by WT RIG-I (Figure 37, lane 2). This time we did not detect ISG56 expression upon transfection of Flag-RIG-I K172R or upon cotransfection of Flag-RIG-I K172R and OASL-V5 (Figure 37, lane 5 and 6), indicating that the transfected DNA amounts may not have been sufficient to induce detectable ISG56 expression.

However, we found that KSHV ORF20 did not alter the expression level of ISG56 induced by WT RIG-I overexpression, as the detected protein expression of ISG56 was equal after transfection of RIG-I alone or after cotransfection of RIG-I and ORF20 (Figure 37, lane 1 and 4). Moreover, induction of ISG56 protein expression by RIG-I and OASL was not reduced in the presence of ORF20. On the contrary, ISG56 expression was increased upon cotransfection of ORF20, OASL and RIG-I (Figure 37, lane 3), compared to ISG56 expression induced by RIG-I alone, or RIG-I and OASL in combination (Figure 37, lane 1 and 2). This effect was detected in two of three independent experiments.

A weak expression of ISG56 was detected in the sample with cotransfected RIG-I K172R and ORF20, but this was probably due to spill over from the right lane with lysates from RIG-I-N transfected cells, since this was not observed in the two replicates of this experiment. As expected, the constitutive active mutant RIG-I-N strongly induced ISG56 expression. Expression of ORF20 did not result in a detectable alteration of ISG56 induction by RIG-I-N (Figure 37, lane 9). Interestingly, expression of RIG-I-N, but not WT RIG-I, induced expression of endogenous OASL (Figure 37, anti-OASL immunoblot).

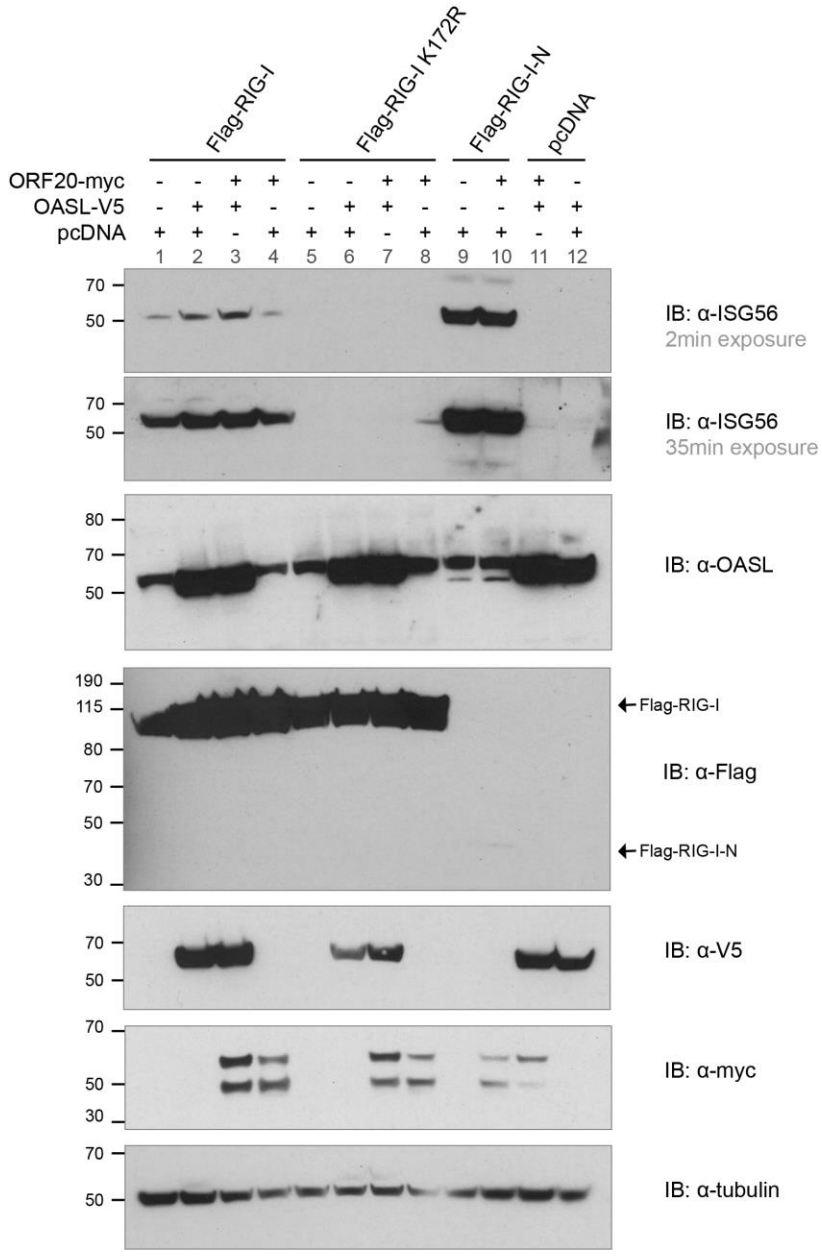

Figure 37 KSHV ORF20 does not inhibit RIG-I mediated ISG56 induction in the absence or presence of OASL. HEK293T VH cells were transfected in a 1:1:1 ratio with the indicated constructs, or were transfected in a 1:2 ratio with Flag-RIG-I, Flag-RIG-I K172R, Flag-RIG-I-N, or OASL-V5 and empty vector pcDNA. Cells were lysed 48 h p.t. with RIPA-100 buffer. Lysates were subjected to NuPAGE gelelectrophoresis followed by anti-ISG56, anti-Flag, anti-V5, anti-OASL, and anti-myc immunoblotting on the same membrane. Anti-tubulin immunoblotting served as a protein loading control. Experiment was repeated three times. Left margin gives molecular sizes in kilodaltons (kDa).

3.3.9 Mild enhancing effect of OASL and inhibitory effects of KSHV ORF20 on RIG-I-mediated induction of IFNβ

OASL weakly enhances RIG-I-mediated induction of IFNβ

Our experiments confirmed that OASL overexpression increased RIG-I induced ISG expression, and partially rescued ISG induction by RIG-I ubiquitin-binding mutants (Figure 36). However, the presence of ORF20 did not affect this phenotype. As a next step, we used a different readout to address the role of ORF20 on OASL enhanced RIG-I signalling, using the IFNβ luciferase reporter assay. Since RIG-I activation induces transcription of type I IFNs, and type I IFNs subsequently induce transcription of ISGs (1.4.2 and 1.4.3 Introduction), a readout based on type I IFN induction is a more direct approach to analyse a functional RIG-I signalling pathway than a readout based on ISG expression.

Zhu and colleagues showed that human OASL expression increased RIG-I-mediated induction of IFNβ in a luciferase reporter assay, similar to our approach in Figure 9. They used stable HEK293T OASL-V5 or empty vector cell lines cotransfected with pcDNA as a control, N-terminally tagged WT RIG-I, or ubiquitination mutants RIG-I K172R and RIG-I T55I. IFNβ-luciferase activity was shown as fold induction of the samples whereby IFNβ-luciferase activity of the empty vector control cell line was set to 1. In detail, the data show that in the absence of OASL, the RIG-I mutants did not induce IFNβ induction in the pcDNA cell line, while WT RIG-I induced IFNβ by twofold. In contrast, OASL expressing cell lines showed a more pronounced IFNβ activity: WT RIG-I expression induced IFNβ promoter activity fivefold, RIG-I K172R fourfold, RIG-I T55I threefold, and pcDNA about 1.5-fold. From this, the authors concluded that OASL enhanced WT RIG-I-mediated induction of the IFNβ response. As coexpression of OASL with the ubiquitination mutants of RIG-I induced IFNβ, they reasoned that OASL expression may functionally rescue the RIG-I ubiquitin-binding mutants (Zhu et al. 2014).

To confirm the data by Zhu et al. we generated HEK293T cells stably expressing OASL-V5, or empty vector pcDNA3.1 as a control. As HEK293T cell lines have been used in most labs for decades, some of the cell lines seem to have developed differing characteristics in some assays (personal communication with Veit Hornung). To avoid differences in our results due to the used 293T cell line, we generated two independent 293T cell lines. We used HEK293T cells received from Veit Hornung (HEK293T VH) which were used in the study of Zhu et al. and HEK293T cells commonly used in our lab (HEK293T VIMM). Expression of OASL in the stable cell lines was validated by anti-V5 immunoblotting (Figure 38).

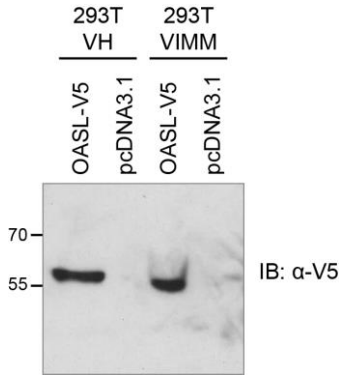

Figure 38 OASL is expressed in HEK293T VH and HEK293T VIMM stable cell lines. The plasmids pcDNA3.1 OASL-V5 and pcDNA3.1 were linearised and transfected into HEK293T VH and HEK293T VIMM cells. Cells were selected by G418 treatment for 14 cell days p.t, lysed 15 days p.t. and subjected to anti-V5 immunoblotting. Left margin gives molecular sizes in kilodaltons (kDa).

Next, HEK293T VH and HEK293T VIMM cells stably expressing OASL or empty vector pcDNA were transfected in a 1:1 ratio with empty vector pcDNA3.1 in combination with N-terminally Flag-tagged versions of WT RIG-I, RIG-I K172R, RIG-I-N, or empty vector pcDNA3.1 as a control, along with IFNβ-Firefly luciferase reporter and Renilla luciferase reporter plasmids. Cotransfection of RIG-I plasmids with empty vector pcDNA3.1 allowed substitution of pcDNA3.1 with expression constructs of interest, like KSHV ORF20, in continuative experiments. The 1:1 ratio was used based on a previous IFNβ luciferase reporter assay in HEK293T cells, where the Flag-RIG-I DNA amount was titrated to determine the amount needed for a sufficient induction of the IFNβ reporter (data not shown). Values of the RIG-I, RIG-I K172R, and RIG-I-N transfected samples are shown as fold induction to the empty vector control of the corresponding cell line, which were set to 1 (Figure 39). Selected sample-control pairs were statistically analysed. Expression of the transiently and stably transfected constructs was verified by immunoblotting of the lysates (data not shown).

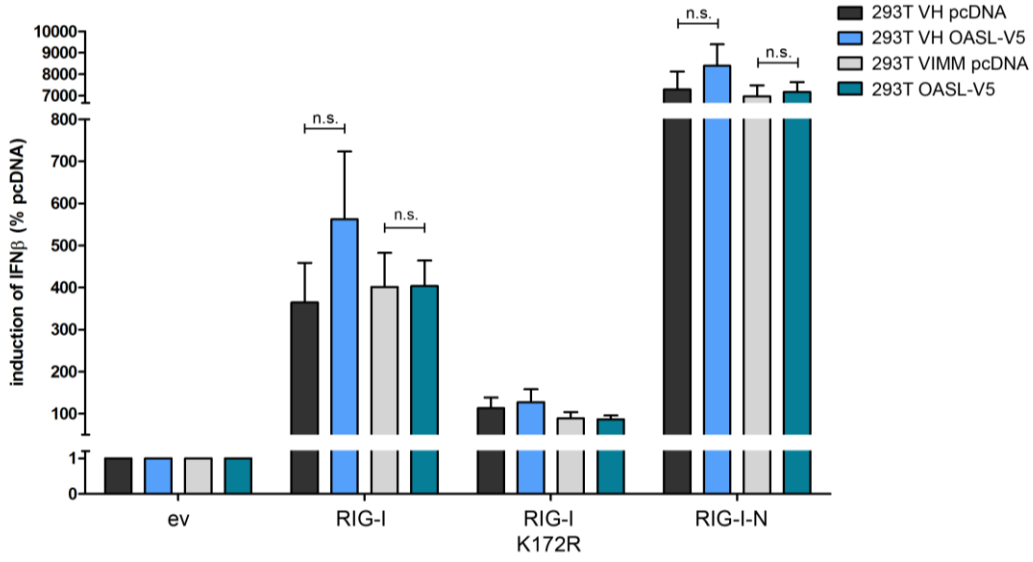

Figure 39 OASL expression weakly enhances RIG-I mediated IFNβ induction in HEK293T VH cells. HEK293T VH and VIMM cells stably transfected with OASL-V5 or empty vector pcDNA3.1 (ev) were transfected in a 1:1 ratio with pcDNA3.1 in combination with Flag-tagged RIG-I, RIG-I K172R, RIG-I-N, or pcDNA3.1 as a control, along with IFNβ-Firefly luciferase and Renilla luciferase reporter plasmids. 48 h p.t. cells were lysed and luciferase activity was measured. The Firefly values were normalised to the corresponding Renilla values. Normalised data are shown as fold induction to the corresponding pcDNA3.1 control. Data shows averages with standard deviation from three independent experiments. Log-transformed results of select control-sample pairs were analysed by two-tailed unpaired *t* test: n.s., not statistically significant; ***, $P < 0.001$; ****, $P < 0.0001$.

We found that transient expression of RIG-I induced strong IFNβ activity in all generated cell lines by more than 300 fold compared to the corresponding empty vector control (Figure 39). In 293T VH cells, OASL expression resulted in a slightly higher RIG-I-induced IFNβ activity (562 fold) compared to the empty vector control, although this effect was not statistically significant. However, this elevating effect of OASL expression on RIG-I signalling was not detected in HEK293T VIMM cells (Figure 39). Expression of RIG-I K172R in HEK293T VH and VIMM empty vector control cell lines activated the IFNβ promoter, indicating that the introduced mutation did not completely abrogate RIG-I signalling, although the induction was reduced to one third compared to WT RIG-I. Importantly, RIG-I K172R-mediated IFNβ activity was not enhanced by OASL expression in HEK293T VIMM and VH cells (Figure 39). Transient expression of constitutive active RIG-I-N induced a very strong IFNβ activity, which was increased more than 7000 fold in HEK293T VH and VIMM pcDNA3.1 cells. We measured no statistically significant OASL-mediated enhancement of RIG-I-N-induced IFNβ activity in HEK293T VIMM and VH cells (Figure 39).

The transient transfection of the different RIG-I plasmids induced a much more pronounced IFNβ activity in our assay, as IFNβ activity was increased more than 300 fold upon RIG-I expression, compared to a 2 fold induction of IFNβ activity in the study of Zhu and colleagues. This could implicate that different experimental parameters, like expression constructs, reporter plasmids, or DNA amounts for transfection constructs were used. We detected a mild enhancing effect of OASL expression on RIG-I- and RIG-I-N-induced IFNβ activation, although the high variability of the values indicated by the error bars have to be taken into account. We observed no rescuing effect of OASL on RIG-I K172R induced-IFNβ activity. Elevated RIG-I signalling upon OASL overexpression was detected in HEK293T VH cells, but not in HEK293T VIMM cells, demonstrating diversity of HEK293T cell lines. In summary, we could only partially reproduce the data shown by Zhu et al. with this experimental setup, showing that OASL positively influenced RIG-I-mediated type I IFN signalling.

KSHV ORF20 and ORF20 B inhibit RIG-I-mediated induction of IFNβ independent of OASL overexpression

We next analysed the influence of ORF20 on IFNβ induction downstream of RIG-I activation in the absence and presence of overexpressed OASL using the earlier described luciferase reporter assay.
We have shown that transient expression of ORF20 reduced IFNβ and IFNα4 activation upon NDV infection by about 50% compared to an empty vector control in multiple cell lines, showing that ORF20 interferes with RIG-I signalling (Figure 9). In our initial experiments, we did not analyse the N-terminally truncated form of ORF20, ORF20 B. Therefore, ORF20 B was included in the following experiments.
HEK293T VH and VIMM cell lines stably expressing empty vector or OASL were transfected in a 1:1 ratio with ORF20, ORF20 B, or pcDNA3.1 in combination with WT RIG-I, RIG-I K172R, RIG-I-N, or pcDNA3.1, along with reporters for IFNβ-Firefly luciferase and Renilla luciferase. Transfection of empty vector pcDNA3.1 served as a control for the transfected ORF20 or RIG-I plasmids. The cells were lysed 48 h p.t. and luciferase activity was measured. Firefly luciferase values were normalised to the corresponding Renilla values and were subsequently multiplied by 100 to show the values in a range

above 0.5 (Figure 40). Figure 45 (Appendix) shows fold induction of IFNβ activity, where normalised data of ORF20 and ORF20 B transfected samples were scaled to the corresponding control samples that expressed empty vector pcDNA3.1 together with RIG-I, RIG-I K172R, RIG-I-N, or pcDNA3.1. Expression of transiently and stably transfected constructs was verified by immunoblotting (data not shown).
The following data were produced along with the data shown in Figure 39 in one continuous experiment. The underlying values for controls and the RIG-I expressing samples are the same. But while Figure 39 shows the data as fold induction scaled to the corresponding empty vector control for each cell line, Figure 40 shows IFNβ induction as normalised Firefly values that are not scaled to the empty vector controls.

HEK293T VH and VIMM cells transiently transfected with empty vector control showed equal IFNβ activity, irrespective of stable expression of OASL or pcDNA3.1. This indicates that overexpression of OASL alone does not induce a detectable IFNβ activation. Similarly, ORF20 or ORF20 B expression did not induce the RIG-I signalling pathway, as coexpression of ORF20 or ORF20 B with pcDNA3.1 activated IFNβ to the same extent as the corresponding empty vector control in HEK293T VH and VIMM OASL or pcDNA3.1 stable cell lines (Figure 40 A, B and C).

As shown before, expression of WT RIG-I induced a very potent IFNβ induction with similar values in HEK293T VH and VIMM cells stably expressing pcDNA3.1 control. In HEK293T VH, but not HEK293T VIMM cells, coexpression of OASL with RIG-I resulted in a higher IFNβ activity compared to the corresponding empty vector control cell line (Figure 40 A). Expression of ORF20 did not affect RIG-I-induced IFNβ activity in the absence or presence of OASL expression, as IFNβ activity upon RIG-I and ORF20 cotransfection was similar in OASL and pcDNA3.1 expressing HEK293T VH and VIMM stable cell lines (Figure 40 A).

Interestingly, we found that, unlike ORF20, co-expression of ORF20 B with RIG-I reduced RIG-I-mediated IFNβ activity to about one third of the IFNβ activity induced by RIG-I and pcDNA3.1 expression, irrespective of OASL expression in HEK293T VH or VIMM cells (Figure 40 A). These data showed that ORF20 B strongly interfered with the RIG-I signalling pathway activated by WT RIG-I overexpression, independent of OASL overexpression.
As observed earlier, expression of the RIG-I mutant K172R induced a moderate IFNβ activity in HEK293T VH and VIMM cells, independent of OASL overexpression. In the presence of RIG-I K172R, IFNβ activity was reduced to about one third of the IFNβ activity induced by WT RIG-I (Figure 40, compare A and B). We found that coexpression of ORF20 or ORF20 B with RIG-I K172R diminished the induction of IFNβ by about half and two thirds, respectively, compared to coexpression of RIG-I K172R with empty vector pcDNA control in HEK293T VH and VIMM cells stably expressing OASL or empty vector (Figure 40 B).

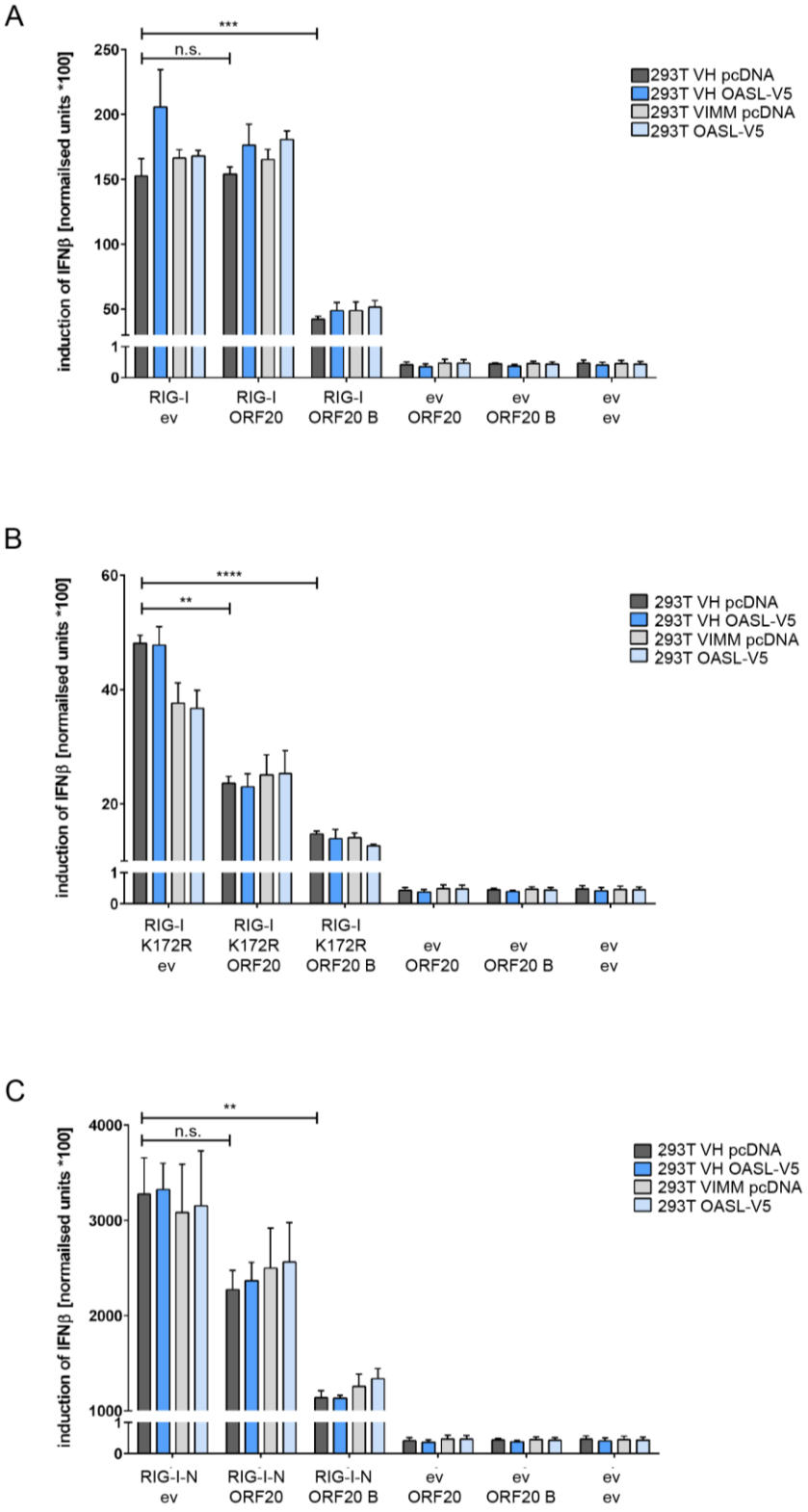

Figure 40 ORF20 B and partially ORF20 inhibit IFNβ induction downstream of RIG-I activation independent of OASL expression. HEK293T VH and VIMM cells stably expressing OASL-V5 or pcDNA3.1 were transfected with IFNβ-Firefly luciferase and Renilla luciferase reporter constructs along with ORF20-myc, ORF20 B-myc, or pcDNA3.1 (ev) in combination with Flag-tagged RIG-I, RIG-I K172R, RIG-I-N, or pcDNA3.1 in a 1:1 ratio. Transfection of empty vector pcDNA3.1 (ev) served as control. Cells were lysed 48 h p.t. and luciferase activity was measured. Shown is induction of IFNβ, determined as follows: Firefly values normalised to the corresponding Renilla values multiplied by 100. Data shows averages with standard deviation from three independent experiments. Log-transformed results of select control-sample pairs were analysed by two-tailed unpaired *t* test: n.s., not statistically significant; **, $P < 0.1$; ***; $P < 0.01$; ****, $P < 0.0001$.

A similar effect of ORF20 and ORF20 B was observed for RIG-I-N-induced IFNβ activity. Expression of RIG-I-N induced a very strong IFNβ activity, while coexpression of RIG-I-N with ORF20 or ORF20 B reduced IFNβ activity by about one third and two thirds, respectively. This effect was similar in HEK293T VH and VIMM stable cell lines (Figure 40 C).
These findings suggest that both forms of ORF20, ORF20 and ORF20 B, were able to interfere with type I IFN signalling downstream of RIG-I, whereby expression of ORF20 B resulted in a twofold stronger inhibition of IFNβ activity than full length ORF20. Importantly, inhibition of RIG-I signalling by ORF20 and ORF20 B was independent of OASL overexpression.

In summary, we found that ORF20 B strongly diminished RIG-I dependent IFNβ activation induced upon WT RIG-I, RIG-I K172R, and RIG-I-N overexpression, while full length ORF20 diminished RIG-I K172R and RIG-I-N induced IFNβ induction, but not WT RIG-I induced IFNβ activity. These effects were independent of overexpression of OASL, and comparable in HEK293T VH and VIMM cells.

3.3.10 KSHV ORF20 and ORF20 B inhibit RIG-I-mediated induction of ISG56 independent of OASL overexpression

We next analysed whether ORF20 or ORF20 B also negatively affected ISG56 promoter induction upon activation of RIG-I signalling. Similar to the luciferase reporter assay used to study IFNβ promoter induction, we analysed ISG56 promoter induction upon RIG-I overexpression in the absence and presence of KSHV ORF20 and ORF20 B. We furthermore studied the influence of OASL expression on RIG-I-induced ISG56 activation and analysed whether ORF20 and ORF20 B expression altered the effect of OASL in this assay.
We transfected HEK293T VH cells stably expressing OASL or empty vector with an ISG56-Firefly luciferase reporter and a Renilla luciferase reporter for normalisation along with two expression constructs in a 1:1 ratio: WT RIG-I or empty vector pcDNA3.1 in combination with ORF20, ORF20 B, or pcDNA3.1. Stable cell lines transfected solely with empty vector served as a control for the basal level of ISG56 activation, while coexpression of ORF20 or ORF20 B with empty vector controlled for the influence of the ORF20 expression constructs on the Firefly and Renilla values. Cells were lysed 48 h after transfection and luciferase activity was measured. Normalised Firefly luciferase values are shown in Figure 41. The empty vector controls were not set to 1 to give insight into the measured values.

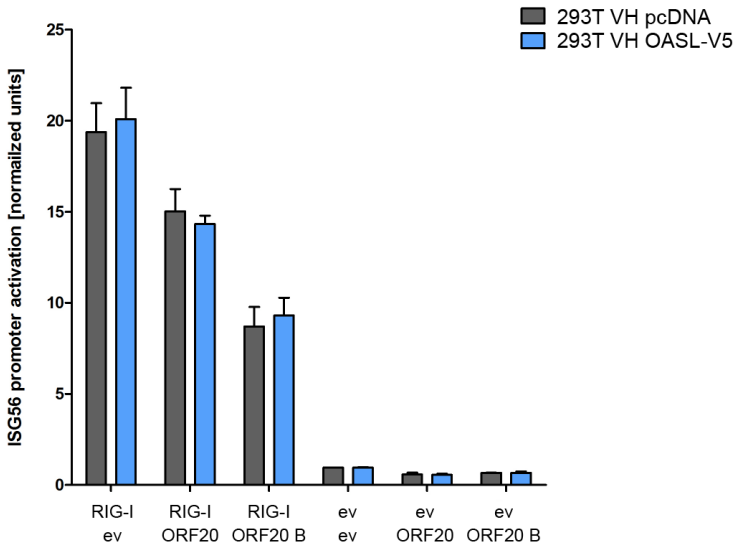

Figure 41 KSHV ORF20 and ORF20 B diminish ISG56 induction downstream of RIG-I activation independent of OASL overexpression. HEK293T VH cells stably expressing OASL-V5 or empty vector pcDNA3.1 were transfected in a 1:1 ratio with Flag-RIG-I or empty vector pcDNA3.1 (ev) and ORF20-myc, ORF20 B-myc, or empty vector pcDNA3.1 (ev) as a control, along with the reporter constructs ISG56-Firefly luciferase and Renilla luciferase. Cells were lysed 48 h p.t. and luciferase activity was measured. Firefly values were normalised to the corresponding Renilla values. Data shows averages of normalised non-scaled values with standard deviation from three independent experiments.

As expected we found that the basal level of ISG56 activation induced by empty vector transfection was very low in HEK293T VH cells stably expressing OASL or empty vector, showing that neither empty vector transfection nor expression of OASL was sufficient to induce a measurable ISG56 induction. Expression of ORF20 and ORF20 B in the absence of RIG-I expression resulted in a similar ISG56 activity as the empty vector control, indicating that expression of the constructs did not influence reporter plasmid expression (Figure 41, group 4, 5, and 6). Activation of the RIG-I signalling upon WT RIG-I overexpression strongly induced the ISG56 promoter by about 20 fold compared to the corresponding empty vector control. Coexpression of OASL with RIG-I resulted in the same IS56 induction as coexpression of empty vector with RIG-I, showing that OASL did not enhance RIG-I-mediated ISG56 promoter induction in this assay (Figure 41, compare group 1 and 4). This finding was contrary to our immunoblotting results of ISG56 protein expression in HEK293T cells expressing RIG-I in combination with empty vector pcDNA or OASL, where we could show that RIG-I-induced ISG56 expression was enhanced by overexpression of OASL (Figure 36).

We found that expression of ORF20 reduced WT RIG-I-induced ISG56 promoter activity from 20 fold to about 15 fold compared the corresponding empty vector control. In the presence of ORF20 B the RIG-I induced ISG56 promoter induction was even reduced from 20 fold to 10 fold. OASL expression did not influence the effect of ORF20 and ORF20 B on RIG-I signalling, as the measured ISG56 promoter induction was equal in HEK293T VH cells stably expressing OASL or empty vector control (Figure 41, compare group 1 to group 2 and 3). In accordance with our IFNβ luciferase data (Figure 40), we found that ORF20 moderately and ORF20 B strongly interfered with the RIG-I signalling pathway, as IFNβ and ISG56 promoter induction was diminished by ORF20 and ORF20 B expression. This function of ORF20 and ORF20 B was independent of OASL overexpression.

In summary, we found that KSHV ORF20 and ORF20 B interact with human OASL. We confirmed published data showing that OASL binds to RIG-I and enhances RIG-I signalling, measured by increased IRF3 nuclear translocation, IFNβ promoter induction, and ISG56 protein expression. KSHV ORF20 did not inhibit colocalisation or binding of RIG-I and OASL, and did not diminish ISG56 protein expression induced by RIG-I and OASL. Nonetheless, KSHV ORF20 interfered with the RIG-I signalling pathway, as IRF3 localisation was altered and IFNβ and ISG56 promoter induction were diminished by ORF20 expression. An inhibition of IFNβ and ISG56 promoter induction was weakly to moderately detectable upon ORF20 expression, but strongly detectable upon ORF20 B expression, indicating that the two different forms ORF20 and ORF20 B may have different phenotypes. Our findings suggest that ORF20 and ORF20 B can interfere with the RIG-I signalling pathway, but not by manipulating the OASL effect on RIG-I activation.

3.3.11 Interactome of human OASL

Given the interaction of OASL and ORF20, the colocalisation of both proteins in the nucleolus and cytoplasm, and our results showing that ORF20 did not affect the role of OASL on RIG-I, we sought to determine unknown cellular interaction partners of OASL to gain insights into unknown mechanistic functions. With the results we aimed to draw conclusion about further functions of OASL and the role of the interaction between ORF20 and OASL.

We therefore used the unbiased approach of q-AP-MS with myc-tagged OASL as bait, as introduced in 3.1.3 and outlined in Figure 15 A. Briefly, heavy or light arginine and lysine were incorporated into proteins of HeLa S3 in 10 days of cell culture and heavy labelled cells were transfected with OASL-myc, while light labelled cells were transfected with LacZ-myc. Myc-tagged LacZ was used as a control for unspecific co-precipitating proteins, since LacZ should not have the same binding partners as OASL, but shared the same vector backbone and epitope tag with OASL, as well as its cytoplasmic localisation. The cells were lysed 24 h p.t. and subjected to anti-myc IP. Heavy and light labelled samples were combined for affinity purification, followed by ethanol precipitation of the eluates. Samples were prepared for mass spectrometry and measured by LC-MS/MS by Josef Wissing of the Cellular Proteome Research group at the HZI. The results were bioinformatically analysed and heavy to light fold change values were calculated to compare the relative abundance of each precipitated protein in the heavy and light labelled sample. The value is based on the relative intensity of the identified peptides of a protein. True interaction partners should be more abundant for OASL, while co-purifying contaminants have a 1:1 ratio in the OASL and LacZ sample. In parallel, a crossover experiment with switched SILAC labels was performed and analysed to reliably detected unspecific binding partners and furthermore serving as biological replicate of the experiment. In the crossover experiment, the label switch results in reciprocal SILAC ratios for true interaction partners (Paul et al. 2011). The values of the forward and the crossover experiment were graphed together and are shown in Figure 42 A and Table 26 (Appendix).

In addition, we determined the interactome of OASL in NDV infected cells to identify potential protein interaction partners of OASL upon activation of RIG-I signalling. For this, we performed q-AP-MS as described above, but infected the transiently transfected HeLa S3 cells with NDV. We observed significant nuclear translocation of IRF3 at 12 h p.i. with NDV in HeLa S3 cells (Figure 34) and therefore

lysed the cells 14 h p.i. to assure that the RIG-I signalling pathway was activated. The samples were processed and analysed as described earlier and are shown in Figure 42 B and Table 27 (Appendix).

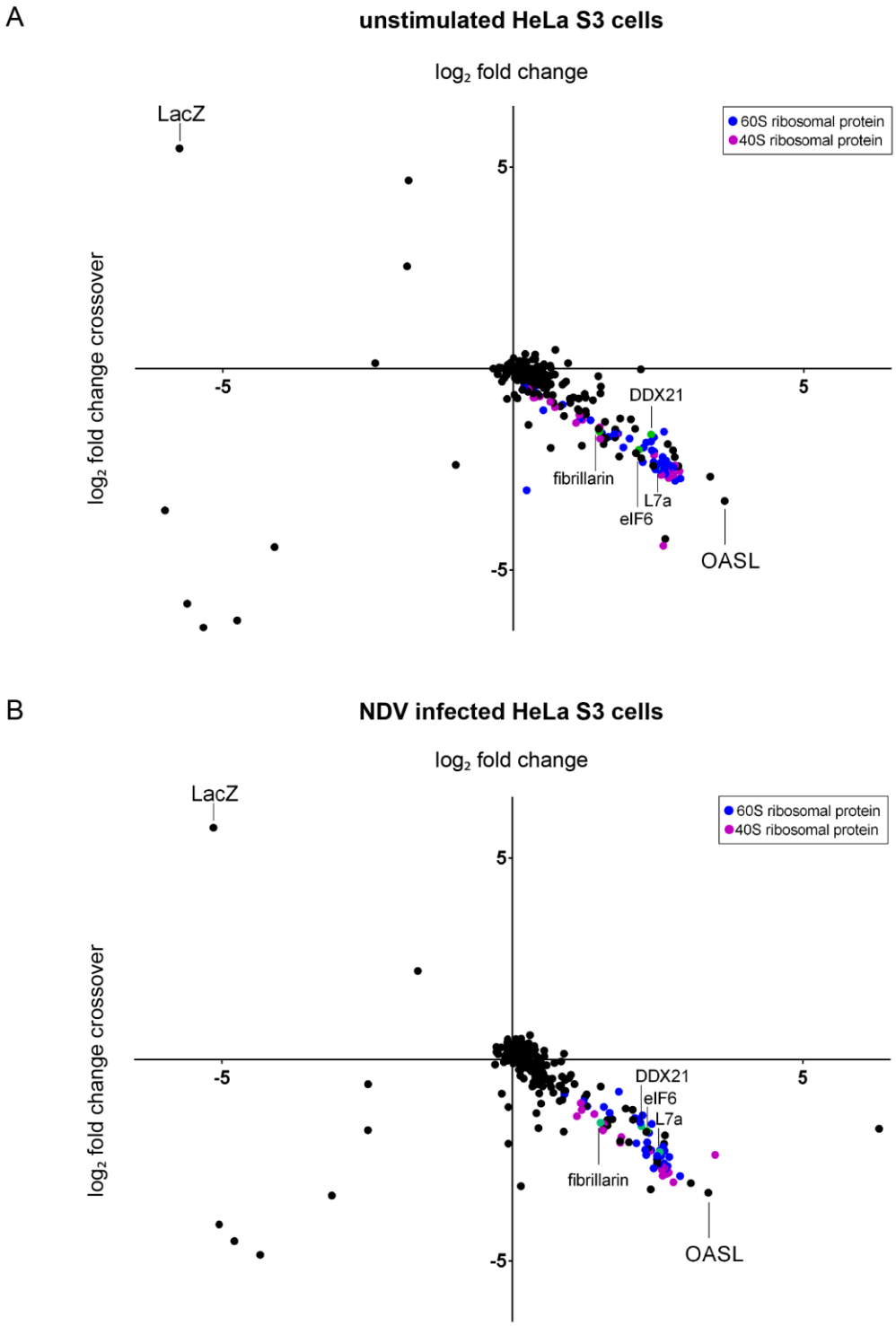

Figure 42 Interactome of human OASL in unstimulated and NDV infected HeLa S3 cells analysed q-AP-MS. HeLa S3 cells incorporated heavy or light arginine and lysine for 10 days of cell culture. Heavy labelled cells were transfected with OASL-myc, and light labelled cells with LacZ-myc as a control (forward experiment). In parallel a crossover experiment with switched isotope labels was performed. Here light labelled cells were transfected with OASL-myc and heavy labelled cells with LacZ-myc. Unstimulated cells were lysed 24 h p.t (**A**). 24 h p.t. cells were infected with NDV for 1 h and lysed 14 h p.i. (**B**). Samples were further processed as described in **Figure 15**. Heavy/light fold change values were calculated for the identified proteins based on their relative intensity in the sample, corresponding to their relative abundance. The values of each protein identified in the forward and in the crossover experiment were graphed together. Proteins that were identified only in the forward or crossover experiment are not shown.

We found that OASL mainly precipitated the same proteins in unstimulated cells and NDV infected cells. All highly confident interaction partners of OASL were identified under both conditions. Interestingly, OASL interacted with a high number of ribosomal proteins. The human ribosome contains 47 proteins in the large ribosomal subunit (60S) and 33 proteins in the small ribosomal subunit (40S). We identified 39 60S proteins and 25 40S proteins under unstimulated conditions and 28 60S and 28 40S proteins under stimulated conditions as potential interaction partners of OASL. In addition a range of (i) ribosome-associated proteins such as Ribosome production factor 2 (RPF2), Ribosome biogenesis protein BRX1, and Ribosome biogenesis regulatory protein homolog (RRS1) and (ii) RNA-binding proteins such as RNA-binding protein 34 (RBM34), RNA-binding protein 28 (RBM28), and Probable rRNA-processing protein EBP2 were identified as highly potential interaction partners of OASL (Table 26 and Table 27 Appendix). Furthermore, OASL bound a variety of nucleolar proteins like rRNA 2'-O-methyltransferase fibrillarin, eukaryotic translation initiation factor 6 (eIF6), and nucleolar RNA helicase 2 also named DEAD Box protein 21 (DDX21). Many of the OASL interacting partners are described to bind RNA, rDNA, or DNA. Together with the high number of ribosomal proteins identified as potential interacting partners, our data suggest that OASL might play a role in the biogenesis of ribosomes, RNA maturation or processing in the nucleus. Notably, we did not detect RIG-I or components of the RIG-I signalling cascade to interact with OASL.

Strikingly, many of the potential binding partners of OASL have also been identified as binding partners of KSHV ORF20. The common binding partners of OASL in unstimulated and NDV stimulated cells are listed together with the binding partners of KSHV ORF20 in Table 23, demonstrating that OASL and ORF20 have a largely overlapping cellular interactome. We found that ORF20 and OASL both interacted with 46 of 80 known ribosomal proteins. Non-ribosomal common interaction partners of ORF20 and OASL were fibrillarin, eIF6, DDX21, nuclease-sensitive element-binding protein 1 (YBOX1), putative ATP-dependent RNA helicase DHX30, double-stranded RNA-binding protein Staufen homolog 2 (STAU2), ribosome-binding protein 1 (RRBP1), and proline-rich coiled-coil 2C (PRC2C). Except for eIF6, all of these proteins have been described to bind RNA and are involved in RNA synthesis, maturation, processing, and decay. STAU2 for example is involved in cytoplasmic mRNA decay by binding to the 3’ untranslated region (3’UTR) of target mRNAs (Park & Maquat 2013) and might be involved in nuclear RNA export (Miki et al. 2005). YBOX-1 participates in almost all DNA- and mRNA-dependent processes in the cell, as it is a multifunctional transcription and translation factor (Kosnopfel et al. 2014). RNA helicase DHX30 influences viral replication in a zinc-finger antiviral protein (ZAP)-dependent (Ye et al. 2010) or independent way (Zhou et al. 2008). Although eIF6 is not described to bind RNA directly, it was shown to be involved in miRNA-mediated post-transcriptional silencing (Chendrimada et al. 2007). Also, the proteins fibrillarin, eIF6, and DDX21 are localised in the nucleolus where they influence ribosome biogenesis, as well as transcriptional and translational regulation, and thereby broadly contribute to the fate of proteins (Amin et al. 2007, Miluzio et al. 2009, Calo et al. 2014).

In summary, we found that human OASL precipitated a variety of proteins that are connected with transcription, translation, or the biogenesis of ribosomes. Moreover, many potential interaction partners were proteins described to be localised in the nucleus or nucleolus, which goes in line with our IF studies

showing that OASL was strongly enriched in the nucleolus (Figure 29 and Figure 30). Stimulation of the RIG-I signalling pathway did not result in a significant change of the cellular interactome of OASL. Notably, the interactome of OASL (Figure 42) showed a high conformance with the interactome of KSHV ORF20 (Figure 15 and Table 23), indicating a functional connection of both proteins.

Table 23 Common binding partners of OASL (in unstimulated or NDV infected cells) and of KSHV ORF20 identified by q-AP-MS. Samples of the forward (fwd) and crossover (cro) experiment were prepared as described in Figure 15/Figure 42 and were analysed by mass spectrometry. Heavy to light fold change values (H/L) were calculated for the identified proteins, based on the relative intensity for their peptides in the forward or crossover experiment. Not detected (n.d.) proteins in a sample are indicated. Proteins are listed in alphabetical order.

	OASL (-NDV)		**OASL (+NDV)**		**ORF20**	
common partners of KSHV ORF20 and OASL (-/+ NDV)	**fwd H/L**	**cro H/L**	**fwd H/L**	**cro H/L**	**fwd H/L**	**cro H/L**
Nucleolar RNA helicase 2 GN=DDX21 [DDX21_HUMAN]	2,371	-1,632	2,221	-1,652	1,343	n.d.
Putative ATP-dependent RNA helicase DHX30 GN=DHX30 [DHX30_HUMAN]	1,968	n.d.	1,950	-1,215	n.d.	-0,933
rRNA 2'-O-methyltransferase fibrillarin GN=FBL [FBRL_HUMAN]	1,480	-1,555	1,516	-1,567	0,618	-0,876
Eukaryotic translation initiation factor 6 GN=EIF6 [IF6_HUMAN]	2,111	-2,093	2,320	-1,774	n.d.	-4,470
Protein PRRC2C GN=PRRC2C [PRC2C_HUMAN]	0,920	n.d.	3,571	n.d.	n.d.	-0,811
Ribosome-binding protein 1 GN=RRBP1 [RRBP1_HUMAN]	0,874	-1,174	0,889	-0,764	2,391	-2,467
Double-stranded RNA-binding protein Staufen homolog 2 GN=STAU2 [STAU2_HUMAN]	1,554	-1,874	1,568	-1,717	n.d.	-1,744
Nuclease-sensitive element-binding protein 1 GN=YBX1 [YBOX1_HUMAN]	1,823	-2,181	2,005	-2,051	0,249	-1,048
common <u>ribosomal</u> partners of KSHV ORF20 and OASL (-/+ NDV)						
60S acidic ribosomal protein P0 GN=RPLP0 [RLA0_HUMAN]	2,698	-2,403	2,540	-2,256	2,049	-2,598
60S acidic ribosomal protein P1 GN=RPLP1 [RLA1_HUMAN]	2,671	-2,498	2,586	-2,273	2,173	-2,173
60S acidic ribosomal protein P2 GN=RPLP2 [RLA2_HUMAN]	2,591	-2,371	2,559	-2,388	1,860	-2,224
60S ribosomal protein L3 GN=RPL3 [RL3_HUMAN]	2,423	-2,058	2,353	-1,818	1,831	-2,463
60S ribosomal protein L4 GN=RPL4 [RL4_HUMAN]	2,419	-1,704	2,166	-1,482	2,111	-2,867
60S ribosomal protein L6 GN=RPL6 [RL6_HUMAN]	2,505	-2,508	2,556	-2,296	2,002	-2,516
60S ribosomal protein L7a GN=RPL7A [RL7A_HUMAN]	2,457	-2,470	2,535	-2,293	2,126	-2,422
60S ribosomal protein L7 GN=RPL7 [RL7_HUMAN]	2,592	-1,567	2,108	-1,451	1,712	-2,114
60S ribosomal protein L8 GN=RPL8 [RL8_HUMAN]	2,631	-2,285	2,620	-2,265	2,027	-2,385
60S ribosomal protein L10 GN=RPL10 [RL10_HUMAN]	1,741	-1,616	1,675	-1,323	1,530	-2,498
60S ribosomal protein L10a GN=RPL10A [RL10A_HUMAN]	2,754	-2,453	2,610	-2,242	2,396	-2,876
60S ribosomal protein L11 GN=RPL11 [RL11_HUMAN]	2,415	-2,318	2,390	-2,249	0,535	-0,950
60S ribosomal protein L12 GN=RPL12 [RL12_HUMAN]	2,664	-2,553	2,636	-2,696	1,625	-2,055
60S ribosomal protein L13 GN=RPL13 [RL13_HUMAN]	2,228	-2,319	2,303	-2,368	1,157	-1,756
60S ribosomal protein L14 GN=RPL14 [RL14_HUMAN]	2,541	-2,329	2,594	-2,157	1,254	-2,225

	OASL (-NDV)		OASL (+NDV)		ORF20	
60S ribosomal protein L15 GN=RPL15 [RL15_HUMAN]	2,285	-1,836	2,202	-1,559	2,272	-2,858
60S ribosomal protein L17 GN=RPL17 [RL17_HUMAN]	0,850	-0,892	0,897	-0,862	0,714	-1,432
60S ribosomal protein L18 GN=RPL18 [RL18_HUMAN]	2,368	-1,811	2,241	-1,384	1,926	-2,353
60S ribosomal protein L19 GN=RPL19 [RL19_HUMAN]	1,331	-1,279	1,226	-1,032	1,293	-1,886
60S ribosomal protein L23 GN=RPL23 [RL23_HUMAN]	1,526	-1,600	1,575	-1,174	1,542	-2,238
60S ribosomal protein L24 GN=RPL24 [RL24_HUMAN]	1,803	-1,612	1,833	-0,796	2,200	-3,036
60S ribosomal protein L27 GN=RPL27 [RL27_HUMAN]	2,453	-2,423	2,490	-2,393	2,009	-2,400
60S ribosomal protein L27a GN=RPL27A [RL27A_HUMAN]	1,150	-1,245	1,289	-1,158	0,784	-1,513
60S ribosomal protein L29 GN=RPL29 [RL29_HUMAN]	1,895	-1,952	2,135	-2,076	1,005	-1,531
60S ribosomal protein L30 GN=RPL30 [RL30_HUMAN]	2,582	-2,449	2,537	-2,263	1,913	-4,404
60S ribosomal protein L34 GN=RPL34 [RL34_HUMAN]	2,601	-2,464	2,526	-2,587	2,044	-2,889
60S ribosomal protein L35a GN=RPL35A [RL35A_HUMAN]	2,571	-2,194	2,318	-2,052	1,851	-2,386
60S ribosomal protein L36 GN=RPL36 [RL36_HUMAN]	2,875	-2,727	2,609	-2,576	2,510	-2,515
40S ribosomal protein S2 GN=RPS2 [RS2_HUMAN]	1,772	-1,653	1,570	-1,593	1,404	-1,914
40S ribosomal protein S3 GN=RPS3 [RS3_HUMAN]	2,696	-2,544	2,492	-2,566	0,352	-0,986
40S ribosomal protein S3a GN=RPS3A [RS3A_HUMAN]	1,082	-1,349	1,109	-1,406	0,981	-1,722
40S ribosomal protein S4, X isoform GN=RPS4X [RS4X_HUMAN]	0,456	-0,692	0,523	-0,662	0,713	-1,617
40S ribosomal protein S6 GN=RPS6 [RS6_HUMAN]	1,138	-1,150	1,178	-1,082	2,178	-3,063
40S ribosomal protein S8 GN=RPS8 [RS8_HUMAN]	1,487	-1,458	1,413	-1,350	0,990	-1,678
40S ribosomal protein S9 GN=RPS9 [RS9_HUMAN]	0,639	-0,823	0,705	-0,821	0,573	-1,544
40S ribosomal protein S11 GN=RPS11 [RS11_HUMAN]	0,264	-0,507	0,379	-0,632	0,350	-1,146
40S ribosomal protein S12 GN=RPS12 [RS12_HUMAN]	0,448	0,046	2,590	-2,674	2,452	-3,281
40S ribosomal protein S14 GN=RPS14 [RS14_HUMAN]	1,497	-1,739	1,560	-1,754	0,898	-1,993
40S ribosomal protein S16 GN=RPS16 [RS16_HUMAN]	2,672	-2,546	2,594	-2,668	n.d.	-1,253
40S ribosomal protein S18 GN=RPS18 [RS18_HUMAN]	2,673	-2,712	2,586	-2,880	-0,407	-0,531
40S ribosomal protein S20 GN=RPS20 [RS20_HUMAN]	2,546	-2,635	2,613	-2,685	0,404	-1,282
40S ribosomal protein S23 GN=RPS23 [RS23_HUMAN]	1,190	-1,270	1,194	-1,247	1,383	-1,631
40S ribosomal protein S24 GN=RPS24 [RS24_HUMAN]	0,719	-0,958	0,816	-1,027	2,270	-2,461
40S ribosomal protein S25 GN=RPS25 [RS25_HUMAN]	2,642	-2,567	2,560	-2,680	-0,079	-0,686
40S ribosomal protein S26 GN=RPS26 [RS26_HUMAN]	0,385	-0,702	0,473	-0,619	1,731	-2,700
40S ribosomal protein S27 GN=RPS27 [RS27_HUMAN]	1,725	n.d.	1,644	n.d.	n.d.	-2,624
Ubiquitin-40S ribosomal protein S27a GN=RPS27A [RS27A_HUMAN]	2,782	-2,403	2,646	-2,837	-3,786	-1,677

4 Discussion

The oncogenic gammaherpesvirus KSHV inhibits the production of the type I IFNs IFNα and IFNβ to evade the innate antiviral defence (Bisson et al. 2009, Paludan et al. 2011). This enables the virus to establish a lifelong infection in its host and effectively replicate upon reactivation from latency. A number of different studies have shown that KSHV encodes a multitude of proteins that interfere with the type I IFN activation or the subsequent induction of ISGs. Interestingly, evasion by the described viral factors is achieved through diverse mechanisms and by targeting different innate immune signalling components (Bussey & Brinkmann 2018).

Nonetheless, our knowledge of viral immune evasion, as well as the host innate immune response is far from complete, as the recent discovery of the important cGAS sensor illustrates (Sun et al. 2013, Wu et al. 2013). The study of virus-host interactions can provide a wealth of insight into host and virus biology, including which distinct viral factors contribute to the manipulation of innate immune responses. Eventually, identification of these factors might lead to the discovery of novel drug targets.

4.1 Modulation of the type I IFN response downstream of RIG-I

4.1.1 Identification of KSHV-encoded inhibitors of the RIG-I signalling pathway

The starting point of this thesis was an unbiased screen of 85 KSHV-encoded ORFs for their ability to inhibit IFNα4 and IFNβ induction downstream of the cellular pattern recognition receptor (PRR) RIG-I. This important cellular sensor detects viral RNA as well as viral DNA, transcribed by RNA Polymerase II, and subsequently mediates a potent type I IFN induction.

We analysed the effect of each single KSHV-encoded protein on the transcriptional induction of the IFNβ or IFNα4 promoter, that were activated upon infection with the RNA virus New Castle disease virus (NDV) in a luciferase reporter assay (Figure 44).

Though the performed luciferase reporter assay is a powerful tool to identify novel inhibitors of a specific signalling pathway, the assay underlies certain restrictions. We used NDV to stimulate type I IFN signalling. NDV is a well described RNA virus and known to activate RIG-I (M. Yoneyama et al. 2005) and TLR3 signalling in HeLa cells (J. Cheng et al. 2014). While RIG-I mediates signalling via its adapter MAVS, TLR3 uses the adaptor TRIF. Subsequently, both signalling pathways merge at the level of the kinase TKB1, which activates IRF3. NDV is commonly used to induce type I IFN signalling, but it is likely that the measured type I IFN response is initiated by more than one PRR. This has to be taken into account when analysing ORF-mediated inhibition of IFNα4/IFNβ induction, since activation of more than one pathway might rescue an existing inhibitory effect, at least to some extent, based on the signalling component or the step in the signalling pathway that it manipulated by the viral protein. Furthermore, the ectopic expression of the viral ORFs can mask the identification of type I IFN inhibitors that require additional viral factors like other ORFs, viral mRNA, or miRNA.

Nonetheless, similar approaches have been very successfully used by Bisson and colleagues, who screened 80 KSHV-encoded ORFs for their ability to inhibit IFNAR-dependent ISRE promoter induction upon IFNα treatment and identified ORF10 as a novel inhibitor of innate immune signalling (Bisson et

al. 2009). Wu and colleagues used a luciferase reporter assay to screen for EBV-encoded antagonists of the type I IFN response upon Sendai virus (SeV) infection (L. Wu et al. 2009). These and other studies show that the experimental setup used in this study is a powerful method to identify virus-encoded antagonists of innate immune signalling. This is underlined by our results, which are in line with published data and moreover revealed KSHV ORF20 as a novel inhibitor of the type I IFN response downstream of RIG-I.

KSHV-encoded inhibitors of the type I IFN response downstream of RIG-I

Based on the data gained with the KSHV library screen, selected ORFs were analysed in small scale assays and in different cell lines. In our type I IFN reporter assay several ORFs potently inhibited IFNα4 and/or IFNβ induction upon NDV infection (Figure 9).

KSHV ORF36 was shown to interfere with type I IFN signalling (Hwang et al. 2009) and its murine homolog in MHV68 is described to bind phosphorylated IRF3 leading to inhibition of IRF3 binding to promoter sites (Hwang et al. 2009). In accordance with the published data, ORF36 expression strongly inhibited type I IFN promoter induction in all analysed cell types, thereby serving as a positive control for our assay.

KSHV ORF10, herpesvirus homologues of ORF11, and KSHV ORF54 are also already described inhibitors of the type I IFN response.

ORF10 is reported to form an inhibitory complex with the IFNAR, JAK and STAT, preventing ISGF3-mediated transcriptional induction (Bisson et al. 2009). In our reporter assay, ORF10 inhibited IFNβ induction in Hela S3 and Vero cells, but not IFNα4 in HeLa S3 and NIH3T3 cells. It is possible that IFNβ promoter inhibition by ORF10 resulted from a blocked positive feedback loop on transcriptional induction of type I IFNs. The positive feedback loop is mediated by an IFNAR signalling, leading to IFR7 protein expression and further induction of IFNα/β expression (Honda et al. 2006). The used cell lines in our assay should minimize IFNAR signalling dependent effects, since Vero and Hela S3 cells, arisen from HeLa cells, are described to be deficient in IFN production upon NDV infection (Blach-Olszewska et al. 1977, Desmyter et al. 1968). It is also possible that ORF10 has several functions, which is common for herpesvirus-encoded gene products (Pellet & Roizman 2013), and that we detected a novel function of ORF10 in this study. To test this hypothesis, an IFNAR$^{-/-}$ cell line could be used to analyse type I IFN promoter induction and mRNA levels upon RIG-I pathway activation in the presence of ORF10.

Similar to ORF10, KSHV ORF54 and MHV68-encoded ORF54 are described to interfere with IFNAR signalling. KSHV ORF54 decreases protein levels of IFNAR and additional receptors (Madrid & Ganem 2012), and MHV68 ORF54 induces the degradation of the IFNAR subunit IFNAR1 (Leang et al. 2011). We observed ORF54-dependent inhibition of the IFNα4 and IFNβ promoter downstream of RIG-I activation in HeLa S3 and NIH3T3 cells, which has not been reported previously. As described earlier for ORF10, the ORF54-mediated inhibition of IFNAR signalling could contribute to the impaired IFNα/β promoter induction. Future studies will be necessary to determine if ORF54 plays an additional role in inhibition of RIG-I signalling, for example mediating degradation of RIG-I signalling components.

ORF11 mildly inhibited IFNβ induction in HeLa S3 cells but did not reduce IFNα4 promoter induction in HeLa S3 or NIH3T3 cells. The MHV68- and EBV-encoded homologues of ORF11 are described to interfere with type I IFN signalling by different mechanisms. EBV-encoded LF2 interacts with IRF7 and prevents IRF7 dimerization (Wu et al. 2009), while MHV68-encoded ORF11 interacts with TBK1 and thereby abolishes interaction of TBK1 and IRF7 (Wu et al. 2009). Though we did not find a strong inhibitory effect of ORF11 on the RIG-I pathway, it might be possible that KSHV ORF11 interferes with type I IFN signalling as well. Experiments analysing the IFNα/β promoter induction upon SeV infection in 293T cells or analysing the interaction of ORF11 with TBK1 or IRF7 by co-IP studies as performed by Wu and colleagues, would help to address this question.

K10, also known as vIRF4, was described to interact with IRF7 thereby preventing IRF7 dimerization and activation resulting in inhibition of IFNα4 activation (Hwang et al. 2017). Additionally, vIRF4 promotes KSHV replication and survival in infected cells by interacting with molecules of NOTCH signalling (Heinzelmann et al. 2010) and promotes degradation of p53 to prevent cell cycle arrest (Lee et al. 2009). In our hands, K10 expression inhibited IFNα4 and IFNβ induction in all analysed cell lines. Noteworthy, expression of K10 potently induced IFNα4 and IFNβ promoter activation in unstimulated cells, which we did not observe for the other expression constructs, with the exception of a mild activation by ORF75 (data not shown). This could diminish further activation upon NDV infection, as the promoter was already induced. Further investigations are necessary to analyse whether this is a biological effect or an experimental artefact.

KSHV-encoded proteins with no effect on the type I IFN response downstream of RIG-I

No inhibitory effects on IFNα4/IFNβ promoters were detect for ORF23, ORF55, ORF64, or ORF75.

ORF23 is a predicted membrane glycoprotein (Kolar et al. 2008) and no immune evasive functions are described for ORF23 so far, being in accordance with our results.

ORF75 and MHV68-encoded ORF75c are described to deamidate RIG-I resulting in activation of the signalling pathway (He et al. 2015). We detected slightly elevated IFNα4 and IFNβ promoter induction in unstimulated cells in the presence of ORF75 (data not shown), being in accordance with data by He and colleagues.

ORF55, a predicted tegument protein (O'Connor & Kedes 2006), was shown to abolish cGAS-STING pathway activation upon overexpression of STING and cGAS in an IFNβ-luciferase reporter assay (Z. Ma et al. 2015). Since we did not detect ORF55-mediated inhibition of RIG-I signalling, this may suggest that ORF55 inhibits the cGAS-STING pathway far upstream in the signalling cascade, interfering with pathway components that are not required for RIG-I signalling. It would be interesting to perform follow-up experiments to verify these results and analyse how ORF55 inhibits the cGAS-STING pathway.

We observed that ORF64 expression enhanced IFNα4 and IFNβ induction upon NDV infection in HeLa S3 cells but not in NIH3T3 cells. In contrast to our results, KSHV ORF64 and its MHV68-encoded homolog are described to antagonise RIG-I signalling (Inn et al. 2011, Sun et al. 2015). Similar to our approach, Inn and colleagues analysed the effect of ORF64 on IFNβ promoter induction upon activation with a constitutive active RIG-I mutant or upon SeV infection in a luciferase reporter assay in Vero cells and found that ORF64 inhibited IFNβ activation. The differences between our results and those of Inn

et al. might be explained by different experimental conditions, e.g. the use of different cell lines or transfection reagents.

4.1.2 KSHV ORF20 inhibits the RIG-I-mediated type I IFN response

We observed that KSHV-encoded ORF20 inhibited IFNα4 induction in NIH3T3 cells and IFNβ induction in Vero cells upon NDV infection, in our initial luciferase reporter screen (Figure 44 Appendix). To verify these data, we performed small scale assays and furthermore included the analysis of the IFNα4 and IFNβ response in HeLa S3 cells upon NDV infection (Figure 9). We saw that ORF20 expression significantly inhibited IFNα4 and IFNβ induction upon NDV infection in all analysed cell types (Figure 9). The results were carefully controlled by comparing the inhibitory capacity to known virus-encoded type I IFN inhibitors like influenza A virus-encoded NS1 and KSHV-encoded ORF36, which showed only a slightly stronger inhibition than ORF20.

In a similar reporter assay, we analysed the role of ORF20 on IFNβ activation upon overexpression of RIG-I variants in HEK293T cells (Figure 40). We found that ORF20 expression inhibited IFNβ induction upon expression of constitutive active RIG-I-N and the RIG-I mutant K172R (Figure 40 B and C). Curiously, we did not observe that ORF20 diminished WT RIG-I induced signalling (Figure 40 A). The saturation of the luciferase signal can most certainly be excluded as an explanation, since we observed much higher Firefly luciferase values upon RIG-I-N than upon WT RIG-I expression. However, the results showed that the inhibitory effect of ORF20 on type I IFN induction was not influenced by NDV-induced TLR3 signalling but was dependent on RIG-I signalling.

As an additional read-out, we analysed ORF20 in a RIG-I-induced ISG56 promoter luciferase reporter assay in HEK293T cells and observed mild inhibition of ORF20 on the type I IFN signalling pathway (Figure 44). Most likely this confirmed that ORF20 inhibited the production of type I IFN downstream of RIG-I, which leads to a reduced activation of IFNAR signalling, which then leads to a diminished ISG56 promoter induction. To specifically detect ORF20-mediated effects on IFNAR signalling, cells should be stimulated with IFNβ in the presence or absence of ORF20.

Additionally, we analysed subcellular localisation of the important type I IFN transcription factor IRF3 upon NDV infection. Upon activation, cytoplasmic IRF3 dimerizes and translocates to the nucleus, where it binds to the promoter of IFNα and IFNβ genes (Honda & Taniguchi 2006). We observed cytoplasmic IRF3 localisation in unstimulated cells, and IRF3 localisation in the nucleoplasm omitted from the nucleolus upon NDV infection (Figure 34 and Figure 35). In the majority of ORF20-expressing cells, however, IRF3 was evenly distributed in the cytoplasm, nucleoplasm and nucleolus in unstimulated as well as in NDV infected cells (Figure 35 C). This might indicate that ORF20 manipulates proper cellular IRF3 localisation, thereby inhibiting IRF3 trafficking and subsequent binding to type I IFN promoter regions. However, this finding needs to be evaluated carefully, since the experiment was performed only once, and we cannot completely exclude that the observed IRF3 localisation was due to sample handling or labelling procedure. Usage of fluorochrome-coupled IRF3 and ORF20 constructs and subsequent live cell imaging would be a suitable alternative to IF staining, as it would exclude fixation and antibody dependent artefacts and would allow to analyse IRF3 trafficking upon activation in ORF20 expressing cells.

Altogether, our data suggest that KSHV-encoded ORF20 inhibits the type I IFN response downstream of RIG-I. Further experiments should address whether ORF20 inhibits additional PRR signalling pathways. Due to the experimental setup, ORF20 was identified independent of the viral context, since other KSHV-encoded gene products were absent. Future experiments should therefore address the inhibitory role of ORF20 during KSHV infection. To study lytic KSHV proteins like ORF20, a genetically modified form of KSHV is commonly used that does not undergo latency but exclusively performs lytic replication (Bussey et al. 2018, Bussey et al. 2014, Gallo et al. 2017). In this $KSHV_{LYT}$ strain, the promoter of the key protein replication and transcription activator (RTA) is substituted by an active PGK promoter. Importantly, an ORF20 stop virus on the $KSHV_{LYT}$ background has been recently generated in our lab (Bussey et al. 2018), which could be used to determine whether inhibition of IFNα/IFNβ induction is dependent on the presence of ORF20. Since KSHV encodes several type I IFN signalling inhibitors like ORF11, ORF36, and ORF64, expression of these proteins could mask ORF20-mediated inhibition. Nonetheless, similar approaches have successfully been used to study herpesvirus-encoded innate immune modulators (Hwang et al. 2009, Kang et al. 2014, Wu et al. 2015).

4.1.3 The ORF20 isoform ORF20 B is a novel inhibitor of the type I IFN pathway

KSHV encodes more than 85 ORFs and moreover maximizes its genome capacity by mRNA splicing, mRNA editing, translational frame shifting, internal translation initiation sites, and alternative start codons (Pellet & Riozman 2013, Arias et al. 2014, Bussey et al. 2018). The functions of these alternative gene products have only begun to be studied. A prominent example for herpesvirus protein isoforms with different functions are HSV-1 encoded UL26 and UL26.5. UL26.5 is expressed from an internal start codon and therefore shares a domain of identical amino acid sequence with UL26 (Liu & Roizman 1991, reviewed in Pellet & Riozman 2013).

The ORF20 gene product contributes to the KSHV genome complexity with an internal translation initiation site and an alternative start codon, thereby encoding the 320 aa full length isoform ORF20 (ORF20 FL), the 297 aa isoform ORF20 A, and the 257 aa isoform ORF20 B (1.3.2 Introduction). Previous studies with ORF20 were predominantly performed with an ORF20 construct which has all starting codons in frame with the first methionine. Therefore, the concurrent presence of all isoforms cannot be excluded here. But it is possible that ORF20 A and B are not as strongly expressed as ORF20 FL, since they lack a Kozak sequence.

When analysing the basic molecular properties of ORF20, we observed that the KSHV ORF20 construct that was used in our KSHV library screen expressed a 35 kDa and a 29 kDa protein (Figure 10). We found that the 29 kDa form correlated with the apparent protein size of ORF20 B (Figure 10) and concluded that the ORF20 construct used in this study expressed both, ORF20 FL and ORF20 B. Since the biological relevance of the different ORF20 isoforms is unclear, we included ORF20 B in several experiments.

In many experiments we found the same result for ORF20 and ORF20 B. ORF20 and ORF20 B showed the same localisation pattern and were strongly associated with the nucleolus (Figure 12 and Figure 13). They co-precipitated with endogenous nucleolar proteins L7a and DDX21 (Figure 17), as well as transiently expressed interferon-inducible OASL and its mutant OASLΔUbi (Figure 27). ORF20 and

ORF20 B colocalised with nucleolar proteins (Figure 18) and induced dispersal of nucleolar proteins (Figure 18 and Figure 19).

Notably, when analysing the type I IFN response, we found that ORF20 B expression inhibited induction of IFNβ and ISG56 promoters more potently than ORF20 (Figure 40 and Figure 41). Precisely, in the presence of ORF20 B, IFNβ and ISG56 promoter induction was significantly reduced downstream of WT RIG-I, mutant RIG K172R, and constitutive active RIG-I-N. ORF20 B was not included in the initial KSHV library screen, where we detected ORF20-mediated inhibition of the IFNα4 and IFNβ promoter upon NDV infection (Figure 9). It is possible that expression of ORF20 B from the ORF20 construct is partially or even completely responsible for this observed inhibition.

Experiments performed by Baca Chan in our lab showed that ORF20 B but not ORF20 strongly inhibited the IFNβ promoter induction upon transient cGAS-STING expression in 293T cells in a luciferase reporter assay (data not shown). Interestingly, Ma and colleagues showed that ORF20 strongly interfered with the cGAS-STING DNA sensing pathway (Z. Ma et al. 2015). In a KSHV library screen, they identified ORF20 and other KSHV-encoded proteins to inhibit IFNβ promoter induced by cGAS-STING overexpression using a luciferase assay in HEK293T cells. Since the study did not differentiate between the ORF20 isoforms, a complete comparison of the data is difficult. The variance in cGAS-STING pathway inhibition by ORF20 may be due to the used ORF20 expression constructs, which were part of two different KSHV libraries (Davis et al. 2015, Sander et al. 2008) and might express the ORF20 isoforms in varying amounts. Furthermore, differences in the experimental setup like the transfection reagent, the length of the IFNβ promoter in the Firefly luciferase reporter construct, as well as cell density and passage number (Hughes et al. 2007) may influence the experimental outcome.

Taken together these results indicate that the ORF20 isoform ORF B is a potent inhibitor of the RIG-I- and cGAS-mediated type I IFN response, suggesting that ORF20 B interferes with the type I IFN signalling pathway at a point where RIG-I and cGAS signalling have merged. This could consequently suggest that ORF20 FL fulfils another function, independent of ORF20 B-mediated IFN modulation.

Since our ORF20 expression construct expressed both ORF20 FL and ORF20 B, and ORF20 B showed stronger inhibitory capacity than ORF20, it is possible that ORF20 B but not ORF20 FL is an inhibitor of type I IFN signalling. To ascertain is hypothesis, different experiments should be performed that address the inhibitory role of ORF20 FL and ORF20 B in the type I IFN pathway using plasmid constructs that express each isoform singly or in combination. Such constructs have recently been generated in our lab (Bussey et al. 2018).

Future experiments could furthermore address the question at which level of the PRR signalling cascade ORF20 FL and ORF20 A inhibit. To do this, transient reporter assays that induce signalling by overexpression of different signalling components like MAVS, TBK-1, constitutive active IRF3, or IRF7 could be used.

It would be interesting to study if ORF20 FL and ORF20 B are expressed at different time points during viral replication, or if they are expressed preferentially in different cell types, as this could give hints about their relevance for the viral function. Lytic KSHV ORF20 FL and ORF20 B mutants could be used to address this question.

In summary, in this study we have identified KSHV ORF20 as a modulator of the type I IFN response. We found that the ORF20 isoform ORF20 B potently inhibits the type I IFN response downstream of RIG-I and further propose that inhibition is achieved far downstream since the PRR RIG-I and cGAS are both affected.

4.2 The KSHV ORF20 interactome

KSHV ORF20 is a poorly described protein. It belongs to the conserved UL24 family, whose members have been associated with diverging functions. HSV-1, HCMV, KSHV, and MHV68 UL24 family members have shown implications in cell cycle arrest (Nascimento & Parkhouse 2007, Nascimento et al. 2009, Paladino et al. 2014). HSV-1 UL24 is described to disperse nucleolar proteins (Lymberopoulos & Pearson 2007) and HCMV UL24 family member UL76 induces DNA damage response-mediated cytokine interleukin 8 (IL-8) expression (Costa et al. 2013) and formation of nuclear aggresomes (Lin et al. 2013).

To better understand the role of KSHV ORF20, we analysed the cellular ORF20 interactome which could indicate towards the function of ORF20. We used q-AP-MS to identify cellular interaction partners of ORF20 and found many specific binding partners (Figure 15 B and C, Table 24 Appendix).
Interestingly, most identified proteins are described to localise to nuclei and the vast majority binds RNA or DNA. We found a strong tendency for ORF20 to interact with ribosomal and ribosome-associated proteins, as we identified more than half of the 47 60S ribosomal proteins and more than one third of the 33 40S ribosomal proteins. Ribosomal proteins are highly concentrated in the nucleolus, the site of ribosome biogenesis. While ORF20 is not described to be able to bind RNA or DNA, we and others have found that ORF20 is localised in the nucleus and especially the nucleolus (Sander et al. 2008) (Figure 11). It is therefore reasonable that ORF20 interacts with nuclear and nucleolar proteins.
Ribosomal proteins are commonly referred to as contaminants during standard AP-MS and some are listed in the “contaminant repository for affinity purification”, or CRAPome (Mellacheruvu et al. 2013).
However, we used q-AP-MS, which allows discrimination of true and false interaction partners based on their relative abundance for the bait protein in comparison to a control protein. Moreover, labelling with heavy amino acids identifies procedural contaminants, which exclusively show binding in the light label sample. We furthermore controlled for ribosomal proteins by analysing the interactome of KSHV ORF75, a nuclear protein (Table 25 Appendix). We did not identify specific interactions with ribosomal proteins for ORF75, underlining that interaction of ORF20 with ribosomal proteins was not caused by the experimental procedure.
Nonetheless, experimental conditions can affect the outcome. For example, supplementation of the lysis buffer with the magnesium-chelating reagent EDTA destabilizes ribosomes and promotes dissociation into 60S and 40S ribosomal subunits, while in the absence of EDTA polysomes and ribosomes are retained in cell lysates (Fuchs et al. 2011). We used EDTA-free lysis buffer for q-AP-MS since only small quantities of EDTA are suitable for electrospray mass spectrometry. We transiently expressed ORF20 from a pcDNA vector construct to perform q-AP-MS, which is a commonly used strategy in AP-MS.

However, this can lead to overexpression artefacts, as excessive bait protein might interact with spurious proteins, leading to the identification of false-positive and false-negative results (Meyer & Selbach 2015). These side-effects can be limited by expression of the bait protein at near-endogenous levels by utilizing for example expression from bacterial artificial chromosomes (Hubner et al. 2010).
We controlled interaction of ORF20 with selected cellular binding partners by co-IP and IF studies. We found that ORF20 co-localised with the ribosomal protein L7a, as well as the nucleolar proteins DDX21, eIF6, and fibrillarin in the nucleolus (Figure 18) and additionally found co-precipitated ORF20 with L7a and DDX21 (Figure 17). These findings strengthened our q-AP-MS experimental setup and confirmed interaction of ORF20 with nucleolar proteins. The role of ORF20 on the ribosome maturation and translation will be discussed in 4.4.3.

During the course of this study, Davis and colleagues published a global mapping study of 89 KSHV proteins (Davis et al. 2015). The authors analysed cellular interaction of each individual ORF by performing AP-MS of strep-tagged expression constructs and evaluated the result with a developed MS interaction statistic scoring algorithm. They identified coiled-coil domain containing protein 86 (CCDC86) as a high-confident ORF20 interacting partner (Davis et al. 2015). The function of CCDC86, also known as cytokine-induced protein with coiled-coil domain or cyclon, is poorly understood. It is induced by IL-3 expression and associated with T-cell homeostasis. In line with our findings, CCDC86 is a nucleolar protein and has the ability to bind RNA (Castello et al. 2012). We did not detect CCDC86 as an interaction partner of ORF20. This may be due to differences in the experimental setup. We used HeLa S3 cells, while Davis et al. used 293T cells, and we performed SILAC based q-AP-MS instead of label free AP-MS. Additionally, the chosen protein tag could result in binding of different proteins - we used a myc-tag and not a strep-tag. In accordance with our findings, Davis and colleagues identified 542 weak interactions for ORF20, including nucleolar proteins like fibrillarin and ribosomal proteins (Davis et al. 2015).

Noteworthy, we did not detect type I IFN signalling components to interact with ORF20, although we found that ORF20 inhibited IFNα4, IFNβ, and ISG56 promoters, as discussed in 4.1.2 and 4.1.3. This could either suggest that ORF20 inhibits type I IFN activation not by directly binding to proteins involved in signalling, but achieves its inhibitory function via indirect mechanisms, like chromatin modulation, effects on translation or rearrangement of nuclear and nucleolar protein localisations. Since we found that the ORF20 B isoform was a stronger inhibitor of the type I IFN response, our result could also suggest that we did not enrich for ORF20 B protein interaction partners, though our ORF20 expression construct expressed both isoforms, ORF20 FL and ORF20 B. To discriminate between the ORF20 FL and the ORF20 B interactome and to unravel their individual function, q-AP-MS studies could be performed with expression constructs encoding each isoform singly.

Importantly, our q-AP-MS studies revealed interaction of ORF20 with two different antiviral proteins. We found DDX21, a nucleolar helicase, to bind KSHV ORF20 (Figure 15 B and C, Table 24 Appendix), confirmed their interaction by IP (Figure 17), and showed colocalisation of DDX21 and ORF20 in the

nucleolus (Figure 18). DDX21 interferes with Influenza A virus replication by binding to a component of the viral polymerase complex, whereby a large proportion of this protein complex re-translocates to the nucleus (G. Chen et al. 2014). The role of DDX21 during herpesvirus infection is not understood. We found that ORF20 dispersed DDX21 and other nucleolar proteins from the nucleolus (discussed in 4.3.3 in detail). Future studies would be needed to determine whether DDX21 is able to diminish KSHV replication and whether ORF20 interaction with DDX21 or dispersal of DDX21 could prevent this.
As a major finding of this study, we identified the interferon-inducible oligoadenylate synthetase-like protein (OASL) as a specific ORF20 interaction partner. We subsequently characterised the interaction of ORF20 and OASL and the function of this interaction. These results will be discussed in 4.4.

In summary, we used the sophisticated q-AP-MS technique to identify a complete cellular protein-protein interaction map of KSHV ORF20. We identified several specific interaction partners of ORF20, whereby ORF20 predominantly interacted with nucleolar RNA/DNA-binding proteins, ribosomal proteins and the signature ISG OASL.

4.3 The role of KSHV ORF20 in the nucleolus

4.3.1 ORF20 is a nucleolar protein

As part of the basic protein characterisation of ORF20, we analysed subcellular localisation of ORF20 and ORF20 B. Since the subcellular localisation is closely related to the protein function due to the cellular processes that are concentrated in a distinct compartment or cellular area, localisation studies are a common and helpful starting point to study viral protein function (Salsman et al. 2008).

We found transiently expressed ORF20 localised in the nucleolus and the nucleoplasm, additionally we detected cytoplasmic localisation in several cells (Figure 11). We verified localisation in cell types of different origin (Figure 11). These results were in accordance with published data that showed ectopically expressed ORF20 to be localised in the nucleolus und nucleus (Sander et al. 2008).
The subcellular localisation of the isoforms ORF20 B and ORF20 A was not known. We found that ORF20 B showed the same localisation as ORF20 (Figure 13). Subsequent studies of our group compared localisation of ORF20 and the ORF20 FL, ORF20 B, and ORF20 A isoforms, using expression constructs that expressed each isoform exclusively. They found that all isoforms predominantly localised to the nucleoli and nuclei, and were indistinguishable from the original ORF20 expression construct (Bussey et al. 2018).

In the present study, ORF20 and ORF20 B localisation was not analysed in the context of KSHV infection. However, interactions between viral proteins can alter the localisation of individual ORFs (Salsman et al. 2008). Further studies of our group observed the same subcellular localisation of myc-tagged ORF20, ORF20 FL, and ORF20 B in cells latently infected with KSHV and upon KSHV reactivation (Bussey et al. 2018). For this approach Bussey et al. used HuARLT2-rKSHV.219 cells, a conditionally immortalized human endothelial cell line latently infected with a genetically modified KSHV

strain. This recombinant rKSHV.219 allows detection of latently infected cells by expression of GFP, while reactivation and subsequent lytic gene expression can be detected by RFP expression.

While overexpression of proteins can potentially lead to artificial localisation, our results clearly show that ORF20 has the potential to localise to the nucleolus under some circumstances. Our findings are strengthened by localisation studies of herpesvirus UL24 family members, where ORF20 belongs to. We observed predominant nuclear and nucleolar localisation of the MCMV encoded UL24 family member M76 in different cell types of different species (Figure 23 and Figure 24), suggesting that the nucleolar localisation was conserved between ORF20 and M76. Based on these results, succeeding studies of our group systematically analysed the localisation of the UL24 family members of the *Alpha*-, *Beta*-, and *Gammherpesvirinae*. HSV-1 UL24, HCMV UL76, MCMV M76, and MHV68 ORF20 were detected in the nucleus and cytoplasm, and distinctly in the nucleolus in transiently transfected in HeLa cells (Bussey et al. 2018).
Moreover, our results were in accordance with previous studies. HSV-1 UL24 and HCMV UL76 were identified to have significant nucleolar localisation, but were also detected in the nucleus and in the cytoplasm (Salsman et al. 2008). Additionally, EBV-encoded UL24 family member BXRF1 is a described nucleoprotein with nucleolar localisation (M. Cai et al. 2017). These results confirm that the subcellular localisation is conserved among UL24 family members.

4.3.2 ORF20 affects chromatin structure in the nucleus

We found that ORF20 and ORF20 B showed a more diverse localisation, as we observed distinct localisation in different subnuclear areas (Figure 11 and Figure 13) and therefore categorised ORF20 localisation into four categories (Figure 12). Next to the well described nucleolar und nuclear localisation of ORF20, here referred to as ORF20-i localisation, we observed cells that expressed ORF20 in the nucleoplasm and in nucleolar-ring-like structures, probably reflecting the nucleolar border (ORF20-ii), and cells that showed nuclear localisation but were lacking nucleolar ORF20 (ORF20-iii). Additionally, we observed cells that showed distinct expression of ORF20 at the nuclear periphery and the nucleolar border but no expression in the nucleoplasm (ORF20-iv). This observation was verified in different cell lines of different species. Interestingly, we found an altered DNA staining that corresponded to the ORF20 localisation ORF20-ii to iv (Figure 11), which was best detectable in HeLa S3 cells, probably due to the size of the nuclei.
It is possible that these observations were reflecting antibody and dye accessibility of subcellular regions, which might have varied within the sample based on the amount of expressed protein in each cell. It was shown that a high concentration of a transiently expressed antigen led to insufficient antigen detection in the nucleolus, which was detected as peripheral staining of the nucleolus resembling nucleolar ring-like structures (Svistunova et al. 2012). However, fixation of the cells with cold methanol led to a complete antibody accessibility, as the nuclear and nucleolar proteins were partially extracted and thus antigen concentration was reduced (Svistunova et al. 2012). We used a combination of cold methanol and PFA fixation in our localisation studies, which should have reduced staining problems originating in the before mentioned antigen concentration.

Subsequent studies of our group that analysed localisation of transduced ORF20 upon lytic KSHV infection in HuARLT2-rKSHV.219 cells did not confirm ORF20 localisation phenotypes or altered DNA localisation (Bussey et al. 2018 and personal comunication with Kendra Bussey).
However, virus-induced DNA marginalisation has been overserved during herpesvirus replication. During this process the chromatin within the nucleus condenses, while viral replication compartments expand and the interchromatin domains enlarge, allowing large macromolecular assemblies like ribonucleoprotein particles and herpesvirus capsids to reach the nuclear periphery and exit the nucleus (Bosse et al. 2015 and references within). The viral factors that accomplish alteration of the nuclear architecture are unknown. It would therefore be of interest to study if ORF20 is able to induce DNA marginalisation and rearranges the nuclear architecture to promote KSHV lytic replication.

4.3.3 ORF20 interacts with nucleolar proteins and induces their dispersal

We found KSHV ORF20 to be localised in the nucleolus and nucleus and identified several nucleolar interactions partners of ORF20 by q-AP-MS. KSHV encodes 21 ORFs that are described or predicted to be at least partially localised in the nucleus (Sander et al. 2008, Davis et al. 2015). A study of our group found that of these 21 ORFs, ORF20 was the only KSHV protein that was convincingly located in the nucleolus in the absence of other viral factors (Osbelt 2016), indicating that ORF20 has an important function in this subcellular compartment.
To further characterize the function of ORF20 in the nucleolus, we verified interaction of ORF20 with ribosomal L7a and helicase DDX21 by co-IP (Figure 17). Additionally, we performed colocalisation studies of ORF20 with several nuclear and nucleolar proteins. We found that ORF20 colocalised with the previously identified interaction partners fibrillarin, eIF6, L7a, and DDX21 in the nucleolus. We used signature proteins of subnuclear compartments to further investigate localisation of ORF20 and observed colocalisation with the important nucleolar protein nucleolin, but no colocalisation with PML, the marker of nuclear bodies (NBs), or coilin, the marker of Cajal bodies (Figure 18). On further inspection we found that transient expression of ORF20 strongly correlated with the absence of ribosomal L7a, nucleolin, DDX21, eIF6, and fibrillarin expression in the nucleolus in HeLa S3 cells (Figure 18), as about one third of the analysed cells showed no expression of these proteins in the nucleolus in the presence of ORF20 (data not shown). This effect was even more pronounced in cells with ORF20 localisation phenotype ORF20-ii, iii, and iv (as illustrated in Figure 12), where more than half of the ORF20 cells lacked nucleolar protein expression (Figure 19). ORF20 did not alter the subnuclear localisation of PML, but changed coilin expression in more than two thirds of the analysed cells, whereby coilin was either absent or expressed in the nucleolus instead of Cajal bodies (Figure 18 and Figure 19). We confirmed our results in different cell types and species (Figure 20 and Figure 21).

We were wondering whether the missing expression signals of the nucleolar proteins were due to manipulation on the protein level. Analysis of whole cell lysate samples showed that the nucleolar proteins L7a and DDX21 were equally expressed in the presence or absence of ORF20 (Figure 17), indicating that ORF20 did probably not affect overall protein expression or protein stability.
Another possibility would be that ORF20 induced dispersal of nucleolar proteins. Notably, we did not observe redistribution of the nucleolar proteins to other subcellular compartments (Figure 18 and Figure

20). For sample fixation, we used cold methanol and subsequent PFA treatment to allow detection of endogenous nucleolar protein expression. However, as mentioned earlier, methanol treatment extracts nuclear and nucleolar proteins and might change the cellular morphology (Sheval et al. 2005, Svistunova et al. 2012). To exclude that redistribution of the analysed nucleolar proteins was not detected due to methanol fixation, short proteinase treatment of the cells prior to PFA fixation could be used to reduce the density of the cellular contents and hence allow antigen detection in the nucleolus (Svistunova et al. 2012).

Notably, we observed redistribution of coilin to the nucleolus in the presence of ORF20. Coilin is a major component of Cajal bodies, which are closely connected to the nucleolus as distinct proteins traffic between these subnuclear structures (Machyna et al. 2014). Hence, we propose that ORF20 manipulates a distinct subset of nuclear proteins that are functionally connected to the nucleolus, resulting in their dispersal or dissociation from original subnuclear compartments. In line with our results, ORF20 homologue HSV-1 UL24 was shown to disperse the nucleolar proteins nucleolin and B23 (Lymberopoulos & Pearson 2007, Lymberopoulos et al. 2011). While HSV-1 infection induces fibrillarin redistribution to spots in the nucleoplasm (Lymberopoulos & Pearson, 2010), this is supposed to be independent of UL24 function (Lymberopoulos & Pearson, 2007).

Since we did not find a nucleolar protein that was unaffected by ORF20 expression, future experiments could analyse if ORF20 directly interacts with nucleolar proteins like fibrillarin, ribosomal proteins, and DDX21, or if ORF20 indirectly interacts with these proteins, maybe by binding to the same RNA or DNA, or by interacting with the same macromolecular complex e.g. ribosomal subunits. Unbiased quantitative MS analysis of cell infected with lytic KSHV, KSHV ORF20 stop virus, and uninfected cells could be used to analyse the nucleolar proteome composition upon KSHV infection and the effect of ORF20 within. A similar approach has revealed that influenza-A virus targets specific nucleolar pathways by manipulating the nucleolar proteome composition (Emmott et al. 2010).

These results would be especially interesting since recent research provides evidences that nucleoli are an important target of almost all types of viruses, though the implications of viral-nucleolar protein interactions are only beginning to emerge (Matthews et al. 2011, Rawlinson & Moseley 2015). The interactions can be broadly divided into two classes: viral proteins that recruit nuclear or nucleolar proteins to facilitate proviral functions and viral proteins that target nucleolar proteins to modify host cell functions (Davis et al. 2015). The identified redistribution of several nucleolar proteins by ORF20 would suggest that ORF20 induces a broad change in the nucleolar protein composition, whereby the implications for the host cell function and especially ribosome biogenesis, transcription, and cell cycle are unclear. Intrudingly, absence of each nucleolar protein from the nucleolus itself could result in broad changes of the cell function. Exemplary, nucleolin is a highly multifunctional protein. It is involved in nearly all nuclear-associated process, including transcription, ribosome biogenesis, trafficking of nuclear proteins, DNA replication and chromatin organisation (Tajrishi et al. 2011, Durut & Sáez-Vásquez 2015). Furthermore, downregulation of nucleolin is reported to increase expression of p53, leading to inhibition of RNA polymerase I transcription and induction of cell cycle arrest in the G_2 phase (Tajrishi et al. 2011). Studies by Nascimento and colleagues found that transient expression of KSHV ORF20, HSV-1 UL24, HCMV UL76, and MHV68 ORF20 interfered with cell progression to mitosis in a Cdc2-cyclin B complex

dependent manner, resulting in cell cycle arrest in the G_2 phase. It is possible that rearrangement of the nucleolar proteome composition and dispersal of nucleolin by ORF20 is connected with these observations. However, we did not observe a subsequent induction of cell death in the presence of ORF20, as reported in these studies. Future studies should confirm if KSHV ORF20 induces cell cycle arrest and analyse whether this would be mediated or caused by the dispersal of nucleolar proteins like nucleolin.

As described before, KSHV ORF20 belongs to the conserved UL24 protein family, and HSV-1-encoded family member UL24 was shown to induce dispersal of the nucleolar proteins nucleolin and B23 (Bertrand & Pearson 2008, Bertrand et al. 2010, Lymberopoulos et al. 2011). These studies described that the UL24 homology domain was involved in proper function of UL24. Hence, we were wondering whether manipulation of nucleolar proteins was conserved in the UL24 protein family. We analysed localisation and presence of nucleolar protein expression in cells transiently expressing the murine herpesvirus MCMV-encoded UL24 family member M76 (Figure 24 and Figure 25). Like ORF20, M76 was predominantly located in the nucleolus and was additionally expressed in the nucleoplasm and in some cells in the cytoplasm. The nucleolar proteins fibrillarin, eIF6, and DDX21 colocalised with M76 in the nucleolus. Though their expression was frequently diminished in the presence of M76, an absence of nucleolar protein expression was seldomly observed. This could indicate that M76 has the capability to alter nucleolar protein localisation but might require viral cofactors to gain full function. MCMV has a much larger genome than the alpha- and gammaherpesviruses, which is encoding for more than 170 ORFs (Tang et al. 2006). This could argue that MCMV ORFs orchestrate their functions by interlinking different gene products. It is also possible that dispersal of nucleolar proteins is not a conserved function of the UL24 family members, but that the functions of these proteins may vary. This hypothesis is strengthened by the observation that HCMV UL76 but not HSV-1 UL24 is described to reduce the number of PML NBs per cell (Salsman et al. 2008).
As described in 4.3.1, predominant nucleolar localisation is conserved throughout the members of the UL24 protein family. A complete comparison of alpha-, beta-, and gammaherpesvirus-encoded UL24 proteins would be needed to investigate if dispersal of nucleolar proteins is conserved in all subfamilies, or limited to some subfamilies or even restricted to distinct herpesviruses.

Conclusively, unravelling the ORF20-induced effects on the molecular composition of nucleoli and the corresponding outcome on cellular function might provide key insights into the molecular mechanisms of KSHV infection and might moreover provide a better understanding of the molecular biology of nucleoli. Finally, these findings could result in new targets for intervention of herpesvirus infection.

4.4 Characterisation of the interaction of KSHV ORF20 and human OASL

4.4.1 KSHV ORF20 interacts with OASL

Using the unbiased q-AP-MS approach, we identified the cellular OASL protein as binding partner of ORF20 (Figure 15 and Table 24). This interferon-stimulated gene (ISG) product was of special interest

since it was described to possess antiviral activity against a number of RNA viruses, but an implication for DNA virus infection had not been shown. OASL belongs to the OAS protein family, which is characterised by the presence of the OAS domain (1.4.4 Introduction). Based on this domain, OAS family members OAS1, 2, and 3 are capable to synthesize 2'-5'-linked oligoadenylates, which activate an RNaseL-mediated RNA decay pathway. The OAS domain of OASL, however, shows important sequence differences, resulting in an enzymatically inactive OASL protein. In addition, OASL has a unique C-terminus composed of two ubiquitin-like domains which are absent in OAS1-3 (1.4.4 Introduction and Figure 26).

ORF20 specifically interacts with OASL

To verify interaction of ORF20 and OASL, we performed co-IP experiments and found that ORF20 precipitated with OASL and vice versa (Figure 27 A and B). In the same way, the ORF20 B isoform showed interaction with OASL (Figure 27 A and B), which showed that aa 1-64 of ORF20 were dispensable for its interaction with OASL.

To understand which domains of OASL were required for interaction with ORF20, we used an OASL truncation mutant (OASLΔUbi), expressing aa 1-339 and therefore lacking the C-terminal ubiquitin domains of OASL. We found that ORF20 interacted with OASLΔUbi, showing that ubiquitin domains of OASL were not required for the interaction with ORF20 (Figure 27 A and B). Importantly, ORF20 interacted specifically with the OAS domain of OASL, as ORF20 did not interact with OAS family member OAS1, which contains one enzymatically active OAS domain, but interacted with OASLΔUbi, which has the OASL-specific OAS domain (Figure 27 A and B).

OASL is able to bind RNA, due its dsRNA binding groove in the OAS domain (Ibsen et al. 2015). Therefore, we were wondering whether the interaction with ORF20 occurred indirectly or by binding to the same RNA. Subsequent studies of our group used OASL RNA binding mutants to show that the interaction of ORF20 and OASL was not dependent on RNA binding of OASL (Bussey et al. 2018).

Since the experimental setup presented here was using overexpressed proteins, it might be possible that a post-lysis interaction was accounting for the observed interaction of ORF20 and OASL. However, subsequent studies performed by Kendra Bussey in our lab showed that only minor interaction of ORF20 and OASL occurred if the both proteins were expressed singly and lysates were combined for IP, which proofed that the interaction was not artificial. In the following, our group was able to overcome the difficulties to detect endogenous OASL by using polyclonal antibodies against OASL. Based on this, subsequent studies of our group could show that endogenous OASL co-precipitated with ORF20 in HeLa S3 cells, as well as in RIG-I-induced 293T cells, but not in 293T OASL-/- cells (Bussey et al. 2018), validating the ORF20-OASL interaction results presented in this study.

ORF20 colocalises with OASL

Additionally, we performed IF studies to analyse the subcellular localisation and colocalisation of ORF20 and OASL. We found that OASL was located in the cytoplasm and the nucleolus and omitted from the nucleoplasm, which was in accordance with previous studies (Rebouillat et al. 1998, Zhu et al. 2014).

OASL localisation was not affected by coexpression of ORF20 and we detected clear colocalisation of ORF20 and OASL in the nucleolus and to a minor extent in the cytoplasm of transiently transfected cells (Figure 29).

In contrast to full length OASL, we found the truncated OASLΔUbi mutant localised in the cytoplasm and nucleoplasm and omitted from the nucleolus. However, we detected a few cells with OASLΔUbi expression at the nucleolar border (Figure 29), which might indicate that the nucleolar localisation was not completely dependent on the protein sequence encoded by aa 340-514 of OASL, expressing the Ubi domains. Therefore, it might be possible that translocation of OASL from the nucleoplasm to the nucleolus is at least partially dependent on the Ubi domains. A potential nucleolar localisation signal (NoLS) was predicted for OASL within the Ubi domains at aa 376-386 (Rebouillat et al. 1998). In line with our results, subsequent studies performed in our lab analysed localisation of several OASL mutants and found that the predicted NoLS was not required for nucleolar localisation, but aa 340-350 were necessary (Osbelt 2016).

We found cytoplasmic colocalisation of ORF20 and OASLΔUbi in cells with cytoplasmic ORF20 expression and nucleolar colocalisation in cells with nucleolar OASLΔUbi (Figure 29). Since we less frequently detected colocalisation of ORF20 and OASLΔUbi and found weaker interaction of ORF20 or ORF20 B with OASLΔUbi after IP, our results suggest that nucleolar localisation of OASL is beneficial but not required for interaction with ORF20.

ORF20 interacts with all OASL isoforms

In humans three OASL isoforms are described. The pristine isoform OASL-a is commonly referred to as OASL protein and has been predominantly studied. The OASL-b and OASL-d isoforms, however, are barley described (see also 3.3.1 and Figure 26).

To gain further insight into the ORF20-OASL interaction, we analysed subcellular localisation of each OASL isoform, which has not been studied before (Figure 30). In addition to the cytoplasmic localisation that all OASL isoforms showed, we found that OASL-a was exclusively located in the nucleolus but omitted from the nucleoplasm. In contrast, OASL-b and OASL-d were located in the nucleoplasm but not the nucleolus. OASL-a has a unique amino acid sequence (aa 250-350), encoding the C-terminal part of the OAS domain, which OASL-b and-d are lacking. Therefore, our result led to the conclusion that not a sequence within the Ubi domains (aa 350-514 of OASL-a), like the predicted NoLS between aa 376-386 (Rebouillat et al. 1998), is required for nucleolar localisation, but supports the hypothesis, that the sequence encoded by aa 340-350 of OASL-a is functioning as an NoLS (Osbelt 2016). For secluding analysis whether weak nucleolar expression of OASL-b and/or OASL-d was undetected by our approach, extraction of the cytoplasm prior to fixation could improve visualisation of the nucleolar expression signals.

Using co-IP studies, we found that ORF20, as well as the ORF20 B isoform, were able to interact with all three OASL isoforms. However, the strength of expression of the corresponding interaction partner indicated that ORF20 and ORF20 B interacted strongest with OASL-a, moderately with OASL-b, and weakly with OASL-d (Figure 28). This might indicate that binding affinity to ORF20 correlated with the overall length of the OASL isoform, as OASL-a is a 514 aa protein, OASL-d a 384 aa protein, and OASL-

d a 255 aa protein (Figure 26 A) and interaction occurs over the overall length of OASL. The interaction between ORF20 and OASL-b, which is lacking the Ubi domains, supports our results gained with the OASLΔUbi mutant (Figure 27), showing that ORF20-OASL interacted independently of the Ubi domains of OASL. Moreover, absence of nucleolar localisation of OASL-b and OASL-d and concomitant binding to ORF20 supports our hypothesis that nucleolar localisation is not mandatory but supportive for interaction of ORF20 and OASL.
It has been shown that expression of all three OASL isoforms can be induced by interferons and that different interferons induced discrete isoforms (Guo et al. 2012). However, the biological relevance of the existing OASL isoforms is still under debate (personal communication with Rune Hartmann) and future experiments are required to determine endogenous relevance and existing discrete functions.

In summary, this is the first study that showed interaction of a viral protein with human OASL. We found that ORF20, as well as its isoform ORF20 B, predominately colocalised with isoform OASL-a in the nucleolus but interacted with all three known OASL isoforms, independent of nucleolar localisation or presence of the Ubi-domains of OASL.

Subsequent studies of our lab emphasised the relevance of the ORF20-OASL interaction, as they found that interaction with OASL was conserved among the UL24 family members (Bussey et al. 2018). By using a similar approach as presented in this study, they showed interaction of OASL with the ORF20 homologues MCMV M76, HCMV UL76, and HSV-1 UL24 using co-IP.

4.4.2 KSHV ORF20 does not interfere with the OASL effect on RIG-I

During the course of this study, OASL has been shown to amplify RIG-I-mediated type I IFN induction. OASL directly binds to RIG-I and substitutes for its polyubiquitination, which is leading to further activation of this cellular RNA sensor (Zhu et al. 2014). A subsequent study showed that dsRNA-binding of the OAS domain of OASL was crucial to mediate RIG-I signalling enhancement (Ibsen et al. 2015). Since we identified ORF20 was an inhibitor of the RIG-I signalling pathway and showed interaction and colocalisation of ORF20 and OASL, we performed several experiments to analyse if ORF20 interfered with the OASL-mediated effect on RIG-I function.

Using IF microscopy, we found RIG-I and OASL colocalisation in the cytoplasm, which was in accordance with the published results (Zhu et al. 2014). ORF20 did not colocalise with RIG-I in the absence or presence of transiently transfected OASL (Figure 31). Furthermore, ORF20 expression did not alter subcellular localisation of RIG-I or OASL, nor prevented colocalisation of RIG-I and OASL (Figure 31), showing that ORF20 did not manipulate colocalisation of OASL and RIG-I.
Using co-IP experiments, we confirmed the published interaction of OASL and RIG-I (Figure 32). We found that ORF20 co-precipitated with OASL, as observed before, but did not co-precipitate with RIG-I in the absence of OASL. Moreover, we found that ORF20 co-precipitated with RIG-I and OASL, suggesting that ORF20 did not inhibit interaction of RIG-I and OASL, but that OASL was able to bind both, RIG-I and ORF20 (Figure 32).

To analyse whether ORF20 interfered with OASL-mediated enhancement of RIG-I signalling, we performed several experiments analysing OASL function on type I IFN induction. We found that overexpression of OASL induced IRF3 nuclear translocation in unstimulated cells and further increased IRF3 nuclear translocation upon NDV-induced RIG-I pathway activation. Overexpression of the truncated OASLΔUbi mutant did not lead to enhanced IRF3 nuclear translocation, showing that the Ubi domains were indispensable for this effect (Figure 33 and Figure 34).
These results have to be carefully interpreted, since liposomal transfection reagents are known to induce IFNβ and ISGs expression (X. Li et al. 1998). However, the transfection reagent LF, that was used in our study, was one of three reagents that showed only minimal induction effects (Jensen et al. 2014). We carefully controlled our experiment by including untransfected cells and cells transfected with the control protein LacZ. Importantly, our results were in accordance with the published data by Zhu and colleagues, showing that OASL enhanced IRF3 dimerization and nuclear translocation in an Ubi domains-dependent manner (Zhu et al. 2014).

Additionally, we analysed the effect of OASL on RIG-I-induced ISG56 expression using IB experiments. As expected, transient transfection of WT RIG-I induced ISG56 expression, while the constitutively active RIG-I-N mutant had an even stronger effect (Figure 36). In contrast to the published data, the RIG-I ubiquitin-binding mutants RIG-I K172R and RIG-I T55I did not show a completely abolished type I IFN induction (Zhu et al. 2014), but had a mildly inducing effect on ISG56 expression (Figure 36). This might be due to differences in the transfection procedure, like incubation time and used transfection reagent, the passage number of the used cells, or due to differences in the antibody concentration during immunoblotting. When using less expression construct for transfection, we could not measure induction of ISG56 expression by RIG-I K172R and RIG-I T55I, suggesting that the used DNA amount was able to change the experimental outcome and could account for the observed difference in ISG56 expression (Figure 37). However, our results suggest that the introduced mutations K172R and T55I in RIG-I did not completely abrogate RIG-I function in our hands. This was supported by the observation that expression of the RIG-I K172R mutant induced IFNβ promoter activation in a luciferase reporter assay, although induction was strongly reduced compared to WT RIG-I (Figure 39).
We found that overexpression of OASL alone was not sufficient to induce ISG56 expression, while co-expression of OASL and RIG-I increased ISG56 expression compared to RIG-I alone. OASL did not enhance RIG-I-N-mediated ISG56 expression, probably because pathway activation was already saturated by RIG-I-N expression. Overexpression of OASL partially rescued RIG-I K172R and RIG-I T55I pathway activation (Figure 36), confirming that OASL was able to substitute for hindered polyubiquitination of the RIG-I mutants (Zhu et al. 2014). When we used this experimental setup to analyse ORF20 coexpression effects, we found no inhibitory effects of ORF20 on RIG-I-induced ISG56 expression or OASL-mediated enhancement of ISG56 expression (Figure 37).

We used an IFNβ luciferase reporter assay as a different read-out to analyse type I IFN induction downstream of RIG-I. We found that stable expression of OASL was mildly enhancing WT RIG-I induced IFNβ induction in one of two HEK293T cells lines from different origin. OASL was not affecting RIG-I

K172R or RIG-I-N induced signalling (Figure 39). This was in contrast to the published data showing that stable OASL expression led to an elevated IFNβ induction in the presence of WT RIG-I and RIG-I K172R and T55I mutants (Zhu et al. 2014).

Notably, we measured high levels of luciferase activity with our experimental approach, which was probably accounting for the high standard variations within the experiment. However, we could clearly detect the varying effects of the different RIG-I mutants on IFNβ activation, which were in accordance with the published data (Figure 39 and Figure 40). Additionally, we found significant inhibitory effects of ORF20 B coexpression (Figure 40), suggesting that the experimental setup was a useful approach to study the influence of different factors on the RIG-I signalling pathway. Although we verified OASL expression in the generated stable cell lines (Figure 38), it might be possible that less OASL protein was expressed in the cell line compared to transient transfection approaches, and might not have been sufficient to mediate OASL enhancement of RIG-I signalling.

We performed this experiment in HEK293T cell lines that were commonly used in our lab (HEK293T VIMM) and HEK293T cells that were originally used by Zhu et al., which we received from Veit Hornung (HEK293T VH). While OASL had a mild enhancing effect on IFNβ activity in HEK293T VH cells, this was not the case in VIMM cells. This could be explained by differences in cell density and passage number of the used 293T cell lines, as these factors are described to affect the experimental outcome (Hughes et al. 2007). HEK293T cells are used in many labs since decades. It should be considered that HEK293T cell lines have developed lab-specific characteristics, which may result in differing experimental outcomes, as suggested by Veit Hornung.

Analysing the effect of ORF20 and ORF20 B co-expression, we found that ORF20 slightly and ORF20 B strongly inhibited IFNβ induction, which was independent of stable OASL expression (Figure 40). To completely exclude a contribution of OASL for ORF20 inhibition of the type I IFN pathway, ORF20 should be studied in the absence of endogenous OASL. Hence, OASL knockout cells should be used for future experiments and a HEK293T OASL-/- cell line is now available in our lab.

Additionally, we analysed OASL expression and ORF20-OASL co-expression in a RIG-I ISG56 luciferase-based reporter assay. As observed for IFNβ promoter induction, we found that stable expression of OASL in HEK293T VH cells had no effect on ISG56 promoter induction in the presence or absence of WT RIG-I, RIG-I K172R, or RIG-I-N (Figure 41). This was in contrast to our results gained by ISG56 IB, where we found that ISG56 protein expression was enhanced in the presence of OASL (Figure 36). As mentioned earlier, it might be possible that OASL expression in the stable cell line was not sufficient to measurably increase RIG-I pathway activation. Since we used the same HEK293T VH cells in both experiments, cell line dependent effects can be neglected. In addition, it cannot be excluded that detection of the ISG56 protein by IB and detection of ISG56 promoter induction by an ISG56-repoter construct was leading to different results.

In line with the IFNβ luciferase data (Figure 40), we found that ORF20 mildly and ORF20 B strongly inhibited ISG56 induction downstream of RIG-I activation, which was independent of OASL expression (Figure 41). However, we did not detect inhibition of ISG56 protein expression by ORF20 by IB (Figure 36). Since we detected only moderate inhibitory capacity of ORF20, it is possible that ORF20 expression

in the ISG56 IB experimental setup was not sufficient to measurably inhibit ISG56 expression. Comparative analysis of ORF20, ORF20 B, and ORF20 FL should reveal whether the isoforms have a distinct inhibitory function on ISG56 expression upon RIG-I activation (see also 4.1.3).
In summary, we could confirm the published data by Zhu and colleagues (2014) showing that OASL colocalised and interacted with RIG-I and was furthermore able to enhance RIG-I-mediated type I IFN induction. We found that ORF20 did not prevent colocalisation or interaction of RIG-I and OASL, nor inhibited the RIG-I pathway in an OASL-dependent manner. Our results indicate that activation of the RIG-I pathway was manipulated by ORF20 independent of its interaction with OASL.

4.4.3 OASL and ORF20 show a highly overlapping interactome and interact with ribosomal proteins

OASL is highly upregulated upon viral infection, interferon treatment and IRF3 activation (Melchjorsen et al. 2009, Schoggins et al. 2011). Overexpressed OASL was shown to possess antiviral activity against a number of distinct RNA viruses, while other RNA viruses were unaffected (Schoggins et al. 2011, Schoggins et al. 2014). The role of OASL during DNA virus infection is barely studied. OASL did not affect replication of the DNA viruses vaccinia (Schoggins et al. 2014), or HSV-1 (Marques et al. 2008), while a contradictory study described an antiviral effect of OASL on HSV-1 (Zhu et al. 2014).
To date two cellular interaction partners of OASL are described. The transcriptional repressor methyl CpG binding protein 1 (MBD1) was identified to interact with OASL in a yeast two-hybrid screen of a human leukocyte cDNA library (Andersen et al. 2004). Secondly, OASL was shown to interact with the cellular sensor RIG-I, thereby enhancing type I IFN signalling. Co-precipitation of OASL and RIG-I was shown for transiently expressed and endogenous proteins (Zhu et al. 2014). However, no global interaction studies were available of OASL. Our study is the first to show that a viral protein, KSHV ORF20, interacts with OASL.

To better understand why and how ORF20 and OASL may interact, we used the unbiased approach of q-AP-MS to identify cellular interaction partners of OASL and unravel its cellular function. As OASL was shown to play a role in the RIG-I signalling pathway, we analysed the OASL interactome in unstimulated and NDV infected cells (Figure 42, Table 26, and Table 27).
We identified numerous highly confident interaction partners of OASL under both conditions. We did not detect MBD1 or RIG-I in our analysis. This may be due to differences in the experimental approach, or due to the cell lines used, as we used q-AP-MS to detect endogenous interaction partners in HeLa S3 cells, while interaction with endogenous RIG-I was detected in HEK293T cells infected with SeV and in primary human fibroblasts. OASL interaction with MBD1 was shown with expression constructs but not for endogenous proteins.
Comparing the interactome of unstimulated and NDV-infected cells, we found the same highly confident interaction partners of OASL and only found differences among the less reliable binding proteins (Table 26 and Table 27). It is possible that the performed NDV infection was not sufficiently to induce type I IFN signalling. This might have been due to the high number of cells and media volume, that was required during this experimental step. Furthermore, transient interactions, which occur during pathway activation, might have been obscured in this experimental setup. To verify induction of type I IFN

signalling, phosphorylation of signalling components e.g. p-TBK1 or p-IRF3 could have been analysed by IB. However, these results are suitable to further strengthen the observed protein interactions of OASL, if both experiments are regarded as replicates.

In accordance with its nucleolar localisation, we identified several nucleolar interaction partners of OASL. Additionally, we found many ribosome-associated and 40S or 60S ribosomal proteins to interact with OASL. In the nucleolus, ribosomal proteins and rRNAs assemble to the 60S and 40S ribosomal subunits in a process called ribosome biogenesis. The subunits are transported to the cytoplasm, where they form the mature 80S eukaryotic ribosome utilizing further proteins like eIF6. One or more ribosomes bind to a mRNA molecule thereby forming actively replicating ribosomes or polysomes (Khatter et al. 2015, Brina et al. 2014).

Comparing the interactome of OASL and ORF20, we identified a large amount of common binding partners (Table 23). This was underlined by the observation that OASL and ORF20 co-precipitated DDX21 and ribosomal L7a (Figure 17) and colocalised with DDX21 and L7a in the nucleolus (Figure 18 and Figure 30). These findings emphasise the functional connection between the two proteins and shows that ORF20 interacts with the same molecular machinery as OASL. Because we did not detect many cytoplasmic proteins as binding partners of ORF20 and OASL, we hypothesise that ORF20 and OASL act in the nucleolus and nucleus, at least under our own experimental conditions. Since 46 of 80 known ribosomal proteins have been identified to interact with ORF20 and OASL, OASL and ORF20 may play a role in the nucleolus, the site of ribosome biogenesis, or may interact with ribosomes. Our findings suggest that OASL might be involved in the maturation of ribosomes and transcriptional control in the nucleolus, and translational control in the cytoplasm, as OASL interacted with a network of proteins implicated in these mechanisms. By interaction with OASL, ORF20 might manipulate exactly these networks and the related functions. Recent publications showed that translating ribosomes vary in their ribosomal protein composition, thereby generating an incredible number of specialised ribosomes that are able to distinctively translate specific subpools of mRNAs (Shi et al. 2017, Shi et al. 2017). By interacting with OASL, ORF20 might influence the incorporation of specific ribosomal proteins and contribute to the generation of specialised ribosomes to promote the translation of desirable mRNAs.

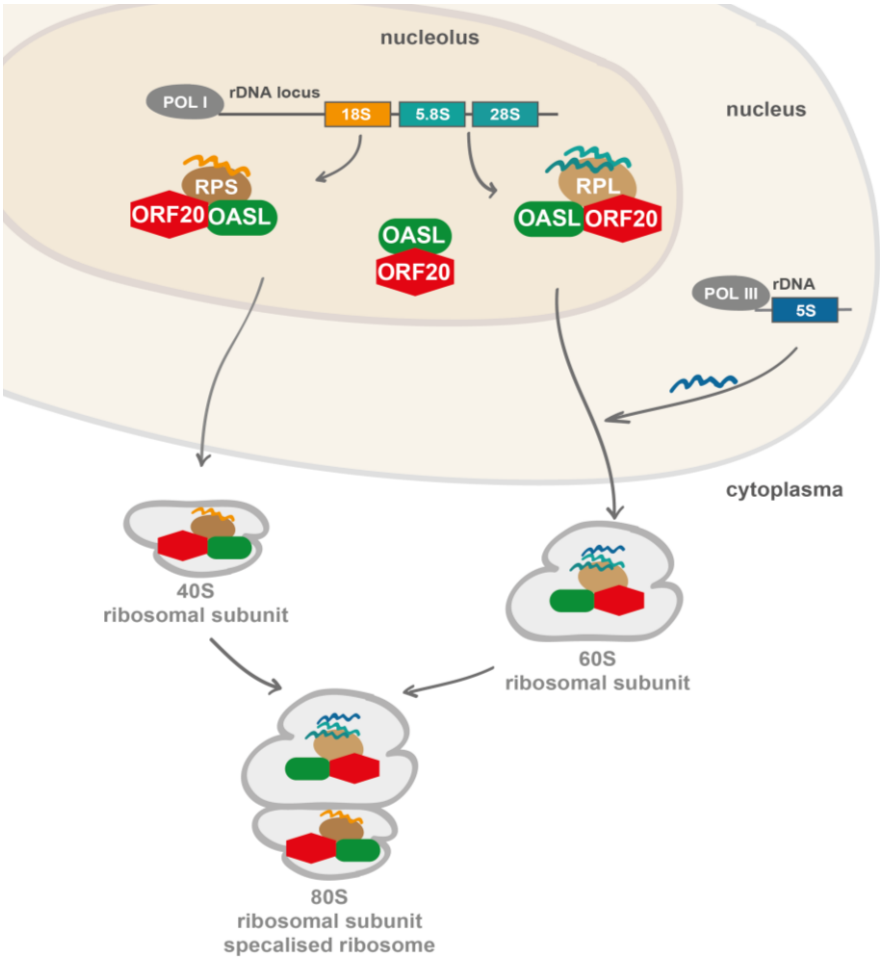

Figure 43 Putative generation of specialised ribosomes by interaction of OASL and ORF20 with ribosomal and nucleolar proteins. ORF20 and OASL have been identified to interact and colocalise with various common ribosomal and nucleolar proteins in the nucleolus, the site of ribosome biogenesis. OASL might be involved in the maturation of the ribosomes and translational control. ORF20 might use the interaction with OASL and ribosomal proteins to manipulate ribosome biogenesis and translation, which could lead to formation of specialised ribosomes that would promote translation of proviral proteins.

Subsequent studies of our group found that ORF20 and OASL co-sedimented with ribosomal subunits and polysomes utilizing sucrose gradient fractionation of ribosomes from transfected cells (Bussey et al. 2018). This verified our identification of 60S and 40S ribosomal proteins as interaction partners of ORF20 and OASL. However, this interaction did not affect global cellular translation, as shown with a puromycin incorporation assay. Interestingly, coexpression of ORF20 increased OASL expression in this assay, which was in accordance with our observation (Figure 37). Quantitative reverse transcriptase polymerase chain reaction (q-RT-PCR) showed that OASL mRNA levels were unregulated in the presence of ORF20 upon RIG-I-N expression and RIG-I activation by 5'pppRNA. This effect was dependent on IRF3 but not INFAR or STAT1, showing that upregulation of OASL was dependent on RIG-I signalling but independent of IFNAR signalling (Bussey et al. 2018). It was shown that OASL mRNA was induced at late time points during de novo KSHV infection using microarray studies (Alkharsah et al. 2011). Bussey and colleagues found that OASL transcript levels were increased in latently infected HuARLT-rKSHV.219 cells compared to uninfected cells and were further increased upon reactivation, which occurred concomitantly with increased ORF20 mRNA levels. When analysing the effect of OASL on gammaherpesvirus infection, OASL reconstituted 293T OASL$^{-/-}$ cells showed

inhibition of VSV-GFP infection as expected but resulted in enhancement of MHV68-GFP and $KSHV_{LYT}$ infected cells. This effect was dependent on ORF20, as a KSHVLYTORF20stop virus mutant failed to achieve enhancement of infection (Bussey et al. 2018).

In summary, based on the results presented here, Bussey et al. identified a unique proviral role for OASL during gammaherpesvirus infection, which is mediated by KSHV-encoded ORF20. The increased expression of OASL by ORF20 and the interaction of ORF20 and OASL with ribosomal proteins might manipulate ribosomal protein composition to generate specialised ribosomes that benefit KSHV infection. The implications of formation of specialised ribosomes during gammaherpesvirus infection will be an interesting topic for future studies and might furthermore lead to novel approaches for antiviral treatments.

I List of abbreviations

40S	small ribosomal subunit
60S	large ribosomal subunit
aa	amino acid
AIDS	acquired immunodeficiency syndrome
ART	antiretroviral treatment
BSA	Bovine serum albumin
CARDs	caspase activation and recruitment domains
CCDC86	coiled-coil domain-containing protein 86
Cdk2	cyclin-dependent kinase 2
cGAMP	cytosolic receptors cyclic GMP-AMP
cGAS	cytosolic receptors cyclic GMP-AMP synthase
co-IP	co-immunoprecipitation
CTD	C-terminal domain
DDX21	nucleolar RNA helicase 2
DFC	dense fibrillar component
dsDNA	double stranded DNA
EBV	Epstein-Barr virus
eIF	eukaryotic translation initiation factor
eIF6	eukaryotic translation initiation factor 6
ER	endoplasmic reticulum
EtBr	ethidium bromide
ev	empty vector
FBS	Dialyzed fetal bovine serum
FC	fibrillar centre
FCS	Fetal Calf Serum
GC	granular component
HCMV	human cytomegalovirus
HHV-6A	human herpesvirus 6A
HHV-6B	human herpesvirus 6B
HHV-7	human herpesvirus 7
HHV-8	Human Herpesvirus 8
HIV	human immunodeficiency virus
HMW	high molecular weight
HRP	horseradish peroxidase
HSV-1	herpes simplex virus 1
HSV-2	herpes simplex virus 2
IB	immunoblotting
IF	immunofluorescence

IFI16	nuclear receptor IFNγ-inducible protein 16
IFIT	interferon-induced proteins with tetratricopeptide repeats
IFIT	interferon-induced protein with tetratricopeptide repeats
IFN	interferon
IFNAR	type I IFN receptor
IL	interleukin
IP	immunoprecipitation
IRF	interferon regulatory factor
ISG	interferon-stimulated gene
ISGF3	ISG factor 3
JAK1	Janus kinase 1
kb	Kilo base pairs
kDa	kilodaltons
KS	Kaposi's Sarcoma
KSHV	Kaposi's sarcoma-associated herpesvirus
L7a	60S ribosomal proteins L7a
LA0	acidic ribosomal protein P0
LacZ	β-galactosidase enzyme
LC-MS/MS	Liquid chromatography coupled to tandem mass spectrometry
LF	Lipofectamine 2000
MAPK	mitogen-activated protein kinase
MAVS	mitochondrial antiviral signalling protein
MBD1	methyl CpG binding protein 1
MCMV	murine cytomegalovirus
MDA-5	Melanoma differentiation associated gene 5
MHV68	murine gammaherpesvirus 68
miRNAs	micro RNAs
MS	mass spectrometry
mTOR	phosphoinositide 3-kinase (PI3K)–mammalian target of rapamycin
MxA	myxovirus resistance A
NDV	Newcastle disease virus
NoLS	nucleolar localisation signals
OAS	2'-5'-oligoadenylate synthetase
OASL	2'-5'-oligoadenylate synthetase-like protein
ORF	open reading frame
ORF20 FL	320 aa full length isoform of ORF20
p.i.	post infection
p.t.	post transfection
PAMPs	pathogen-associated molecular patterns
PCR	polymerase chain reaction

pDC	plasmacytoid dendritic cell
PEL	Primary Effusion Lymphoma
PFA	paraformaldehyde
pI3K	phosphoinositide 3-kinase
PKR	serine/threonine protein kinase R
PML	promyelocytic leukaemia
PPI	protein-protein interaction
PRR	pathogen recognition receptors
pUb	polyubiquitination
q-AP-MS	quantitative affinity purification coupled to mass spectrometry
RBM	RNA-binding protein
rDNA	ribosomal DNA
RIG-I	retinoic acid inducible gene
RLR	retinoic acid inducible gene-like receptor
SeV	Sendai virus
SILAC	stable isotope labelling by amino acids in cell culture
ssRNA	single stranded RNA
STAT1/2	signal transducer and activator of transcription1/2
STAU2	Staufen homolog 2
STING	stimulator of interferon genes
TBK1	TANK binding kinase 1
TLR	Toll-like receptor
TRIM	tripartite motif
TYK2	tyrosine kinase 2
Ubi	ubiquitin-like
VSV	vesicular stomatitis virus
VZV	varicella-zoster virus
WT	wild type
YBOX1	nuclease-sensitive element-binding protein 1

II List of tables

III List of figures

IV List of references

Abbas, Y. M., Pichlmair, A., Górna, M. W., Superti-Furga, G., & Nagar, B. (2013). Structural basis for viral 5′-PPP-RNA recognition by human IFIT proteins. *Nature*, *494*(7435), 60–64. http://doi.org/10.1038/nature11783

Abdeljelil, N. Ben, Rochette, Pieree-Alexandre, & Pearson, A. (2013). The UL24 protein of herpes simplex virus 1 affects the sub-cellular distribution of viral glycoproteins involved in fusion. *Virology*, *444*(1–2), 263–273. http://doi.org/10.1016/j.virol.2013.06.021

Ablasser, A., Bauernfeind, F., Hartmann, G., Latz, E., Fitzgerald, K. A., & Hornung, V. (2009). RIG-I-dependent sensing of poly(dA:dT) through the induction of an RNA polymerase III–transcribed RNA intermediate. *Nature Immunology*, *10*(10), 1065–1072. http://doi.org/10.1038/ni.1779

Akula, S. M., Pramod, N. P., Wang, F.-Z., & Chandran, B. (2001). Human Herpesvirus 8 Envelope-Associated Glycoprotein B Interacts with Heparan Sulfate-like Moieties. *Virology*, *284*(2), 235–249. http://doi.org/10.1006/viro.2001.0921

Alkharsah, K. R., Singh, V. V., Bosco, R., Santag, S., Grundhoff, A., Konrad, A.& Schulz, T. F. (2011). Deletion of Kaposi's Sarcoma-Associated Herpesvirus FLICE Inhibitory Protein, vFLIP, from the Viral Genome Compromises the Activation of STAT1-Responsive Cellular Genes and Spindle Cell Formation in Endothelial Cells. *Journal of Virology*, *85*(19), 10375–10388. http://doi.org/10.1128/JVI.00226-11

Amin, M. A., Matsunaga, S., Ma, N., Takata, H., Yokoyama, M., Uchiyama, S., & Fukui, K. (2007). Fibrillarin, a nucleolar protein, is required for normal nuclear morphology and cellular growth in HeLa cells. *Biochemical and Biophysical Research Communications*, *360*(2), 320–326. http://doi.org/10.1016/j.bbrc.2007.06.092

Andersen, J. B., Strandbygård, D. J., Hartmann, R., & Justesen, J. (2004). Interaction between the 2′-5′ oligoadenylate synthetase-like protein p59 OASL and the transcriptional repressor methyl CpG-binding protein. *European Journal of Biochemistry*, *271*(3), 628–636. http://doi.org/10.1046/j.1432-1033.2003.03966.x

Aneja, K. K., & Yuan, Y. (2017). Reactivation and Lytic Replication of Kaposi's Sarcoma-Associated Herpesvirus: An Update. *Frontiers in Microbiology*, *8*, 613. http://doi.org/10.3389/fmicb.2017.00613

Ansari, M. A., Dutta, S., Veettil, M. V., Dutta, D., Iqbal, J., Kumar, B., & Chandran, B. (2015). Herpesvirus Genome Recognition Induced Acetylation of Nuclear IFI16 Is Essential for Its Cytoplasmic Translocation, Inflammasome and IFN-β Responses. *PLoS Pathogens*, *11*(7), e1005019. http://doi.org/10.1371/journal.ppat.1005019

Arias, C., Weisburd, B., Stern-Ginossar, N., Mercier, A., Madrid, A. S., Bellare, P., & Ganem, D. (2014). KSHV 2.0: A Comprehensive Annotation of the Kaposi's Sarcoma-Associated Herpesvirus Genome Using Next-Generation Sequencing Reveals Novel Genomic and Functional Features. *PLoS Pathogens*, *10*(1). http://doi.org/10.1371/journal.ppat.1003847

Bergonzini, V., Salata, C., Calistri, A., Parolin, C., Palù, G., Ferrucci, S., & Wojna, V. (2010). View and review on viral oncology research. *Infectious Agents and Cancer*, *5*(1), 11. http://doi.org/10.1186/1750-9378-5-11

Bernardi, R., & Pandolfi, P. P. (2007). Structure, dynamics and functions of promyelocytic leukaemia nuclear bodies. *Nature Reviews. Molecular Cell Biology*, *8*(12), 1006–1016. http://doi.org/10.1038/nrm2277

Bertrand, L., Leiva-Torres, G. A., Hyjazie, H., & Pearson, A. (2010). Conserved residues in the UL24 protein of herpes simplex virus 1 are important for dispersal of the nucleolar protein nucleolin. *Journal of Virology*, *84*(1), 109–118. http://doi.org/10.1128/JVI.01428-09

Bertrand, L., & Pearson, A. (2008). The conserved N-terminal domain of herpes simplex virus 1 UL24 protein is sufficient to induce the spatial redistribution of nucleolin. *Journal of General Virology*, *89*(5), 1142–1151. http://doi.org/10.1099/vir.0.83573-0

Bisson, S. A., Page, A.-L., & Ganem, D. (2009). A Kaposi's Sarcoma-Associated Herpesvirus Protein That Forms Inhibitory Complexes with Type I Interferon Receptor Subunits, Jak and STAT Proteins, and Blocks Interferon-Mediated Signal Transduction. *Journal of Virology*, *83*(10), 5056–5066. http://doi.org/10.1128/JVI.02516-08

Blach-Olszewska, Z., Halasa, J., Matej, H., & Cembrzyńska-Nowak, M. (1977). Why HeLa cells do not produce interferon? *Archivum Immunologiae et Therapiae Experimentalis*, *25*(5), 683–91. Retrieved from http://www.ncbi.nlm.nih.gov/pubmed/597016

Boisvert, F.-M., van Koningsbruggen, S., Navascués, J., & Lamond, A. I. (2007). The multifunctional nucleolus. *Nature Reviews. Molecular Cell Biology*, *8*(7), 574–585. http://doi.org/10.1038/nrm2184

Bortz, E., Whitelegge, J. P., Jia, Q., Zhou, Z. H., Stewart, J. P., Wu, T., & Sun, R. (2003). Identification of Proteins Associated with Murine Gammaherpesvirus 68 Virions Identification of Proteins Associated with Murine Gammaherpesvirus 68 Virions, *Journal of Virology 77*(24), 13425–13432. http://doi.org/10.1128/JVI.77.24.13425

Bosse, J. B., Hogue, I. B., Feric, M., Thiberge, S. Y., Sodeik, B., Brangwynne, C. P., & Enquist, L. W. (2015). Remodeling nuclear architecture allows efficient transport of herpesvirus capsids by diffusion. *Proceedings of the National Academy of Sciences*, *112*(42), E5725–E5733. http://doi.org/10.1073/pnas.1513876112

Brina, D., Miluzio, A., Ricciardi, S., & Biffo, S. (2014). eIF6 anti-association activity is required for ribosome biogenesis, translational control and tumor progression. *Biochimica et Biophysica Acta*, *1849*(7), 830–835. http://doi.org/10.1016/j.bbagrm.2014.09.010

Brulois, K., & Jung, J. U. (2014). Interplay between Kaposi's sarcoma-associated herpesvirus and the innate immune system. *Cytokine & Growth Factor Reviews*, *25*(5), 597–609. http://doi.org/10.1016/j.cytogfr.2014.06.001

Bussey, K. A., & Brinkmann, M. M. (2018). Strategies for immune evasion by human tumor viruses. *Current Opinion in Virology*, *32*, 30–39. http://doi.org/10.1016/j.coviro.2018.08.015

Bussey, K. A., Lau, U., Schumann, S., Gallo, A., Osbelt, L., Stempel, M., & Brinkmann, M. M. (2018). The interferon-stimulated gene product oligoadenylate synthetase-like protein enhances replication of Kaposi's sarcoma-associated herpesvirus (KSHV) and interacts with the KSHV ORF20 protein. *PLOS Pathogens* (Vol. 14). http://doi.org/10.1371/journal.ppat.1006937

Bussey, K. A., Reimer, E., Todt, H., Denker, B., Gallo, A., Konrad, A., & Brinkmann, M. M. (2014). The gammaherpesviruses Kaposi's sarcoma-associated herpesvirus and murine gammaherpesvirus 68 modulate the Toll-like receptor-induced proinflammatory cytokine response. *Journal of Virology*, *88*(16), 9245–59. http://doi.org/10.1128/JVI.00841-14

Cai, M., Liao, Z., Chen, T., Wang, P., Zou, X., Wang, Y., B Li, M. (2017). Characterization of the subcellular localization of Epstein-Barr virus encoded proteins in live cells. *Oncotarget*, *8*(41), 70006–70034. http://doi.org/10.18632/oncotarget.19549

Cai, Q., Verma, S. C., Lu, J., & Robertson, E. S. (2010). Molecular Biology of Kaposi's Sarcoma-associated Herpesvirus and Related Oncogenesis. *Advances in Virus Research* (Vol. 78). NIH Public Access. http://doi.org/10.1016/B978-0-12-385032-4.00003-3

Calo, E., Flynn, R. a, Martin, L., Spitale, R. C., Chang, H. Y., & Wysocka, J. (2014). RNA helicase DDX21 coordinates transcription and ribosomal RNA processing. *Nature*, *518*(7538), 249–253. http://doi.org/10.1038/nature13923

Castello, A., Fischer, B., Eichelbaum, K., Horos, R., Beckmann, B. M., Strein, C., & Hentze, M. W. (2012). Insights into RNA Biology from an Atlas of Mammalian mRNA-Binding Proteins. *Cell*,

149(6), 1393–1406. http://doi.org/10.1016/j.cell.2012.04.031

Ceci, M., Gaviraghi, C., Gorrini, C., Sala, L. a, Offenhäuser, N., Marchisio, P. C., & Biffo, S. (2003). Release of eIF6 (p27BBP) from the 60S subunit allows 80S ribosome assembly. *Nature*, *426*(6966), 579–584. http://doi.org/10.1038/nature02160

Chandran, B. (2010). Early events in Kaposi's sarcoma-associated herpesvirus infection of target cells. *Journal of Virology*, *84*(5), 2188–99. http://doi.org/10.1128/JVI.01334-09

Chang, Y., Cesarman, E., Pessin, M. S., Lee, F., Culpepper, J., Knowles, D. M., & Moore, P. S. (1994). Identification of herpesvirus-like DNA sequences in AIDS-associated Kaposi's sarcoma. *Science (New York, N.Y.)*, *266*(5192), 1865–9. http://doi.org/10.1126/science.7997879

Chen, G., Liu, C.-H., Zhou, L., & Krug, R. M. (2014). Cellular DDX21 RNA helicase inhibits influenza A virus replication but is counteracted by the viral NS1 protein. *Cell Host & Microbe*, *15*(4), 484–93. http://doi.org/10.1016/j.chom.2014.03.002

Chen, Q., Sun, L., & Chen, Z. J. (2016). Regulation and function of the cGAS–STING pathway of cytosolic DNA sensing. *Nature Immunology*, *17*(10), 1142–1149. http://doi.org/10.1038/ni.3558

Chendrimada, T. P., Finn, K. J., Ji, X., Baillat, D., Gregory, R. I., Liebhaber, S. a, & Shiekhattar, R. (2007). MicroRNA silencing through RISC recruitment of eIF6. *Nature*, *447*(7146), 823–828. http://doi.org/10.1038/nature05841

Cheng, G., Zhong, J., Chung, J., & Chisari, F. V. (2007). Double-stranded DNA and double-stranded RNA induce a common antiviral signaling pathway in human cells. *Proceedings of the National Academy of Sciences of the United States of America*, *104*(21), 9035–9040. http://doi.org/10.1073/pnas.0703285104

Cheng, J., Sun, Y., Zhang, X., Zhang, F., Zhang, S., Yu, S., B Ding, C. (2014). Toll-like receptor 3 inhibits Newcastle disease virus replication through activation of pro-inflammatory cytokines and the type-1 interferon pathway. *Archives of Virology*, *159*(11), 2937–2948. http://doi.org/10.1007/s00705-014-2148-6

Chiu, Y. H., MacMillan, J. B., & Chen, Z. J. (2009). RNA Polymerase III Detects Cytosolic DNA and Induces Type I Interferons through the RIG-I Pathway. *Cell*, *138*(3), 576–591. http://doi.org/10.1016/j.cell.2009.06.015

Choi, U. Y., Kang, J. S., Hwang, Y. S., & Kim, Y. J. (2015). Oligoadenylate synthase-like (OASL) proteins: dual functions and associations with diseases. *Experimental & Molecular Medicine*, *47*(3), e144. http://doi.org/10.1038/emm.2014.110

Coen, D. M., & Schaffer, P. A. (2003). Antiherpesvirus drugs: a promising spectrum of new drugs and drug targets. *Nature Reviews Drug Discovery*, *2*(4), 278–288. http://doi.org/10.1038/nrd1065

Costa, H., Nascimento, R., Sinclair, J., & Parkhouse, R. M. E. (2013). Human Cytomegalovirus Gene UL76 Induces IL-8 Expression through Activation of the DNA Damage Response. *PLoS Pathogens*, *9*(9). http://doi.org/10.1371/journal.ppat.1003609

Damania, B. A., & Cesarman, E. (2013). Kaposi's Sarcoma-Associated Herpesvirus. In H. P. M. Fields Bernard N, Knipe David M (Ed.), *Fields Virology* (pp. 2080–2128). Wolters Kluwer Health/Lippincott Williams & Wilkins.

Davis, Z. H., Verschueren, E., Jang, G. M., Kleffman, K., Johnson, J. R., Park, J., B Glaunsinger, B. A. (2015). Global mapping of herpesvirus-host protein complexes reveals a transcription strategy for late genes. *Molecular Cell*, *57*(2), 349–360. http://doi.org/10.1016/j.molcel.2014.11.026

De Veer, M. J., Holko, M., Frevel, M., Walker, E., Der, S., Paranjape, J. M., & Williams, B. R. G. (2001). Functional classification of interferon-stimulated genes identified using microarrays. *Journal of Leukocyte Biology*. http://doi.org/10.1189/jlb.69.6.912

Desmyter, J., Melnick, J. L., & Rawls, W. E. (1968). Defectiveness of interferon production and of rubella virus interference in a line of African green monkey kidney cells (Vero). *Journal of Virology*, *2*(10), 955–61. Retrieved from http://www.ncbi.nlm.nih.gov/pubmed/4302013

Dixit, E., & Kagan, J. C. (2013). Intracellular Pathogen Detection by RIG-I-Like Receptors. *Advances in Immunology* (1st ed., Vol. 117). Elsevier Inc. http://doi.org/10.1016/B978-0-12-410524-9.00004-9

Dupin, N., Grandadam, M., Calvez, V., Aubin, J. T., Huraux, J. M., Agut, H., & Escande, J. P. (1995). Herpesvirus-like DNA sequences in patients with Mediterranean Kaposi's sarcoma. *The Lancet*, *345*(8952), 761–762. http://doi.org/10.1016/S0140-6736(95)90642-8

Durut, N., & Sáez-Vásquez, J. (2015). Nucleolin: Dual roles in rDNA chromatin transcription. *Gene*, *556*(1), 7–12. http://doi.org/10.1016/j.gene.2014.09.023

Duus, K. M., Lentchitsky, V., Wagenaar, T., Grose, C., & Webster-Cyriaque, J. (2004). Wild-Type Kaposi's Sarcoma-Associated Herpesvirus Isolated from the Oropharynx of Immune-Competent Individuals Has Tropism for Cultured Oral Epithelial Cells. *Journal of Virology*, *78*(8), 4074–4084. http://doi.org/10.1128/JVI.78.8.4074-4084.2004

Ebrahimi, B., Dutia, B. M., Roberts, K. L., Garcia-Ramirez, J. J., Dickinson, P., Stewart, J. P., & Nash, A. A. (2003). Transcriptome profile of murine gammaherpesvirus-68 lytic infection. *Journal of General Virology*, *84*(1), 99–109. http://doi.org/10.1099/vir.0.18639-0

Emmott, E., Wise, H., Loucaides, E. M., Matthews, D. A., Digard, P., & Hiscox, J. A. (2010). Quantitative Proteomics Using SILAC Coupled to LC−MS/MS Reveals Changes in the Nucleolar Proteome in Influenza A Virus-Infected Cells. *Journal of Proteome Research*, *9*(10), 5335–5345. http://doi.org/10.1021/pr100593g

Eskildsen, S., Hartmann, R., Kjeldgaard, N. O., & Justesen, J. (2002). Gene structure of the murine 2′-5′-oligoadenylate synthetase family. *Cellular and Molecular Life Sciences (CMLS)*, *59*(7), 1212–1222. http://doi.org/10.1007/s00018-002-8499-2

Eskildsen, S., Justesen, J., Schierup, M. H., & Hartmann, R. (2003). Characterization of the 2′-5′-oligoadenylate synthetase ubiquitin-like family. *Nucleic Acids Research*, *31*(12), 3166–3173. http://doi.org/10.1093/nar/gkg427

Fuchs, G., Diges, C., Kohlstaedt, L. A., Wehner, K. A., & Sarnow, P. (2011). Proteomic analysis of ribosomes: Translational control of mRNA populations by glycogen synthase GYS1. *Journal of Molecular Biology*, *410*(1), 118–130. http://doi.org/10.1016/j.jmb.2011.04.064

Gack, M. U. (2014). Mechanisms of RIG-I-Like Receptor Activation and Manipulation by Viral Pathogens. *Journal of Virology*, *88*(10), 5213–5216. http://doi.org/10.1128/JVI.03370-13

Gack, M. U., Albrecht, R. A., Urano, T., Inn, K. S., Huang, I. C., Carnero, E., & García-Sastre, A. (2009). Influenza A Virus NS1 Targets the Ubiquitin Ligase TRIM25 to Evade Recognition by the Host Viral RNA Sensor RIG-I. *Cell Host and Microbe*, *5*(5), 439–449. http://doi.org/10.1016/j.chom.2009.04.006

Gack, M. U., Kirchhofer, A., Shin, Y. C., Inn, K.-S., Liang, C., Cui, S., & Jung, J. U. (2008). Roles of RIG-I N-terminal tandem CARD and splice variant in TRIM25-mediated antiviral signal transduction. *Proceedings of the National Academy of Sciences of the United States of America*, *105*(43), 16743–16748. http://doi.org/10.1073/pnas.0804947105

Gallo, A., Lampe, M., Günther, T., & Brune, W. (2017). The Viral Bcl-2 Homologs of Kaposi's Sarcoma-Associated Herpesvirus and Rhesus Rhadinovirus Share an Essential Role for Viral Replication. *Journal of Virology*, *91*(6), e01875-16. http://doi.org/10.1128/JVI.01875-16

Galluzzi, L., Vanpouille-Box, C., Bakhoum, S. F., & Demaria, S. (2018). SnapShot: CGAS-STING Signaling. *Cell*, *173*(1), 276–276.e1. http://doi.org/10.1016/j.cell.2018.03.015

Ganem, D. (2010). KSHV and the pathogenesis of Kaposi sarcoma: Listening to human biology and medicine. *Journal of Clinical Investigation*. American Society for Clinical Investigation. http://doi.org/10.1172/JCI40567

Griffin, B. D., Verweij, M. C., & Wiertz, E. J. H. J. (2010). Herpesviruses and immunity: The art of evasion. *Veterinary Microbiology*. http://doi.org/10.1016/j.vetmic.2010.02.017

Guo, X., Li, X., Xu, Y., Sun, T., Yang, G., Wu, Z., & Li, E. (2012). Identification of OASL d, a splice variant of human OASL, with antiviral activity. *International Journal of Biochemistry and Cell Biology*, *44*(7), 1133–1138. http://doi.org/10.1016/j.biocel.2012.04.001

Hartmann, R., Olsen, H. S., Widder, S., Jørgensen, R., & Justesen, J. (1998). a Novel Human Gene Related To the 2 ′ – 5 ′ Oligoadenylate Synthetase Family, *Nucleic Acids Research*, *26*(18), 4121–4127.

He, S., Zhao, J., Song, S., He, X., Minassian, A., Zhou, Y., & Feng, P. (2015). Viral pseudo-enzymes activate RIG-I via deamidation to evade cytokine production. *Molecular Cell*, *58*(1), 134–146. http://doi.org/10.1016/j.molcel.2015.01.036

Heinzelmann, K., Scholz, B. A., Nowak, A., Fossum, E., Kremmer, E., Haas, J., & Kempkes, B. (2010). Kaposi's sarcoma-associated herpesvirus viral interferon regulatory factor 4 (vIRF4/K10) is a novel interaction partner of CSL/CBF1, the major downstream effector of Notch signaling. *Journal of Virology*, *84*(23), 12255–64. http://doi.org/10.1128/JVI.01484-10

Honda, K., Takaoka, A., & Taniguchi, T. (2006). Type I Inteferon Gene Induction by the Interferon Regulatory Factor Family of Transcription Factors. *Immunity*, *25*(3), 349–360. http://doi.org/10.1016/j.immuni.2006.08.009

Honda, K., & Taniguchi, T. (2006). IRFs: master regulators of signalling by Toll-like receptors and cytosolic pattern-recognition receptors. *Nature Reviews Immunology*, *6*(9), 644–658. http://doi.org/10.1038/nri1900

Hornung, V., Hartmann, R., Ablasser, A., & Hopfner, K. (2014). OAS proteins and cGAS: unifying concepts in sensing and responding to cytosolic nucleic acids. *Nature Reviews Immunology*, *14*(8), 521–528. http://doi.org/10.1038/nri3719

Hovanessian, A. G., & Justesen, J. (2007). The human 2′-5′oligoadenylate synthetase family: Unique interferon-inducible enzymes catalyzing 2′-5′ instead of 3′-5′ phosphodiester bond formation. *Biochimie*, *89*(6–7), 779–788. http://doi.org/10.1016/j.biochi.2007.02.003

Hubner, N. C., Bird, A. W., Cox, J., Splettstoesser, B., Bandilla, P., Poser, I., & Mann, M. (2010). Quantitative proteomics combined with BAC TransgeneOmics reveals in vivo protein interactions. *Journal of Cell Biology*, *189*(4), 739–754. http://doi.org/10.1083/jcb.200911091

Hughes, P., Marshall, D., Reid, Y., Parkes, H., & Gelber, C. (2007). The costs of using unauthenticated, over-passaged cell lines: How much more data do we need? *BioTechniques*. http://doi.org/10.2144/000112598

Hwang, S.-W., Kim, D., Jung, J. U., & Lee, H.-R. (2017). KSHV-encoded viral interferon regulatory factor 4 (vIRF4) interacts with IRF7 and inhibits interferon alpha production. *Biochemical and Biophysical Research Communications*, *486*(3), 700–705. http://doi.org/10.1016/J.BBRC.2017.03.101

Hwang, S., Kim, K. S., Flano, E., Wu, T. T., Tong, L. M., Park, A. N., & Sun, R. (2009). Conserved Herpesviral Kinase Promotes Viral Persistence by Inhibiting the IRF-3-Mediated Type I Interferon Response. *Cell Host and Microbe*, *5*(2), 166–178. http://doi.org/10.1016/j.chom.2008.12.013

Ibsen, M. S., Gad, H. H., Andersen, L. L., Hornung, V., Julkunen, I., Sarkar, S. N., & Hartmann, R. (2015). Structural and functional analysis reveals that human OASL binds dsRNA to enhance RIG-I signaling. *Nucleic Acids Research*, *43*(10), 5236–5248. http://doi.org/10.1093/nar/gkv389

Inn, K.-S., Lee, S.-H., Rathbun, J. Y., Wong, L.-Y., Toth, Z., Machida, K., & Jung, J. U. (2011). Inhibition of RIG-I-mediated signaling by Kaposi's sarcoma-associated herpesvirus-encoded deubiquitinase ORF64. *Journal of Virology*, *85*(20), 10899–904. http://doi.org/10.1128/JVI.00690-11

Ishibashi, M., Wakita, T., & Esumi, M. (2010). 2',5'-Oligoadenylate synthetase-like gene highly induced by hepatitis C virus infection in human liver is inhibitory to viral replication in vitro. *Biochemical and Biophysical Research Communications*, *392*(3), 397–402. http://doi.org/10.1016/j.bbrc.2010.01.034

Ishikawa, H., & Barber, G. N. (2008). STING is an endoplasmic reticulum adaptor that facilitates innate immune signalling. *Nature*, *455*(7213), 674–678. http://doi.org/10.1038/nature07317

Ivashkiv, L., & Donlin, L. (2013). Regulation of type I interferon responses. *Nature Reviews Immunology*, *14*(1), 36–49. http://doi.org/10.1038/nri3581

Jackson, C. C., Dickson, M. A., Sadjadi, M., Gessain, A., Abel, L., Jouanguy, E., & Casanova, J.-L. (2016). Kaposi Sarcoma of Childhood: Inborn or Acquired Immunodeficiency to Oncogenic HHV-8. *Pediatric Blood & Cancer*, (63), 392–397.

Jacobson, J. G., Martin, S. L., & Coen, D. M. (1989). A conserved open reading frame that overlaps the herpes simplex virus thymidine kinase gene is important for viral growth in cell culture. *Journal of Virology*, *63*(4), 1839–1843.

Jensen, K., Anderson, J. A., & Glass, E. J. (2014). Comparison of small interfering RNA (siRNA) delivery into bovine monocyte-derived macrophages by transfection and electroporation. *Veterinary Immunology and Immunopathology*, *158*(3–4), 224–232. http://doi.org/10.1016/J.VETIMM.2014.02.002

Jentsch, S., & Pyrowolakis, G. (2000). Ubiquitin and its kin: how close are the family ties? *Trends in Cell Biology*, *10*(8), 335–342. http://doi.org/10.1016/S0962-8924(00)01785-2

Kang, H.-R., Cheong, W.-C., Park, J.-E., Ryu, S., Cho, H.-J., Youn, H., & Song, M. J. (2014). Murine gammaherpesvirus 68 encoding open reading frame 11 targets TANK binding kinase 1 to negatively regulate the host type I interferon response. *Journal of Virology*, *88*(12), 6832–46. http://doi.org/10.1128/JVI.03460-13

Kawai, T., & Akira, S. (2010). The role of pattern-recognition receptors in innate immunity: update on Toll-like receptors. *Nature Immunology*, *11*(5), 373–384. http://doi.org/10.1038/ni.1863

Kerr, I. M., Brown, R. E., & Hovanessian, A. G. (1977). Nature of inhibitor of cell-free protein synthesis formed in response to interferon and double-stranded RNA. *Nature*, *268*(5620), 540–2. http://doi.org/10.1038/268540a0

Kerur, N., Veettil, M. V., Sharma-Walia, N., Bottero, V., Sadagopan, S., Otageri, P., & Chandran, B. (2011). IFI16 acts as a nuclear pathogen sensor to induce the inflammasome in response to Kaposi Sarcoma-associated herpesvirus infection. *Cell Host and Microbe*, *9*(5), 363–375. http://doi.org/10.1016/j.chom.2011.04.008

Khatter, H., Myasnikov, A. G., Natchiar, S. K., & Klaholz, B. P. (2015). Structure of the human 80S ribosome. *Nature*. http://doi.org/10.1038/nature14427

Knizewski, L., Kinch, L., Grishin, N. V., Leszek, R., & Ginalski, K. (2006). Human Herpesvirus 1 UL24 Gene Encodes a Potential PD-(D/E)XK Endonuclease. *Journal of Virology*, *80*(5), 2575–2577. http://doi.org/10.1128/JVI.80.5.2575

Kolar, M., Lassig, M., & Berg, J. (2008). From protein interactions to functional annotation: graph alignment in Herpes. *BMC Systems Biology*, *2*(1), 90. http://doi.org/10.1186/1752-0509-2-90

Kosnopfel, C., Sinnberg, T., & Schittek, B. (2014). Y-box binding protein 1 - A prognostic marker and target in tumour therapy. *European Journal of Cell Biology*, *93*(1–2), 61–70. http://doi.org/10.1016/j.ejcb.2013.11.007

Leang, R. S., Wu, T.-T., Hwang, S., Liang, L. T., Tong, L., Truong, J. T., & Sun, R. (2011). The Anti-interferon Activity of Conserved Viral dUTPase ORF54 is Essential for an Effective MHV-68 Infection. *PLoS Pathogens*, *7*(10), e1002292. http://doi.org/10.1371/journal.ppat.1002292

Lee, H.-R., Choi, U. Y., Hwang, S.-W., Kim, S., & Jung, J. U. (2016). Viral Inhibition of PRR-Mediated Innate Immune Response: Learning from KSHV Evasion Strategies. *Molecules and Cells*, *39*(11), 777–782. http://doi.org/10.14348/molcells.2016.0232

Lee, H.-R., Toth, Z., Shin, Y. C., Lee, J.-S., Chang, H., Gu, W., & Jung, J. U. (2009). Kaposi's sarcoma-associated herpesvirus viral interferon regulatory factor 4 targets MDM2 to deregulate the p53 tumor suppressor pathway. *Journal of Virology*, *83*(13), 6739–47. http://doi.org/10.1128/JVI.02353-08

Li, X. L., Boyanapalli, M., Weihua, X., Kalvakolanu, D. V, & Hassel, B. A. (1998). Induction of interferon synthesis and activation of interferon-stimulated genes by liposomal transfection reagents. *Journal of Interferon & Cytokine Research* , *18*(11), 947–52. http://doi.org/10.1089/jir.1998.18.947

Li, Y., Li, C., Xue, P., Zhong, B., Mao, A.-P., Ran, Y., & Shu, H.-B. (2009). ISG56 is a negative-feedback regulator of virus-triggered signaling and cellular antiviral response. *Proceedings of the National Academy of Sciences of the United States of America*, *106*(19), 7945–7950. http://doi.org/10.1073/pnas.0900818106

Lin, S.-R., Jiang, M. J., Wang, H.-H., Hu, C.-H., Hsu, M.-S., Hsi, E., & Wang, S.-K. (2013). Human cytomegalovirus UL76 elicits novel aggresome formation via interaction with S5a of the ubiquitin proteasome system. *Journal of Virology*, *87*(21), 11562–78. http://doi.org/10.1128/JVI.01568-13

Liu, F., & Roizman, B. (1991). The Herpes Simplex Virus 1 Gene Encoding a Protease Also Contains within Its Coding Domain the Gene Encoding the More Abundant Substrate. *Journal of Virology*, *65*(10), 5149–5156. Retrieved from http://www.ncbi.nlm.nih.gov/pubmed/1654435

Longnecker, R. M., Kieff, E., & Cohen, J. I. (2013). Epstein-Barr Virus. In H. P. M. Fields Bernard N, Knipe David M (Ed.), *Fields Virology* (6th ed.). Wolters Kluwer Health/Lippincott Williams & Wilkins.

Luo, L., Gassman, K. L., Petell, L. M., Wilson, C. L., Bewersdorf, J., & Shopland, L. S. (2009). The nuclear periphery of embryonic stem cells is a transcriptionally permissive and repressive compartment. *Journal of Cell Science*, *122*(20), 3729–3737. http://doi.org/10.1242/jcs.052555

Lymberopoulos, M. H., Bourget, A., Abdeljelil, N. Ben, & Pearson, A. (2011). Involvement of the UL24 protein in herpes simplex virus 1-induced dispersal of B23 and in nuclear egress. *Virology*, *412*(2), 341–348. http://doi.org/10.1016/j.virol.2011.01.016

Lymberopoulos, M. H., & Pearson, A. (2007). Involvement of UL24 in herpes-simplex-virus-1-induced dispersal of nucleolin. *Virology*, *363*(2), 397–409. http://doi.org/10.1016/j.virol.2007.01.028

Lymberopoulos, M. H., & Pearson, A. (2010). Relocalization of Upstream Binding Factor to Viral Replication Compartments Is UL24 Independent and Follows the Onset of Herpes Simplex Virus 1 DNA Synthesis. *Journal of Virology*, *84*(9), 4810–4815. http://doi.org/10.1128/JVI.02437-09

Ma, F., Li, B., Liu, S., Iyer, S. S., Yu, Y., Wu, A., & Cheng, G. (2015). Positive Feedback Regulation of Type I IFN Production by the IFN-Inducible DNA Sensor cGAS. *The Journal of Immunology*, *194*(4), 1545–1554. http://doi.org/10.4049/jimmunol.1402066

Ma, Z., Jacobs, S. R., West, J. A., Stopford, C., Zhang, Z., Davis, Z., & Damania, B. (2015). Modulation of the cGAS-STING DNA sensing pathway by gammaherpesviruses. *Proceedings of the National Academy of Sciences*, *112*(31), E4306–E4315. http://doi.org/10.1073/pnas.1503831112

Machyna, M., Kehr, S., Straube, K., Kappei, D., Buchholz, F., Butter, F., & Neugebauer, K. M. (2014). The Coilin Interactome Identifies Hundreds of Small Noncoding RNAs that Traffic through Cajal Bodies. *Molecular Cell*, *56*(3), 389–399. http://doi.org/10.1016/j.molcel.2014.10.004

Madrid, a. S., & Ganem, D. (2012). Kaposi's Sarcoma-Associated Herpesvirus ORF54/dUTPase Downregulates a Ligand for the NK Activating Receptor NKp44. *Journal of Virology*, *86*(16), 8693–8704. http://doi.org/10.1128/JVI.00252-12

Marcel, V., Ghayad, S., Belin, S., Therizols, G., Morel, A. P., Solano-Gonzàlez, E., & Diaz, J. J. (2013). P53 Acts as a Safeguard of Translational Control by Regulating Fibrillarin and rRNA Methylation in Cancer. *Cancer Cell*, *24*(3), 318–330. http://doi.org/10.1016/j.ccr.2013.08.013

Marques, J., Anwar, J., Eskildsen-Larsen, S., Rebouillat, D., Paludan, S. R., Sen, G., & Hartmann, R. (2008). The p59 oligoadenylate synthetase-like protein possesses antiviral activity that requires the C-terminal ubiquitin-like domain. *Journal of General Virology*, *89*(11), 2767–2772. http://doi.org/10.1099/vir.0.2008/003558-0

Martró, E., Esteve, A., Schulz, T. F., Sheldon, J., Gambús, G., Muñoz, R., & Casabona, J. (2007). Risk factors for human Herpesvirus 8 infection and AIDS-associated Kaposi's sarcoma among men who have sex with men in a European multicentre study. *International Journal of Cancer*, *120*(5), 1129–1135. http://doi.org/10.1002/ijc.22281

Matthews, D., Emmott, E., & Hiscox, J. (2011). Viruses and the Nucleolus. In *The Nucleolus* (pp. 321–345). New York, NY: Springer New York. http://doi.org/10.1007/978-1-4614-0514-6_14

McGeoch, D. J., & Davison, A. J. (1999). The descent of human herpesvirus 8. *Seminars in Cancer Biology*, *9*(3), 201–9. http://doi.org/10.1006/scbi.1999.0093

McNab, F., Mayer-Barber, K., Sher, A., Wack, A., & O'Garra, A. (2015). Type I interferons in infectious disease. *Nature Reviews Immunology*, *15*(2), 87–103. http://doi.org/10.1038/nri3787

Mekhail, K., & Moazed, D. (2010). The nuclear envelope in genome organization, expression and stability. *Nature Reviews.Molecular Cell Biology*, *11*(5), 317–328. http://doi.org/10.1038/nrm2894

Melchjorsen, J., Kristiansen, H., Christiansen, R., Rintahaka, J., Matikainen, S., Paludan, S. R., & Hartmann, R. (2009). Differential regulation of the OASL and OAS1 genes in response to viral infections. *Journal of Interferon & Cytokine Research* , *29*(4), 199–207. http://doi.org/10.1089/jir.2008.0050

Mellacheruvu, D., Wright, Z., Couzens, A. L., Lambert, J. P., St-Denis, N. A., Li, T., & Nesvizhskii, A. I. (2013). The CRAPome: A contaminant repository for affinity purification-mass spectrometry data. *Nature Methods*. http://doi.org/10.1038/nmeth.2557

Mesri, E. A., Cesarman, E., & Boshoff, C. (2010). Kaposi's sarcoma and its associated herpesvirus. *Nature Reviews Cancer*, *10*(10), 707–719. http://doi.org/10.1038/nrc2888

Meyer, K., & Selbach, M. (2015). Quantitative affinity purification mass spectrometry: A versatile technology to study protein-protein interactions. *Frontiers in Genetics*. Frontiers Media SA. http://doi.org/10.3389/fgene.2015.00237

Meylan, E., Curran, J., Hofmann, K., Moradpour, D., Binder, M., Bartenschlager, R., & Tschopp, J. (2005). Cardif is an adaptor protein in the RIG-I antiviral pathway and is targeted by hepatitis C virus. *Nature*, *437*(7062), 1167–1172. http://doi.org/10.1038/nature04193

Miki, T., Takano, K., & Yoneda, Y. (2005). The role of mammalian Staufen on mRNA traffic: a view from its nucleocytoplasmic shuttling function. *Cell Structure and Function*, *30*(2), 51–56. http://doi.org/10.1247/csf.30.51

Miller, G., Heston, L., Grogan, E., Gradoville, L., Rigsby, M., Sun, R., & Chang, Y. (1997). Selective switch between latency and lytic replication of Kaposi's sarcoma herpesvirus and Epstein-Barr virus in dually infected body cavity lymphoma cells. *Journal of Virology*, *71*(1), 314–24. Retrieved from http://www.ncbi.nlm.nih.gov/pubmed/8985352

Miluzio, A., Beugnet, A., Volta, V., & Biffo, S. (2009). Eukaryotic initiation factor 6 mediates a continuum between 60S ribosome biogenesis and translation. *EMBO Reports*, *10*(5), 459–465. http://doi.org/10.1038/embor.2009.70

Morimoto, M., & Boerkoel, C. F. (2013). The role of nuclear bodies in gene expression and disease. *Biology*, *2*(3), 976–1033. http://doi.org/10.3390/biology2030976

Nascimento, R., Dias, J. D., & Parkhouse, R. M. E. (2009). The conserved UL24 family of human alpha, beta and gamma herpesviruses induces cell cycle arrest and inactivation of the cyclinB/cdc2 complex. *Archives of Virology*, *154*(7), 1143–1149. http://doi.org/10.1007/s00705-009-0420-y

Nascimento, R., & Parkhouse, R. M. E. (2007). Murine gammaherpesvirus 68 ORF20 induces cell-cycle arrest in G2 by inhibiting the Cdc2-cyclin B complex. *Journal of General Virology*, *88*(5), 1446–1453. http://doi.org/10.1099/vir.0.82589-0

Newton, K., Petfalski, E., Tollervey, D., & Cáceres, J. F. (2003). Fibrillarin is essential for early development and required for accumulation of an intron-encoded small nucleolar RNA in the mouse. *Molecular and Cellular Biology*, *23*(23), 8519–8527. http://doi.org/10.1128/MCB.23.23.8519-8527.2003

Ni, L., Wang, S., & Zheng, C. (2012). The nucleolus and herpesviral usurpation. *Journal of Medical Microbiology*, *61*(PART12), 1637–1643. http://doi.org/10.1099/jmm.0.045963-0

O'Connor, C. M., & Kedes, D. H. (2006). Mass spectrometric analyses of purified rhesus monkey rhadinovirus reveal 33 virion-associated proteins. *Journal of Virology*, *80*(3), 1574–83. http://doi.org/10.1128/JVI.80.3.1574-1583.2006

Orzalli, M. H., Broekema, N. M., Diner, B. A., Hancks, D. C., Elde, N. C., Cristea, I. M., & Knipe, D. M. (2015). cGAS-mediated stabilization of IFI16 promotes innate signaling during herpes simplex virus infection. *Proceedings of the National Academy of Sciences*, *112*(14), E1773–E1781. http://doi.org/10.1073/pnas.1424637112

Osbelt, L. (2016). Characterization of the Kaposi's sarcoma-associated herpesvirus (KSHV) ORF20 interaction with human oligoadenylate synthetase-like (OASL). University of Veterinary Medicine Hannover.

Paladino, P., Marcon, E., Greenblatt, J., & Frappier, L. (2014). Identification of herpesvirus proteins that contribute to G1/S arrest. *Journal of Virology*, *88*(8), 4480–92. http://doi.org/10.1128/JVI.00059-14

Paludan, S. R., Bowie, A. G., Horan, K. A., & Fitzgerald, K. A. (2011). Recognition of herpesviruses by the innate immune system. *Nature Reviews Immunology*, *11*(2), 143–154. http://doi.org/10.1038/nri2937

Park, E., & Maquat, L. E. (2013). Staufen-mediated mRNA decay. *Wiley Interdisciplinary Reviews: RNA*, *4*(4), 423–435. http://doi.org/10.1002/wrna.1168

Parkin, D. M. (2006). The global health burden of infection-associated cancers in the year 2002. *International Journal of Cancer*, *118*(12), 3030–3044. http://doi.org/10.1002/ijc.21731

Pauk, J., Huang, M. L., Brodie, S. J., Wald, A., Koelle, D. M., Schacker, T., & Corey, L. (2000). Mucosal shedding of human herpesvirus 8 in men. *The New England Journal of Medicine*, *343*(19), 1369–77. http://doi.org/10.1056/NEJM200011093431904

Paul, F. E., Hosp, F., & Selbach, M. (2011). Analyzing protein-protein interactions by quantitative mass spectrometry. *Methods*, *54*(4), 387–395. http://doi.org/10.1016/j.ymeth.2011.03.001

Pauli, E.-K., Chan, Y. K., Davis, M. E., Gableske, S., Wang, M. K., Feister, K. F., & Gack, M. U. (2014). The Ubiquitin-Specific Protease USP15 Promotes RIG-I-Mediated Antiviral Signaling by Deubiquitylating TRIM25. *Science Signaling*, *7*(307), ra3-ra3. http://doi.org/10.1126/scisignal.2004577

Pearson, A., & Coen, D. M. (2002). Identification, localization, and regulation of expression of the UL24 protein of herpes simplex virus type 1. *Journal of Virology*, *76*(21), 10821–10828. http://doi.org/10.1128/JVI.76.21.10821-10828.2002

Pellet, P. E., & Roizman, B. (2013). Herpesviridae. In H. P. M. Fields Bernard N, Knipe David M (Ed.), *Fields Virology* (6th ed., pp. 1802–1822). Wolters Kluwer Health/Lippincott Williams & Wilkins.

Pestka, S., Krause, C. D., & Walter, M. R. (2004). Interferons, interferon-like cytokines, and their receptors. *Immunological Reviews*, 202:8-32. http://doi.org/10.1111/j.0105-2896.2004.00204.x

Rawlinson, S. M., & Moseley, G. W. (2015). The nucleolar interface of RNA viruses. *Cellular Microbiology*, *17*(8), 1108–1120. http://doi.org/10.1111/cmi.12465

Razonable, R. R. (2011). Antiviral drugs for viruses other than human immunodeficiency virus. In *Mayo Clinic Proceedings* (Vol. 86, pp. 1009–1026). http://doi.org/10.4065/mcp.2011.0309

Rebouillat, D., Marié, I., & Hovanessian, A. G. (1998). Molecular cloning and characterization of two related and interferon- induced 56-kDa and 30-kDa proteins highly similar to 2'-5' oligoadenylate synthetase. *European Journal of Biochemistry*, *257*(2), 319–330. http://doi.org/10.1046/j.1432-1327.1998.2570319.x

Renne, R., Lagunoff, M., Zhong, W., & Ganem, D. (1996). The Size and Conformation of Kaposi's Sarcoma-Associated Herpesvirus (Human Herpesvirus 8) DNA in Infected Cells and Virions. *Journal of Virology*, *70*(11), 8151–8154.

Roberts, W., Hovanessian, A., Brown, R., Clemens, M., & Kerr, I. (1976). Interferon-mediated protein kinase and low-molecular-weight inhibitor of protein synthesis. *Nature*, *264*(5585), 477–480. http://doi.org/10.1038/264477a0

Roy, A., Dutta, D., Iqbal, J., Pisano, G., Gjyshi, O., Ansari, M. A., & Chandran, B. (2016). Nuclear Innate Immune DNA Sensor IFI16 Is Degraded during Lytic Reactivation of Kaposi's Sarcoma-Associated Herpesvirus (KSHV): Role of IFI16 in Maintenance of KSHV Latency. *Journal of Virology*, *90*(19), 8822–8841. http://doi.org/10.1128/JVI.01003-16

Russo, J. J., Bohenzky, R. A., Chien, M.-C., Chen, J., Yan, M., Maddalena, D., & Moore, P. S. (1996). Nucleotide sequence of the Kaposi sarcoma-associated herpesvirus (HHV8). *Proceedings of the National Academy of Sciences*, *93*(25), 14862–14867.

Sadler, A. J., & Williams, B. R. G. (2008). Interferon-inducible antiviral effectors. *Nature Reviews Immunology*, *8*(7), 559–568. http://doi.org/10.1038/nri2314

Salahuddin, S. Z., Nakamura, S., Biberfeld, P., Kaplan, M. H., Markham, P. D., Larsson, L., & Gallo, R. C. (1988). Angiogenic properties of Kaposi's sarcoma-derived cells after long-term culture in vitro. *Science*, *242*(4877), 430–433. http://doi.org/10.1126/science.2459779

Salsman, J., Zimmerman, N., Chen, T., Domagala, M., & Frappier, L. (2008). Genome-Wide Screen of Three Herpesviruses for Protein Subcellular Localization and Alteration of PML Nuclear Bodies. *PLoS Pathogens*, *4*(7), e1000100. http://doi.org/10.1371/journal.ppat.1000100

Sander, G., Konrad, A., Thurau, M., Wies, E., Leubert, R., Kremmer, E., & Stürzl, M. (2008). Intracellular localization map of human herpesvirus 8 proteins. *Journal of Virology*, *82*(4), 1908–1922. http://doi.org/10.1128/JVI.01716-07

Sathish, N., Wang, X., & Yuan, Y. (2012). Tegument proteins of kaposi's sarcoma-associated herpesvirus and related gamma-herpesviruses. *Frontiers in Microbiology*, *3*(MAR). http://doi.org/10.3389/fmicb.2012.00098

Sathish, N., & Yuan, Y. (2011). Evasion and Subversion of Interferon-Mediated Antiviral Immunity by Kaposi's Sarcoma-Associated Herpesvirus: an Overview. *Journal of Virology*, *85*(21), 10934–10944. http://doi.org/10.1128/JVI.00687-11

Schoggins, J. W., MacDuff, D. A., Imanaka, N., Gainey, M. D., Shrestha, B., Eitson, J. L., & Rice, C. M. (2014). Pan-viral specificity of IFN-induced genes reveals new roles for cGAS in innate immunity. *Nature*. 505(7485):691-5. http://doi.org/10.1038/nature12862

Schoggins, J. W., Wilson, S. J., Panis, M., Murphy, M. Y., Jones, C. T., Bieniasz, P., & Rice, C. M. (2011). A diverse range of gene products are effectors of the type I interferon antiviral response. *Nature*, *472*(7344), 481–485. http://doi.org/10.1038/nature09907

Seth, R. B., Sun, L., Ea, C. K., & Chen, Z. J. (2005). Identification and characterization of MAVS, a mitochondrial antiviral signaling protein that activates NF-κB and IRF3. *Cell*, *122*(5), 669–682. http://doi.org/10.1016/j.cell.2005.08.012

Sheval, E. V., Polzikov, M. A., Olson, M. O., & Zatsepina, O. V. (2005). A higher concentration of an antigen within the nucleolus may prevent its proper recognition by specific antibodies. *European Journal of Histochemistry : EJH.*, *49*(2), 117–123.

Shi, Z., Fujii, K., Kovary, K. M., Genuth, N. R., Röst, H. L., Teruel, M. N., & Barna, M. (2017). Heterogeneous Ribosomes Preferentially Translate Distinct Subpools of mRNAs Genome-wide. *Molecular Cell*, *67*(1), 71–83.e7. http://doi.org/10.1016/j.molcel.2017.05.021

Sinfield, R. L., Molyneux, E. M., Banda, K., Borgstein, E., Broadhead, R., Hesseling, P., & Liomba, G. (2007). Spectrum and presentation of pediatric malignancies in the HIV era: Experience from Blantyre, Malawi, 1998-2003. *Pediatric Blood and Cancer*, *48*(5), 515–520. http://doi.org/10.1002/pbc.20917

Steffens, C. (2015). *Characterisation of the herpesviral UL24 protein family*. Technische Universität Carolo-Wilhelmina zu Braunschweig.

Steiner, I., Kennedy, P. G., & Pachner, A. R. (2007). The neurotropic herpes viruses: herpes simplex and varicella-zoster. *Lancet Neurology*. http://doi.org/10.1016/S1474-4422(07)70267-3

Sun, C., Schattgen, S. A., Pisitkun, P., Jorgensen, J. P., Hilterbrand, A. T., Wang, L. J., & Paludan, S. R. (2015). Evasion of innate cytosolic DNA sensing by a gammaherpesvirus facilitates establishment of latent infection. *Journal of Immunology*, *194*(4), 1819–31. http://doi.org/10.4049/jimmunol.1402495

Sun, L., Wu, J., Du, F., Chen, X., & Chen, Z. J. (2013). Cyclic GMP-AMP Synthase Is a Cytosolic DNA Sensor That Activates the Type I Interferon Pathway. *Science*, *339*(6121), 786–791. http://doi.org/10.1126/science.1232458

Svistunova, D. M., Musinova, Y. R., Polyakov, V. Y., & Sheval, E. V. (2012). A Simple Method for the Immunocytochemical Detection of Proteins Inside Nuclear Structures That Are Inaccessible to Specific Antibodies. *Journal of Histochemistry and Cytochemistry*, *60*(2), 152–158. http://doi.org/10.1369/0022155411429704

Tajrishi, M. M., Tuteja, R., & Tuteja, N. (2011). Nucleolin: The most abundant multifunctional phosphoprotein of nucleolus. *Communicative and Integrative Biology*, *4*(3), 267–275. http://doi.org/10.4161/cib.4.3.14884

Talon, J., Horvath, C. M., Polley, R., Basler, C. F., Muster, T., Palese, P., & García-Sastre, a. (2000). Activation of interferon regulatory factor 3 is inhibited by the influenza A virus NS1 protein. *Journal of Virology*, *74*(17), 7989–7996. http://doi.org/10.1128/JVI.74.17.7989-7996.2000

Tang, Q., Murphy, E. A., & Maul, G. G. (2006). Experimental Confirmation of Global Murine Cytomegalovirus Open Reading Frames by Transcriptional Detection and Partial Characterization of Newly Described Gene Products. *Journal of Virology*, *80*(14), 6873–6882. http://doi.org/10.1128/JVI.00275-06

Taylor, T. J., Brockman, M. A., McNamee, E. E., & Knipe, D. M. (2002). Herpes simplex virus. *Frontiers in Bioscience*, *7*, d752-64. http://doi.org/10.2741/TAYLOR

Terenzi, F., Hui, D. J., Merrick, W. C., & Sen, G. C. (2006). Distinct induction patterns and functions of two closely related interferon-inducible human genes, ISG54 and ISG56. *Journal of Biological Chemistry*, *281*(45), 34064–34071. http://doi.org/10.1074/jbc.M605771200

Thakker, S., & Verma, S. C. (2016). Co-infections and pathogenesis of KSHV-associated malignancies. *Frontiers in Microbiology*, *7*(FEB), 151. http://doi.org/10.3389/fmicb.2016.00151

Tollervey, D., Lehtonen, H., Jansen, R., Kern, H., & Hurt, E. C. (1993). Temperature-sensitive mutations demonstrate roles for yeast fibrillarin in pre-rRNA processing, pre-rRNA methylation, and ribosome assembly. *Cell*, *72*(3), 443–457. http://doi.org/10.1016/0092-8674(93)90120-F

Torre, L. A., Bray, F., Siegel, R. L., Ferlay, J., Lortet-Tieulent, J., & Jemal, A. (2015). Global cancer statistics, 2012. *A Cancer Journal for Clinicians*, *65*(2), 87–108. http://doi.org/10.3322/caac.21262 [doi]

van Diemen, F. R., & Lebbink, R. J. (2017). CRISPR/Cas9, a powerful tool to target human herpesviruses. *Cellular Microbiology*, *19*(2), e12694. http://doi.org/10.1111/cmi.12694

Vladimer, G. I., Górna, M. W., & Superti-Furga, G. (2014). IFITs: Emerging roles as key anti-viral proteins. *Frontiers in Immunology*, *5*(MAR), 1–6. http://doi.org/10.3389/fimmu.2014.00094

Ward, K. N. (2013). Human Herpesviruses-6 and -7 (HHV-6A, HHV-6B and HHV-7). *eLS*. http://doi.org/10.1002/9780470015902.a0023616

Wei, T. (2003). In situ visualization of rDNA arrangement and its relationship with subnucleolar structural regions in Allium sativum cell nucleolus. *Journal of Cell Science*, *116*(6), 1117–1125. http://doi.org/10.1242/jcs.00323

West, J. A., Gregory, S. M., Sivaraman, V., Su, L., & Damania, B. (2011). Activation of Plasmacytoid Dendritic Cells by Kaposi's Sarcoma-Associated Herpesvirus. *Journal of Virology*, *85*(2), 895–904. http://doi.org/10.1128/JVI.01007-10

West, J. A., Wicks, M., Gregory, S. M., Chugh, P., Jacobs, S. R., Zhang, Z., & Damania, B. (2014). An Important Role for Mitochondrial Antiviral Signaling Protein in the Kaposi's Sarcoma-Associated Herpesvirus Life Cycle. *Journal of Virology*, *88*(10), 5778–5787. http://doi.org/10.1128/JVI.03226-13

Wu, J. J., Li, W., Shao, Y., Avey, D., Fu, B., Gillen, J., & Zhu, F. (2015). Inhibition of cGAS DNA Sensing by a Herpesvirus Virion Protein. *Cell Host and Microbe*, *18*(3), 333–344. http://doi.org/10.1016/j.chom.2015.07.015

Wu, J., Sun, L., Chen, X., Du, F., Shi, H., Chen, C., & Chen, Z. J. (2013). Cyclic GMP-AMP is an endogenous second messenger in innate immune signaling by cytosolic DNA. *Science*, *339*(6121), 826–30. http://doi.org/10.1126/science.1229963

Wu, L., Fossum, E., Joo, C. H., Inn, K.-S., Shin, Y. C., Johannsen, E., & Jung, J. U. (2009). Epstein-Barr virus LF2: an antagonist to type I interferon. *Journal of Virology*, *83*(2), 1140–6. http://doi.org/10.1128/JVI.00602-08

Ye, P., Liu, S., Zhu, Y., Chen, G., & Gao, G. (2010). DEXH-Box protein DHX30 is required for optimal function of the zinc-finger antiviral protein. *Protein and Cell*, *1*(10), 956–964. http://doi.org/10.1007/s13238-010-0117-8

Yoneyama, M., Kikuchi, M., Matsumoto, K., Imaizumi, T., Miyagishi, M., Taira, K., & Fujita, T. (2005). Shared and Unique Functions of the DExD/H-Box Helicases RIG-I, MDA5, and LGP2 in Antiviral Innate Immunity. *The Journal of Immunology*, *175*(5), 2851–2858. http://doi.org/10.4049/jimmunol.175.5.2851

Yoneyama, M., Kikuchi, M., Natsukawa, T., Shinobu, N., Imaizumi, T., Miyagishi, M., & Fujita, T. (2004). The RNA helicase RIG-I has an essential function in double-stranded RNA-induced innate antiviral responses. *Nature Immunology*, *5*(7), 730–737. http://doi.org/10.1038/ni1087

Zhang, G., Chan, B., Samarina, N., Abere, B., Weidner-Glunde, M., Buch, A., & Schulz, T. F. (2016). Cytoplasmic isoforms of Kaposi sarcoma herpesvirus LANA recruit and antagonize the innate immune DNA sensor cGAS. *Proceedings of the National Academy of Sciences*, *113*(8), E1034–E1043. http://doi.org/10.1073/pnas.1516812113

Zhang, Y., Baysac, K. C., Yee, L., Saporita, A. J., & Weber, J. D. (2014). Elevated DDX21 regulates c-Jun activity and rRNA processing in human breast cancers. *Breast Cancer Research* , *16*(5), 449. http://doi.org/10.1186/s13058-014-0449-z

Zhou, Y., Ma, J., Bushan Roy, B., Wu, J. Y.-Y., Pan, Q., Rong, L., & Liang, C. (2008). The packaging of human immunodeficiency virus type 1 RNA is restricted by overexpression of an RNA helicase DHX30. *Virology*, *372*(1), 97–106. http://doi.org/10.1016/j.virol.2007.10.027

Zhu, J., Zhang, Y., Ghosh, A., Cuevas, R. a., Forero, A., Dhar, J., & Sarkar, S. N. (2014). Antiviral Activity of Human OASL Protein Is Mediated by Enhancing Signaling of the RIG-I RNA Sensor. *Immunity*, *40*(6), 936–948. http://doi.org/10.1016/j.immuni.2014.05.007

V Appendix

a. Luciferase-based reporter assays

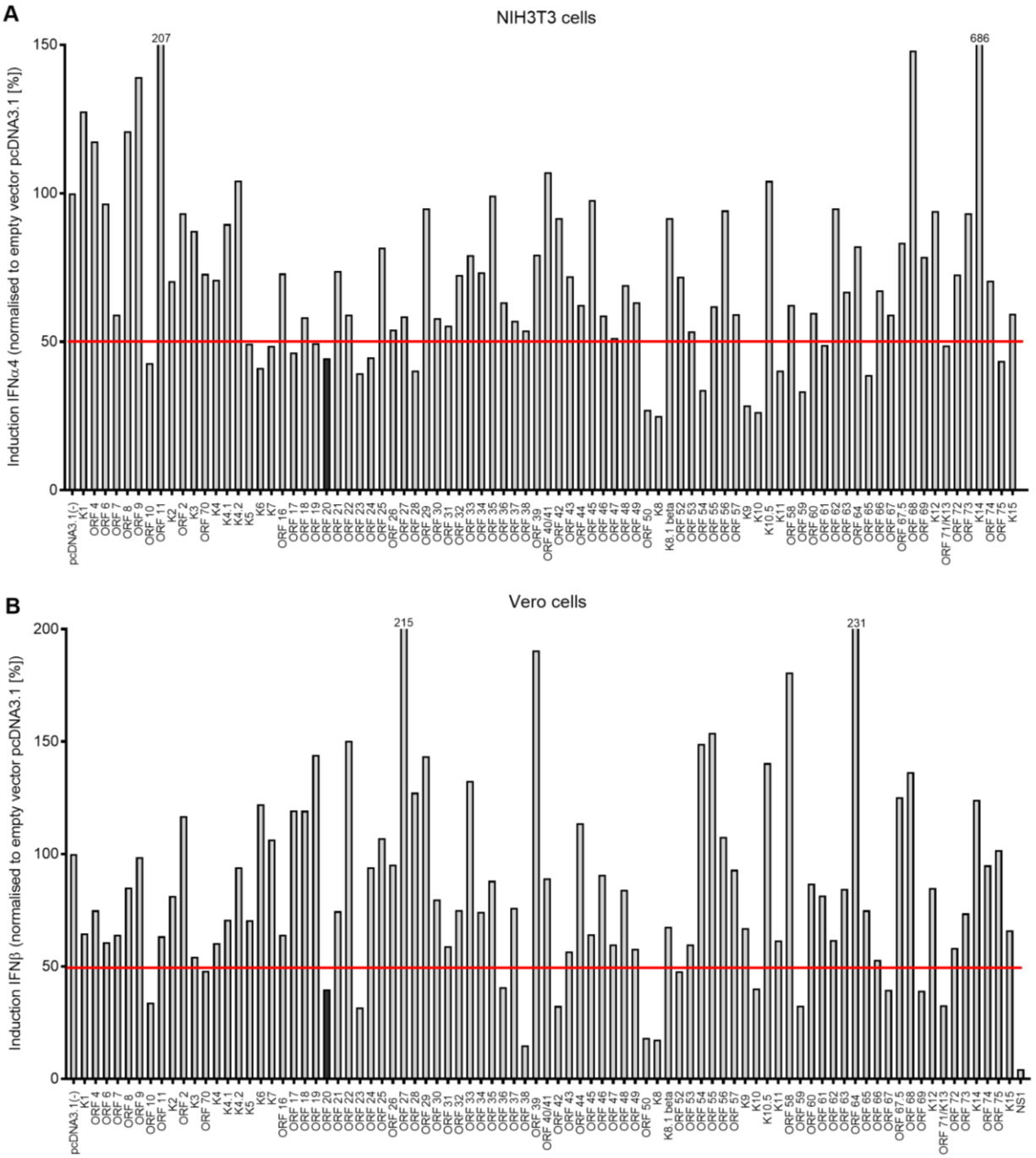

Figure 44 Screen for KSHV ORFs that negatively modulate the RIG-I-induced type I IFN response upon NDV infection. NIH3T3 cells (**A**) or Vero cells (**B**) were transfected with three constructs: IFNβ-Firefly luciferase (**A**) or IFNα4-Firefly luciferase (**B**), Renilla luciferase, and the indicated vector construct. 24 h p.t. cells were unstimulated or stimulated with the RIG-I agonist Newcastle disease virus (NDV). 21h later cells were lysed and luciferase activity was measured. Firefly luciferase values were normalised to the corresponding Renilla values and were subsequently scaled to empyt vector control pcDNA3.1(-), which was set to 100%. The NS1 protein of influenza A virus was used as a positive control for inhibition of RIG-I signalling. Red line highlights a 50% induction of the promoter compared to the empty vector control. Experiments was performed once.

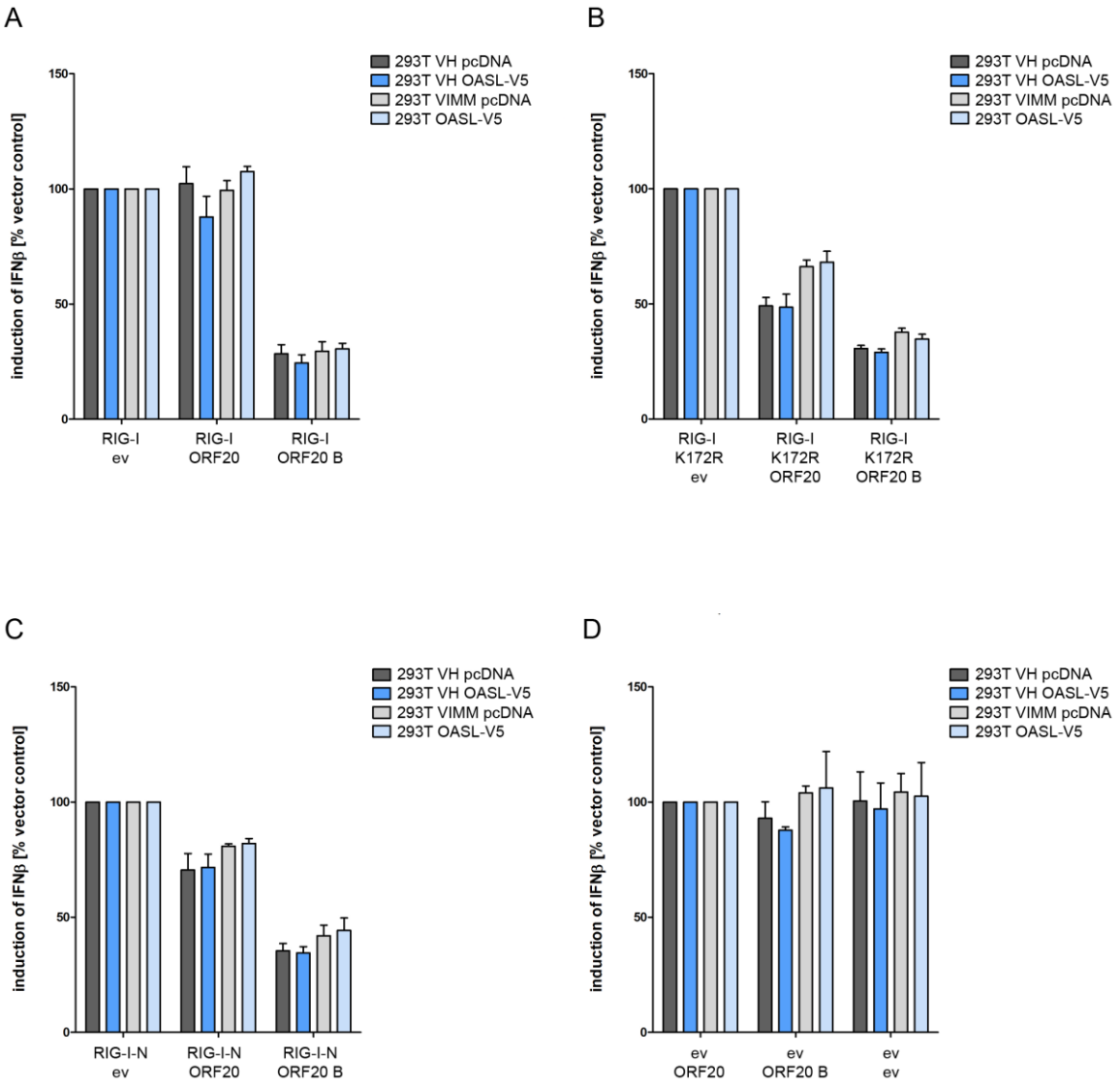

Figure 45 KSHV ORF20 B and ORF20 diminish IFNβ induction downstream of RIG-I activation independent of OASL expression. HEK293T VH and HEK293T VIMM cells stably expressing OASL-V5 or pcDNA3.1 were transfected with IFNβ-Firefly luciferase and Renilla luciferase reporter constructs along with ORF20-myc, ORF20 B-myc, or pcDNA3.1 in combination with Flag-RIG-I, Flag-RIG-I K172R, Flag-RIG-I-N, or pcDNA3.1 in a 1:1 ratio. Transfection of empty vector pcDNA3.1 (ev) served as control. Cells were lysed 48 h p.t. and Firefly and Renilla luciferase activity was measured. Shown is induction of IFNβ in response to plasmid transfection, determined as follows: Firefly values normalised to the corresponding Renilla values and subsequently scaled to the corresponding empty vector control. Non-scaled data are shown in Figure 39. Data shows averages with standard deviation from three independent experiments.

b. Proteomics

i. ORF20 Interactome

Table 24 Binding partners of KSHV ORF20 identified by affinity purification followed by quantitative mass spectrometry. HeLa S3 cells were labelled with heavy or light amino acids in cell culture (SILAC). In the forward experiment (fwd) heavy labelled cells transiently expressed ORF20-myc and light labelled cells expressed LacZ-myc as a control. Labels were switched in the crossover experiment (cro). 24 h p.t. cells were lysed. Samples were subjected to anti-myc IP. Eluates were analysed by mass spectrometry. Heavy to light fold change values (H/L) were calculated for the identified proteins, based on the relative intensity for their peptides in the forward or crossover experiment. The values of the "heavy/light-fold change" for each protein pair were transformed into log_2 fold changes. Peptide filters were applied during bioinformatical analysis. Data are arranged according to size (descending) of the "H/L fwd" values. Shown are to top 150 proteins.

protein name	H/L fwd	H/L cro	log_2 fold change fwd	log_2 fold change cro	H/L Count fwd	H/L Count cro	Area fwd	Area cro	Score fwd	Score cro
ORF20 protein OS=Human herpesvirus 8 GN=ORF20 [E5LBU3_HHV8]	31.96	0.01	5.00	-6.31	4	1	8.4E7	5.9E7	640.65	500.08
Beta-galactosidase OS=Escherichia coli GN=lacZ [BGAL_ECOLX]	0.04	28.60	-4.49	4.84	17	38	3.8E8	3.2E8	6259.46	8969.05
60S ribosomal protein L36 GN=RPL36 [RL36_HUMAN]	5.70	0.17	2.51	-2.52	4	3	3.0E6	2.7E6	170.58	68.06
40S ribosomal protein S12 GN=RPS12 [RS12_HUMAN]	5.47	0.10	2.45	-3.28	3	1	1.8E6	2.6E6	86.61	28.00
60S ribosomal protein L10a GN=RPL10A [RL10A_HUMAN]	5.26	0.14	2.40	-2.88	1	1	3.3E6	4.5E6	71.33	52.42
Ribosome-binding protein 1 GN=RRBP1 [RRBP1_HUMAN]	5.25	0.18	2.39	-2.47	1	1	4.5E5	8.0E5	57.24	35.95
60S ribosomal protein L15 GN=RPL15 [RL15_HUMAN]	4.83	0.14	2.27	-2.86	3	3	3.5E6	2.9E6	100.88	116.18
40S ribosomal protein S24 GN=RPS24 [RS24_HUMAN]	4.82	0.18	2.27	-2.46	2	1	8.3E6	8.6E6	264.58	153.02
60S ribosomal protein L24 GN=RPL24 [RL24_HUMAN]	4.60	0.12	2.20	-3.04	5	5	2.3E6	6.2E6	196.56	321.93
40S ribosomal protein S6 GN=RPS6 [RS6_HUMAN]	4.52	0.12	2.18	-3.06	11	10	2.0E7	2.4E7	758.89	629.80
60S acidic ribosomal protein P1 GN=RPLP1 [RLA1_HUMAN]	4.51	0.22	2.17	-2.17	2	2	1.3E7	9.7E6	498.80	426.09
Elongation factor Tu, mitochondrial GN=TUFM [EFTU_HUMAN]	4.49	2.60	2.17	1.38	1	1	1.8E6	4.6E5	33.96	38.16
60S ribosomal protein L7a GN=RPL7A [RL7A_HUMAN]	4.37	0.19	2.13	-2.42	8	10	3.7E7	2.4E7	1056.37	659.68
60S ribosomal protein L4 GN=RPL4 [RL4_HUMAN]	4.32	0.14	2.11	-2.87	3	4	1.4E6	1.7E6	234.29	231.82
60S acidic ribosomal protein P0 GN=RPLP0 [RLA0_HUMAN]	4.14	0.17	2.05	-2.60	7	6	5.1E6	3.0E6	322.94	226.68
60S ribosomal protein L34 GN=RPL34 [RL34_HUMAN]	4.12	0.13	2.04	-2.89	4	3	7.2E6	6.2E6	106.34	69.32
60S ribosomal protein L8 GN=RPL8 [RL8_HUMAN]	4.08	0.19	2.03	-2.38	10	7	4.2E7	5.1E7	1014.24	900.74
60S ribosomal protein L27 GN=RPL27 [RL27_HUMAN]	4.02	0.19	2.01	-2.40	2	4	8.1E6	5.0E6	146.34	124.94
60S ribosomal protein L6 GN=RPL6 [RL6_HUMAN]	4.01	0.17	2.00	-2.52	9	9	4.0E7	3.9E7	574.39	612.48
60S ribosomal protein L18 GN=RPL18 [RL18_HUMAN]	3.80	0.20	1.93	-2.35	3	3	9.3E6	7.4E6	380.69	364.03
60S ribosomal protein L30 GN=RPL30 [RL30_HUMAN]	3.77	0.05	1.91	-4.40	1	1	2.5E6	9.5E5	51.43	62.39
60S acidic ribosomal protein P2 GN=RPLP2 [RLA2_HUMAN]	3.63	0.21	1.86	-2.22	7	12	2.3E7	1.8E7	1141.87	1120.62
60S ribosomal protein L35a GN=RPL35A [RL35A_HUMAN]	3.61	0.19	1.85	-2.39	1	2	7.0E6	4.4E6	27.60	67.53
60S ribosomal protein L3 GN=RPL3 [RL3_HUMAN]	3.56	0.18	1.83	-2.46	1	4	2.8E6	2.6E6	79.53	163.40
2'-5'-oligoadenylate synthase-like protein GN=OASL [OASL_HUMAN]	3.42	0.24	1.77	-2.04	2	1	1.3E6	2.8E6	127.32	95.71

protein name	H/L fwd	H/L cro	log_2 fold change fwd	log_2 fold change cro	H/L Count fwd	H/L Count cro	Area fwd	Area cro	Score fwd	Score cro
40S ribosomal protein S26 GN=RPS26 [RS26_HUMAN]	3.32	0.15	1.73	-2.70	3	3	5.2E6	6.9E6	280.44	276.03
60S ribosomal protein L7 GN=RPL7 [RL7_HUMAN]	3.28	0.23	1.71	-2.11	1	1	2.0E6	2.7E6	57.68	92.05
60S ribosomal protein L12 GN=RPL12 [RL12_HUMAN]	3.08	0.24	1.63	-2.06	1	1	3.9E6	2.5E6	31.49	93.97
60S ribosomal protein L23 GN=RPL23 [RL23_HUMAN]	2.91	0.21	1.54	-2.24	7	5	7.7E6	6.8E6	493.09	179.77
60S ribosomal protein L10 GN=RPL10 [RL10_HUMAN]	2.89	0.18	1.53	-2.50	1	6	3.1E6	2.4E6	190.04	234.11
40S ribosomal protein S2 GN=RPS2 [RS2_HUMAN]	2.65	0.27	1.40	-1.91	3	7	2.1E6	5.3E6	63.59	260.51
40S ribosomal protein S23 GN=RPS23 [RS23_HUMAN]	2.61	0.32	1.38	-1.63	6	3	1.2E7	8.0E6	492.96	367.91
Nucleolar RNA helicase 2 GN=DDX21 [DDX21_HUMAN]	2.54		1.34		3		9.2E5	0.0E0	115.45	
60S ribosomal protein L19 GN=RPL19 [RL19_HUMAN]	2.45	0.27	1.29	-1.89	1	2	1.7E6	2.9E6	139.74	209.56
BAG family molecular chaperone regulator 2 GN=BAG2 [BAG2_HUMAN]	2.43	0.52	1.28	-0.94	6	6	1.7E7	1.0E7	578.87	458.58
60S ribosomal protein L14 GN=RPL14 [RL14_HUMAN]	2.39	0.21	1.25	-2.23	1	1	1.4E6	1.4E6	109.11	116.70
60S ribosomal protein L23a GN=RPL23A [RL23A_HUMAN]	2.31		1.21		1		5.2E6	4.9E6	195.82	131.75
28S ribosomal protein S28. mitochondrial GN=MRPS28 [RT28_HUMAN]	2.24	0.29	1.16	-1.81	1	1	5.8E5	1.3E6	50.66	40.02
60S ribosomal protein L13 GN=RPL13 [RL13_HUMAN]	2.23	0.30	1.16	-1.76	6	6	4.4E6	5.1E6	311.80	347.67
Heterogeneous nuclear ribonucleoprotein F GN=HNRNPF [HNRPF_HUMAN]	2.22	0.38	1.15	-1.40	2	5	6.6E6	2.4E7	879.33	990.20
Protein LTV1 homolog GN=LTV1 [LTV1_HUMAN]	2.22	0.35	1.15	-1.51	2	1	6.1E5	9.2E5	208.76	107.00
40S ribosomal protein S7 GN=RPS7 [RS7_HUMAN]	2.14		1.10		1		7.0E5	0.0E0	26.61	
U4/U6 small nuclear ribonucleoprotein Prp3 GN=PRPF3 [PRPF3_HUMAN]	2.05	0.50	1.03	-1.00	1	8	2.1E7	2.4E7	72.15	302.57
60S ribosomal protein L29 GN=RPL29 [RL29_HUMAN]	2.01	0.35	1.01	-1.53	1	1	1.4E6	2.7E6	73.51	60.77
40S ribosomal protein S8 GN=RPS8 [RS8_HUMAN]	1.99	0.31	0.99	-1.68	3	7	9.7E6	1.7E7	370.20	550.51
40S ribosomal protein S3a GN=RPS3A [RS3A_HUMAN]	1.97	0.30	0.98	-1.72	1	3	3.2E6	3.6E6	94.46	153.48
40S ribosomal protein S14 GN=RPS14 [RS14_HUMAN]	1.86	0.25	0.90	-1.99	5	3	3.5E6	9.1E6	492.95	289.73
Apoptosis-inducing factor 1, mitochondrial GN=AIFM1 [AIFM1_HUMAN]	1.84	0.35	0.88	-1.50	1	1	8.0E5	1.0E6	51.39	34.80
DNA-directed RNA polymerase I subunit RPA1 GN=POLR1A [RPA1_HUMAN]	1.83	0.52	0.87	-0.95	2	2	8.6E5	1.0E6	55.29	106.96
H/ACA ribonucleoprotein complex subunit 1 GN=GAR1 [GAR1_HUMAN]	1.80	0.51	0.85	-0.96	3	1	2.5E6	1.0E6	98.04	44.97
60S ribosomal protein L27a GN=RPL27A [RL27A_HUMAN]	1.72	0.35	0.78	-1.51	1	1	3.2E6	7.7E6	100.13	100.45
60 kDa SS-A/Ro ribonucleoprotein GN=TROVE2 [RO60_HUMAN]	1.72	0.80	0.78	-0.32	1	1	9.1E5	8.2E5	53.18	137.50
Pre-mRNA-processing factor 6 GN=PRPF6 [PRP6_HUMAN]	1.71	0.48	0.78	-1.05	8	9	2.9E6	3.8E6	414.64	553.10
U4/U6 small nuclear ribonucleoprotein Prp31 GN=PRPF31 [PRP31_HUMAN]	1.71	0.43	0.78	-1.22	2	2	1.1E6	2.3E6	47.76	90.39
Advillin GN=AVIL [AVIL_HUMAN]	1.70		0.77		1		5.9E5	0.0E0	42.29	
U4/U6 small nuclear ribonucleoprotein Prp4 GN=PRPF4 [PRP4_HUMAN]	1.66	0.51	0.73	-0.98	5	10	1.6E6	3.8E6	415.16	607.62
60S ribosomal protein L17 GN=RPL17 [RL17_HUMAN]	1.64	0.37	0.71	-1.43	1	3	2.6E5	4.0E6	38.91	94.72
40S ribosomal protein S4, X isoform GN=RPS4X [RS4X_HUMAN]	1.64	0.33	0.71	-1.62	4	3	4.7E6	5.6E6	393.20	361.52

protein name	H/L fwd	H/L cro	log_2 fold change fwd	log_2 fold change cro	H/L Count fwd	H/L Count cro	Area fwd	Area cro	Score fwd	Score cro
U6 snRNA-associated Sm-like protein LSm2 GN=LSM2 [LSM2_HUMAN]	1.64	0.70	0.71	-0.51	2	2	2.5E6	2.7E6	340.55	431.15
60 kDa heat shock protein, mitochondrial GN=HSPD1 [CH60_HUMAN]	1.59	0.65	0.67	-0.63	49	53	9.1E7	9.8E7	8255.49	10866.5
Peptidyl-prolyl cis-trans isomerase H GN=PPIH [PPIH_HUMAN]	1.58		0.66		2		1.5E6	0.0E0	154.19	
DNA-directed RNA polymerase I subunit RPA34 GN=CD3EAP [RPA34_HUMAN]	1.57	0.73	0.65	-0.46	4	7	6.0E6	1.0E7	297.12	604.14
60S ribosomal protein L36a GN=RPL36A [RL36A_HUMAN]	1.57	0.61	0.65	-0.71	1	2	3.8E5	1.2E6	53.86	64.94
NHP2-like protein 1 GN=NHP2L1 [NH2L1_HUMAN]	1.56		0.64		1		1.2E6	0.0E0	76.54	
rRNA 2'-O-methyltransferase fibrillarin GN=FBL [FBRL_HUMAN]	1.53	0.54	0.62	-0.88	4	1	3.1E6	9.5E5	134.35	43.68
Transcription termination factor 1 GN=TTF1 [TTF1_HUMAN]	1.52		0.61		1		2.1E6	0.0E0	29.73	
DNA-directed RNA polymerases I and III subunit RPAC1 GN=POLR1C [RPAC1_HUMAN]	1.51	0.52	0.60	-0.95	3	3	8.3E5	7.8E5	155.01	186.22
Histone-binding protein RBBP4 GN=RBBP4 [RBBP4_HUMAN]	1.49	0.45	0.58	-1.17	1	1	1.2E6	7.2E5	106.36	48.69
40S ribosomal protein S9 GN=RPS9 [RS9_HUMAN]	1.49	0.34	0.57	-1.54	4	3	2.3E6	2.6E6	153.59	138.09
FACT complex subunit SSRP1 GN=SSRP1 [SSRP1_HUMAN]	1.47		0.56		1		1.2E6	0.0E0	36.19	
H/ACA ribonucleoprotein complex subunit 2 GN=NHP2 [NHP2_HUMAN]	1.46		0.55		3		2.0E6	0.0E0	113.30	
60S ribosomal protein L11 GN=RPL11 [RL11_HUMAN]	1.45	0.52	0.53	-0.95	2	1	3.5E6	3.1E6	232.04	221.86
U6 snRNA-associated Sm-like protein LSm3 GN=LSM3 [LSM3_HUMAN]	1.42	0.55	0.51	-0.85	1	1	5.2E6	4.2E6	28.53	37.22
Splicing factor 3A subunit 2 GN=SF3A2 [SF3A2_HUMAN]	1.39	1.24	0.48	0.31	1	2	6.4E5	4.8E5	28.98	43.16
Coilin GN=COIL [COIL_HUMAN]	1.38	1.40	0.47	0.49	2	2	1.6E6	2.1E6	51.57	77.54
Heterogeneous nuclear ribonucleoprotein H GN=HNRNPH1 [HNRH1_HUMAN]	1.37	0.64	0.45	-0.65	4	2	9.6E6	3.3E7	1127.25	1639.37
Nucleolar and coiled-body phosphoprotein 1 GN=NOLC1 [NOLC1_HUMAN]	1.37	0.63	0.45	-0.66	2	1	6.2E5	4.3E5	134.80	25.42
Far upstream element-binding protein 2 GN=KHSRP [FUBP2_HUMAN]	1.34	0.72	0.42	-0.48	2	8	1.0E6	3.1E6	61.62	356.17
40S ribosomal protein S20 GN=RPS20 [RS20_HUMAN]	1.32	0.41	0.40	-1.28	3	4	2.5E6	1.3E6	161.40	108.23
U4/U6.U5 tri-snRNP-associated protein 1 GN=SART1 [SNUT1_HUMAN]	1.31	0.55	0.39	-0.86	15	14	1.0E7	8.3E6	1549.60	1162.91
Protein SREK1IP1 GN=SREK1IP1 [SR1IP_HUMAN]	1.31		0.38		4		3.0E6	0.0E0	248.99	
Protein CASC3 GN=CASC3 [CASC3_HUMAN]	1.30	0.72	0.38	-0.47	2	3	8.1E5	4.1E6	83.54	80.95
SRA stem-loop-interacting RNA-binding protein, mitochondrial GN=SLIRP [SLIRP_HUMAN]	1.30		0.38		1		6.2E5	0.0E0	27.06	
SWI/SNF-related matrix-associated actin-dependent regulator of chromatin subfamily E member 1 GN=SMARCE1 [SMCE1_HUMAN]	1.29		0.37		1		1.5E6	0.0E0	112.45	
DNA topoisomerase 1 GN=TOP1 [TOP1_HUMAN]	1.29	0.67	0.37	-0.58	10	8	9.2E6	6.1E6	628.67	433.53
Protein FAM133B GN=FAM133B [F133B_HUMAN]	1.28	0.92	0.36	-0.12	2	1	6.7E6	7.2E6	233.36	85.74
40S ribosomal protein S3 GN=RPS3 [RS3_HUMAN]	1.28	0.50	0.35	-0.99	5	4	2.1E6	2.8E6	266.12	216.65
40S ribosomal protein S11 GN=RPS11 [RS11_HUMAN]	1.27	0.45	0.35	-1.15	2	1	1.0E6	1.8E6	73.20	42.29

protein name	H/L fwd	H/L cro	log_2 fold change fwd	log_2 fold change cro	H/L Count fwd	H/L Count cro	Area fwd	Area cro	Score fwd	Score cro
60S ribosomal protein L26 GN=RPL26 [RL26_HUMAN]	1.27	0.60	0.34	-0.74	1	1	1.3E6	1.7E6	26.32	30.67
Splicing factor 3A subunit 1 GN=SF3A1 [SF3A1_HUMAN]	1.26	0.65	0.33	-0.63	6	9	2.7E6	4.1E6	335.87	639.83
Coiled-coil domain-containing protein 12 GN=CCDC12 [CCD12_HUMAN]	1.24	0.63	0.31	-0.68	1	2	4.0E6	7.1E5	86.72	39.60
Splicing factor 3A subunit 3 GN=SF3A3 [SF3A3_HUMAN]	1.24	0.72	0.31	-0.48	1	2	2.8E6	3.3E6	131.88	216.70
Putative pre-mRNA-splicing factor ATP-dependent RNA helicase DHX15 GN=DHX15 [DHX15_HUMAN]	1.24	0.54	0.31	-0.89	29	26	2.8E7	2.5E7	3660.57	2514.86
Single-stranded DNA-binding protein, mitochondrial GN=SSBP1 [SSBP_HUMAN]	1.23	0.85	0.30	-0.24	1	2	2.2E6	1.2E6	120.65	128.16
G patch domain-containing protein 4 GN=GPATCH4 [GPTC4_HUMAN]	1.20	0.93	0.27	-0.10	5	6	4.1E6	3.2E6	511.63	572.06
Heat shock cognate 71 kDa protein GN=HSPA8 [HSP7C_HUMAN]	1.20	0.64	0.27	-0.64	37	32	1.0E8	7.9E7	5367.60	4163.95
Peptidyl-prolyl cis-trans isomerase E GN=PPIE [PPIE_HUMAN]	1.19	0.78	0.25	-0.35	3	2	1.1E6	1.4E6	88.52	61.62
Protein SON GN=SON [SON_HUMAN]	1.19	0.61	0.25	-0.71	5	11	1.9E6	5.9E6	367.64	727.87
Nuclease-sensitive element-binding protein 1 GN=YBX1 [YBOX1_HUMAN]	1.19	0.48	0.25	-1.05	11	18	2.6E8	2.5E8	5692.59	6427.18
H/ACA ribonucleoprotein complex subunit 4 GN=DKC1 [DKC1_HUMAN]	1.18	1.07	0.24	0.10	9	7	9.3E6	9.5E6	542.14	583.64
Transcription initiation factor TFIID subunit 12 GN=TAF12 [TAF12_HUMAN]	1.18	0.66	0.23	-0.60	1	2	3.5E5	1.2E6	31.38	76.39
Splicing factor 45 GN=RBM17 [SPF45_HUMAN]	1.17	0.65	0.22	-0.62	12	9	8.1E6	5.2E6	826.30	401.03
Splicing factor 3B subunit 5 GN=SF3B5 [SF3B5_HUMAN]	1.16	0.64	0.22	-0.65	1	1	7.2E6	9.1E6	221.58	184.58
Treacle protein GN=TCOF1 [TCOF_HUMAN]	1.16	0.90	0.21	-0.16	55	51	1.1E8	1.2E8	5708.84	5240.79
PHD finger protein 6 GN=PHF6 [PHF6_HUMAN]	1.15		0.20		1		5.8E5	0.0E0	37.18	
Transcription initiation factor TFIID subunit 10 GN=TAF10 [TAF10_HUMAN]	1.14	0.59	0.19	-0.76	1	2	2.7E6	6.2E6	178.44	505.15
Cell growth-regulating nucleolar protein GN=LYAR [LYAR_HUMAN]	1.14	1.03	0.19	0.04	1	1	1.6E6	2.9E6	236.07	67.90
Transcriptional activator protein Pur-alpha GN=PURA [PURA_HUMAN]	1.14	0.59	0.19	-0.77	1	1	2.3E6	2.1E6	105.65	51.22
Transcription initiation factor TFIID subunit 8 GN=TAF8 [TAF8_HUMAN]	1.14	0.69	0.18	-0.53	2	3	1.8E6	2.8E6	220.39	202.26
Transcription initiation factor TFIID subunit 4 GN=TAF4 [TAF4_HUMAN]	1.14	0.65	0.18	-0.63	9	15	7.4E6	7.1E6	1355.55	1474.19
THO complex subunit 5 homolog GN=THOC5 [THOC5_HUMAN]	1.12	0.76	0.16	-0.39	4	3	9.6E5	9.5E5	191.89	63.98
Transcription initiation factor TFIID subunit 9 GN=TAF9 [TAF9_HUMAN]	1.12	0.62	0.16	-0.69	6	6	2.0E6	3.3E6	308.75	297.73
Splicing factor 3B subunit 1 GN=SF3B1 [SF3B1_HUMAN]	1.11	0.63	0.15	-0.66	24	19	1.3E7	1.2E7	1582.91	1241.16
Splicing factor 3B subunit 4 GN=SF3B4 [SF3B4_HUMAN]	1.10	0.65	0.14	-0.63	1	1	7.2E6	1.0E7	286.37	200.29
WD40 repeat-containing protein SMU1 GN=SMU1 [SMU1_HUMAN]	1.10		0.14		2		8.1E5	0.0E0	86.32	
Poly(rC)-binding protein 1 GN=PCBP1 [PCBP1_HUMAN]	1.10	0.69	0.14	-0.54	4	5	6.1E6	6.8E6	655.49	806.58
Immortalization up-regulated protein GN=IMUP [IMUP_HUMAN]	1.09	1.13	0.13	0.18	1	2	1.7E6	4.0E5	64.68	83.15
Splicing factor 3B subunit 3 GN=SF3B3 [SF3B3_HUMAN]	1.09	0.65	0.13	-0.62	17	15	1.1E7	1.2E7	1983.86	1467.58
Transcription initiation factor TFIID subunit 2 GN=TAF2 [TAF2_HUMAN]	1.09	0.79	0.13	-0.33	1	2	6.7E5	6.0E5	25.39	45.58

protein name	H/L fwd	H/L cro	log_2 fold change fwd	log_2 fold change cro	H/L Count fwd	H/L Count cro	Area fwd	Area cro	Score fwd	Score cro
DNA-directed RNA polymerase I subunit RPA43 GN=TWISTNB [RPA43_HUMAN]	1.09	1.21	0.13	0.28	2	2	2.5E6	1.9E6	176.85	98.09
Splicing factor 3B subunit 2 GN=SF3B2 [SF3B2_HUMAN]	1.09	0.64	0.12	-0.65	12	19	4.5E6	2.1E7	855.97	1415.91
Serine/threonine-protein kinase PRP4 homolog GN=PRPF4B [PRP4B_HUMAN]	1.09	0.92	0.12	-0.12	8	4	9.3E6	5.3E6	824.47	757.73
Transcription initiation factor TFIID subunit 6 GN=TAF6 [TAF6_HUMAN]	1.08	0.62	0.12	-0.70	8	8	1.8E6	3.1E6	423.76	481.82
Zinc finger CCCH-type antiviral protein 1 GN=ZC3HAV1 [ZCCHV_HUMAN]	1.07	0.35	0.10	-1.53	10	9	9.3E6	1.4E7	942.31	914.40
Actin. gamma-enteric smooth muscle GN=ACTG2 [ACTH_HUMAN]	1.07	1.43	0.10	0.52	1	1	3.1E7	2.6E7	1222.21	1367.81
Intron-binding protein aquarius GN=AQR [AQR_HUMAN]	1.07	0.51	0.09	-0.98	4	2	1.3E6	1.1E6	135.27	130.57
Myosin regulatory light chain 12A GN=MYL12A [ML12A_HUMAN]	1.06	1.08	0.09	0.11	4	4	3.4E6	2.7E6	296.86	396.85
BAG family molecular chaperone regulator 3 GN=BAG3 [BAG3_HUMAN]	1.06	0.71	0.08	-0.50	1	2	1.3E6	8.4E5	111.14	144.95
Clathrin heavy chain 1 GN=CLTC [CLH1_HUMAN]	1.05		0.08		1		3.9E5	0.0E0	29.68	
Pinin GN=PNN [PININ_HUMAN]	1.05	0.65	0.07	-0.62	4	3	1.2E6	6.4E5	119.56	63.02
Pre-mRNA-splicing factor ISY1 homolog GN=ISY1 [ISY1_HUMAN]	1.05	0.67	0.07	-0.57	3	2	7.6E5	1.9E6	253.63	272.67
THO complex subunit 3 GN=THOC3 [THOC3_HUMAN]	1.04		0.06		3		2.5E6	0.0E0	135.97	
PHD finger-like domain-containing protein 5A GN=PHF5A [PHF5A_HUMAN]	1.03	0.62	0.05	-0.69	1	2	1.2E6	1.5E6	49.88	146.80
RNA-binding protein with serine-rich domain 1 GN=RNPS1 [RNPS1_HUMAN]	1.03	0.75	0.05	-0.41	5	4	6.9E6	7.5E6	333.96	266.30
Probable ATP-dependent RNA helicase DHX36 GN=DHX36 [DHX36_HUMAN]	1.03	0.43	0.04	-1.21	3	1	2.2E6	9.7E5	306.69	55.16
Myosin-9 GN=MYH9 [MYH9_HUMAN]	1.03	1.06	0.04	0.08	74	83	1.6E7	2.1E7	7815.88	9231.54
Serine/threonine-protein phosphatase PGAM5, mitochondrial GN=PGAM5 [PGAM5_HUMAN]	1.03	0.80	0.04	-0.32	6	2	3.3E6	2.2E6	282.34	184.22
Major vault protein GN=MVP [MVP_HUMAN]	1.02	0.34	0.03	-1.55	6	4	2.3E6	1.6E6	293.01	125.92
Heat shock 70 kDa protein 1A/1B GN=HSPA1A [HSP71_HUMAN]	1.02	0.74	0.03	-0.43	30	36	1.2E8	1.1E8	5384.61	5446.69
Nucleophosmin GN=NPM1 [NPM_HUMAN]	1.02	0.61	0.03	-0.72	3	2	4.2E6	4.5E6	242.86	399.22
60S ribosomal protein L31 GN=RPL31 [RL31_HUMAN]	1.02		0.02		1		5.5E5	0.0E0	34.44	
Heterogeneous nuclear ribonucleoprotein Q GN=SYNCRIP [HNRPQ_HUMAN]	1.01	1.00	0.02	0.01	1	1	2.0E6	2.0E6	208.09	110.63
Transcription initiation factor TFIID subunit 3 GN=TAF3 [TAF3_HUMAN]	1.01	0.68	0.01	-0.56	1	2	1.5E6	6.4E5	122.68	38.89
DBIRD complex subunit ZNF326 GN=ZNF326 [ZN326_HUMAN]	1.00	0.64	0.00	-0.65	4	5	1.6E6	3.0E6	205.42	302.08
Bromodomain and PHD finger-containing protein 3 GN=BRPF3 [BRPF3_HUMAN]	1.00	0.56	0.00	-0.84	1	1	9.0E5	1.8E6	41.62	44.14
Pre-mRNA-splicing factor SYF1 GN=XAB2 [SYF1_HUMAN]	1.00	0.60	0.00	-0.74	2	5	1.4E6	1.7E6	47.83	155.28
Heterogeneous nuclear ribonucleoprotein U-like protein 1 GN=HNRNPUL1 [HNRL1_HUMAN]	1.00	0.46	-0.01	-1.13	4	7	1.8E6	7.0E6	255.43	444.78

ii. ORF75 Interactome

Table 25 Binding partners of KSHV ORF75 identified by affinity purification followed by quantitative mass spectrometry. HeLa S3 cells were labelled with heavy or light amino acids in cell culture (SILAC). In the forward experiment (fwd) heavy labelled cells transiently expressed ORF75-myc and light labelled cells expressed LacZ-myc as a control. Labels were switched in the crossover experiment (cro). 24 h p.t. cells were lysed. Samples were subjected to anti-myc IP. Eluates were analysed by mass spectrometry. Heavy to light fold change values (H/L) were calculated for the identified proteins, based on the relative intensity for their peptides in the forward or crossover experiment. The values of the "heavy/light-fold change" for each protein pair were transformed into log_2 fold changes. Peptide filters were applied during bioinformatical analysis. Data are arranged according to size (descending) of the "H/L fwd" values. Shown are to top 150 proteins.

protein name	H/L fwd	H/L cro	log_2 fold change fwd	log_2 fold change cro	H/L count fwd	H/L count cro	Area fwd	Area cro	Score fwd	Score cro
ORF75 OS=Human herpesvirus 8 GN=ORF75 [D0UZU4_HHV8]	28.01	0.03	4.81	-5.10	73	38	3.5E8	3.1E8	10948.22	8439.82
Beta-galactosidase OS=Escherichia coli GN=lacZ [BGAL_ECOLX]	0.02	34.72	-5.64	5.12	26	54	8.1E8	6.0E8	10184.15	10341.11
Protein transport protein Sec16A GN=SEC16A [SC16A_HUMAN]	60.62	0.01	5.92	-6.06	7	2	2.4E6	2.4E6	379.89	294.78
Protein SEC13 homolog GN=SEC13 [SEC13_HUMAN]	21.97	0.04	4.46	-4.61	2	1	1.2E6	1.0E6	84.38	65.42
DNA-directed RNA polymerases I, II, and III subunit RPABC3 GN=POLR2H [RPAB3_HUMAN]	7.26		2.86		2		6.7E5	0.0E0	124.21	
Structural maintenance of chromosomes flexible hinge domain-containing protein 1 GN=SMCHD1 [SMHD1_HUMAN]	2.64	0.31	1.40	-1.71	1	5	1.2E6	1.4E6	61.00	239.26
BAG family molecular chaperone regulator 2 GN=BAG2 [BAG2_HUMAN]	2.62	0.31	1.39	-1.67	21	15	3.3E7	2.7E7	1150.29	1334.28
Far upstream element-binding protein 2 GN=KHSRP [FUBP2_HUMAN]	1.77	2.10	0.82	1.07	2	2	6.9E5	6.4E5	44.17	110.69
Mediator of RNA polymerase II transcription subunit 4 GN=MED4 [MED4_HUMAN]	1.76	0.24	0.82	-2.04	1	1	3.2E5	1.4E5	62.26	56.47
Zinc finger matrin-type protein 2 GN=ZMAT2 [ZMAT2_HUMAN]	1.76	0.85	0.81	-0.23	1	1	2.5E6	2.4E6	61.73	104.17
AT-rich interactive domain-containing protein 2 GN=ARID2 [ARID2_HUMAN]	1.73		0.79		1		1.0E5	0.0E0	50.33	
Proliferation-associated protein 2G4 GN=PA2G4 [PA2G4_HUMAN]	1.69		0.76		1		1.7E5	0.0E0	42.07	
Intron-binding protein aquarius GN=AQR [AQR_HUMAN]	1.67	0.93	0.74	-0.11	1	1	2.3E5	4.3E5	30.48	27.00
Mediator of RNA polymerase II transcription subunit 18 GN=MED18 [MED18_HUMAN]	1.66	0.37	0.74	-1.42	1	1	1.1E6	5.5E5	51.55	42.22
Mediator of RNA polymerase II transcription subunit 20 GN=MED20 [MED20_HUMAN]	1.54	0.11	0.62	-3.19	2	2	6.1E5	2.6E5	55.39	59.04
Luc7-like protein 3 GN=LUC7L3 [LC7L3_HUMAN]	1.49	0.57	0.57	-0.80	2	1	7.2E5	1.7E6	104.35	113.16
Parathymosin GN=PTMS [PTMS_HUMAN]	1.44	1.38	0.53	0.47	1	1	4.3E5	2.6E5	42.29	38.30
GC-rich sequence DNA-binding factor 1 GN=GCFC1 [GCFC1_HUMAN]	1.43	0.57	0.51	-0.80	3	5	1.5E6	1.2E6	290.73	266.60
Peptidyl-prolyl cis-trans isomerase-like 1 GN=PPIL1 [PPIL1_HUMAN]	1.38	0.73	0.47	-0.45	2	3	1.1E6	1.8E6	78.95	56.85
Far upstream element-binding protein 1 GN=FUBP1 [FUBP1_HUMAN]	1.37	1.06	0.46	0.09	1	1	6.0E5	5.4E5	30.69	25.44

protein name	H/L fwd	H/L cro	log_2 fold change fwd	log_2 fold change cro	H/L count fwd	H/L count cro	Area fwd	Area cro	Score fwd	Score cro
ATP-dependent RNA helicase A GN=DHX9 [DHX9_HUMAN]	1.37	0.79	0.45	-0.34	13	20	2.6E6	3.7E6	788.83	1020.81
THO complex subunit 3 GN=THOC3 [THOC3_HUMAN]	1.33	0.96	0.41	-0.07	2	2	2.7E6	2.0E6	129.55	124.20
Pre-mRNA-splicing factor RBM22 GN=RBM22 [RBM22_HUMAN]	1.28	0.67	0.35	-0.59	7	6	2.4E6	2.2E6	239.50	192.16
Pre-mRNA-splicing factor CWC22 homolog GN=CWC22 [CWC22_HUMAN]	1.28	0.73	0.35	-0.46	2	3	1.7E6	2.0E6	143.37	150.89
Splicing factor 3B subunit 4 GN=SF3B4 [SF3B4_HUMAN]	1.26	0.77	0.33	-0.37	2	1	1.4E6	2.1E6	221.06	209.65
Putative pre-mRNA-splicing factor ATP-dependent RNA helicase DHX15 GN=DHX15 [DHX15_HUMAN]	1.25	0.82	0.32	-0.28	24	19	6.6E6	6.4E6	1657.57	1473.66
Small ubiquitin-related modifier 2 GN=SUMO2 [SUMO2_HUMAN]	1.25	0.57	0.32	-0.80	1	1	8.7E5	3.7E5	86.53	51.55
Coilin GN=COIL [COIL_HUMAN]	1.24	0.98	0.31	-0.02	1	1	2.2E6	1.5E6	28.14	52.55
U1 small nuclear ribonucleoprotein A GN=SNRPA [SNRPA_HUMAN]	1.24		0.31		1		1.3E6	0.0E0	28.65	
SUMO-conjugating enzyme UBC9 GN=UBE2I [UBC9_HUMAN]	1.24		0.31		1		6.7E5	0.0E0	26.69	
Microfibrillar-associated protein 1 GN=MFAP1 [MFAP1_HUMAN]	1.23	0.76	0.30	-0.39	7	8	4.2E6	8.1E6	517.22	499.03
60S ribosomal protein L23a GN=RPL23A [RL23A_HUMAN]	1.22	0.86	0.29	-0.22	1	1	6.2E5	8.8E5	49.31	59.52
Caspase activity and apoptosis inhibitor 1 GN=CAAP1 [CAAP1_HUMAN]	1.22		0.29		1		1.3E5	0.0E0	24.96	
Immortalization up-regulated protein GN=IMUP [IMUP_HUMAN]	1.21		0.28		1		5.3E5	0.0E0	103.36	
Bromodomain and PHD finger-containing protein 3 GN=BRPF3 [BRPF3_HUMAN]	1.20	0.64	0.27	-0.65	1	1	7.9E5	1.4E6	26.36	35.10
RNA-binding protein 14 GN=RBM14 [RBM14_HUMAN]	1.20	1.08	0.26	0.11	1	2	2.2E5	7.2E5	37.96	94.04
Protein FAM133B GN=FAM133B [F133B_HUMAN]	1.20	1.04	0.26	0.05	5	5	2.8E6	3.3E6	150.69	337.06
Splicing factor 3A subunit 2 GN=SF3A2 [SF3A2_HUMAN]	1.19	1.05	0.25	0.07	2	1	1.1E6	9.1E5	53.62	29.31
Pre-mRNA-splicing factor 38A GN=PRPF38A [PR38A_HUMAN]	1.19	0.55	0.25	-0.85	1	1	1.9E6	3.7E6	96.66	153.13
Mediator of RNA polymerase II transcription subunit 19 GN=MED19 [MED19_HUMAN]	1.19	0.78	0.25	-0.36	1	2	2.4E6	1.9E6	74.00	75.69
Splicing factor 45 GN=RBM17 [SPF45_HUMAN]	1.19	0.73	0.25	-0.45	13	13	5.6E6	6.5E6	687.35	817.55
Heat shock cognate 71 kDa protein GN=HSPA8 [HSP7C_HUMAN]	1.19	0.72	0.25	-0.47	41	45	1.1E8	1.1E8	6058.70	5952.89
40S ribosomal protein S17-like GN=RPS17L [RS17L_HUMAN]	1.18	0.96	0.24	-0.05	1	1	1.3E6	8.4E5	38.88	31.67
THO complex subunit 1 GN=THOC1 [THOC1_HUMAN]	1.18	0.79	0.23	-0.34	2	4	1.3E6	1.5E6	199.11	193.87
DNA-directed RNA polymerase I subunit RPA43 GN=TWISTNB [RPA43_HUMAN]	1.17	0.91	0.23	-0.13	2	1	1.7E6	2.2E6	92.39	66.98
DNA-directed RNA polymerases I and III subunit RPAC1 GN=POLR1C [RPAC1_HUMAN]	1.17	0.80	0.23	-0.31	1	1	5.1E5	3.1E5	29.99	38.37
Tuftelin-interacting protein 11 GN=TFIP11 [TFP11_HUMAN]	1.17	0.63	0.23	-0.67	1	4	9.8E5	1.2E6	171.02	188.10

protein name	H/L fwd	H/L cro	log_2 fold change fwd	log_2 fold change cro	H/L count fwd	H/L count cro	Area fwd	Area cro	Score fwd	Score cro
Advillin GN=AVIL [AVIL_HUMAN]	1.17		0.23		1		3.1E5	0.0E0	41.34	
Nuclear cap-binding protein subunit 1 GN=NCBP1 [NCBP1_HUMAN]	1.17	0.88	0.23	-0.19	2	2	1.1E6	1.4E6	159.88	225.41
Chromatin target of PRMT1 protein GN=CHTOP [CHTOP_HUMAN]	1.17	0.70	0.22	-0.51	1	1	5.3E5	1.4E5	87.71	42.93
Coiled-coil domain-containing protein 12 GN=CCDC12 [CCD12_HUMAN]	1.16	0.79	0.22	-0.34	1	1	9.5E5	1.6E6	38.89	53.47
Splicing factor 3B subunit 1 GN=SF3B1 [SF3B1_HUMAN]	1.16	0.75	0.22	-0.42	5	6	1.4E6	1.9E6	182.63	378.63
U2 small nuclear ribonucleoprotein A' GN=SNRPA1 [RU2A_HUMAN]	1.16	0.73	0.22	-0.45	13	14	6.0E6	6.7E6	1053.20	1140.56
Small nuclear ribonucleoprotein Sm D3 GN=SNRPD3 [SMD3_HUMAN]	1.16	0.77	0.21	-0.38	4	4	9.2E6	1.3E7	312.42	452.70
SNW domain-containing protein 1 GN=SNW1 [SNW1_HUMAN]	1.15	0.74	0.21	-0.43	36	36	2.1E7	2.6E7	2489.69	3126.89
Serine/threonine-protein kinase PRP4 homolog GN=PRPF4B [PRP4B_HUMAN]	1.15	0.99	0.20	-0.02	5	6	5.2E6	4.5E6	512.05	615.07
Werner syndrome ATP-dependent helicase GN=WRN [WRN_HUMAN]	1.15		0.20		1		7.7E5	0.0E0	24.53	
Coiled-coil domain-containing protein 9 GN=CCDC9 [CCDC9_HUMAN]	1.14	0.79	0.19	-0.34	1	1	4.4E5	3.5E5	36.75	33.62
Splicing factor 3B subunit 2 GN=SF3B2 [SF3B2_HUMAN]	1.14	0.89	0.19	-0.17	8	4	2.9E6	2.1E6	526.03	270.06
H/ACA ribonucleoprotein complex subunit 4 GN=DKC1 [DKC1_HUMAN]	1.14	0.97	0.19	-0.04	5	5	5.4E6	3.1E6	319.23	321.32
Eukaryotic initiation factor 4A-III GN=EIF4A3 [IF4A3_HUMAN]	1.14	0.79	0.19	-0.34	24	25	1.6E7	1.9E7	1840.12	1855.30
Brain acid soluble protein 1 GN=BASP1 [BASP1_HUMAN]	1.13	0.92	0.18	-0.12	1	4	3.2E6	2.3E6	154.73	120.57
THO complex subunit 6 homolog GN=THOC6 [THOC6_HUMAN]	1.13	0.88	0.18	-0.19	5	5	1.8E6	1.3E6	382.25	358.20
U5 small nuclear ribonucleoprotein 200 kDa helicase GN=SNRNP200 [U520_HUMAN]	1.13	0.81	0.17	-0.31	32	39	4.2E6	5.6E6	2332.61	3286.75
Small nuclear ribonucleoprotein-associated proteins B and B' GN=SNRPB [RSMB_HUMAN]	1.13	0.61	0.17	-0.71	7	6	5.3E6	8.0E6	738.75	693.47
Heterogeneous nuclear ribonucleoprotein A3 GN=HNRNPA3 [ROA3_HUMAN]	1.13		0.17		1		5.4E5	0.0E0	33.38	
Retinitis pigmentosa 9 protein GN=RP9 [RP9_HUMAN]	1.12	0.95	0.17	-0.07	2	2	7.1E5	4.2E5	67.11	77.27
Transcription initiation factor TFIID subunit 7 GN=TAF7 [TAF7_HUMAN]	1.11	0.87	0.16	-0.21	2	2	1.8E6	1.3E6	54.93	147.60
RNA-binding protein Raly GN=RALY [RALY_HUMAN]	1.11	0.85	0.15	-0.24	6	8	2.1E6	3.0E6	431.93	409.33
Protein SREK1IP1 GN=SREK1IP1 [SR1IP_HUMAN]	1.11	0.99	0.15	-0.01	4	3	2.2E6	3.2E6	358.54	221.88
Protein CASC3 GN=CASC3 [CASC3_HUMAN]	1.11	0.81	0.15	-0.30	5	4	1.9E6	1.5E6	121.49	188.34
Pre-mRNA-processing-splicing factor 8 GN=PRPF8 [PRP8_HUMAN]	1.11	0.78	0.15	-0.35	11	18	2.4E6	2.7E6	388.21	781.14
Splicing factor 3B subunit 3 GN=SF3B3 [SF3B3_HUMAN]	1.11	0.79	0.15	-0.35	16	15	3.9E6	2.8E6	1556.03	1441.37
Small nuclear ribonucleoprotein E GN=SNRPE [RUXE_HUMAN]	1.10	0.73	0.14	-0.45	3	2	1.1E7	1.1E7	347.91	354.00
Treacle protein GN=TCOF1 [TCOF_HUMAN]	1.10	0.80	0.14	-0.32	43	42	7.3E7	6.3E7	4334.81	4236.84

protein name	H/L fwd	H/L cro	log_2 fold change fwd	log_2 fold change cro	H/L count fwd	H/L count cro	Area fwd	Area cro	Score fwd	Score cro
Probable ATP-dependent RNA helicase DHX35 GN=DHX35 [DHX35_HUMAN]	1.10	0.80	0.14	-0.32	8	9	2.0E6	2.5E6	271.95	540.38
Plasminogen activator inhibitor 1 RNA-binding protein GN=SERBP1 [PAIRB_HUMAN]	1.10	0.98	0.14	-0.03	1	2	7.1E5	9.6E5	184.19	122.66
Splicing factor 3A subunit 1 GN=SF3A1 [SF3A1_HUMAN]	1.09	0.87	0.13	-0.20	1	1	1.1E6	1.0E6	27.64	46.55
Small nuclear ribonucleoprotein Sm D1 GN=SNRPD1 [SMD1_HUMAN]	1.09	0.79	0.13	-0.35	4	4	1.2E7	1.6E7	522.78	569.20
H/ACA ribonucleoprotein complex subunit 1 GN=GAR1 [GAR1_HUMAN]	1.09	0.80	0.13	-0.33	2	3	9.7E5	6.2E5	95.14	65.78
Nucleolin GN=NCL [NUCL_HUMAN]	1.09	0.97	0.12	-0.04	6	8	8.5E5	1.1E6	179.33	389.72
Protein mago nashi homolog GN=MAGOH [MGN_HUMAN]	1.09	0.82	0.12	-0.28	7	5	7.0E6	7.9E6	504.74	526.50
Protein BUD31 homolog GN=BUD31 [BUD31_HUMAN]	1.09	0.79	0.12	-0.34	1	1	1.7E6	3.0E5	26.10	30.80
RNA-binding protein 25 GN=RBM25 [RBM25_HUMAN]	1.08	0.91	0.12	-0.13	2	2	1.9E6	1.3E6	51.60	82.54
E3 ubiquitin-protein ligase RBBP6 GN=RBBP6 [RBBP6_HUMAN]	1.08	1.01	0.12	0.02	6	11	3.5E6	4.8E6	159.02	363.39
Heterogeneous nuclear ribonucleoproteins C1/C2 GN=HNRNPC [HNRPC_HUMAN]	1.08	0.83	0.11	-0.27	18	16	3.5E7	3.6E7	1931.59	2137.79
Transcription initiation factor TFIID subunit 8 GN=TAF8 [TAF8_HUMAN]	1.08	0.92	0.11	-0.12	3	6	9.3E5	1.4E6	206.90	402.45
116 kDa U5 small nuclear ribonucleoprotein component GN=EFTUD2 [U5S1_HUMAN]	1.08	0.78	0.11	-0.36	26	30	4.8E6	7.8E6	2081.71	2752.36
Small nuclear ribonucleoprotein Sm D2 GN=SNRPD2 [SMD2_HUMAN]	1.08	0.80	0.11	-0.33	7	5	9.7E6	9.8E6	724.39	638.18
Splicing factor 3B subunit 5 GN=SF3B5 [SF3B5_HUMAN]	1.08	0.69	0.11	-0.53	3	1	4.8E6	3.5E6	197.07	193.74
Small nuclear ribonucleoprotein F GN=SNRPF [RUXF_HUMAN]	1.07	0.80	0.10	-0.32	4	3	7.8E6	9.0E6	430.66	213.88
Thioredoxin-dependent peroxide reductase, mitochondrial GN=PRDX3 [PRDX3_HUMAN]	1.07		0.10		1		6.0E5	0.0E0	125.09	
RNA-binding protein 8A GN=RBM8A [RBM8A_HUMAN]	1.07	0.81	0.10	-0.30	8	8	2.1E7	2.2E7	663.05	725.53
U5 small nuclear ribonucleoprotein 40 kDa protein GN=SNRNP40 [SNR40_HUMAN]	1.07	0.83	0.09	-0.27	7	9	2.8E6	3.2E6	405.90	452.72
Heat shock 70 kDa protein 1A/1B GN=HSPA1A [HSP71_HUMAN]	1.06	0.78	0.09	-0.35	51	51	1.2E8	1.2E8	7389.26	7232.86
Interleukin enhancer-binding factor 2 GN=ILF2 [ILF2_HUMAN]	1.06	0.69	0.09	-0.53	1	1	6.2E5	2.8E5	41.97	39.07
PHD finger-like domain-containing protein 5A GN=PHF5A [PHF5A_HUMAN]	1.06	0.83	0.08	-0.26	1	1	1.3E6	1.0E6	50.94	34.62
Transcription initiation factor TFIID subunit 9 GN=TAF9 [TAF9_HUMAN]	1.05		0.08		1		4.4E5	0.0E0	27.35	
DNA-directed RNA polymerase I subunit RPA34 GN=CD3EAP [RPA34_HUMAN]	1.05	0.93	0.07	-0.10	4	4	3.5E6	4.8E6	396.44	296.03
40S ribosomal protein S25 GN=RPS25 [RS25_HUMAN]	1.05	0.88	0.07	-0.18	2	1	1.6E6	2.0E6	149.44	154.22

protein name	H/L fwd	H/L cro	log_2 fold change fwd	log_2 fold change cro	H/L count fwd	H/L count cro	Area fwd	Area cro	Score fwd	Score cro
G patch domain-containing protein 4 GN=GPATCH4 [GPTC4_HUMAN]	1.05	0.77	0.07	-0.38	4	3	2.1E6	1.9E6	355.92	180.85
Cleavage and polyadenylation specificity factor subunit 6 GN=CPSF6 [CPSF6_HUMAN]	1.05	1.18	0.07	0.24	3	4	5.3E5	5.3E5	253.17	229.21
Pre-mRNA-processing factor 19 GN=PRPF19 [PRP19_HUMAN]	1.04	0.82	0.06	-0.28	6	3	1.1E6	1.3E6	227.93	199.41
CWF19-like protein 2 GN=CWF19L2 [C19L2_HUMAN]	1.04		0.05		1		2.2E5	0.0E0	28.62	
Peptidyl-prolyl cis-trans isomerase B GN=PPIB [PPIB_HUMAN]	1.04	0.95	0.05	-0.07	8	9	8.1E6	8.9E6	725.09	799.43
40S ribosomal protein S26 GN=RPS26 [RS26_HUMAN]	1.03		0.05		1		1.1E6	0.0E0	65.57	
40S ribosomal protein S3a GN=RPS3A [RS3A_HUMAN]	1.03	0.79	0.05	-0.35	2	2	9.3E5	4.2E5	74.78	65.16
60S ribosomal protein L22 GN=RPL22 [RL22_HUMAN]	1.03	0.91	0.04	-0.13	2	3	6.7E6	6.5E6	365.48	311.38
Pre-mRNA branch site protein p14 GN=SF3B14 [PM14_HUMAN]	1.03	0.87	0.04	-0.19	3	1	5.9E5	4.5E5	135.65	79.03
rRNA 2'-O-methyltransferase fibrillarin GN=FBL [FBRL_HUMAN]	1.03	0.74	0.04	-0.44	4	4	1.4E6	1.5E6	90.91	142.58
RNA-binding protein FUS GN=FUS [FUS_HUMAN]	1.03	0.88	0.04	-0.18	1	2	5.1E5	1.1E6	38.99	78.49
Putative RNA-binding protein Luc7-like 2 GN=LUC7L2 [LC7L2_HUMAN]	1.02	1.00	0.03	-0.01	3	5	9.1E5	1.1E6	182.07	440.90
60S ribosomal protein L34 GN=RPL34 [RL34_HUMAN]	1.02	1.08	0.03	0.11	4	1	3.1E6	2.0E6	100.59	26.30
Poly(U)-binding-splicing factor PUF60 GN=PUF60 [PUF60_HUMAN]	1.01	0.91	0.02	-0.14	37	39	7.4E7	1.2E8	4716.86	5368.77
Multiple myeloma tumor-associated protein 2 GN=MMTAG2 [MMTA2_HUMAN]	1.01	1.00	0.02	0.00	7	8	4.3E6	5.7E6	730.22	877.45
RNA-binding protein with serine-rich domain 1 GN=RNPS1 [RNPS1_HUMAN]	1.01	0.87	0.02	-0.20	5	5	2.4E6	3.0E6	287.30	349.19
60S ribosomal protein L4 GN=RPL4 [RL4_HUMAN]	1.01	1.08	0.01	0.11	2	2	3.1E5	3.2E5	59.41	171.69
Pre-mRNA 3'-end-processing factor FIP1 GN=FIP1L1 [FIP1_HUMAN]	1.01	0.93	0.01	-0.10	3	4	7.4E5	1.0E6	95.82	210.77
Heterogeneous nuclear ribonucleoproteins A2/B1 GN=HNRNPA2B1 [ROA2_HUMAN]	1.00	0.92	0.00	-0.12	9	8	4.4E6	4.4E6	499.94	604.85
60S acidic ribosomal protein P2 GN=RPLP2 [RLA2_HUMAN]	1.00	0.93	0.00	-0.10	1	2	5.7E5	5.9E5	46.49	145.97
RNA-binding protein 7 GN=RBM7 [RBM7_HUMAN]	1.00	0.84	0.00	-0.25	2	1	6.1E5	4.5E5	117.95	127.02
60S ribosomal protein L7a GN=RPL7A [RL7A_HUMAN]	1.00	0.93	0.00	-0.10	6	8	7.2E6	9.5E6	424.92	655.38
Stress-70 protein. mitochondrial GN=HSPA9 [GRP75_HUMAN]	1.00	0.91	-0.01	-0.14	38	37	4.4E7	4.3E7	4854.16	4783.82
Serine/arginine-rich splicing factor 6 GN=SRSF6 [SRSF6_HUMAN]	1.00	1.00	-0.01	0.00	2	2	1.5E6	2.1E6	99.94	144.87
Histone H3.3C GN=H3F3C [H3C_HUMAN]	0.99	0.42	-0.01	-1.25	1	1	1.7E6	3.4E6	54.40	66.19
UPF0468 protein C16orf80 GN=C16orf80 [CP080_HUMAN]	0.99	0.82	-0.02	-0.28	5	4	6.2E6	3.9E6	407.10	339.72
Serine/threonine-protein phosphatase PGAM5, mitochondrial GN=PGAM5 [PGAM5_HUMAN]	0.99	0.94	-0.02	-0.10	9	8	6.7E6	5.1E6	640.50	573.19

protein name	H/L fwd	H/L cro	log_2 fold change fwd	log_2 fold change cro	H/L count fwd	H/L count cro	Area fwd	Area cro	Score fwd	Score cro
40S ribosomal protein S9 GN=RPS9 [RS9_HUMAN]	0.99	0.93	-0.02	-0.11	1	1	5.8E5	7.1E5	33.88	35.27
Serine/arginine-rich splicing factor 1 GN=SRSF1 [SRSF1_HUMAN]	0.98	1.04	-0.03	0.06	6	4	1.8E6	2.2E6	203.40	259.60
Pleiotropic regulator 1 GN=PLRG1 [PLRG1_HUMAN]	0.98	0.58	-0.03	-0.78	2	1	2.4E6	2.4E6	164.57	215.37
40S ribosomal protein S6 GN=RPS6 [RS6_HUMAN]	0.98	0.86	-0.03	-0.21	2	3	9.8E5	1.0E6	83.29	89.55
Spliceosome-associated protein CWC15 homolog GN=CWC15 [CWC15_HUMAN]	0.97	0.73	-0.04	-0.46	5	8	4.9E6	6.3E6	423.04	492.36
60S ribosomal protein L8 GN=RPL8 [RL8_HUMAN]	0.97	0.94	-0.04	-0.09	7	8	8.6E6	8.3E6	643.31	670.66
Zinc finger protein 207 GN=ZNF207 [ZN207_HUMAN]	0.97	0.87	-0.05	-0.20	1	3	1.4E6	2.9E6	115.09	150.09
60S ribosomal protein L19 GN=RPL19 [RL19_HUMAN]	0.96	0.84	-0.05	-0.25	1	1	1.4E6	8.8E5	91.55	62.87
60 kDa heat shock protein, mitochondrial GN=HSPD1 [CH60_HUMAN]	0.96	0.97	-0.05	-0.04	54	47	3.3E7	2.6E7	6015.03	5807.86
SAP30-binding protein GN=SAP30BP [S30BP_HUMAN]	0.96	0.79	-0.06	-0.34	1	1	6.3E5	9.6E5	74.28	112.00
FACT complex subunit SSRP1 GN=SSRP1 [SSRP1_HUMAN]	0.96		-0.07		1		5.3E5	0.0E0	28.57	
Protein FRG1 GN=FRG1 [FRG1_HUMAN]	0.95	0.90	-0.07	-0.15	4	3	2.0E6	1.5E6	300.17	255.17
Spliceosome RNA helicase DDX39B GN=DDX39B [DX39B_HUMAN]	0.95	0.87	-0.07	-0.21	3	4	8.7E5	1.1E6	174.45	199.30
Transcription initiation factor TFIID subunit 10 GN=TAF10 [TAF10_HUMAN]	0.95	0.77	-0.07	-0.38	2	3	2.8E6	1.6E6	426.71	378.71
Transcription initiation factor TFIID subunit 4 GN=TAF4 [TAF4_HUMAN]	0.95	0.87	-0.08	-0.20	13	13	5.9E6	6.8E6	1385.81	1552.07
Crooked neck-like protein 1 GN=CRNKL1 [CRNL1_HUMAN]	0.95	0.69	-0.08	-0.54	1	2	9.5E5	6.2E5	76.42	118.07
Cell growth-regulating nucleolar protein GN=LYAR [LYAR_HUMAN]	0.94	0.78	-0.09	-0.36	1	1	7.3E5	4.9E5	65.70	62.22
Pinin GN=PNN [PININ_HUMAN]	0.94	0.70	-0.09	-0.50	3	1	4.0E5	3.1E5	79.94	32.46
Protein SET GN=SET [SET_HUMAN]	0.94	0.70	-0.09	-0.52	1	2	8.4E5	1.2E6	127.48	152.19
60S ribosomal protein L3 GN=RPL3 [RL3_HUMAN]	0.94	0.84	-0.09	-0.26	1	1	1.3E6	1.1E6	45.72	53.68
Zinc finger CCCH domain-containing protein 14 GN=ZC3H14 [ZC3HE_HUMAN]	0.94	0.87	-0.09	-0.20	1	6	1.3E6	9.5E5	35.36	298.44
DNA topoisomerase 1 GN=TOP1 [TOP1_HUMAN]	0.94	0.69	-0.09	-0.54	4	4	2.8E6	1.9E6	176.63	153.16
Cleavage and polyadenylation specificity factor subunit 5 GN=NUDT21 [CPSF5_HUMAN]	0.94	1.14	-0.10	0.19	8	8	4.6E6	5.6E6	305.04	422.17

iii. OASL Interactome

Table 26 Binding partners of OASL identified by affinity purification followed by quantitative mass spectrometry. Samples were prepared as described in Figure 42. Briefly, SILAC labelled HeLa S3 cells were used. In the forward experiment (fwd) heavy labelled cells transiently expressed OASL a-myc and light labelled cells expressed LacZ-myc as a control. Labels were switched in the crossover experiment (cro). 24 h p.t. cells were lysed. Samples of the forward and crossover experiment were combined for anti-myc affinity purification. Eluates were analysed by mass spectrometry. Heavy to light fold change values (H/L) were calculated for the identified proteins. The values of the "heavy/light-fold change" for each protein pair were transformed into log_2 fold changes. Peptide filters were applied during bioinformatical analysis. Data are arranged according to size (descending) of the "H/L fwd" values. Shown are to top 150 proteins.

protein name	H/L fwd	H/L cro	log_2 fold change fwd	log_2 fold change cro	H/L Count fwd	H/L Count cro	Area fwd	Area cro	Score fwd	Score cro
2'-5'-oligoadenylate synthase-like protein GN=OASL [OASL_HUMAN]	12.41	0.10	3.63	-3.28	9	9	3.6E8	2.6E8	479.75	412.39
Beta-galactosidase OS=Escherichia coli GN=lacZ [BGAL_ECOLX]	0.02	44.22	-5.75	5.47	6	4	0.0E0	0.0E0		
Ribosome production factor 2 homolog GN=RPF2 [RPF2_HUMAN]	10.47	0.16	3.39	-2.68	1	1	1.7E7	2.1E7	50.59	68.05
60S ribosomal protein L36 GN=RPL36 [RL36_HUMAN]	7.33	0.15	2.87	-2.73	6	1	6.1E8	1.2E9	257.14	124.54
40S ribosomal protein S10 GN=RPS10 [RS10_HUMAN]	7.25	0.17	2.86	-2.55	2	2	2.7E7	7.2E7	54.69	41.15
RNA-binding protein 34 GN=RBM34 [RBM34_HUMAN]	7.15	0.19	2.84	-2.42	7	5	8.2E7	5.1E7	283.13	130.44
60S ribosomal protein L5 GN=RPL5 [RL5_HUMAN]	6.89	0.15	2.78	-2.78	18	12	7.9E8	7.8E8	903.52	667.77
Ubiquitin-40S ribosomal protein S27a GN=RPS27A [RS27A_HUMAN]	6.88	0.19	2.78	-2.40	3	1	3.6E8	4.8E7	193.19	90.32
Probable rRNA-processing protein EBP2 GN=EBNA1BP2 [EBP2_HUMAN]	6.85	0.22	2.78	-2.19	8	7	2.6E8	2.3E8	379.24	313.44
60S ribosomal protein L10a GN=RPL10A [RL10A_HUMAN]	6.74	0.18	2.75	-2.45	14	10	8.6E8	8.9E8	709.68	668.36
40S ribosomal protein S28 GN=RPS28 [RS28_HUMAN]	6.74	0.16	2.75	-2.64	5	5	3.0E8	4.4E8	279.20	301.66
RNA-binding protein 28 GN=RBM28 [RBM28_HUMAN]	6.71	0.25	2.75	-2.03	2	1	2.5E7	3.0E6	59.45	26.76
60S acidic ribosomal protein P0 GN=RPLP0 [RLA0_HUMAN]	6.49	0.19	2.70	-2.40	20	16	1.7E9	1.2E9	1681.51	1256.31
40S ribosomal protein S3 GN=RPS3 [RS3_HUMAN]	6.48	0.17	2.70	-2.54	14	11	8.1E8	1.2E9	745.96	679.26
40S ribosomal protein S12 GN=RPS12 [RS12_HUMAN]	6.39	0.17	2.67	-2.59	8	7	7.0E8	9.5E8	255.34	263.10
40S ribosomal protein S18 GN=RPS18 [RS18_HUMAN]	6.38	0.15	2.67	-2.71	7	7	3.1E8	3.9E8	328.99	232.21
40S ribosomal protein S16 GN=RPS16 [RS16_HUMAN]	6.37	0.17	2.67	-2.55	3	7	3.8E8	3.4E8	258.44	335.01
60S acidic ribosomal protein P1 GN=RPLP1 [RLA1_HUMAN]	6.37	0.18	2.67	-2.50	2	4	8.8E8	6.5E8	353.61	294.30
60S ribosomal protein L12 GN=RPL12 [RL12_HUMAN]	6.34	0.17	2.66	-2.55	9	9	1.2E9	1.6E9	997.24	911.29
Putative ribosomal RNA methyltransferase NOP2 GN=NOP2 [NOP2_HUMAN]	6.30	0.27	2.66	-1.87	7	4	5.8E7	5.3E7	319.03	252.40
40S ribosomal protein S25 GN=RPS25 [RS25_HUMAN]	6.24	0.17	2.64	-2.57	3	2	1.1E8	4.0E7	71.45	58.12
60S ribosomal protein L8 GN=RPL8 [RL8_HUMAN]	6.19	0.21	2.63	-2.29	20	14	3.0E9	3.2E9	1361.53	1005.32
Ribosome biogenesis protein BRX1 homolog GN=BRIX1 [BRX1_HUMAN]	6.12	0.05	2.61	-4.23	2	2	1.0E7	7.2E6	96.47	68.54

protein name	H/L fwd	H/L cro	log_2 fold change fwd	log_2 fold change cro	H/L Count fwd	H/L Count cro	Area fwd	Area cro	Score fwd	Score cro
60S ribosomal protein L18a GN=RPL18A [RL18A_HUMAN]	6.12	0.16	2.61	-2.61	5	4	3.3E8	2.2E8	232.96	164.47
60S ribosomal protein L21 GN=RPL21 [RL21_HUMAN]	6.08	0.17	2.60	-2.55	10	8	8.5E8	8.2E8	524.64	360.79
60S ribosomal protein L34 GN=RPL34 [RL34_HUMAN]	6.07	0.18	2.60	-2.46	4	2	4.7E8	4.3E8	111.49	53.85
60S ribosomal protein L7 GN=RPL7 [RL7_HUMAN]	6.03	0.34	2.59	-1.57	6	8	3.2E8	4.4E8	429.42	470.21
60S acidic ribosomal protein P2 GN=RPLP2 [RLA2_HUMAN]	6.02	0.19	2.59	-2.37	9	7	1.2E9	1.3E9	613.38	619.06
60S ribosomal protein L30 GN=RPL30 [RL30_HUMAN]	5.99	0.18	2.58	-2.45	4	5	1.9E8	2.5E8	296.40	301.08
40S ribosomal protein S5 GN=RPS5 [RS5_HUMAN]	5.99	0.05	2.58	-4.40	2	2	2.3E7	1.9E7	102.46	130.76
60S ribosomal protein L35a GN=RPL35A [RL35A_HUMAN]	5.94	0.22	2.57	-2.19	4	2	5.9E8	7.3E8	128.76	42.10
60S ribosomal protein L28 GN=RPL28 [RL28_HUMAN]	5.89	0.16	2.56	-2.63	7	3	2.8E8	7.8E7	225.29	161.57
40S ribosomal protein S20 GN=RPS20 [RS20_HUMAN]	5.84	0.16	2.55	-2.63	6	8	8.9E8	1.1E9	242.34	310.50
60S ribosomal protein L14 GN=RPL14 [RL14_HUMAN]	5.82	0.20	2.54	-2.33	6	4	1.0E9	1.0E9	392.24	265.70
60S ribosomal protein L6 GN=RPL6 [RL6_HUMAN]	5.68	0.18	2.51	-2.51	15	12	3.1E9	3.7E9	993.97	653.84
60S ribosomal protein L7a GN=RPL7A [RL7A_HUMAN]	5.49	0.18	2.46	-2.47	16	16	2.9E9	3.2E9	1044.42	1284.42
60S ribosomal protein L27 GN=RPL27 [RL27_HUMAN]	5.48	0.19	2.45	-2.42	6	5	8.4E8	6.9E8	185.39	159.74
60S ribosomal protein L32 GN=RPL32 [RL32_HUMAN]	5.44	0.18	2.44	-2.50	10	7	4.5E8	3.6E8	517.66	220.81
60S ribosomal protein L3 GN=RPL3 [RL3_HUMAN]	5.36	0.24	2.42	-2.06	9	8	9.3E8	1.1E9	558.73	564.07
40S ribosomal protein S17-like GN=RPS17L [RS17L_HUMAN]	5.36	0.23	2.42	-2.14	8	8	4.7E8	3.3E8	483.26	511.52
60S ribosomal protein L4 GN=RPL4 [RL4_HUMAN]	5.35	0.31	2.42	-1.70	11	14	6.4E8	5.7E8	502.68	495.17
60S ribosomal protein L11 GN=RPL11 [RL11_HUMAN]	5.33	0.20	2.41	-2.32	2	2	8.3E8	1.0E9	286.85	184.63
Uncharacterized protein C7orf50 GN=C7orf50 [CG050_HUMAN]	5.31	0.19	2.41	-2.41	1	3	4.1E7	9.0E7	65.77	80.18
60S ribosomal protein L13a GN=RPL13A [RL13A_HUMAN]	5.22	0.25	2.38	-2.03	4	3	5.6E8	5.6E8	111.02	90.35
Nucleolar RNA helicase 2 GN=DDX21 [DDX21_HUMAN]	5.17	0.32	2.37	-1.63	11	8	1.8E8	1.4E8	627.22	462.43
60S ribosomal protein L18 GN=RPL18 [RL18_HUMAN]	5.16	0.29	2.37	-1.81	7	7	8.2E8	6.8E8	588.06	494.93
KRR1 small subunit processome component homolog GN=KRR1 [KRR1_HUMAN]	5.13		2.36		1		2.3E7	0.0E0	65.96	
60S ribosomal protein L15 GN=RPL15 [RL15_HUMAN]	4.87	0.28	2.28	-1.84	8	6	4.1E8	2.5E8	416.18	219.51
60S ribosomal protein L37a GN=RPL37A [RL37A_HUMAN]	4.74	0.26	2.24	-1.96	4	2	1.2E8	6.0E7	309.42	59.81
60S ribosomal protein L13 GN=RPL13 [RL13_HUMAN]	4.69	0.20	2.23	-2.32	8	9	1.4E9	1.4E9	543.79	488.99
Ribosome biogenesis regulatory protein homolog GN=RRS1 [RRS1_HUMAN]	4.60	0.21	2.20	-2.22	2	2	2.3E7	1.7E7	55.94	45.95
Pre-mRNA-processing factor 19 GN=PRPF19 [PRP19_HUMAN]	4.58	0.99	2.19	-0.02	2	4	2.7E7	4.3E7	58.63	156.76
40S ribosomal protein S15 GN=RPS15 [RS15_HUMAN]	4.48	0.25	2.16	-2.01	10	10	1.8E8	2.2E8	758.42	655.80

protein name	H/L fwd	H/L cro	log_2 fold change fwd	log_2 fold change cro	H/L Count fwd	H/L Count cro	Area fwd	Area cro	Score fwd	Score cro
Eukaryotic translation initiation factor 6 GN=EIF6 [IF6_HUMAN]	4.32	0.23	2.11	-2.09	1	2	5.4E7	1.7E7	24.84	52.47
Putative oxidoreductase GLYR1 GN=GLYR1 [GLYR1_HUMAN]	4.27	0.36	2.10	-1.49	1	3	3.2E7	3.3E7	26.64	126.99
Ataxin-2-like protein GN=ATXN2L [ATX2L_HUMAN]	4.06	0.42	2.02	-1.26	3	1	1.3E7	1.8E7	73.97	28.00
Ribosomal L1 domain-containing protein 1 GN=RSL1D1 [RL1D1_HUMAN]	4.00	0.30	2.00	-1.74	1	2	1.1E8	6.5E7	41.69	53.64
Putative ATP-dependent RNA helicase DHX30 GN=DHX30 [DHX30_HUMAN]	3.91		1.97		2		1.4E7	0.0E0	94.40	
60S ribosomal protein L29 GN=RPL29 [RL29_HUMAN]	3.72	0.26	1.89	-1.95	1	1	2.8E9	3.5E9	220.79	250.69
Coiled-coil domain-containing protein 137 GN=CCDC137 [CC137_HUMAN]	3.57	0.42	1.84	-1.23	2	2	3.4E7	6.8E7	171.35	85.42
UPF0488 protein C8orf33 GN=C8orf33 [CH033_HUMAN]	3.56		1.83		1		2.8E7	0.0E0	60.43	
Nuclease-sensitive element-binding protein 1 GN=YBX1 [YBOX1_HUMAN]	3.54	0.22	1.82	-2.18	12	13	2.4E9	4.4E9	2105.91	2360.46
60S ribosomal protein L24 GN=RPL24 [RL24_HUMAN]	3.49	0.33	1.80	-1.61	4	4	4.6E8	1.5E8	215.23	117.50
40S ribosomal protein S2 GN=RPS2 [RS2_HUMAN]	3.42	0.32	1.77	-1.65	7	6	1.2E8	2.7E8	348.04	321.71
Fragile X mental retardation syndrome-related protein 1 GN=FXR1 [FXR1_HUMAN]	3.37	0.35	1.75	-1.51	1	2	4.8E7	1.6E7	152.01	88.50
Protein LLP homolog GN=LLPH PE=2 [LLPH_HUMAN]	3.37	0.31	1.75	-1.71	3	2	1.1E8	1.8E8	180.17	134.09
60S ribosomal protein L10 GN=RPL10 [RL10_HUMAN]	3.34	0.33	1.74	-1.62	9	9	2.2E8	2.4E8	358.95	306.80
Suppressor of SWI4 1 homolog GN=PPAN [SSF1_HUMAN]	3.33		1.74		1		5.5E7	0.0E0	32.43	
40S ribosomal protein S27 GN=RPS27 [RS27_HUMAN]	3.31		1.72		2		4.2E7	0.0E0	71.06	
mRNA turnover protein 4 homolog GN=MRTO4 [MRT4_HUMAN]	3.21		1.68		3		1.1E7	0.0E0	56.49	
60S ribosomal protein L9 GN=RPL9 [RL9_HUMAN]	3.12	0.31	1.64	-1.69	8	9	5.5E8	6.8E8	498.87	506.01
Y-box-binding protein 3 GN=YBX3 [YBOX3_HUMAN]	3.02	0.30	1.59	-1.73	4	7	1.3E9	1.4E9	1565.71	1511.09
Exosome complex component RRP46 GN=EXOSC5 [EXOS5_HUMAN]	2.99	0.40	1.58	-1.32	2	1	2.3E7	3.1E7	61.05	40.62
Double-stranded RNA-binding protein Staufen homolog 2 GN=STAU2 [STAU2_HUMAN]	2.94	0.27	1.55	-1.87	1	3	1.3E7	1.1E7	32.02	57.01
Ribosomal RNA-processing protein 8 GN=RRP8 [RRP8_HUMAN]	2.91		1.54		1		1.9E7	0.0E0	41.25	
Histone H3.3C GN=H3F3C [H3C_HUMAN]	2.90		1.54		1		1.3E8	0.0E0	28.18	
60S ribosomal protein L23 GN=RPL23 [RL23_HUMAN]	2.88	0.33	1.53	-1.60	6	5	9.0E8	7.3E8	533.34	329.95
Glutamate-rich WD repeat-containing protein 1 GN=GRWD1 [GRWD1_HUMAN]	2.87		1.52		1		1.4E7	0.0E0	31.76	
Polyadenylate-binding protein 1 GN=PABPC1 [PABP1_HUMAN]	2.87	0.31	1.52	-1.67	6	3	3.2E7	4.6E7	153.21	104.46
Elongation factor 1-alpha 1 GN=EEF1A1 [EF1A1_HUMAN]	2.84	0.74	1.51	-0.44	1	1	1.8E7	5.1E7	37.51	62.85
RNA-binding protein 10 GN=RBM10 [RBM10_HUMAN]	2.83	0.65	1.50	-0.61	2	2	5.3E6	1.3E7	42.34	42.56
40S ribosomal protein S14 GN=RPS14 [RS14_HUMAN]	2.82	0.30	1.50	-1.74	10	11	1.6E9	2.0E9	738.61	1045.79

protein name	H/L fwd	H/L cro	log_2 fold change fwd	log_2 fold change cro	H/L Count fwd	H/L Count cro	Area fwd	Area cro	Score fwd	Score cro
40S ribosomal protein S8 GN=RPS8 [RS8_HUMAN]	2.80	0.36	1.49	-1.46	9	9	7.7E8	1.0E9	523.17	557.68
rRNA 2'-O-methyltransferase fibrillarin GN=FBL [FBRL_HUMAN]	2.79	0.34	1.48	-1.56	4	1	3.5E7	2.1E8	111.71	44.27
M-phase phosphoprotein 6 GN=MPHOSPH6 [MPH6_HUMAN]	2.77	0.36	1.47	-1.49	1	1	1.7E7	2.6E7	36.57	30.29
pre-rRNA processing protein FTSJ3 GN=FTSJ3 [SPB1_HUMAN]	2.76	0.88	1.46	-0.19	2	1	1.8E7	7.1E6	55.51	38.77
Transmembrane protein 229B GN=TMEM229B PE=2 [T229B_HUMAN]	2.74		1.46		1		4.9E6	0.0E0	27.86	
Tubulin alpha-1C chain GN=TUBA1C [TBA1C_HUMAN]	2.59		1.37		1		9.3E6	0.0E0	116.50	
Histone H4 GN=HIST1H4A [H4_HUMAN]	2.59	0.58	1.37	-0.78	4	2	1.8E8	1.1E8	146.88	135.59
60S ribosomal protein L19 GN=RPL19 [RL19_HUMAN]	2.51	0.41	1.33	-1.28	6	4	2.4E8	3.3E8	377.32	154.21
Nucleolar protein 16 GN=NOP16 [NOP16_HUMAN]	2.38	0.46	1.25	-1.13	2	2	6.0E7	1.4E7	117.43	95.92
Nuclear fragile X mental retardation-interacting protein 2 GN=NUFIP2 [NUFP2_HUMAN]	2.37		1.25		1		4.0E6	0.0E0	27.26	
ATP-dependent RNA helicase A GN=DHX9 [DHX9_HUMAN]	2.37	0.48	1.25	-1.05	7	6	3.1E7	3.3E7	312.35	220.75
Histone H2A type 1-H GN=HIST1H2AH [H2A1H_HUMAN]	2.37	0.61	1.24	-0.72	4	4	7.3E8	2.0E8	301.28	153.49
Core histone macro-H2A.1 GN=H2AFY [H2AY_HUMAN]	2.36		1.24		2		3.7E7	0.0E0	104.96	
Histone H2B type 1-J GN=HIST1H2BJ [H2B1J_HUMAN]	2.35	0.65	1.23	-0.63	1	2	2.8E8	2.5E8	350.77	521.94
40S ribosomal protein S23 GN=RPS23 [RS23_HUMAN]	2.28	0.41	1.19	-1.27	6	5	7.1E8	6.0E8	359.11	222.68
Centromere protein V GN=CENPV [CENPV_HUMAN]	2.27	0.27	1.18	-1.91	3	2	1.8E7	1.9E7	172.49	89.37
Chromobox protein homolog 3 GN=CBX3 [CBX3_HUMAN]	2.27		1.18	#ZAHL!	3		2.3E7	0.0E0	201.16	
Heat shock protein beta-1 GN=HSPB1 [HSPB1_HUMAN]	2.25	0.44	1.17	-1.20	1	1	8.2E6	1.6E7	32.13	29.47
60S ribosomal protein L27a GN=RPL27A [RL27A_HUMAN]	2.22	0.42	1.15	-1.24	9	9	1.3E9	1.6E9	518.62	463.10
40S ribosomal protein S6 GN=RPS6 [RS6_HUMAN]	2.20	0.45	1.14	-1.15	14	9	9.0E8	1.2E9	674.98	542.98
Heterochromatin protein 1-binding protein 3 GN=HP1BP3 [HP1B3_HUMAN]	2.19	0.49	1.13	-1.04	6	5	1.2E8	9.9E7	204.13	261.55
Ribosomal RNA processing protein 1 homolog B GN=RRP1B [RRP1B_HUMAN]	2.18	0.60	1.13	-0.75	2	4	1.6E7	1.1E7	71.21	183.02
Vimentin GN=VIM [VIME_HUMAN]	2.16	0.50	1.11	-1.01	2	6	1.9E7	4.1E7	148.87	200.82
40S ribosomal protein S3a GN=RPS3A [RS3A_HUMAN]	2.12	0.39	1.08	-1.35	16	14	4.9E8	9.1E8	1338.48	1224.08
THO complex subunit 3 GN=THOC3 [THOC3_HUMAN]	2.10		1.07		1		1.9E7	0.0E0	31.13	
Fragile X mental retardation syndrome-related protein 2 GN=FXR2 [FXR2_HUMAN]	2.08		1.06		1		4.3E7	0.0E0	100.24	
Heterogeneous nuclear ribonucleoprotein M GN=HNRNPM [HNRPM_HUMAN]	2.05	0.61	1.03	-0.71	9	9	1.2E8	1.3E8	891.85	557.24

protein name	H/L fwd	H/L cro	log_2 fold change fwd	log_2 fold change cro	H/L Count fwd	H/L Count cro	Area fwd	Area cro	Score fwd	Score cro
MKI67 FHA domain-interacting nucleolar phosphoprotein GN=NIFK [MK67I_HUMAN]	2.05		1.03		1		1.0E7	0.0E0	72.77	
RNA-binding protein PNO1 GN=PNO1 [PNO1_HUMAN]	2.05		1.03		1		1.5E7	0.0E0	55.83	
Tudor domain-containing protein 3 GN=TDRD3 [TDRD3_HUMAN]	2.00		1.00		2		1.1E7	0.0E0	45.70	
Transcriptional repressor NF-X1 GN=NFX1 [NFX1_HUMAN]	1.99		0.99		1		1.0E7	0.0E0	35.27	
Putative RNA-binding protein Luc7-like 2 GN=LUC7L2 [LC7L2_HUMAN]	1.97	0.56	0.98	-0.85	1	1	1.0E7	5.0E6	43.57	49.10
Insulin-like growth factor 2 mRNA-binding protein 3 GN=IGF2BP3 [IF2B3_HUMAN]	1.96	0.60	0.97	-0.75	1	4	7.6E7	9.9E7	136.66	248.51
Cold-inducible RNA-binding protein GN=CIRBP [CIRBP_HUMAN]	1.92	1.10	0.94	0.14	1	1	3.9E6	1.2E7	63.80	30.48
Protein PRRC2C GN=PRRC2C [PRC2C_HUMAN]	1.89		0.92		1		2.9E7	0.0E0	27.71	
Nucleolar and spindle-associated protein 1 GN=NUSAP1 [NUSAP_HUMAN]	1.88	0.80	0.91	-0.32	1	2	2.3E7	2.1E7	29.37	58.21
DNA-directed RNA polymerases I, II, and III subunit RPABC1 GN=POLR2E [RPAB1_HUMAN]	1.84	0.78	0.88	-0.36	2	2	1.1E7	1.1E7	105.20	126.30
Ribosome-binding protein 1 GN=RRBP1 [RRBP1_HUMAN]	1.83	0.44	0.87	-1.17	9	8	4.7E7	5.9E7	548.91	480.64
60S ribosomal protein L17 GN=RPL17 [RL17_HUMAN]	1.80	0.54	0.85	-0.89	14	17	1.0E9	1.0E9	1175.61	772.38
Putative RNA-binding protein 15 GN=RBM15 [RBM15_HUMAN]	1.80	0.76	0.85	-0.40	1	1	1.5E7	2.2E7	26.60	27.81
Zinc finger CCCH-type antiviral protein 1 GN=ZC3HAV1 [ZCCHV_HUMAN]	1.75	0.52	0.81	-0.94	11	12	1.7E8	2.1E8	695.08	660.59
Protein FAM98A GN=FAM98A [FA98A_HUMAN]	1.65		0.73		1		1.4E7	0.0E0	46.18	
116 kDa U5 small nuclear ribonucleoprotein component GN=EFTUD2 [U5S1_HUMAN]	1.65	1.38	0.73	0.46	1	2	8.9E6	1.6E7	38.84	42.25
40S ribosomal protein S24 GN=RPS24 [RS24_HUMAN]	1.65	0.51	0.72	-0.96	5	4	1.0E9	1.2E9	584.23	476.74
RNA-binding protein 14 GN=RBM14 [RBM14_HUMAN]	1.64	0.90	0.72	-0.14	3	4	2.7E7	3.7E7	129.99	181.81
Histone H1.0 GN=H1F0 [H10_HUMAN]	1.63		0.70		2		3.6E7	0.0E0	46.93	
Protein PRRC2A GN=PRRC2A [PRC2A_HUMAN]	1.61		0.69		1		2.5E7	0.0E0	45.48	
Insulin-like growth factor 2 mRNA-binding protein 1 GN=IGF2BP1 [IF2B1_HUMAN]	1.61	0.56	0.69	-0.84	8	6	1.9E8	2.6E8	687.53	334.44
Lysine-rich nucleolar protein 1 GN=KNOP1 [KNOP1_HUMAN]	1.60	0.63	0.68	-0.66	7	5	2.3E7	3.0E7	209.49	179.57
Histone H1.4 GN=HIST1H1E [H14_HUMAN]	1.58		0.66		1		2.9E9	3.4E9	2349.41	2256.12
WW domain-binding protein 11 GN=WBP11 [WBP11_HUMAN]	1.57	1.01	0.65	0.02	9	7	8.5E7	7.3E7	477.40	431.42
Probable ATP-dependent RNA helicase DDX17 GN=DDX17 [DDX17_HUMAN]	1.56	0.76	0.65	-0.39	1	2	4.5E7	5.4E7	104.70	135.85
Glioma tumor suppressor candidate region gene 2 protein GN=GLTSCR2 [GSCR2_HUMAN]	1.56	0.26	0.64	-1.97	1	1	6.3E6	6.9E6	48.56	102.11

protein name	H/L fwd	H/L cro	log_2 fold change fwd	log_2 fold change cro	H/L Count fwd	H/L Count cro	Area fwd	Area cro	Score fwd	Score cro
Coiled-coil domain-containing protein 86 GN=CCDC86 [CCD86_HUMAN]	1.56	0.77	0.64	-0.37	2	2	7.5E7	7.9E7	94.28	125.57
40S ribosomal protein S9 GN=RPS9 [RS9_HUMAN]	1.56	0.57	0.64	-0.82	7	4	1.3E8	8.3E7	302.86	129.70
Histone H1.5 GN=HIST1H1B [H15_HUMAN]	1.55	1.05	0.64	0.07	7	6	8.9E8	9.9E8	859.18	835.67
Peptidyl-prolyl cis-trans isomerase-like 1 GN=PPIL1 [PPIL1_HUMAN]	1.55	0.88	0.64	-0.18	4	7	4.5E7	7.1E7	131.24	359.03
N-acetyltransferase 10 GN=NAT10 [NAT10_HUMAN]	1.52		0.60		2		1.1E7	0.0E0	70.36	
RNA-binding motif protein, X chromosome GN=RBMX [RBMX_HUMAN]	1.49	0.83	0.58	-0.27	9	9	1.2E9	1.3E9	1839.85	1355.09
Heterogeneous nuclear ribonucleoproteins C1/C2 GN=HNRNPC [HNRPC_HUMAN]	1.49	0.64	0.58	-0.64	6	5	9.7E8	1.7E9	1104.61	1062.16
Interleukin enhancer-binding factor 2 GN=ILF2 [ILF2_HUMAN]	1.49	0.71	0.57	-0.49	2	3	6.2E7	7.2E7	234.89	202.16
Heterogeneous nuclear ribonucleoprotein R GN=HNRNPR [HNRPR_HUMAN]	1.48		0.57		1		2.7E7	8.5E7	89.39	30.61
Target of EGR1 protein 1 GN=TOE1 [TOE1_HUMAN]	1.48	0.90	0.56	-0.15	3	1	2.6E7	4.4E7	123.14	25.54
Splicing factor 3B subunit 5 GN=SF3B5 [SF3B5_HUMAN]	1.46	0.89	0.54	-0.18	2	3	7.7E7	9.3E7	111.07	200.00
DNA topoisomerase 2-alpha GN=TOP2A [TOP2A_HUMAN]	1.45	1.08	0.53	0.11	4	2	2.4E7	1.9E7	91.66	83.35
SWI/SNF-related matrix-associated actin-dependent regulator of chromatin subfamily E member 1 GN=SMARCE1 [SMCE1_HUMAN]	1.44	0.72	0.53	-0.48	1	1	1.2E7	1.2E7	39.01	48.75
60S ribosomal protein L36a-like GN=RPL36AL [RL36L_HUMAN]	1.44		0.52		1		2.7E7	0.0E0	52.23	
Interleukin enhancer-binding factor 3 GN=ILF3 [ILF3_HUMAN]	1.43	0.74	0.52	-0.43	17	16	2.3E8	2.1E8	891.94	766.48

Table 27 Binding partners of OASL upon NDV infection identified by affinity purification followed by quantitative mass spectrometry. Samples were prepared as described in Figure 42. Briefly, SILAC labelled HeLa S3 cells were used. In the forward experiment (fwd) heavy labelled cells transiently expressed OASL a-myc and light labelled cells expressed LacZ-myc as a control. Labels were switched in the crossover experiment (cro). 24 h p.t. cells were infected with NDV for 1h and were lysed 14h later. Samples of the forward and crossover experiment were combined for anti-myc affinity purification. Eluates were analysed by mass spectrometry. Heavy to light fold change values (H/L) were calculated for the identified proteins. The values of the “heavy/light-fold change” for each protein pair were transformed into log_2 fold changes. Peptide filters were applied during bioinformatical analysis. Data are arranged according to size (descending) of the ”H/L fwd” values. Shown are to top 150 proteins.

protein name	H/L fwd	H/L cro	log_2 fold change fwd	log_2 fold change cro	H/L Count fwd	H/L Count cro	Area fwd	Area cro	Score fwd	Score cro
2'-5'-oligoadenylate synthase-like protein GN=OASL [OASL_HUMAN]	10.34	0.10	3.37	-3.30	8	10	4.1E8	3.9E8	389.73	525.60
Beta-galactosidase OS=Escherichia coli GN=lacZ [BGAL_ECOLX]	0.03	54.03	-5.15	5.76	4	12	8.6E7	8.5E8	207.00	910.00
Ribosome biogenesis protein BRX1 homolog GN=BRIX1 [BRX1_HUMAN]	79.54	0.30	6.31	-1.72	1	1	1.1E7	1.8E7	130.57	91.29
Actin-like protein 6A GN=ACTL6A [ACL6A_HUMAN]	20.48		4.36		1		5.0E6	0.0E0	36.65	

protein name	H/L fwd	H/L cro	log_2 fold change fwd	log_2 fold change cro	H/L Count fwd	H/L Count cro	Area fwd	Area cro	Score fwd	Score cro
Protein PRRC2C GN=PRRC2C [PRC2C_HUMAN]	11.89		3.57		2		2.0E7	0.0E0	43.14	
40S ribosomal protein S5 GN=RPS5 [RS5_HUMAN]	11.21	0.19	3.49	-2.36	2	2	1.7E7	6.4E7	70.07	61.60
DNA topoisomerase 2-beta GN=TOP2B [TOP2B_HUMAN]	9.73		3.28		1		1.3E7	2.2E7	45.49	31.35
RNA-binding protein 34 GN=RBM34 [RBM34_HUMAN]	8.41	0.12	3.07	-3.07	7	5	1.8E8	4.6E7	276.57	165.17
60S ribosomal protein L5 GN=RPL5 [RL5_HUMAN]	7.39	0.13	2.89	-2.89	16	20	9.2E8	1.3E9	889.58	999.44
40S ribosomal protein S21 GN=RPS21 [RS21_HUMAN]	6.82	0.12	2.77	-3.04	1	1	3.1E7	1.2E7	59.88	38.97
60S ribosomal protein L18a GN=RPL18A [RL18A_HUMAN]	6.49	0.19	2.70	-2.42	11	6	6.8E8	4.1E8	414.30	208.04
40S ribosomal protein S28 GN=RPS28 [RS28_HUMAN]	6.46	0.14	2.69	-2.81	4	3	4.5E8	1.8E8	256.52	156.05
60S ribosomal protein L28 GN=RPL28 [RL28_HUMAN]	6.38	0.16	2.67	-2.64	9	5	4.2E8	1.8E8	203.00	187.73
40S ribosomal protein S10 GN=RPS10 [RS10_HUMAN]	6.34	0.15	2.67	-2.74	2	1	3.5E7	2.6E7	42.21	86.71
Ubiquitin-40S ribosomal protein S27a GN=RPS27A [RS27A_HUMAN]	6.26	0.14	2.65	-2.84	6	2	1.2E8	4.6E8	389.99	91.40
60S ribosomal protein L12 GN=RPL12 [RL12_HUMAN]	6.22	0.15	2.64	-2.70	8	8	1.4E9	9.3E8	1280.11	692.62
mRNA turnover protein 4 homolog GN=MRTO4 [MRT4_HUMAN]	6.17	0.27	2.63	-1.88	1	1	1.2E7	1.2E7	35.13	27.15
60S ribosomal protein L8 GN=RPL8 [RL8_HUMAN]	6.15	0.21	2.62	-2.27	21	16	4.6E9	2.1E9	1488.47	790.95
40S ribosomal protein S20 GN=RPS20 [RS20_HUMAN]	6.12	0.16	2.61	-2.68	6	5	1.6E9	5.5E8	316.99	177.07
60S ribosomal protein L10a GN=RPL10A [RL10A_HUMAN]	6.10	0.21	2.61	-2.24	11	9	8.2E8	7.1E8	549.54	351.04
60S ribosomal protein L36 GN=RPL36 [RL36_HUMAN]	6.10	0.17	2.61	-2.58	5	4	1.3E9	4.8E8	362.46	171.75
Probable rRNA-processing protein EBP2 GN=EBNA1BP2 [EBP2_HUMAN]	6.10	0.24	2.61	-2.09	9	6	2.5E8	1.3E8	474.80	201.82
40S ribosomal protein S16 GN=RPS16 [RS16_HUMAN]	6.04	0.16	2.59	-2.67	5	9	4.2E8	4.0E8	346.88	367.08
60S ribosomal protein L14 GN=RPL14 [RL14_HUMAN]	6.04	0.22	2.59	-2.16	9	4	1.5E9	8.7E8	416.55	237.35
40S ribosomal protein S12 GN=RPS12 [RS12_HUMAN]	6.02	0.16	2.59	-2.67	9	7	1.1E9	8.6E8	335.16	185.08
40S ribosomal protein S18 GN=RPS18 [RS18_HUMAN]	6.00	0.14	2.59	-2.88	4	5	2.5E8	2.2E8	216.13	192.95
60S acidic ribosomal protein P1 GN=RPLP1 [RLA1_HUMAN]	6.00	0.21	2.59	-2.27	3	3	9.5E8	7.1E8	362.94	382.40
60S ribosomal protein L21 GN=RPL21 [RL21_HUMAN]	5.96	0.15	2.58	-2.70	9	6	1.3E9	1.2E9	581.58	426.22
40S ribosomal protein S29 GN=RPS29 [RS29_HUMAN]	5.96	0.15	2.58	-2.75	2	1	7.7E7	1.2E7	75.20	28.04
ATP-dependent RNA helicase DDX24 GN=DDX24 [DDX24_HUMAN]	5.96		2.58		1		8.8E6	0.0E0	38.39	
40S ribosomal protein S25 GN=RPS25 [RS25_HUMAN]	5.90	0.16	2.56	-2.68	2	2	3.6E8	9.9E7	83.95	122.80
60S acidic ribosomal protein P2 GN=RPLP2 [RLA2_HUMAN]	5.89	0.19	2.56	-2.39	10	9	1.7E9	2.7E9	775.89	1080.45
60S ribosomal protein L6 GN=RPL6 [RL6_HUMAN]	5.88	0.20	2.56	-2.30	17	14	4.3E9	1.8E9	1224.46	850.69
60S acidic ribosomal protein P0 GN=RPLP0 [RLA0_HUMAN]	5.81	0.21	2.54	-2.26	17	19	1.9E9	1.6E9	1482.49	1562.49
60S ribosomal protein L30 GN=RPL30 [RL30_HUMAN]	5.80	0.21	2.54	-2.26	5	5	3.8E8	2.5E8	394.78	192.98

protein name	H/L fwd	H/L cro	log_2 fold change fwd	log_2 fold change cro	H/L Count fwd	H/L Count cro	Area fwd	Area cro	Score fwd	Score cro
60S ribosomal protein L7a GN=RPL7A [RL7A_HUMAN]	5.79	0.20	2.53	-2.29	17	13	2.7E9	1.7E9	1095.47	781.70
60S ribosomal protein L34 GN=RPL34 [RL34_HUMAN]	5.76	0.17	2.53	-2.59	2	3	1.1E9	6.0E8	55.45	73.96
RNA-binding protein 28 GN=RBM28 [RBM28_HUMAN]	5.63	0.17	2.49	-2.58	3	2	1.5E7	2.0E7	113.10	46.90
40S ribosomal protein S3 GN=RPS3 [RS3_HUMAN]	5.63	0.17	2.49	-2.57	11	9	3.8E8	4.3E8	434.24	397.15
Uncharacterized protein C7orf50 GN=C7orf50 [CG050_HUMAN]	5.62	0.18	2.49	-2.48	3	1	1.1E8	2.9E7	104.58	42.62
60S ribosomal protein L27 GN=RPL27 [RL27_HUMAN]	5.62	0.19	2.49	-2.39	8	6	1.6E9	1.0E9	225.95	207.91
60S ribosomal protein L32 GN=RPL32 [RL32_HUMAN]	5.39	0.15	2.43	-2.70	7	8	7.3E8	6.5E8	390.16	492.44
60S ribosomal protein L13a GN=RPL13A [RL13A_HUMAN]	5.28	0.33	2.40	-1.60	4	5	6.9E8	4.9E8	122.10	126.43
60S ribosomal protein L11 GN=RPL11 [RL11_HUMAN]	5.24	0.21	2.39	-2.25	3	4	6.1E8	5.3E8	307.44	169.78
Ribosome production factor 2 homolog GN=RPF2 [RPF2_HUMAN]	5.21	0.11	2.38	-3.22	1	3	5.5E6	1.1E7	36.59	75.58
40S ribosomal protein S17-like GN=RPS17L [RS17L_HUMAN]	5.11	0.21	2.35	-2.28	6	9	5.3E8	5.1E8	205.42	468.37
60S ribosomal protein L3 GN=RPL3 [RL3_HUMAN]	5.11	0.28	2.35	-1.82	12	9	9.0E8	7.4E8	616.25	596.83
Ribosome biogenesis regulatory protein homolog GN=RRS1 [RRS1_HUMAN]	5.04	0.22	2.33	-2.19	2	2	5.7E7	1.9E7	52.23	56.46
Eukaryotic translation initiation factor 6 GN=EIF6 [IF6_HUMAN]	4.99	0.29	2.32	-1.77	1	1	8.2E7	5.4E7	43.11	46.76
60S ribosomal protein L35a GN=RPL35A [RL35A_HUMAN]	4.99	0.24	2.32	-2.05	3	2	7.4E8	5.3E8	98.26	47.05
Putative ribosomal RNA methyltransferase NOP2 GN=NOP2 [NOP2_HUMAN]	4.95	0.29	2.31	-1.80	5	4	6.5E7	4.4E7	201.87	159.86
60S ribosomal protein L13 GN=RPL13 [RL13_HUMAN]	4.94	0.19	2.30	-2.37	10	9	1.8E9	1.9E9	481.68	414.81
60S ribosomal protein L37a GN=RPL37A [RL37A_HUMAN]	4.88	0.21	2.29	-2.24	3	2	3.7E8	3.6E7	366.35	63.30
60S ribosomal protein L18 GN=RPL18 [RL18_HUMAN]	4.73	0.38	2.24	-1.38	10	6	9.4E8	6.5E8	659.24	450.24
Nucleolar RNA helicase 2 GN=DDX21 [DDX21_HUMAN]	4.66	0.32	2.22	-1.65	12	10	2.5E8	2.7E8	707.94	424.20
60S ribosomal protein L15 GN=RPL15 [RL15_HUMAN]	4.60	0.34	2.20	-1.56	8	7	3.5E8	3.4E8	282.16	279.74
60S ribosomal protein L4 GN=RPL4 [RL4_HUMAN]	4.49	0.36	2.17	-1.48	17	8	7.0E8	4.1E8	759.61	426.60
60S ribosomal protein L29 GN=RPL29 [RL29_HUMAN]	4.39	0.24	2.13	-2.08	3	2	1.7E9	1.3E9	209.65	217.33
40S ribosomal protein S19 GN=RPS19 [RS19_HUMAN]	4.35		2.12		1		7.6E6	0.0E0	36.73	
60S ribosomal protein L7 GN=RPL7 [RL7_HUMAN]	4.31	0.37	2.11	-1.45	7	8	5.9E8	4.3E8	438.03	506.90
WD repeat-containing protein 5 GN=WDR5 [WDR5_HUMAN]	4.29		2.10		1		2.0E7	0.0E0	24.75	
Putative oxidoreductase GLYR1 GN=GLYR1 [GLYR1_HUMAN]	4.22	0.36	2.08	-1.49	1	2	4.4E7	1.2E7	62.98	75.52
Fragile X mental retardation syndrome-related protein 1 GN=FXR1 [FXR1_HUMAN]	4.20	0.42	2.07	-1.25	1	2	5.5E7	1.7E7	77.43	146.04
Nuclease-sensitive element-binding protein 1 GN=YBX1 [YBOX1_HUMAN]	4.01	0.24	2.00	-2.05	14	5	3.7E9	3.7E9	3031.42	1895.35
Putative ATP-dependent RNA helicase DHX30 GN=DHX30 [DHX30_HUMAN]	3.86	0.43	1.95	-1.21	3	1	1.4E7	7.8E6	86.35	45.93

protein name	H/L fwd	H/L cro	log_2 fold change fwd	log_2 fold change cro	H/L Count fwd	H/L Count cro	Area fwd	Area cro	Score fwd	Score cro
UPF0488 protein C8orf33 GN=C8orf33 [CH033_HUMAN]	3.79		1.92		1		8.0E6	0.0E0	25.80	
40S ribosomal protein S15 GN=RPS15 [RS15_HUMAN]	3.67	0.26	1.87	-1.92	8	5	1.2E8	8.9E7	379.28	302.03
Eukaryotic translation initiation factor 3 subunit G GN=EIF3G [EIF3G_HUMAN]	3.63		1.86		1		8.0E6	0.0E0	26.26	
Ribosomal L1 domain-containing protein 1 GN=RSL1D1 [RL1D1_HUMAN]	3.62	0.24	1.86	-2.06	2	2	9.4E7	2.5E7	114.55	61.90
Protein LLP homolog GN=LLPH [LLPH_HUMAN]	3.62	0.25	1.85	-2.02	4	5	6.0E7	9.8E7	234.56	157.97
60S ribosomal protein L24 GN=RPL24 [RL24_HUMAN]	3.56	0.58	1.83	-0.80	5	2	2.5E8	4.7E8	182.06	163.67
Exosome complex component RRP46 GN=EXOSC5 [EXOS5_HUMAN]	3.56		1.83		1		1.8E7	0.0E0	40.23	
Fragile X mental retardation syndrome-related protein 2 GN=FXR2 [FXR2_HUMAN]	3.42		1.77		1		5.2E7	3.1E7	110.21	30.21
Ataxin-2-like protein GN=ATXN2L [ATX2L_HUMAN]	3.30	0.36	1.72	-1.48	7	3	4.2E7	1.6E7	174.12	77.75
Glutamate-rich WD repeat-containing protein 1 GN=GRWD1 [GRWD1_HUMAN]	3.22		1.69		1		2.1E7	0.0E0	47.90	
60S ribosomal protein L10 GN=RPL10 [RL10_HUMAN]	3.19	0.40	1.67	-1.32	10	8	3.1E8	1.5E8	458.95	348.94
Exosome complex component RRP43 GN=EXOSC8 [EXOS8_HUMAN]	3.15		1.65		1		2.5E7	0.0E0	24.58	
40S ribosomal protein S27 GN=RPS27 [RS27_HUMAN]	3.12		1.64		2		7.3E7	0.0E0	64.19	
Y-box-binding protein 3 GN=YBX3 [YBOX3_HUMAN]	3.11	0.32	1.64	-1.63	5	4	2.2E9	1.4E9	1791.29	1219.66
60S ribosomal protein L9 GN=RPL9 [RL9_HUMAN]	3.10	0.35	1.63	-1.50	5	6	5.9E8	3.7E8	456.77	223.51
Polyadenylate-binding protein 1 GN=PABPC1 [PABP1_HUMAN]	3.10	0.32	1.63	-1.62	4	3	7.2E7	3.9E7	155.54	135.86
60S ribosomal protein L23 GN=RPL23 [RL23_HUMAN]	2.98	0.44	1.57	-1.17	8	6	8.9E8	8.2E8	706.26	448.19
Glioma tumor suppressor candidate region gene 2 protein GN=GLTSCR2 [GSCR2_HUMAN]	2.97		1.57		1		3.2E6	0.0E0	76.67	
40S ribosomal protein S2 GN=RPS2 [RS2_HUMAN]	2.97	0.33	1.57	-1.59	7	4	2.3E8	1.4E8	221.37	131.62
Double-stranded RNA-binding protein Staufen homolog 2 GN=STAU2 [STAU2_HUMAN]	2.96	0.30	1.57	-1.72	1	3	4.1E6	1.1E7	25.53	64.93
40S ribosomal protein S14 GN=RPS14 [RS14_HUMAN]	2.95	0.30	1.56	-1.75	14	12	2.3E9	1.4E9	923.96	662.28
Ribosomal RNA processing protein 1 homolog B GN=RRP1B [RRP1B_HUMAN]	2.87	0.63	1.52	-0.67	1	2	1.0E7	1.7E7	28.13	65.11
rRNA 2'-O-methyltransferase fibrillarin GN=FBL [FBRL_HUMAN]	2.86	0.34	1.52	-1.57	2	3	1.7E8	6.8E7	91.58	78.54
40S ribosomal protein S8 GN=RPS8 [RS8_HUMAN]	2.66	0.39	1.41	-1.35	8	6	9.7E8	5.9E8	516.73	444.81
M-phase phosphoprotein 6 GN=MPHOSPH6 [MPH6_HUMAN]	2.49		1.32		1		9.2E6	0.0E0	30.86	
60S ribosomal protein L27a GN=RPL27A [RL27A_HUMAN]	2.44	0.45	1.29	-1.16	8	6	1.9E9	8.8E8	462.57	356.59
Chromobox protein homolog 3 GN=CBX3 [CBX3_HUMAN]	2.43	0.55	1.28	-0.87	1	1	8.2E6	3.4E7	29.88	29.41

protein name	H/L fwd	H/L cro	log_2 fold change fwd	log_2 fold change cro	H/L Count fwd	H/L Count cro	Area fwd	Area cro	Score fwd	Score cro
Coiled-coil domain-containing protein 137 GN=CCDC137 [CC137_HUMAN]	2.41	0.45	1.27	-1.15	1	1	5.5E7	5.9E7	54.36	63.40
ATP-dependent RNA helicase A GN=DHX9 [DHX9_HUMAN]	2.37	0.52	1.25	-0.94	8	14	5.1E7	4.7E7	418.59	516.43
Interferon-stimulated 20 kDa exonuclease-like 2 GN=ISG20L2 [I20L2_HUMAN]	2.34		1.23		1		5.8E6	0.0E0	31.66	
60S ribosomal protein L19 GN=RPL19 [RL19_HUMAN]	2.34	0.49	1.23	-1.03	6	1	3.7E8	5.1E8	371.12	79.80
40S ribosomal protein S23 GN=RPS23 [RS23_HUMAN]	2.29	0.42	1.19	-1.25	5	6	8.5E8	6.5E8	385.63	330.85
40S ribosomal protein S6 GN=RPS6 [RS6_HUMAN]	2.26	0.47	1.18	-1.08	11	8	1.2E9	6.1E8	752.58	244.25
40S ribosomal protein S3a GN=RPS3A [RS3A_HUMAN]	2.16	0.38	1.11	-1.41	10	16	3.9E8	4.1E8	866.41	973.60
Heterogeneous nuclear ribonucleoprotein M GN=HNRNPM [HNRPM_HUMAN]	2.10	0.66	1.07	-0.61	8	9	5.2E7	1.3E8	504.63	608.89
Protein NPAT GN=NPAT [NPAT_HUMAN]	2.09		1.06		1		3.9E7	0.0E0	24.69	
Histone H3.3C GN=H3F3C [H3C_HUMAN]	2.07		1.05		1		1.4E8	0.0E0	48.92	
Histone H4 GN=HIST1H4A [H4_HUMAN]	2.01	0.77	1.01	-0.38	1	4	1.4E8	1.7E8	94.25	187.84
Transcriptional repressor NF-X1 GN=NFX1 [NFX1_HUMAN]	2.00		1.00		2		1.3E7	0.0E0	136.28	
Nuclear fragile X mental retardation-interacting protein 2 GN=NUFIP2 [NUFP2_HUMAN]	1.97	0.73	0.98	-0.46	1	1	1.1E7	5.5E6	32.96	40.49
Serum response factor-binding protein 1 GN=SRFBP1 [SRFB1_HUMAN]	1.93		0.95		1		2.4E7	0.0E0	26.96	
Nucleolar protein 16 GN=NOP16 [NOP16_HUMAN]	1.92		0.94		3		2.2E7	0.0E0	140.30	
Heterochromatin protein 1-binding protein 3 GN=HP1BP3 [HP1B3_HUMAN]	1.88	0.58	0.91	-0.78	10	8	2.2E8	8.4E7	563.83	269.71
Insulin-like growth factor 2 mRNA-binding protein 3 GN=IGF2BP3 [IF2B3_HUMAN]	1.88	0.70	0.91	-0.51	3	2	5.7E7	4.5E7	199.85	99.57
Protein SPT2 homolog GN=SPTY2D1 [SPT2_HUMAN]	1.87	0.72	0.90	-0.48	2	1	1.1E7	7.0E6	61.62	25.44
60S ribosomal protein L17 GN=RPL17 [RL17_HUMAN]	1.86	0.55	0.90	-0.86	23	13	1.2E9	8.3E8	1257.89	989.18
Ribosome-binding protein 1 GN=RRBP1 [RRBP1_HUMAN]	1.85	0.59	0.89	-0.76	9	6	7.5E7	3.2E7	638.61	353.59
Core histone macro-H2A.1 GN=H2AFY [H2AY_HUMAN]	1.85	1.11	0.89	0.14	2	2	2.6E7	1.7E7	82.71	144.70
Centromere protein V GN=CENPV [CENPV_HUMAN]	1.85	0.29	0.88	-1.79	2	2	2.1E7	3.1E7	210.00	141.13
Protein FAM98A GN=FAM98A [FA98A_HUMAN]	1.82	0.50	0.86	-1.00	3	1	8.7E6	1.4E7	141.06	75.81
Histone H2A type 1-H GN=HIST1H2AH [H2A1H_HUMAN]	1.81	0.75	0.86	-0.42	4	4	5.9E8	7.4E8	303.79	311.16
Serine/arginine-rich splicing factor 2 GN=SRSF2 [SRSF2_HUMAN]	1.79	0.97	0.84	-0.05	2	1	3.0E6	1.0E6	53.45	29.01
Tubulin alpha-1C chain GN=TUBA1C [TBA1C_HUMAN]	1.79	0.64	0.84	-0.64	1	1	2.2E7	1.1E7	361.39	87.36
Insulin-like growth factor 2 mRNA-binding protein 1 GN=IGF2BP1 [IF2B1_HUMAN]	1.78	0.63	0.83	-0.68	6	4	2.4E8	2.2E8	412.59	318.70

protein name	H/L fwd	H/L cro	log_2 fold change fwd	log_2 fold change cro	H/L Count fwd	H/L Count cro	Area fwd	Area cro	Score fwd	Score cro
Protein PRRC2A GN=PRRC2A [PRC2A_HUMAN]	1.76		0.82		2		3.0E7	0.0E0	134.32	
40S ribosomal protein S24 GN=RPS24 [RS24_HUMAN]	1.76	0.49	0.82	-1.03	4	5	9.7E8	1.0E9	527.72	435.37
Zinc finger CCCH-type antiviral protein 1 GN=ZC3HAV1 [ZCCHV_HUMAN]	1.75	0.64	0.81	-0.65	9	9	1.9E8	1.4E8	733.74	802.28
Exosome complex component CSL4 GN=EXOSC1 [EXOS1_HUMAN]	1.75		0.80		1		1.5E7	0.0E0	25.93	
Keratin. type I cytoskeletal 18 GN=KRT18 [K1C18_HUMAN]	1.74		0.80		2		7.2E6	0.0E0	80.72	
ELAV-like protein 1 GN=ELAVL1 [ELAV1_HUMAN]	1.65	0.94	0.73	-0.08	1	4	7.5E6	2.6E7	35.52	159.43
40S ribosomal protein S9 GN=RPS9 [RS9_HUMAN]	1.63	0.57	0.70	-0.82	9	7	2.4E8	2.0E8	296.87	298.49
Lysine-rich nucleolar protein 1 GN=KNOP1 [KNOP1_HUMAN]	1.61	0.72	0.69	-0.47	9	3	4.5E7	1.5E7	328.59	156.65
40S ribosomal protein S13 GN=RPS13 [RS13_HUMAN]	1.59	0.62	0.67	-0.68	3	2	9.5E7	8.2E7	150.89	47.85
60S ribosomal protein L36a-like GN=RPL36AL [RL36L_HUMAN]	1.57	0.65	0.65	-0.62	1	1	8.6E7	1.7E7	100.00	65.46
PEST proteolytic signal-containing nuclear protein GN=PCNP [PCNP_HUMAN]	1.55		0.63		1		1.4E7	0.0E0	28.59	
DBIRD complex subunit ZNF326 GN=ZNF326 [ZN326_HUMAN]	1.55		0.63		1		1.4E7	0.0E0	25.17	
Heterogeneous nuclear ribonucleoproteins C1/C2 GN=HNRNPC [HNRPC_HUMAN]	1.52	0.72	0.61	-0.48	12	10	1.6E9	1.2E9	1506.77	1309.19
RNA-binding protein 39 GN=RBM39 [RBM39_HUMAN]	1.51		0.59		1		1.3E7	0.0E0	91.11	
SWI/SNF-related matrix-associated actin-dependent regulator of chromatin subfamily E member 1 GN=SMARCE1 [SMCE1_HUMAN]	1.51		0.59		2		1.2E7	0.0E0	118.33	
Heterogeneous nuclear ribonucleoprotein Q GN=SYNCRIP [HNRPQ_HUMAN]	1.50	0.91	0.59	-0.14	1	3	2.2E7	4.3E7	59.96	115.15
RNA-binding protein Raly GN=RALY [RALY_HUMAN]	1.49	0.72	0.57	-0.48	4	2	6.3E7	4.9E7	106.71	57.91
Probable ATP-dependent RNA helicase DDX17 GN=DDX17 [DDX17_HUMAN]	1.48		0.57		2		7.3E7	1.1E8	184.49	148.49
Serine/arginine-rich splicing factor 12 GN=SRSF12 PE=2 [SRS12_HUMAN]	1.47	1.06	0.55	0.08	1	1	7.6E6	1.5E7	43.95	29.32
Spermatogenesis-associated serine-rich protein 2 GN=SPATS2 [SPAS2_HUMAN]	1.47		0.55		1		3.5E7	0.0E0	31.93	
DNA-directed RNA polymerases I, II, and III subunit RPABC1 GN=POLR2E [RPAB1_HUMAN]	1.46	1.17	0.55	0.23	3	2	1.4E7	1.6E7	165.26	114.50
Caprin-1 GN=CAPRIN1 [CAPR1_HUMAN]	1.46	0.70	0.54	-0.51	1	2	1.7E7	9.5E6	32.39	32.69
60S ribosomal protein L36a GN=RPL36A [RL36A_HUMAN]	1.45		0.54		1		8.7E7	0.0E0	86.26	
Heterogeneous nuclear ribonucleoprotein R GN=HNRNPR [HNRPR_HUMAN]	1.45	0.78	0.54	-0.36	2	2	1.9E7	3.0E7	95.66	101.74
Interleukin enhancer-binding factor 2 GN=ILF2 [ILF2_HUMAN]	1.44	0.79	0.53	-0.33	1	3	3.4E7	7.5E7	118.15	245.09
40S ribosomal protein S4, X isoform GN=RPS4X [RS4X_HUMAN]	1.44	0.63	0.52	-0.66	21	16	6.0E8	4.3E8	1214.86	1072.03

protein name	H/L fwd	H/L cro	log_2 fold change fwd	log_2 fold change cro	H/L Count fwd	H/L Count cro	Area fwd	Area cro	Score fwd	Score cro
Coiled-coil domain-containing protein 86 GN=CCDC86 [CCD86_HUMAN]	1.43	0.91	0.52	-0.13	2	2	4.7E7	3.8E7	64.94	102.55
U6 snRNA-associated Sm-like protein LSm4 GN=LSM4 [LSM4_HUMAN]	1.43		0.52		2		3.2E7	0.0E0	43.37	
Interleukin enhancer-binding factor 3 GN=ILF3 [ILF3_HUMAN]	1.42	0.82	0.51	-0.28	15	14	2.0E8	1.8E8	682.98	745.80
Fragile X mental retardation protein 1 GN=FMR1 [FMR1_HUMAN]	1.41	0.47	0.50	-1.09	1	1	5.0E7	1.9E7	129.30	108.95
Heterogeneous nuclear ribonucleoprotein L GN=HNRNPL [HNRPL_HUMAN]	1.40	0.96	0.49	-0.05	2	2	4.8E7	6.1E7	75.99	69.02

Contributors and Funding Sources

This work was supervised by a thesis committee consisting of Prof. Dr. Melanie Brinkmann (advisor) of the Research Group Viral Immune Modulation at the Helmholtz Centre for Infection Research Braunschweig (HZI) and professor at the Institute of Genetics at the Technische Universität Braunschweig, Prof. Dr. Lothar Jänsch of the Research Group Cellular Proteome Research at the HZI and professor for Proteome Research of Infectious Processes at the Technische Universität Braunschweig, Prof. Dr. Andrea Kröger of the Research Group Innate Immunity at the HZI and professor for Molecular Microbiology at the Otto-von-Guericke-University in Magdeburg and Prof. Dr. Ingo Schmitz of the Research Group Systems-Oriented Immunology and Inflammation Research of the HZI and Otto-von-Guericke University Magdeburg.
The data analysed for Figure 44 in Chapter 3.1 was conducted by Kendra Bussey of the Viral Immune Modulation group at the HZI. Processing of the ethanol purified eluates for q-AP-MS analysis and subsequent MS from Chapter 3.1.3 and 3.3.11 were conducted by Josef Wissing of the Cellular Proteome Research Group at the HZI. The manual analysis of selected q-AP-MS data from Chapter 3.3.1 were conducted by Manfred Nimtz of the Cellular Proteome Research group at the HZI.

All other work conducted for the dissertation was completed by me, Ulrike Diekmann, independently and personally.

Graduate study was supported by an 18-month scholarship within the framework of the promotion of guest scientist stays at the HZI. Funding for this research project was provided in part by the SFB900 Microbial Persistence and its Control.